

UNCLASSIFIED

AD NUMBER
AD465075
NEW LIMITATION CHANGE
TO Approved for public release, distribution unlimited
FROM Distribution authorized to U.S. Gov't. agencies and their contractors; Administrative/Operational Use; Apr 1965. Other requests shall be referred to Air Force Institute of Technology, Wright-Patterson AFB, OH 45433.
AUTHORITY
AU [AETC] ltr, 29 Oct 2004

THIS PAGE IS UNCLASSIFIED

ARL 65-66
APRIL 1965



465075

Aerospace Research Laboratories

CATALOGED BY: DDC
AS AD 113

EXPERIMENTAL OPTIMIZATION OF THE REVERSE-FLOW SWIRL CHAMBER

1/LT. THOMAS D. FIORINO, JR.
1/LT. ROBERT POPLAWSKI
AIR FORCE INSTITUTE OF TECHNOLOGY

OFFICE OF AEROSPACE RESEARCH
United States Air Force



NOTICES

When Government drawings, specifications, or other data are used for any purpose other than in connection with a definitely related Government procurement operation, the United States Government thereby incurs no responsibility nor any obligation whatsoever; and the fact that the Government may have formulated, furnished, or in any way supplied the said drawings, specifications, or other data, is not to be regarded by implication or otherwise as in any manner licensing the holder or any other person or corporation, or conveying any rights or permission to manufacture, use, or sell any patented invention that may in any way be related thereto.

- - - - -

Qualified requesters may obtain copies of this report from the Defense Documentation Center, (DDC), Cameron Station, Alexandria, Virginia.

- - - - -

DDC release to OTS not authorized.

- - - - -

Copies of ARL Technical Documentary Reports should not be returned to Aerospace Research Laboratories unless return is required by security considerations, contractual obligations or notices on a specified document.

NOTICE: When government or other drawings, specifications or other data are used for any purpose other than in connection with a definitely related government procurement operation, the U. S. Government thereby incurs no responsibility, nor any obligation whatsoever; and the fact that the Government may have formulated, furnished, or in any way supplied the said drawings, specifications, or other data is not to be regarded by implication or otherwise as in any manner licensing the holder or any other person or corporation, or conveying any rights or permission to manufacture, use or sell any patented invention that may in any way be related thereto.

ARL 65-66

EXPERIMENTAL OPTIMIZATION OF THE REVERSE-FLOW SWIRL CHAMBER

THESIS

**Presented to the Faculty of the School of Engineering of the Air Force
Institute of Technology, Air University, in Partial Fulfillment of
the Requirements for the Degree of Master of Science**

APRIL 1965

By

**Thomas D. Fiorino, Jr., B.S.A.E.
1/Lt USAF**

**Robert Poplawski, B.S.M.E.
1/Lt USAF**

Graduate Aerospace-Mechanical Engineering

**AEROSPACE RESEARCH LABORATORIES
OFFICE OF AEROSPACE RESEARCH
UNITED STATES AIR FORCE
WRIGHT-PATTERSON AIR FORCE BASE, OHIO**

FOREWORD

The devices investigated in this study are the first high pressure reverse-flow vortex (swirl) chambers developed primarily for sub-micron particle separation. The concept of the swirl chamber is the direct result of continuing basic research in the field of two phase flow, at the Aerospace Research Laboratories, under the direction of the Chief Scientist, Dr. Hans Von Ohain.

The purpose of this investigation was to test and modify the existing swirl chambers, and to obtain the optimum chamber for given conditions as presented herein.

The authors wish to gratefully acknowledge the guidance and help of Dr. Hans Von Ohain, Dr. Roscoe Mills, and Major Robert Keller of ARL. We also wish to extend thanks to Ömer Göksel who did much of the preliminary testing and modification on the swirl chamber, and to thank our thesis advisor Lt. George Tsongas.

We would like to express our thanks to Stan Petticrew and Don Lowe for vital assistance in preparing Lab equipment, and to Jack McClary, who was responsible for the distribution of the high pressure air supply.

We would also like to thank our wives for their help, patience, and understanding during the preparation of this thesis.

Abstract

A high pressure-reverse flow vortex chamber is a device designed for the purpose of separating sub-micron particles out of a gas flow. The requirements for separation of sub-micron particles from a curved flow are given, and an equation determining the minimum angular velocity necessary for separation in a vortex flow is presented.

Three swirl (vortex) chambers were tested and modified to determine their optimum performance. Results show that inlet geometry, method of injection, injection nozzle size, exhaust diffuser spacing, and internal chamber dimensions are important factors when optimizing chamber performance. The testing and modification has led to the evolution of a swirl chamber that can develop an overall pressure ratio of thirty and a pressure recovery of eighty-five per cent for a chamber inlet total pressure of 300 psig.

The internal flow pattern of the swirl chamber was studied using talcum powder for particles and high speed motion picture photography (7,000 frames per second) as an aid in observing gross particle movements.

This study has verified the fact that the swirl chambers are basically capable of separating sub-micron particles out of a gas flow.

Contents

	Page
I. Introduction	1
Background	1
Principle of Operation	3
Purpose and Scope	6
II. Description of Apparatus	8
III. Theoretical Considerations	11
Rotational Velocity for Separation	11
Performance Parameters	13
Method of Injection	14
IV. Experimental Program	18
Qualitative Analysis	19
Chamber Insert Location	20
Modifications in Inlet Geometry	20
Diffuser Spacing	21
Radial Diffusers	21
Radial Probes	21
Quantitative Analysis	21
Nozzle Diameter Changes	22
Single Cell Swirl Chamber	22
Chamber Insert Size	23
Second Generation Chamber	23
Flow Visualization	24
Axial Pressure Probes	24
V. Data Reduction	25
VI. Results and Discussion	27
Qualitative Analysis	27

	Page
Chamber Insert Location	27
Modifications in Inlet Geometry	30
Diffuser Spacing	32
Radial Diffusers	34
Radial Probes	36
Quantitative Analysis	36
Nozzle Diameter Changes	37
Single Cell Swirl Chamber	39
Chamber Insert Size	39
Second Generation Chamber	40
Flow Visualization	41
Axial Pressure Probes	43
VII. Conclusions	44
VIII. Recommendations	46
Additional Chamber Modification	46
Flow Pattern Mapping	47
Separation Capability of the Chambers	47
References	49
List of Figures	50
List of Tables	98
Appendix A: Engineering Drawings	101
Appendix B: Identification Code and Graphical Data	114

List of Symbols

<u>Symbol</u>	<u>Definition</u>	<u>Units</u>
A	Area	in ²
C _D	Coefficient of Discharge	none
D	Diameter	ft ²
F _D	Drag on a Sphere	lbf
g _c	Constant	$\frac{\text{lbf-ft}}{\text{lbf-sec}^2}$
K	Mass Flow Rate Correction Factor	none
k	Ratio of Specific Heats	none
\dot{m}	Mass Flow Rate	$\frac{\text{lbf}}{\text{sec}}$
P	Pressure	psia
R	Gas Flow Radius of Curvature	ft
\bar{R}	Gas Constant	$\frac{\text{lbf-ft}}{\text{lbf-mole-R}}$
Re	Drift Reynolds Number	none
R _p	Particle Path Radius of Curvature	ft
r	Ratio of Venturi Throat Pressure to Upstream Pressure	none
T	Temperature	°R
u	Velocity of Curved Gas Flow	fps
v _p	Perturbation Velocity	fps
W	Particle Drift Velocity	fps
e	Ratio of Venturi Throat Diameter to Upstream Diameter	none

<u>Symbol</u>	<u>Definition</u>	<u>Units</u>
ΔP_v	Exit Venturi Differential Pressure	psi
μ	Absolute Fluid Viscosity	$\frac{\text{lbf-sec}}{\text{ft}^2}$
ρ	Density of Fluid	$\frac{\text{lbm}}{\text{ft}^3}$
σ	Density of Particle	$\frac{\text{slugs}}{\text{ft}^3}$
ω	Angular Velocity	$\frac{\text{rad}}{\text{sec}}$

Subscripts

e	Exit
h	Venturi Throat
i	Inlet
t	Total Conditions
u	Upstream of Venturi Throat
1,3,4,7 and 9	Pressure and temperature tap locations (See Fig.48)

EXPERIMENTAL OPTIMIZATION OF THE
REVERSE-FLOW SWIRL CHAMBER

I. Introduction

Background

The devices investigated in this project were developed as a possible means of separating sub-micron particles out of a gas flow. In general, the separation of particles from a fluid can be accomplished in six ways; they are (Ref 2:8-21):

1. Entrainment of particles within another fluid, as with washing by water sprays.
2. Filtration, in which a gas containing particles is passed through fiber filters to remove the particles.
3. Ionization, in which particles are given an electrostatic charge and are withdrawn from the gas stream by the attraction of a charged electrode.
4. Inertia, which utilizes an abrupt change in the direction of the flow path.
5. Gravitation, in which there is a sudden reduction in the flow velocity of the gas in which particles are immersed.

6. Centrifugal force, as with the whirling
action of a cyclone separator.

Cyclone separators, electrostatic precipitators, and other commercially available separating devices use one or more of the above mentioned methods for achieving particle separation. Unfortunately, none of these devices is capable of practical and efficient separation of particles, having a size on the order of one micron from fluids with high flow rates.

Since recent advances in technology have placed an increasing demand for a method of sub-micron particle separation, numerous studies have been made to find a satisfactory method particularly in the field of two-phase vortex flow. The feasibility of using vortex flows for sub-micron particle separation was studied at the Aerospace Research Laboratory using low pressure (inlet pressure ≤ 100 psig) vortex chambers with air as the fluid, and smoke, talcum, or mercury as the immersed particles. These studies indicated the possibility of using a high pressure (inlet pressure ≥ 150 psig) reverse flow vortex chamber (hereafter referred to as a swirl chamber) for sub-micron particle separation and consequently led to the design and construction of the swirl chambers investigated in this project.

Principle of Operation

The swirl chambers considered in this investigation use the effect of inertial and centrifugal forces on a gas flow to produce separation. To understand the method of particle separation it is necessary to recognize that:

1. The inertia of a particle is a function of its volume and density.
2. The resistance or drag of a particle in a fluid is a function of the particle shape and size.

For the case of a spherical shape, the inertia of the particle is proportional to the cube of its diameter, while its flow resistance is proportional to the square of its diameter. By Newton's first law of motion, a particle in a moving stream will continue to move in a straight line unless acted upon by an external force. The continuance of this motion is a result of the inertia of the particle, whereas fluid resistance opposes such motion. Thus, if separation is attempted by altering the direction of the flowing stream, the suspended particles will, by virtue of their inertia, tend to continue moving in their original direction and not follow the direction of the general gas flow. However, due to fluid friction the particles will eventually be forced to conform to the pattern of the gas flow. The greater the particle density and size, the

GAM/NE/64-14

greater the inertia effects (relatively speaking) and consequently the better the separation of particles from the gas stream.

From the above discussion it becomes obvious that in order to separate particles in a curved flow, both a high fluid angular velocity and sufficient particle residence time within the curved flow are necessary. Since excessive perturbations within the fluid tend to cancel the centrifugal action of the rotation, a low turbulence level within the curved flow is also required. Thus, for a given fluid and particle (type and size) the requirements for sub-micron particle separation in a swirl chamber are:

1. High angular velocity of the fluid
2. Low turbulence level in the device
3. Sufficient particle residence time within the chamber.

Since the swirl chamber flow consists of a spiralling vortex motion, a high angular velocity can be obtained by maintaining a high pressure ratio between the inner core and outer periphery of the vortex flow. Low turbulence level can hopefully be obtained by proper chamber design and particle residence time can be regulated by varying the geometric dimensions of the chamber.

In the swirl chambers under investigation, part or

all of the fluid is tangentially injected at an inner radius position with a high velocity (See Fig. 1) (in a manner similar to the Hilsch vortex tube) and is allowed to expand along a diffuser section to an outer radius. The fluid continues its motion with both axial and tangential components of velocity along a section of constant radius and is eventually turned radially inward either by a physical boundary or a symmetrical flow pattern. The turning of the flow forces the fluid to become a sink-vortex flow called secondary flow. Eventually, to satisfy continuity, the fluid again turns and flows toward the injection area where a portion of the fluid leaves the chamber as exhaust. The remaining portion of the fluid spirals radially outward (source-vortex) and is recirculated with the incoming fluid. In the region between the secondary and recirculating flow, the flow pattern gradually changes from a sink-vortex to a source-vortex.

In operation, the particle laden gas enters the chamber and follows the pattern previously described to the region of secondary flow. The secondary flow phenomena causes the fluid and particles to accelerate to high angular velocities (assuming a sink-free vortex) causing a high concentration of particles near the inner core of the chamber. As the fluid and particles flow toward the exhaust, the gradual change from a sink-vortex to a

source-vortex allows the high concentration of particles to be recirculated in the chamber, and only a very small portion to leave the system as exhaust (hopefully less than one part per thousand of the incoming particles). The high concentration of particles (recirculated) tends to build-up on the outer radius of the chamber and can be removed by allowing a very small amount of the fluid to exit the chamber at the outer radius (See Figs. 2 and 3 for exits).

Purpose and Scope

The purpose of this investigation was to test and modify the high pressure swirl chambers to improve their capability for sub-micron particle separation. Since the injection of sub-micron particles into the inlet air flow would require the use of a special high pressure injection system, and extremely sensitive measuring devices to detect the presence of such minute particles, this method was not used. Instead, a set of parameters were selected as a measure of the separating effectiveness of the chamber. The reason for using these parameters can be found in the section entitled "Theoretical Considerations".

The selected performance factors define the optimum chamber as having the highest:

1. P_9/P_{it} , overall pressure ratio--the ratio

of the outer wall static pressure to the axial total pressure, (See Fig. 4).

2. P_g/P_{t_i} , pressure recovery--ratio of the outer wall static pressure to the chamber inlet total pressure (See Fig. 4).

The specific objective of this project was to obtain an optimum chamber by geometrical modifications of the original swirl chambers.

II. Description of Apparatus

In the course of this investigation two basic high pressure swirl chambers were tested and modified in an effort to obtain optimum performance. They were designated the first and second generation chambers to note the order of their testing and development. In the first generation chamber the fluid was injected at a single radius, while in the second generation chamber the fluid was injected at four radii. The cross-section assembly drawings of the first and second generation chambers are shown in Figs. 48 and 49 respectively. The first generation dual cell chamber was modified to obtain a single cell chamber for additional testing and visual inspection of the internal flow pattern. The visual single cell swirl chamber (with plexiglass window) is shown in Fig. 50. The dual cell chamber is characterized by inlet sections at both ends of the chamber, whereas the single cell chamber has only one inlet section. The nomenclature used to identify the components of the first and second generation chambers are shown in Tables I and II. Some of the components referenced in the above tables are the nozzle rings, radial diffusers, and chamber inserts.

The three nozzle rings used with the first generation chamber have eight convergent nozzles per ring with a

GAM/ME/64-14

throat diameter of $1/16$ in, $3/32$ in, or $1/8$ in. A $1/16$ in hole diameter nozzle ring is shown in Fig. 51. The multiple nozzle housing for the second generation chamber has twenty-four $1/16$ in convergent nozzles arranged in groups of six at four different radii as shown in Fig. 52.

The blank, bleed, and crank diffusers are shown in Figs. 53, 54, and 55, respectively. The blank diffuser is essentially a flat plate while the bleed and crank diffusers have a concentric ring which allows a portion of the exhausting fluid to leave the chamber in an axial direction. The distance between the radial diffuser and the admission chamber (diffuser gap spacing) is determined by the gaskets used between the two components for the blank and bleed diffusers. The diffuser gap spacing for the crank diffuser is not fixed by the gasket thickness and the spacing is varied by turning the diffuser clockwise and counter-clockwise.

Chamber inserts for the first generation chamber are right circular cylindrical shells having a $3 \frac{9}{16}$ in ID and a length from $2 \frac{3}{16}$ in to $6 \frac{3}{16}$ in. The positioning of three different length chamber inserts are shown in Figs. 56, 57, and 58.

Pressure and temperature tap location for the first and second generation chamber are shown schematically in Fig. 4. The exact location can be determined in Figs. 48 and 59 for the first generation chamber. Pressures

GAM/ME/64-14

were obtained from calibrated bourdon or bellows gages (maximum error $\pm 2\%$). Temperature measurements were obtained using calibrated iron-constantan thermocouples (maximum error $\pm 3^{\circ}\text{F}$). Mass flow rates were determined with the use of calibrated venturis. The air was supplied by the Aerospace Research Laboratory at 3,000 psig after it had been dried to an average of -65°F dewpoint by an absorptive drier. The instrumentation and typical test apparatus are shown in Figs. 5 and 6.

Special axial pressure probes (See Fig. 7) were used in an attempt to determine the axial pressure profile in the first and second generation chambers.

III. Theoretical Considerations

One of the requirements for sub-micron particle separation in a vortex flow is a high angular velocity. To determine the magnitude of this rotational velocity an approximate derivation is included in the next sub-section entitled "Minimum Rotational Velocity for Separation." Since the rotational velocity cannot be measured directly in the present chambers and, therefore, used as a performance parameter, two pressure ratios were selected as a measure of the chambers' performance. The reasons for the rotational velocity can be found in the sub-section "Performance Parameters." The final sub-section deals primarily with the method of injection and justifies the selection of inner radius injection for sub-micron particle separation.

Minimum Rotational Velocity for Separation

For particle separation in a curved flow it is desirable to have a means of estimating the required minimum rotational velocity. In order to obtain an analytical estimate of the rotational velocity, similarity considerations were used for laminar flow with perturbations in the fluid.

For a laminar gas flow with the drift $Re < 1$ (based on

particle drift velocity), Stoke's equation for drag on a spherical particle is:

$$F_D = 3\pi\mu WD \quad (1)$$

Referring to Fig. 3 and summing forces in a direction normal to the path of the particle yields:

$$3\pi\mu WD = \frac{\pi D^3}{6} (\sigma - \rho) \frac{W^2 + U^2}{R_p} \quad (2)$$

Eq (2) can be simplified to yield an expression for the angular velocity,

$$\omega = \frac{W}{U} \frac{\mu}{\sigma D^2} \quad (3)$$

where $U \gg W$ $\sigma \gg \rho$
 $R_p \approx R$ $\omega = U/R$

Eq (3) can be re-written in the form

$$\omega = \frac{W}{v_p} \frac{v_p}{U} \frac{\mu}{\sigma D^2} \quad (4)$$

If separation of the particles from the flow is to be attained, the perturbation velocity (v_p) must be less than the particle drift velocity (W). An estimated value of the ratio of drift to perturbation velocity is:

$$W/v_p > 2.5 \quad (\text{Ref. Dr. Von Ohain})$$

GAM/KE/64-14

Since the turbulence level (v_p/u) at any particular time in the present device is difficult to predict, a lower limit which would give the minimum necessary rotational velocity (based on cyclone separators) is:

$$v_p/u \approx 0.04$$

Substituting in the values for the turbulence level and drift to perturbation velocity ratio into Eq (4) yields

$$\omega > 1.8 \frac{u}{\sigma D^2} \quad (5)$$

If the type and size of particles are known, and the viscosity of the fluid is also known, then Eq (5) gives an estimate of the minimum rotational velocity required for separation for a low turbulence level of 4%.

Performance Parameters

Overall Pressure Ratio. The overall pressure ratio, P_g/P_{it} , is used as a performance parameter indicating the magnitude of the angular velocity. The assumption made in using this parameter is that the higher the pressure ratio the larger the angular velocity. In general, if the inlet pressure to the chamber is increased the mass flow and overall pressure ratio are increased; therefore, to satisfy continuity the flow must accelerate to higher angular velocities especially at the smaller radii near the core of the vortex.

The selection of the outer wall static pressure, P_s , for defining both the overall pressure ratio and pressure recovery was based on calculations assuming isentropic and free vortex flow from the inlet nozzles to the outer radius. The calculations resulted in a difference in static and total pressure (at the outer wall) of less than 5% for inlet nozzles in a choked condition and a chamber insert of 3 9/16 inches diameter.

Pressure Recovery. The so called pressure recovery, P_s/P_{t_t} , is used as a performance parameter to indicate the efficiency of conservation of fluid energy. The importance of having a high pressure recovery is obvious in that the larger the pressure recovery, the higher will be the outer wall static pressure. If the outer wall static pressure is increased, then with other conditions held constant, the pressure ratio increases, which, from our previous discussion induces higher angular velocities.

Method of Injection. In an outer radius injection vortex chamber (See Fig. 9), the magnitude of the radial flow occurring in the boundary layer on the chamber walls has been found to be of the same order of magnitude as the local external (i.e., outside the boundary layer) tangential velocity (Ref 3:7). Thus, if efficient particle separation (i.e., removal of most of the particles before they exhaust) is to be obtained, it is desirable

to eliminate the inward radial velocity component of the flow in the region near the exhaust. If one considers a device in which the fluid and particles are injected tangentially at an outer radius (See Fig. 9), the boundary layer buildup on the chamber walls, coupled with the radial inward velocity, transport the particles along the outer walls and eventually out the exhaust. The amount of fluid that leaves the chamber through the boundary layer has been found to be approximately three-fourths of the total mass flow through the chamber, and more important, as the total mass flow is increased, the boundary layer flow becomes proportionately larger (Ref 3:9 and 4:17). As a result of the boundary layer transporting a large amount of fluid, the fluid in the inner region of the vortex chamber tends to revolve as a rigid body and thereby reduce the rotational velocity. The particles which are centrifuged to the outer wall are transported out the exhaust in the boundary layer while the particles near the central core are carried out the exhaust by the axial component of the flow. The net result of the flow pattern is to remove the particles from the system.

To reverse the flow pattern on the outer walls and eliminate the inward radial velocity in the vicinity of the exhaust, the present swirl chambers under investigation were designed to inject all or part of the fluid at

a small radius (approximately one-half inch). By injecting tangentially at this small radius the flow pattern within the chamber is reversed on the outer boundary as compared to the vortex devices previously described (compare Fig. 9 with Fig. 1). Besides creating a spiral vortex (sink-vortex) in the region of the geometric axial center of the chamber, an additional flow pattern which is called recirculating flow is induced as shown in Fig. 1. The advantage of the recirculating flow pattern lies in its ability to transport the particles from the central axial region of the chamber to the outer wall where they can be recirculated (travel the same path as when originally injected) or collected and exited out of the chamber.

In a confined free vortex gas flow it can be shown that the friction loss is inversely proportional to the square of the radius, and the energy loss inversely proportional to the cube of the radius. As a result, the injection of a fluid at a small radius is inherently inefficient, in that, a considerable amount of fluid kinetic energy is dissipated overcoming frictional forces. This energy dissipation is incurred when the fluid diffuses to a larger radius in the process of developing secondary and recirculating flow patterns.

For efficient particle separation and low energy loss due to friction it becomes apparent that "scheduled" in-

GAN/NE/64-14

jection--a method of injecting the fluid at several radii--must be used. The amount of fluid injected at the smaller radii should be just sufficient to maintain the reverse flow pattern, while the greater mass flow should be injected at larger radii so that friction losses are kept to a minimum.

IV. Experimental Program

The primary objective of the experimental work was to increase the overall pressure ratio and pressure recovery and to determine their variance with changes in the ratio of the exit to inlet mass flow rates (mass flow ratio). Changes in the internal geometry were made in order to try and improve the chambers' pressure ratios. In addition, attempts were made to determine the approximate flow pattern within the swirl chambers using axial pressure probes and visual techniques.

In order to obtain a systematic approach in evaluating the high pressure swirl chambers, the investigation was divided into three parts:

1. Qualitative analysis
2. Quantitative analysis
3. Flow visualization

The pressure ratios (i.e., the overall pressure ratio and pressure recovery) were determined as a function of the exit venturi differential pressure for the qualitative tests, and as a function of the mass flow ratio (exit to inlet mass flow rate) for the quantitative tests. This constitutes the major difference between the two analyses. Since an extensive amount of testing was planned, a swirl chamber code was developed to facilitate identifi-

cation of the various tests along with their results. The identification code is explained in Appendix B.

Qualitative Analysis

In the qualitative analysis, only the first generation swirl chamber was tested using 1/16 in diameter nozzles and chamber total inlet pressures of 225 psig and 300 psig. For each inlet pressure, the pressure ratios, i.e., pressure recovery and overall pressure ratio, were determined as a function of the exit venturi differential pressure, ΔP_v . A flow diagram of the apparatus used in the qualitative analysis is shown in Fig. 10.

Since chamber performance is based on the numerical magnitude of the pressure ratios, numerous geometrical chamber modifications were made to increase their values. The geometrical changes made are:

1. Variation of the fluid exit location within the chamber (Fig. 2 and 3).
2. Modifications of the inlet geometry within the chamber (Fig. 11).
3. Changes in the diffuser spacing within the chamber (Fig. 11).
4. Changes in the type of radial diffuser.

Modifications which increased the pressure ratios were incorporated into all subsequent tests in this project. In addition to the geometric changes, perturbation studies

were made using a solid one-quarter inch stainless steel rod inserted radially into the chamber at the center disc flange.

Prior to the commencement of the first qualitative analysis test run the exhaust nose lip (See Fig. 11) was removed to prevent choking of the fluid. Removal of the lip was necessary because the total cross sectional area (between the nozzle ring and the exhaust nose lip) was less than the total nozzle inlet area.

Chamber Insert Location. The chamber inserts were placed in two positions (See Fig. 2 and 3) in an attempt to determine the influence of the fluid exit location on the pressure ratios. The pressure ratios were determined as a function of the exit venturi differential pressure, ΔP_v .

Modifications in the Inlet Geometry. Variations in the inlet geometry were made in five steps and are shown in Fig. 11. The modifications were:

1. Nozzle holes reamed and polished.
2. Lips on the nozzle ring half removed.
3. Lips on the nozzle ring completely removed.
4. Nozzle ring taper increased.
5. Exhaust cylinder nose shortened.

Inlet geometry modifications which resulted in increased values of the pressure ratios were incorporated into all

subsequent tests.

Diffuser Spacing. The diffuser spacing (See Fig. 11) was varied to determine the spacing that would give the optimum overall pressure ratio and pressure recovery.

Radial Diffusers. All previous tests were accomplished using bleed diffusers (See Fig. 54). In this phase of the investigation a blank (no bleed) diffuser (See Fig. 53) was tested, using various diffuser spacings, to determine if the blank diffusers could obtain pressure ratios that were comparable with the bleed diffusers.

Probes Inserted Radially into the Chamber. The object of this study was to determine if the chamber flow, after being disturbed by a radial probe, would return to the initial conditions. The initial conditions were those values of pressure recovery and overall pressure ratio prior to disturbing the flow with a radial probe. The probe was inserted radially at the center disk flange by drilling a special tap for this purpose.

Quantitative Analysis

In the quantitative analysis, both the first and second generation swirl chambers were tested. The overall pressure ratio and pressure recovery were determined as functions of mass flow ratio (\dot{m}_e/\dot{m}_i). The majority of testing was accomplished by varying the exit mass flow

GAN/HE/64-14

rate while holding the total inlet pressure constant at either 225 psig or 300 psig. A schematic of the flow diagram for the quantitative analysis is shown in Fig. 12.

The studies of the first generation chamber included changing the nozzle diameter size and chamber inserts. Additional data was obtained on a single cell swirl chamber (See Fig. 18).

Only three runs were made using the second generation swirl chamber.

Nozzle Diameter Changes. Modifications in the inlet nozzle cross sectional area were restricted to the first generation chamber. The nozzle hole diameters tested were 3/32 in and 1/8 in. For each of the two nozzle diameters tested, the diffuser spacing was varied until the maximum pressure ratios were obtained. The two nozzles tested in the quantitative analysis and the 1/16 in hole nozzle rings used in the qualitative analysis are shown in Fig. 14.

Single Cell Swirl Chamber. Only the first generation type chamber was used in the testing of the single cell chamber. The nozzle size selected for use in the single cell chamber was based on the optimum pressure ratios obtained in the dual chamber. The data obtained on the single cell chamber was compared to a dual swirl chamber operating under the same inlet conditions. The external view of the single cell chamber is shown in Fig. 13.

Chamber Insert Size. In all previous experiments a 3 9/16 in ID x 2 3/16 in long chamber insert was used ("g" insert). The testing that was conducted by varying chamber insert size was restricted to the first generation chamber. Originally, nine insert sizes were proposed for testing (See Appendix B); however, only three different lengths were tested (g, h, and i inserts). The remaining inserts were not tested because the overall pressure ratio, as defined in this report, loses its significance for small diameter chamber inserts (the outer wall static pressure is not within 5% of the outer wall total pressure). The inserts tested are shown in Fig. 15. The assembly drawings are shown in Figs. 56 to 58 and the physical chambers are shown in Figs. 16 to 18.

Second Generation Chamber. The second generation multiple nozzle housing and physical chamber are shown in Figs. 20 and 21 respectively. Testing of the chamber was accomplished by first optimizing the overall pressure ratio at a mass flow ratio of 0.50 to obtain a basis of comparison between the various tests. The overall pressure ratio was optimized by adjusting the crank diffuser (See Fig. 19 for the bleed, crank, and blank diffusers). Upon optimization, the pressure recovery and overall pressure ratio were determined as functions of the mass flow ratio. The data was obtained for total inlet pres-

tures of 225 psig and 300 psig using a 9/64 in diameter center pressure tap (P_{1t}). Since a pressure gradient was expected across the tap, additional tests were conducted using a 0.047 in diameter center pressure tap. The tests using the 0.047 in tap were performed using a constant mass flow ratio of 0.50, while varying the total inlet pressure (0--350 psig). Analogous data was obtained using the 9/64 in center pressure tap to determine the effect of the pressure gradient on the overall pressure ratio.

Flow Visualization. High speed motion pictures (7,000 frames per second) of the internal flow, on a solid plexiglass boundary in a single cell visual chamber (See Figs 22 and 50), were taken for total inlet pressures of 100 psig, 200 psig, and 300 psig. The fluid flow patterns were made visible by injecting talcum powder at an axial sub-atmospheric pressure position in the chamber.

Axial Pressure Probes. During the course of testing attempts were made to obtain axial static and total pressure profiles in the first and second generation dual cell chambers. The probes used are shown schematically in Fig. 7.

V. Data Reduction

In the qualitative analysis the pressure recovery and overall pressure ratio were computed as functions of the exit venturi differential pressure. In the quantitative analysis the pressure ratios were computed as functions of the mass flow ratio (\dot{m}_e/\dot{m}_i). The mass flow rate equation can be derived using the equations of continuity and perfect gas, the definition of the coefficient of discharge, and the assumption of isentropic flow to yield (Ref 1:47-48)

$$\dot{m} = K A_h \left[2 g_c \frac{P_u}{R T_u} (P_u - P_h) \right]^{1/2} \quad (6)$$

$$\text{where: } K \equiv \phi C_D / \sqrt{1 - \beta^4}$$

$$\phi \equiv \left[r^{2/k} \frac{k}{k-1} \left(\frac{1-r^{k-1}}{1-r} \right) \left(\frac{1-\beta^4}{1-\beta^4 r^{2/k}} \right) \right]^{1/2}$$

Eq (6) was used to calculate the chamber inlet and exit mass flow rates. Simplification in the mass flow rate calculations was made by plotting K vs r and is shown in Fig. 23. The discharge coefficient was assumed to be constant at 0.975 because venturi calibration indicated

GAM/ML/64-14

the coefficient varied from approximately 0.972 to 0.981 for the range of testing.

The visual investigation consisted of the evaluation of approximately 12,000 individual frames of high speed motion pictures. The evaluation of the high speed film was made to determine the radial depth to which the particles could penetrate, and to obtain some insight into the phenomena of gross particle movements inside a swirl chamber.

VI. Results and Discussion

The experimental results of this investigation are presented in Figs. 24-47. The qualitative, quantitative, and flow visualization analyses are shown in Figs. 24-35, 36-44, and 45-47 respectively. The graphical data of the above curves can be found in Appendix B. Each curve is the result of a minimum of two test runs. For purposes of clarity each of the areas of investigation is considered separately and in chronological order.

Qualitative Analysis

The results of the qualitative analysis show the overall pressure ratio could have two values at a given exit venturi differential pressure, ΔP_v , depending on whether the exit mass flow rate was being increased or decreased. This hysteresis effect in the overall pressure ratio appears in the majority of the qualitative tests where the exit mass flow rate was increased and decreased. The hysteresis effect is only shown in Figs. 24, 26, and 28. It is not shown in the subsequent overall pressure ratio curves to avoid crowding of the graphs. The detail graphical data curves can be found in Appendix B.

Chamber Insert Location. The effects of chamber insert location on the performance parameters can be seen in Figs. 24-29. The overall pressure ratio for the two

exiting positions is shown in Fig. 24, while Fig. 25 shows the pressure recovery. The influence of chamber inlet pressure on the performance parameters is shown in Figs. 26 and 27 for the first exiting method, and in Figs 28 and 29 for the second exiting method.

For a chamber inlet total pressure of 225 psig, Fig. 24 shows the first exiting method has a maximum overall pressure ratio of approximately 9.8 while the second exiting method has a maximum of 8.2. However, the hysteresis effect is more pronounced for the first exiting method. At $\Delta P_v = 21.75$ psi, the overall pressure ratio can be either 5.6 or 4.3 depending on whether the exit mass flow rate is increasing or decreasing. If the chamber is initially tested from a fully closed to open position (i.e., ΔP_v is increased from 0 psi to 21.75 psi), the overall pressure will be 5.6 at the full open position. Now, if the system (chamber) is allowed to remain at the high ΔP_v value (21.75 psi) for a period of time greater than ten seconds, the center pressure (P_{1t}) gradually increases until the overall pressure ratio drops from 5.6 to 4.3, at which point the system is in equilibrium (no change). Since the hysteresis effect was extremely pronounced at the low inlet pressure (225 psig) for the first exiting position, the second exiting method was tentatively selected for subsequent testing.

It can be seen from Fig. 25 that pressure recovery is not influenced by the fluid exiting method. As shown in Figs. 27 and 29, the pressure recovery increases slightly (approximately 3%) in a wide range of ΔP_v for the higher inlet pressure. The slight increase is due to a large amount of fluid being available to overcome the frictional drag in the system.

The effect of inlet pressure on the overall pressure ratio for the two exiting positions can be seen in Figs. 26 and 28. The increase in the inlet total pressure, P_{t_i} , tends to minimize the hysteresis effect and increase the overall pressure ratio. The maximum overall pressure ratio for the first and second exiting methods, at an inlet pressure of 300 psig, was 13.35 and 14.50, respectively. The decrease in the hysteresis effect at the higher inlet pressure tends to indicate that hysteresis is primarily due to insufficient fluid within the chamber, which results in fluid attachment and/or detachment on the chambers internal walls. It thus appears that the fluid attachment (or detachment) causes the flow pattern to change in such a manner to cause the region of secondary flow to shift in an axial direction.

Since the maximum overall pressure ratio was higher (for the 300 psig inlet total pressure) for the second exiting position, the pressure recovery was not influenced

GAM/ME/64-14

by the exiting position, and the hysteresis effect was less for the second exiting position (for $P_{7t} = 225$ psig) this exiting position was selected for all subsequent testing.

Inlet Geometry Modifications. The effect of the inlet geometry modifications on the overall pressure ratio and pressure recovery are shown in Figs. 30 and 31, respectively. The curves are for an increasing exit venturi differential pressure with a chamber total inlet pressure of 225 psig. The detail graphical data showing the hysteresis effect and the 300 psig chamber total pressure curves can be found in Appendix B. Neither the hysteresis effect nor the 300 psig curves are shown in the results because the trends are essentially the same as described in the section "Chamber Insert Location."

All inlet geometry modifications except the curve for nozzle ring lip completely removed are shown in Figs. 30 and 31. (See Fig. 11 for inlet geometry modifications). The results of the above modifications were not plotted on Figs. 30 and 31 to avoid any additional obscurement of the curves. The nozzle ring lip completely removed curve is approximately half way between the nozzle ring lip half removed and the nozzle ring taper increased curves.

The first four modifications of the inlet geometry led to an increase in the overall pressure ratio and pres-

GAM/ME/64-14

sure recovery in the range of the exit venturi used in testing. The maximum overall pressure ratio increased from 8.20 to 13.85 while the pressure recovery increased from approximately 0.322 to 0.392. The increase of the pressure ratios is due to minimizing the wetted-area at small radii and to decreasing the nozzle injection losses by increasing the nozzle taper. Minimizing the wetted area at small radii increases the pressure ratios because the power losses due to friction in a free vortex are inversely proportional to the cube of the radius. Decreasing the nozzle injection losses primarily allowed a higher mass flow rate which in turn tended to raise the pressure ratios (see discussion in the section entitled "Chamber Insert Location").

The fifth inlet geometry modification (i.e., exhaust cylinder shortened) decreased the maximum pressure recovery from 0.392 to 0.382 while the maximum overall pressure ratio increased from 13.85 to 14.00. For $\Delta P_v < 5$ and $\Delta P_v > 10$ the fifth modification's overall pressure ratio falls to values below that of the fourth modification (maximum, approximately 14%). The decrease in both pressure ratios tends to indicate secondary flow phenomena occurring in the injection area (i.e., the fluid tends to leave the chamber immediately after injection). Thus, the only advantage the fifth modification has compared

GAM/ME/64-14

to the fourth modification is a higher maximum overall pressure ratio at $\Delta P_v = 0$. If the peak of the overall pressure ratio curve can be shifted from $\Delta P_v = 0$ to some larger value ($\Delta P_v > 2$), the overall performance of the fifth modification should be approximately equal to or greater than the performance for the fourth modification. Since higher mass flow rates into the system (chamber) were expected to cause the shift, and higher mass flow rates were planned for the quantitative portion of this investigation, the fifth inlet geometry modification was used in all subsequent tests.

Diffuser Spacing. Four changes in the diffuser spacing were made to determine the spacing that would give the highest possible overall pressure ratio and a reasonable value of pressure recovery. The pressure recovery becomes secondary in importance because an increase in the pressure recovery generally tends to decrease the overall pressure ratio if the diffuser spacing is properly varied. Since the overall pressure ratio indicates the magnitude of the rotational velocity (i.e., the higher the overall pressure ratio the higher the rotational velocity), and since a high rotational is required for sub-micron particle separation, the overall pressure ratio becomes the deciding parameter in the experimental analysis to determine the optimum diffuser spacing. However, under

GAM/ME/64-14

actual operating conditions it may be possible to increase the pressure recovery and thereby lower the overall pressure ratio if a lower rotational velocity can efficiently separate the particles from the fluid. Under these conditions the conservation of fluid energy becomes equally important as the rotational velocity. Thus, under actual operating conditions the optimum spacing depends on the size, type, and density of the particles.

The four diffuser spacings tested were 1/8, 1/16, 1/32, and 1/64 in. The results of the testing are shown in Figs. 32 and 33. The curves are for an increasing exit venturi differential pressure and a chamber inlet total pressure of 225 psig.

The maximum overall pressure ratio was approximately 14.50 for a 1/16 in diffuser spacing. For $\Delta P_v < 6$ psi, the 1/16 in spacing gave the highest overall pressure ratio while for $\Delta P_v > 6$ psi, a 1/32 in spacing gave the highest overall pressure ratio. The change from the 1/16 in to 1/32 in spacing tends to indicate that the chamber volume, exhaust mass flow rate, and diffuser spacing are related to the highest overall pressure ratio. The exact relationship between these variables was not determined in this investigation because a trial and error procedure could quickly determine the diffuser spacing which gives the highest overall pressure ratio. Thus, Fig. 32 shows that

diffuser spacing must be gradually decreased as the exit mass flow rate is increased to obtain the highest possible overall pressure ratio. The pressure recovery for the four diffuser spacings is shown in Fig. 33.

In general, if the diffuser spacing is decreased from the optimum position (highest possible overall pressure ratio), the pressure recovery increases while the overall pressure ratio decreases (See Figs 32 and 33). Decreasing the spacing from the optimum position is equivalent to choking the flow in the chamber (insufficient exhaust area). If the spacing is increased beyond the optimum position, both pressure ratios decrease. The decrease of both pressure ratios tends to indicate secondary flow occurring near the injection area.

Radial Diffusers. All previous tests, to this point, were made using bleed diffusers. In this series, blank diffusers were tested to determine if the pressure ratios produced were comparable to those produced with the use of bleed diffusers. The diffuser spacing for the blank diffusers was varied until the highest overall pressure ratio was obtained. The results comparing the blank and bleed diffusers are shown in Figs. 34 and 35. The curves are for an increasing exit venturi differential pressure and a chamber inlet total pressure of 225 psig.

The trends of the blank diffusers are similar to the trends previously described in the result section entitled "Diffuser Spacing" for the bleed diffusers. The maximum overall pressure ratio for the blank and bleed diffusers was approximately 7.50 and 14.50, respectively. The maximum pressure recovery was approximately 0.400 for the bleed diffusers and 0.370 for the blank diffusers. The highest pressure ratios for the bleed diffuser remained substantially higher over the entire range of the exit venturi used in testing (See Figs. 34 and 35). Since the use of the blank diffusers resulted in a substantial reduction in both pressure ratios, the bleed diffusers were once again used on all subsequent tests.

The reduction in the pressure ratios is probably due to the formation of a back flow into the chamber from the diffusers face (i.e., the flow travels from the center of the diffuser face in an axial direction toward the geometric center of the center disk flange, at which point, the flow turns 180° and travels in the direction of the exhaust). The formation of the back flow increases the center axial pressure, $P_{t,c}$, and possibly allows secondary flow to occur in the injection region. The increase in the center axial pressure decreases the overall pressure ratio while the secondary flow decreases the pressure recovery.

The back flow could be caused by the tendency of the air to flow from a region of high to low pressure. The bleed diffuser, which allows a portion of the exhausting gas to leave the chamber in an axial direction, minimizes the back flow tendency and thus the higher pressure ratios.

Radial Probing into the Chamber. In all tests made using the stainless steel probe, there was no observed loss or change in the pressure ratios after the removal of the probe. Thus, if extreme turbulence is introduced into the chamber during actual particle separation operation, the chamber will fully recover after the removal of the turbulence inducer. Since the system fully and instantaneously recovered (no noticable time lag) in all tests, the data representing the probings is not presented.

Quantitative Analysis

The results of the qualitative testing indicated higher pressure ratios could be obtained by increasing the mass flow rate into the chamber. They further indicated that the diffuser spacing had to be adjusted for different inlet mass flow rates to obtain the highest overall pressure ratio. Thus, in the quantitative analysis, the mass flow rate into the chamber was increased by changing the nozzle size, and, at the same time, the bleed

diffusers were adjusted for the highest overall pressure ratio. The results of the quantitative investigation show that hysteresis completely disappeared with the use of higher mass flow rates and, the injection nozzles were not choked (sonic) in all tests (see the quantitative graphical data curves for the inlet mass flow rates in Appendix B). Since increasing the chamber inlet pressure increased the pressure ratios in a manner previously discussed, they are not discussed in the quantitative analysis for the first generation swirl chamber. The detail graphical data curve for the higher inlet pressure (300 psig) can be found in Appendix B.

Nozzle Diameter Changes. The test results for the 3/32 in and 1/8 in nozzles are shown in Figs. 36 and 37. The curves shown in the above mentioned figures are for a chamber inlet pressure of 225 psig and increasing or decreasing exit mass flow rates (no hysteresis). They represent the maximum overall pressure ratios that can be obtained by varying the diffuser spacing for the 3/32 in and 1/8 in nozzles.

The maximum overall pressure ratios for the 3/32 in and 1/8 in nozzles were approximately 23.10 and 15.90, respectively. They occurred at mass flow ratios, \dot{m}_e/\dot{m}_i , of approximately 0.32 for the 3/32 in nozzles and at 0.48 for the 1/8 in nozzles. The shifting of the max-

imum overall pressure ratio peak, for higher inlet mass flow rates, is as expected as mentioned in the qualitative analysis. The decrease in the maximum overall pressure ratio is possibly due to a weaker free vortex inside the chamber (i.e., a lower rotational velocity). It appears that the weaker vortex is primarily caused by choking of the fluid inside the chamber because of insufficient exit and exhaust areas. Thus, if the maximum overall pressure ratio is desired for a particular chamber, the nozzle hole size must be matched to the geometric dimensions of the chamber.

Under conditions of insufficient chamber volume, exit and exhaust areas, the maximum pressure recovery increases as the maximum overall pressure ratio decreases (for two different nozzle sizes in identical chambers). This is verified by Fig. 37 where the maximum pressure recovery is approximately 0.82 for the 1/8 in nozzles and 0.68 for the 3/32 in nozzles.

Since the pressure recovery is above 50% for mass flow ratios less than 0.50, it was arbitrarily decided to restrict the optimization in such a manner so as to increase the overall pressure ratio while maintaining the pressure recovery above 50% for $\dot{m}_e/\dot{m}_i = 0.50$. Thus, all subsequent tests on the first generation chamber were performed primarily to determine the effect on the

the overall pressure ratio. As a result, the 3/32 in nozzles were incorporated in the chambers for subsequent tests.

Single Cell Swirl Chamber. The results for the first generation single cell chamber show that the frictional losses, due to an additional solid boundary, reduce the maximum overall pressure ratio to a value far below those obtained for the dual cell chamber (approximately 65% reduction). The graphical comparison of the performance parameters for the dual and single cell chamber are shown in Figs. 38 and 39. The maximum pressure ratios for the single cell chamber were found to be 7.70 and 0.580, while the dual cell chamber maximum pressure ratios were 23.10 and 0.688. Thus, if a given overall pressure ratio is required for particle separation, the dual cell swirl chamber should be used to sustain smaller frictional losses (i.e., conserve fluid energy).

Chamber Insert Size. The effect the variation in chamber insert length has on the performance parameters is shown in Figs. 40 and 41. For these figures it can be seen that as the chamber insert length is increased, both pressure ratios decrease. The maximum overall pressure ratio for the g, h, and i inserts (see Appendix B for explanation of letters) were found to be 23.10, 9.60, and 8.30, respectively. The maximum pressure recovery for the g,

h, and i inserts were found to be 0.682, 0.580, and 0.550, respectively. The reduction of the pressure ratios is due to the increase in wetted surface area and chamber volume. If longer chamber lengths are needed to increase particle residence time within the chamber, greater pressure ratios can be obtained by increasing the inlet mass flow rate and adjusting the exit and exhaust areas (to eliminate the possibility of choking).

Second Generation Chamber. The first set of results obtained using the second generation chamber are shown in Figs. 42 and 43. The results indicate significant increases in both pressure ratios compared to the highest values obtained with the first generation chamber. The maximum pressure recovery and overall pressure ratio increased approximately 22% and 30%, respectively (compare Figs. 42 and 43 with Figs. 40 and 41, respectively). The values of the maximum overall pressure ratio and pressure recovery for the second generation chamber having an inlet pressure of 225 psig are 30.00 and 0.840, respectively. Since Fig. 42 is the result of using a 9/64 in diameter center pressure tap (P_{it}) the above overall pressure ratio is extremely conservative (See Fig. 44). The large increases in both pressure ratios for the second generation chamber are merely the experimental verification of the discussion in the section entitled "Method of Injection".

Flow Visualization. Still photographs obtained from high speed motion picture film (7,000 frames/sec) taken at inlet pressures of 100, 200, and 300 psig are shown in Figs. 45-47, respectively. The flow visualization section of this investigation consisted in the use of high speed photography, as well as visual inspection of the flow patterns. Flow visualization was made possible by injecting talcum powder into the gas flow in a single cell visual chamber. The high speed motion pictures were then taken, and the resulting film was studied. The results of these studies showed:

1. The flow is a spiral vortex.
2. The velocity of the secondary flow pattern increased with increasing chamber inlet pressure. Tests were made at 100, 200, and 300 psig. It was easily seen from the motion pictures that as the inlet pressure was increased (from 100 to 300 psig) the rotational velocity of the flow increased.
3. As the inlet pressure is increased (from 100 to 300 psig) the particles are able to penetrate to a smaller radius; however, it was observed that although the particles penetrated to a smaller radius they were quickly centrifuged outward. For the 100 psig inlet

pressure test the particles did not penetrate to as small a radius as for the 200 psig or 300 psig tests, but they remained at some larger radius for a longer period of time before being centrifuged outward.

4. No particles could penetrate beyond a certain void region. This was observed in the motion picture film, and can also be seen in Figs. 45, 46, and 47.

At inlet pressures of 100, 200, and 300 psig the respective diameters of the void region were 0.24 in, 0.22 in, and 0.20 in (± 0.005 in). These distances were measured during observation of individual frames of the motion picture film. The decreases mentioned above (3) cannot be inferred in the case of the dual cell swirl chamber where a solid boundary is not present. When a solid boundary is not present, frictional losses are a minimum due to the symmetrical flow pattern. The particles in this region retain high angular velocities, and it is likely that centrifugal forces are greater than those created by the high overall pressure ratio. If this is the case then the higher the inlet pressure, the larger the minimum radius of particle penetration. When a solid boundary is present the boundary layer buildup and frictional losses tend to slow the particles. Consequently, the overall pressure ratio becomes the dominant

force rather than the centrifugal force. This being so, the higher the inlet pressure, the smaller the radius of particle penetration.

During the flow visualization test runs, exhaust gas samples were collected and examined under a microscope. Limitations of the available microscopes prevented an exact measurement of the exhaust particle size, but indicated they were of a sub-micron nature. The original particles (talcum) were reduced in size due to friction within the chamber.

Axial Pressure Probes. During the course of testing attempts were made to obtain axial static and total pressure profiles in the first and second generation chambers; however, no results were obtained since all probes failed before a total inlet pressure of 100 psig was achieved in the chamber. Failure was of two types:

1. Extreme probe vibration, making it impossible to obtain readings of any value.
2. Probe structural damage due to its extreme vibration.

VII. Conclusions

The results of this investigation indicate some of the variables that influence the effectiveness of sub-micron particle separation in a high pressure swirl chamber. Also, they demonstrate that the swirl chambers tested are capable of developing high overall pressure ratios needed for sub-micron particle separation.

The geometrical modifications of the first generation chamber increased the overall pressure ratio and pressure recovery from approximately 10 and 0.35 to 30 and 0.60. Tests on the second generation chamber resulted in values of overall pressure ratio and pressure recovery of approximately 35 and 0.85.

The specific conclusions of this experimental investigation are:

1. The bleed diffusers substantially increase the overall pressure ratio and pressure recovery when compared to the blank diffusers.
2. The diffuser spacing must be varied, for each inlet condition, to obtain optimum chamber performance.
3. Minimizing the wetted-area at small radii increases the pressure ratios.
4. The nozzle hole diameter must be matched to

the chamber volume for optimum performance.

5. The dual cell chamber is superior, from a performance standpoint, to the single cell chamber.
6. From the results of the flow visualization studies it is apparent that in the range of testing, 0 psig to 300 psig, the rotational velocity increased with an increase in overall pressure ratio.
7. From the exhaust particle samples obtained during testing of the visual chamber, it appears that the dual cell swirl chamber is basically capable of separating sub-micron particles from a gas flow with a high mass flow rate (i.e., one lbm /sec).

VIII. Recommendations

The recommendations for future testing of the high pressure swirl chambers are divided into three sections as follows: (1.) Additional chamber modification, (2.) Flow pattern mapping, (3.) Separation capability of the chambers.

Additional Chamber Modification

The results of the investigation indicate that the exhaust cylinder ID should be varied so that optimum chamber performance can be obtained over the entire range of the mass flow ratio. As shown in the results, the curves of overall pressure ratio and pressure recovery tend to increase or decrease rapidly at the high and low mass flow ratios ($0.35 \geq \dot{m}_e / \dot{m}_i \geq 0.45$). By varying the exhaust cylinder ID, these curves would tend toward the limiting case of constant values for overall pressure ratio and pressure recovery over the entire range of mass flow ratio. For this reason, exhaust cylinder inserts must be fabricated to determine the effect the exhaust area has on the various pressure ratios. Since it is expected that the exhaust inserts must be changed for each particular inlet mass flow rate and mass flow ratio, it would be desirable to fabricate a variable exhaust insert for ease in testing

GAM/ME/64-14

the chambers

Flow Pattern Mapping

To further improve the sub-micron particle separation capability of the swirl chambers it is necessary to determine the exact flow pattern within the device. To assist future investigations, three means of flow pattern mapping are suggested; they are:

1. Axial static pressure probes.
2. Radial static pressure probes.
3. Flow visualization.

The axial static pressure probes must be rigidly supported in tension and measure approximately $3/16$ in ID x $.020$ in ID to insure sufficient strength, and keep the flow disturbance as small as possible. The radial static pressure probes should be inserted through the center disk flange and rigidly supported in tension. The radial probe dimensions should be approximately $1/16$ in ID x 0.010 in ID to minimize flow pattern disturbances.

Glass windows mounted on the periphery of the swirl chambers could be used to trace gross particle movements within the device. The particle movements could be determined through the use of high speed motion pictures or stroboscopic photographic techniques.

Separation Capability of the Chambers

As a means of testing the particle separation capa-

GAM/ME/64-14

bility of the chambers, the following method is suggested:

1. Close exits, and optimize the overall pressure ratio.
2. Inject talcum powder at an axial sub-atmospheric pressure position.
3. Collect exhaust samples on glass slides for microscopic examination to determine the size of the particles that escape from the chamber through the exhaust.

References

1. ASME Research Publication. Fluid Meters, Their Theory and Application (Fourth Edition). New York: ASME, 1937.
2. Babcox and Wilcox Co. Steam, Its Generation and Use. New York: Babcox and Wilcox Co., 1960.
3. Kendall, James M. Jr. Exoerimental Study of a Compressible Viscous Vortex. JPL Technical Report No. 32-290. Pasadena, California: Jet Propulsion Laboratory, 1962.
4. Ragsdale, Robert G. NASA Research on the Hydrodynamics of the Gaseous Vortex Reactor. NASA TN D-288. Washington: National Aeronautics and Space Administration, 1960.

List of Figures

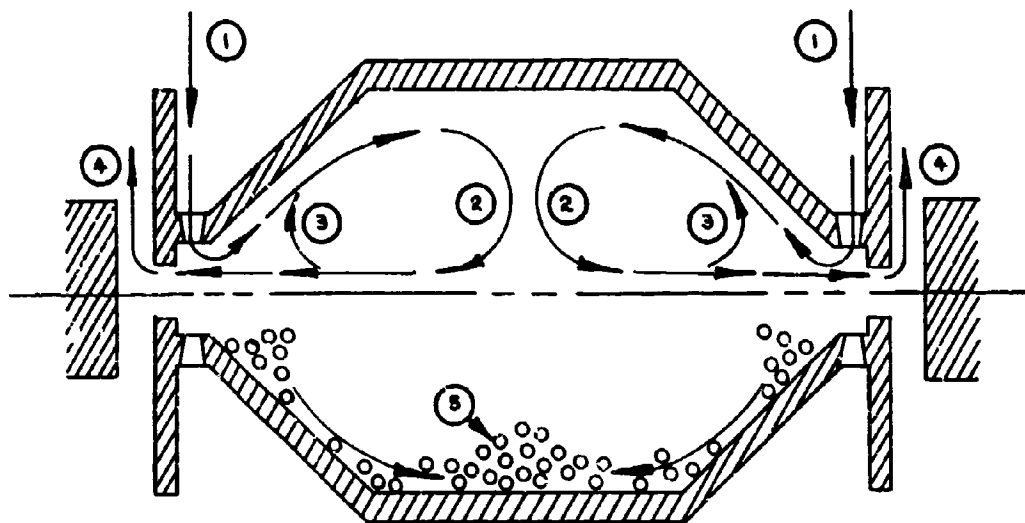
Figure		Page
1	Inner Radius Injection Chamber	55
2	Inserts in First Exiting Position	56
3	Inserts in Second Exiting Position	56
4	Schematic of Pressure and Temperature Taps . . .	57
5	Instrumentation	58
6	Instrumentation and Swirl Chamber	58
7	Schematics of Axial Pressure Probes	59
8	Sketch of Flow Velocities in Two Phase Flow . .	60
9	Outer Radius Injection Chamber	61
10	Flow Diagram of Qualitative Testing Apparatus .	62
11	Inlet Geometry Modifications	63
12	Flow Diagram of Quantitative Testing Apparatus .	64
13	First Generation Single Swirl Chamber	65
14	Nozzle Rings for First Generation Chamber . . .	66
15	Inserts for First Generation Chamber	66
16	First Generation Chamber with g-Insert	67
17	First Generation Chamber with h-Insert	68
18	First Generation Chamber with i-Insert	69
19	Radial Exhaust Diffusers	70
20	Injection Housing for Second Generation Chamber.	70
21	Second Generation Chamber	71
22	First Generation Visual Chamber	72
23	Curve for Venturi Correction Factor	73

Figure		Page
	Qualitative Results--Performance Parameters as a Function of the Exit Venturi Differential Pressure	
24	Effect of Fluid Exiting Position on the Over- all Pressure Ratio	75
25	Effect of Fluid Exiting Position on the Pressure Recovery	76
26	Effect of Inlet Pressure on the Overall Pressure Ratio for the First Fluid Exit- ing Position	77
27	Effect of Inlet Pressure on the Pressure Recovery for the First Fluid Exiting Position	78
28	Effect of Inlet Pressure on the Overall Pressure Ratio for the Second Fluid Exit- ing Position	79
29	Effect of Inlet Pressure on the Pressure Recovery for the Second Fluid Exiting Position	80
30	Effect of Inlet Geometry on the Overall Pressure Ratio	81
31	Effect of Inlet Geometry on the Pressure Recovery	82

Figure		Page
32	Effect of Diffuser Gap Spacing on the Overall Pressure Ratio	83
33	Effect of Diffuser Gap Spacing on the Pressure Recovery	84
34	Overall Pressure Ratio for Blank and Bleed Diffusers.	85
35	Pressure Recovery for Blank and Bleed Diffusers	86
Quantitative Results--Performance Parameters as a Function of the Mass Flow Ratio .		
36	Overall Pressure Ratio for 3/32 in and 1/8 in Nozzle Rings	87
37	Pressure Recovery for 3/32 in and 1/8 in Nozzle Rings	88
38	Overall Pressure Ratio for Single and Dual Cell Chambers	89
39	Pressure Recovery for Single and Dual Cell Chambers	90
40	Overall Pressure Ratio for Three Chamber Inserts	91
41	Pressure Recovery for Three Chamber Inserts	92

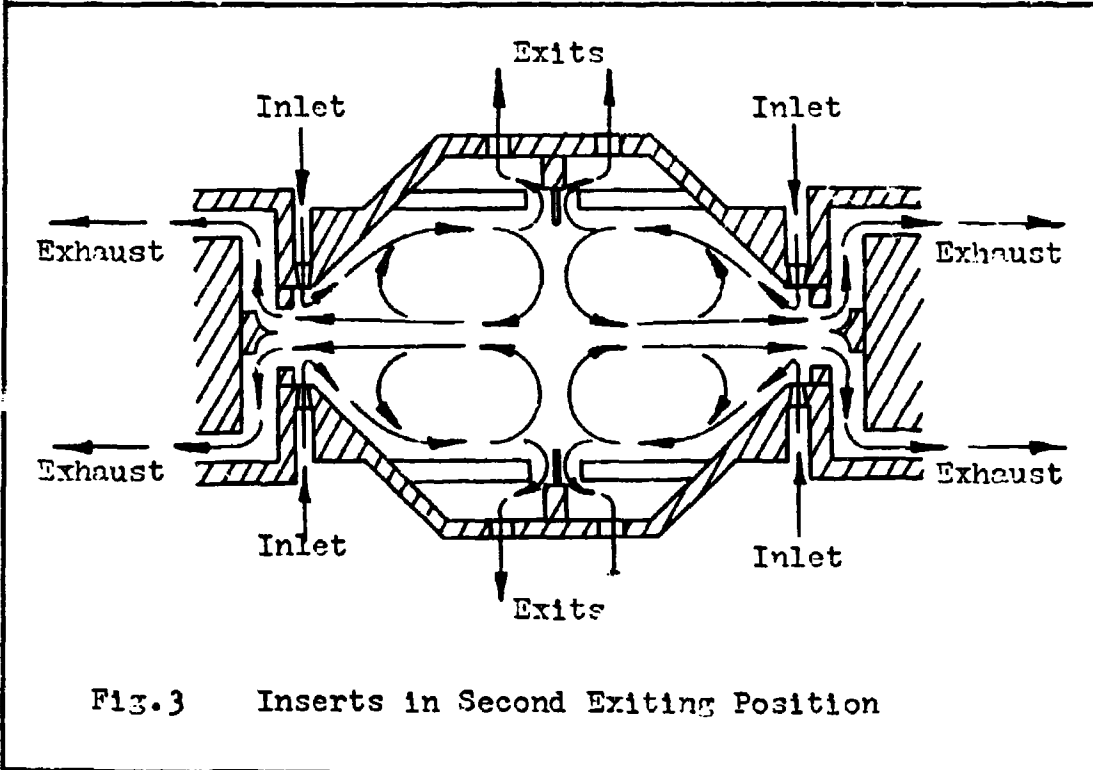
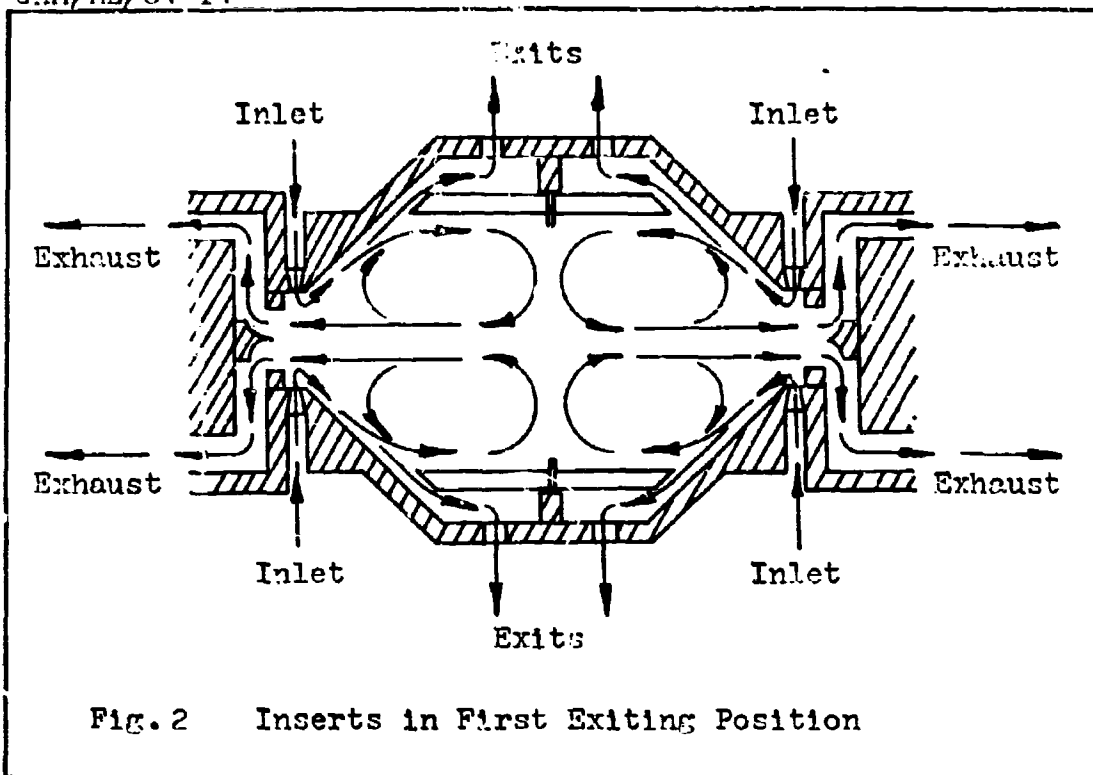
Figure		Page
42	Second Generation Chamber Overall Pressure Ratio for Two Inlet Pressures	93
43	Second Generation Chamber Pressure Recovery for Two Inlet Pressures	94
44	Pressure Ratios for Two Center Pressure Probes	95
45	Flow Pattern for 100 psig Inlet Pressure	96
46	Flow Pattern for 200 psig Inlet Pressure	96
47	Flow Pattern for 300 psig Inlet Pressure	97
 Engineering Drawings		
48	Assembly of First Generation Dual Cell Swirl Chamber	102
49	Assembly of Second Generation Dual Cell Swirl Chamber	103
50	Assembly of Visual Single Cell Swirl Chamber	104
51	Nozzle Ring for First Generation Swirl Chambers	105
52	Multiple Nozzle Housing for Second Generation Chamber	106
53	Cross Section of Blank Diffusers	107
54	Cross Section of Bleed Diffusers	108

Figure		Page
55	Crank Diffuser for Second Generation Swirl Chamber	109
56	First Generation Swirl Chamber with g-Insert	110
57	First Generation Swirl Chamber with h-Insert	111
58	First Generation Swirl Chamber with i-Insert	112
59	Pressure and Temperature Connections for First Generation Chamber	113
60-84	Qualitative Graphical Data	121
85-101	Quantitative Graphical Data	147



- Inlet ----- ①
- Secondary Flow ----- ②
- Recirculating Flow ----- ③
- Exhaust ----- ④
- Particle Flow Near Wall ----- ⑤

Fig. 1 Inner Radius Injection Chamber



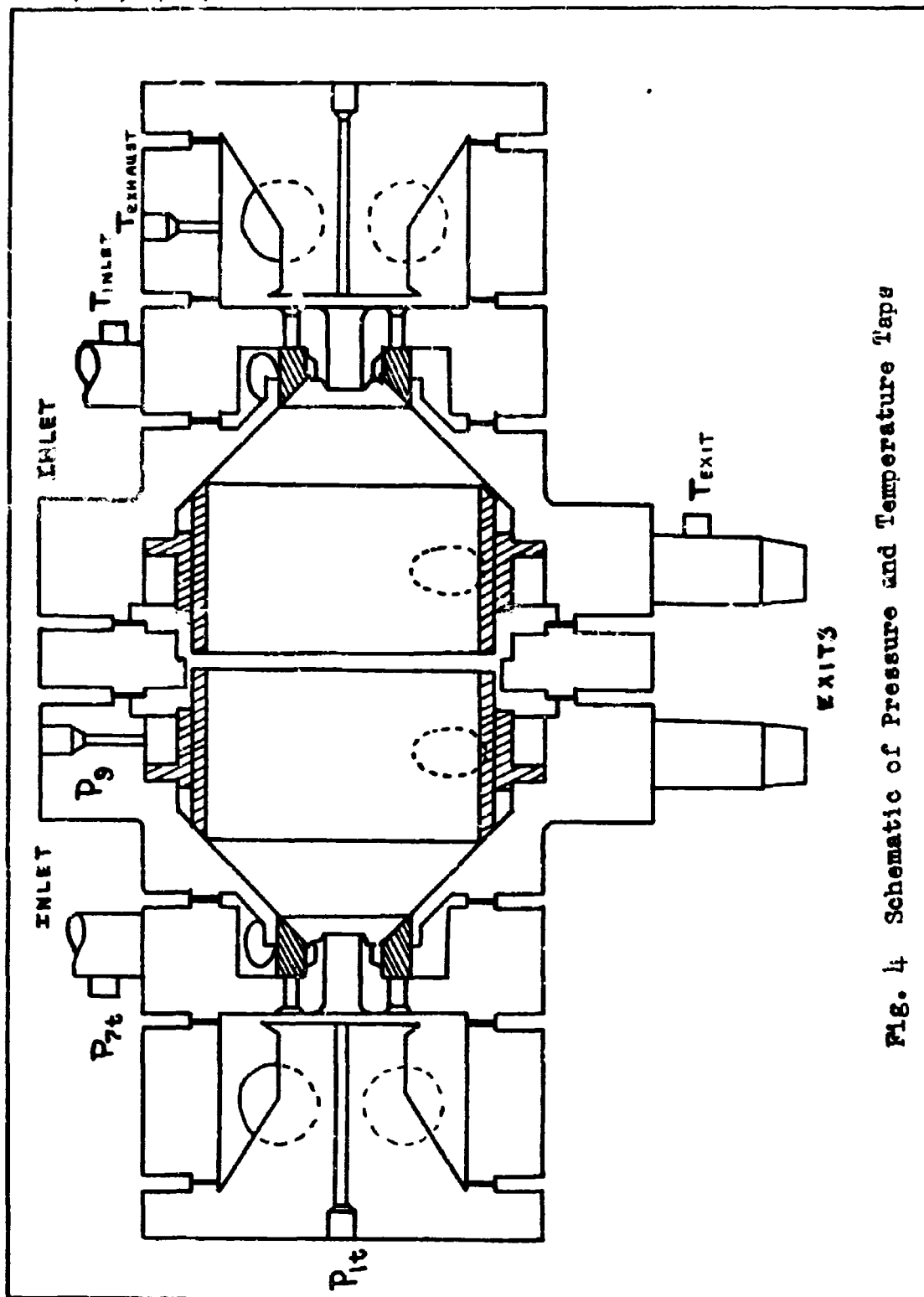


Fig. 4 Schematic of Pressure and Temperature Taps

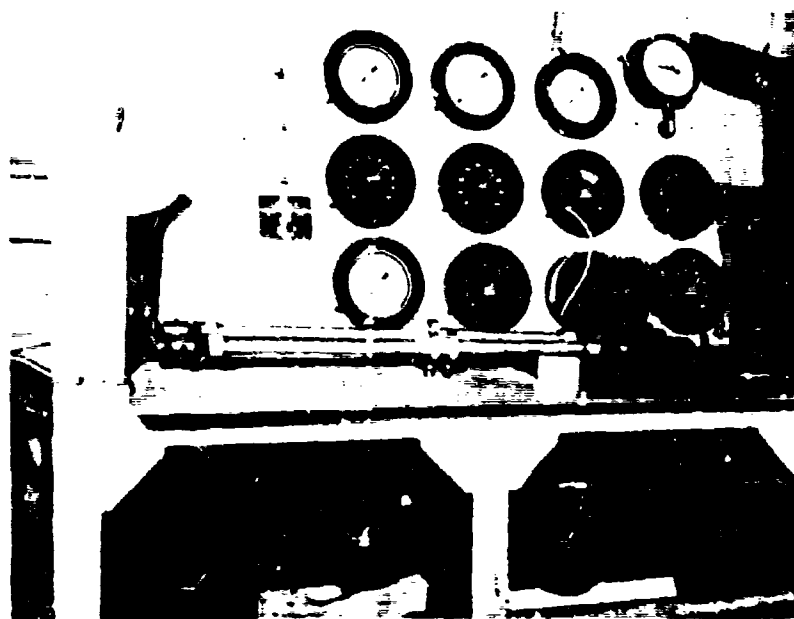


Fig. 5 Instrumentation

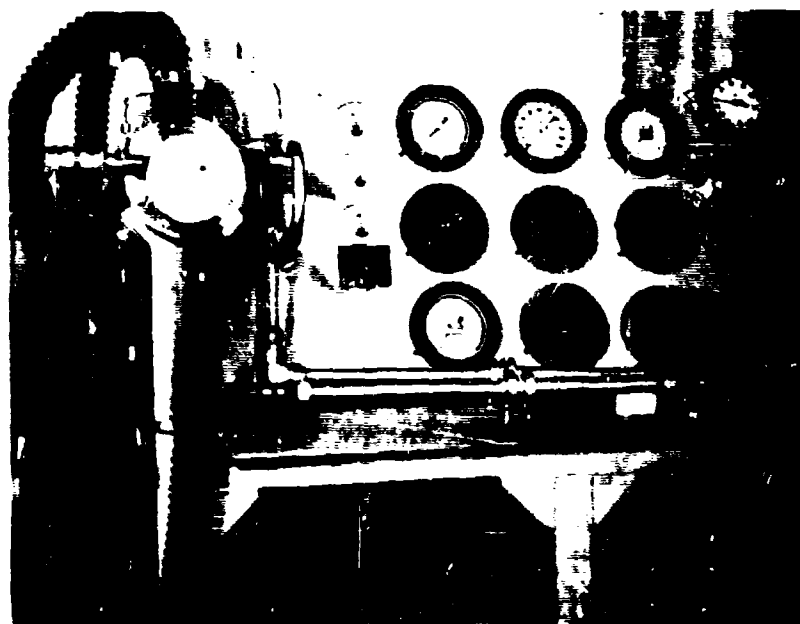
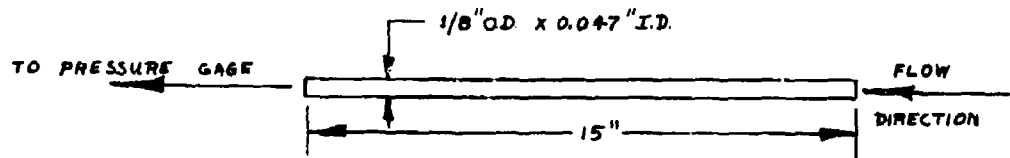
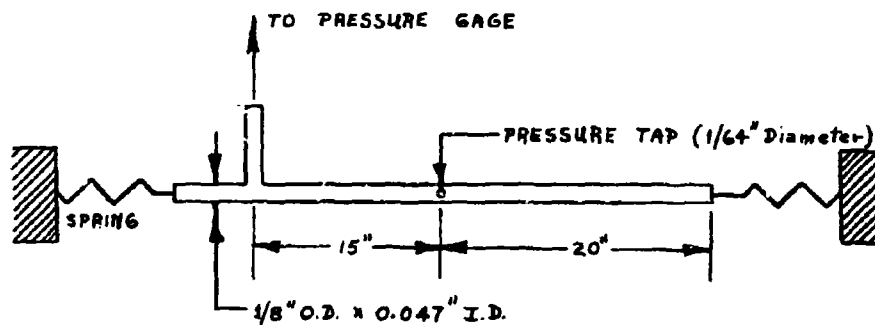


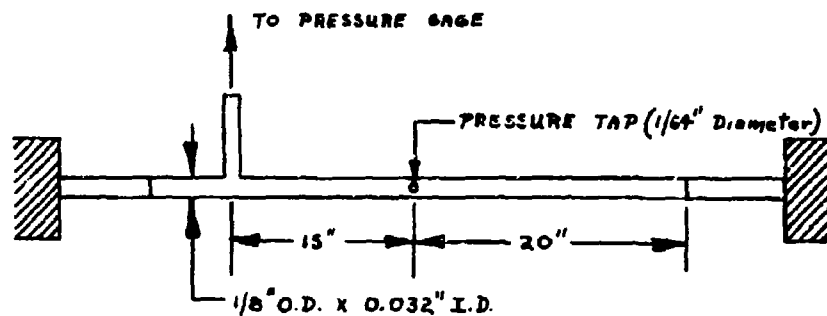
Fig. 6 Instrumentation and Swirl Chamber



Total Pressure Probe

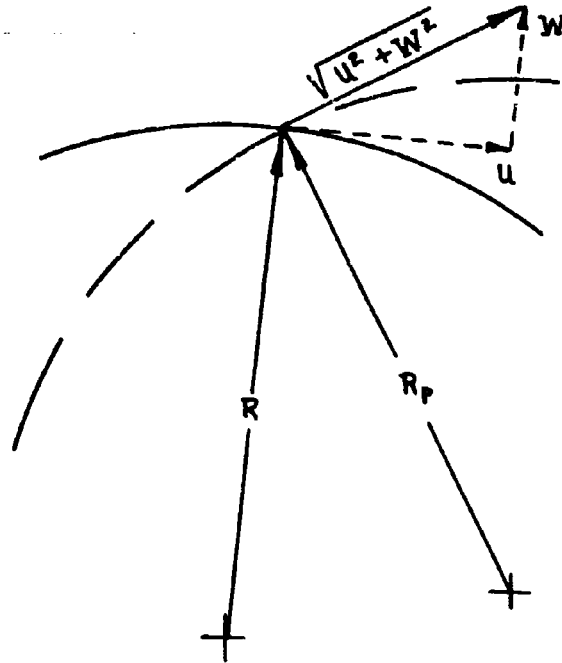


Static Pressure Probe



Static Pressure Probe

Fig. 7 Schematics of Axial Pressure Probes



$\sqrt{u^2 + W^2}$ = Particle Velocity

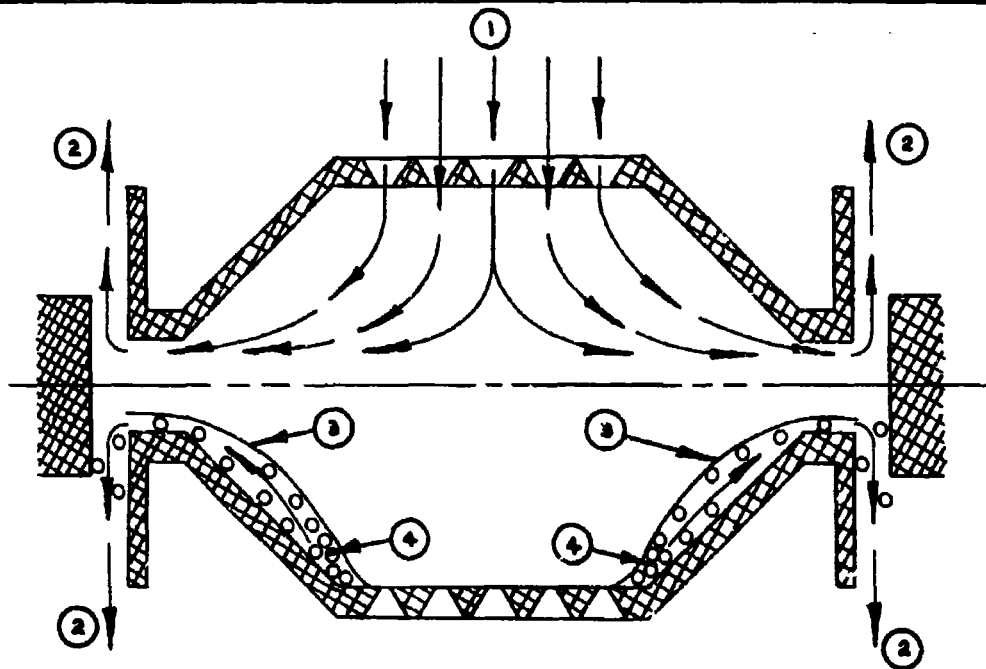
u = Flow Velocity

W = Particle Drift Velocity

R = Radius of Curvature of Gas Flow

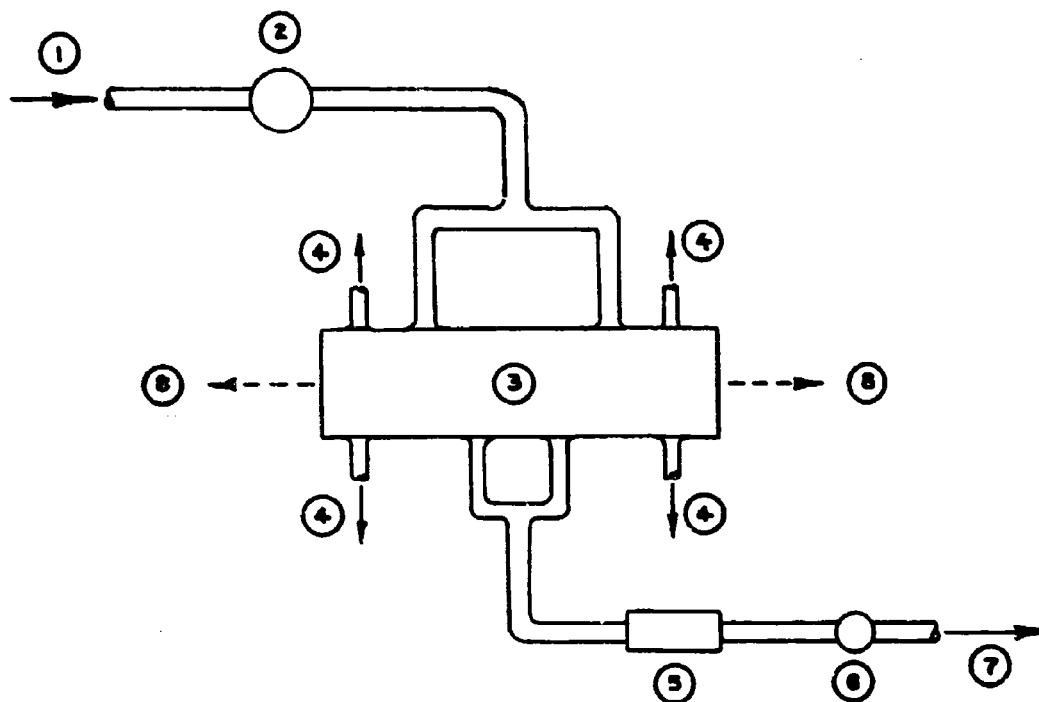
R_p = Radius of Curvature of Particle Flow

Fig. 8 Sketch of Flow Velocities in Two Phase Flow



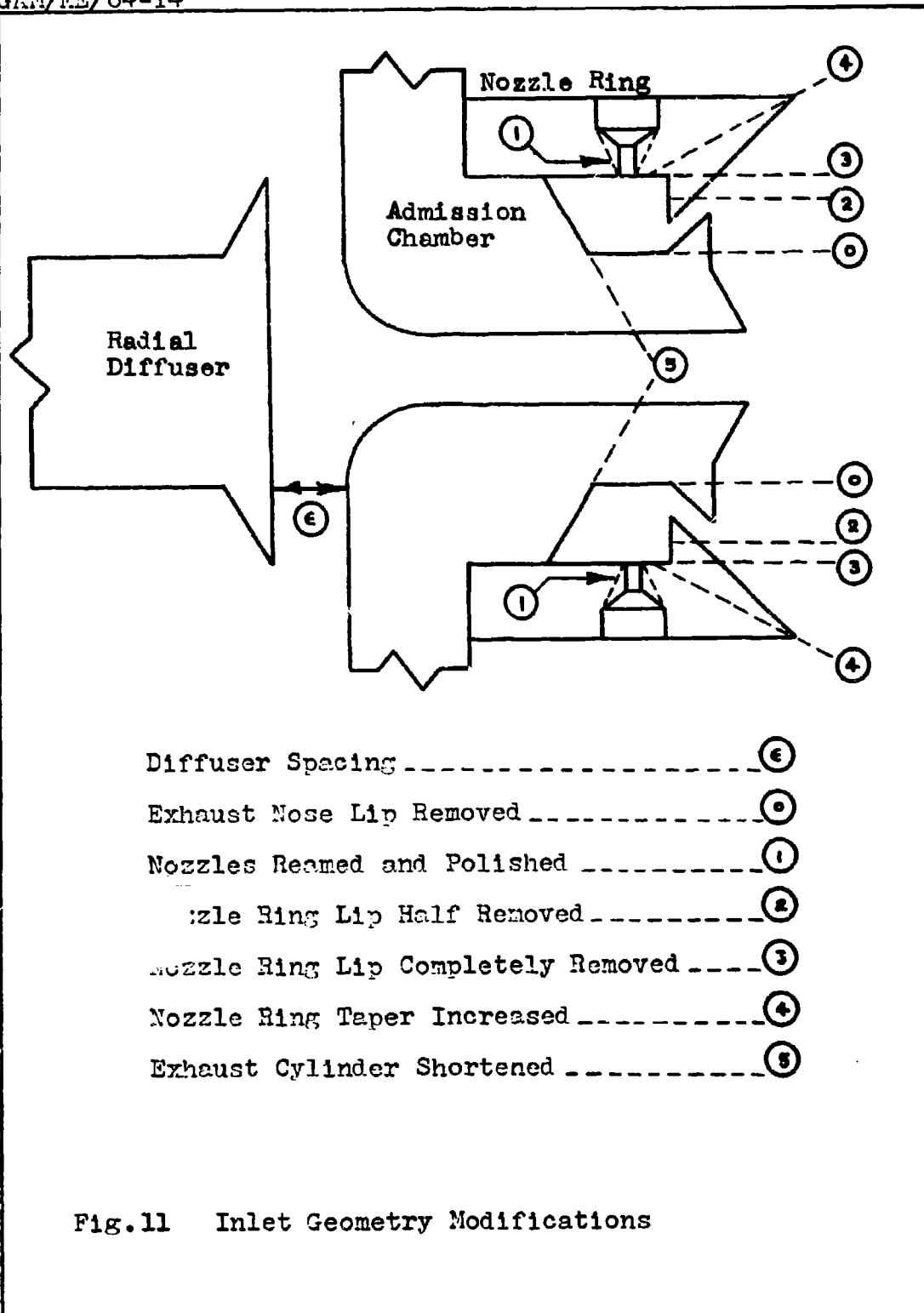
- Inlets ----- (1)
- Exhaust ----- (2)
- Wall Boundary Layer ----- (3)
- Particles Within Boundary Layer ----- (4)

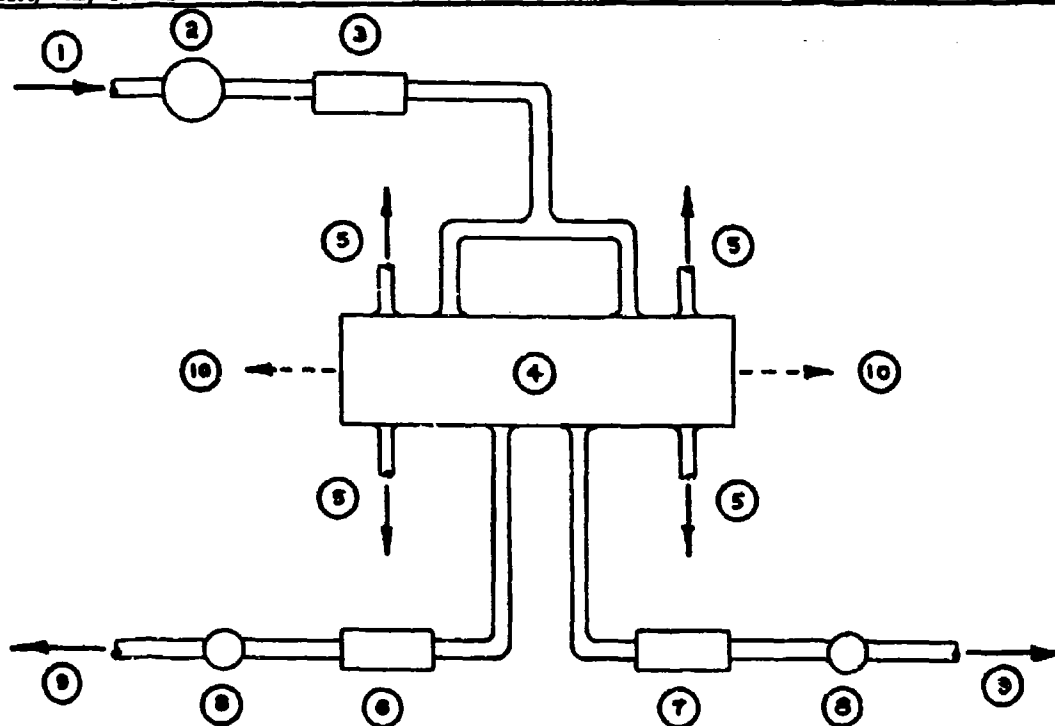
Fig. 9 Outer Radius Injection Chamber



- | | |
|--------------------------------------|---|
| Flow from Tank Farm | ① |
| Pressure Regulator | ② |
| Swirl Chamber | ③ |
| Flow Exhaust | ④ |
| Exit Venturi (0.650" x 0.375") | ⑤ |
| Exit Control Valve | ⑥ |
| Flow Exit | ⑦ |
| Exhaust Thru Bleed Diffuser | ⑧ |

Fig. 10 Flow Diagram of Qualitative Testing Apparatus





- Flow from Tank Farm.....①
- Pressure Regulator.....②
- Inlet Venturi (1.257" x 0.750").....③
- Swirl Chamber.....④
- Flow Exhaust.....⑤
- Left Exit Venturi (0.875" x 0.500").....⑥
- Right Exit Venturi (0.840" x 0.500").....⑦
- Exit Control Valve.....⑧
- Flow Exit.....⑨
- Exhaust Thru Bleed Diffuser.....⑩

Fig. 12 Flow Diagram of Quantitative Testing Apparatus

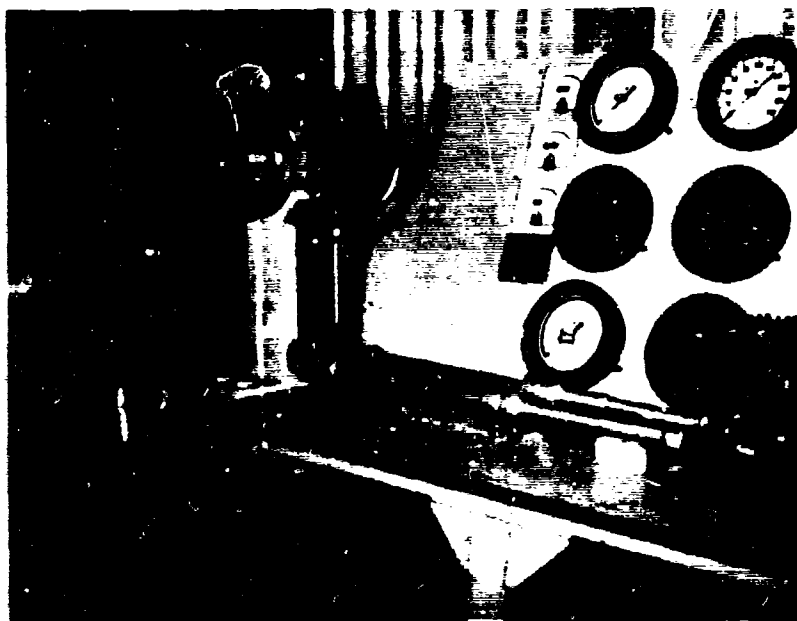


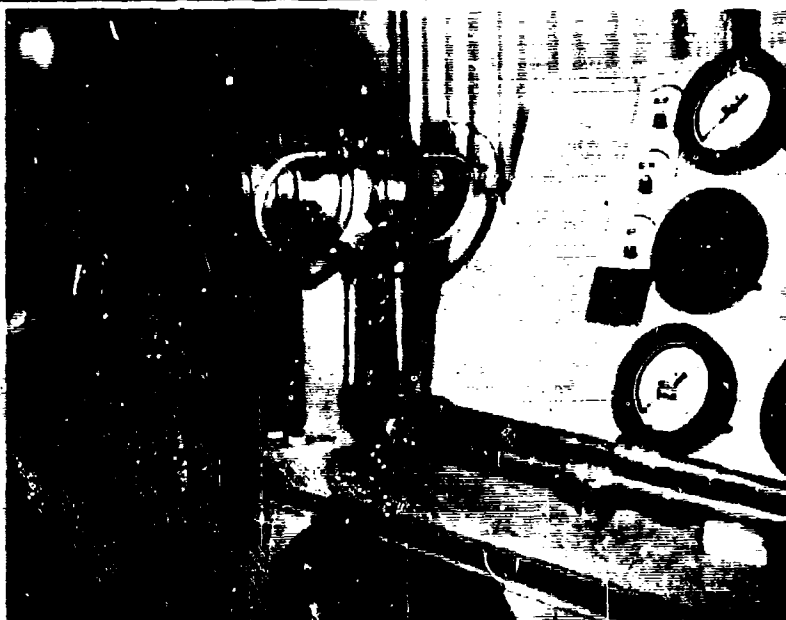
Fig. 13 First Generation Single Swirl Chamber



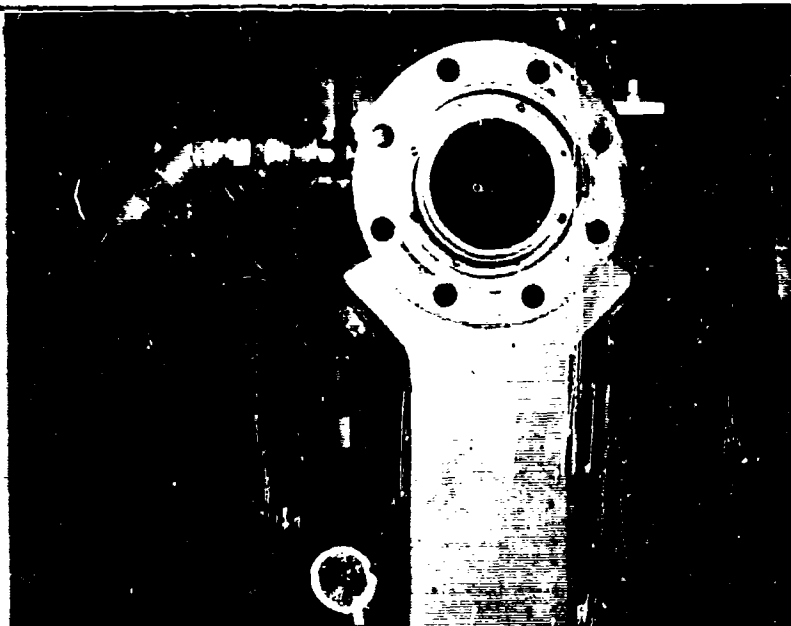
Fig. 14 Nozzle Rings for First Generation Chamber



Fig. 15 Inserts for First Generation Chamber

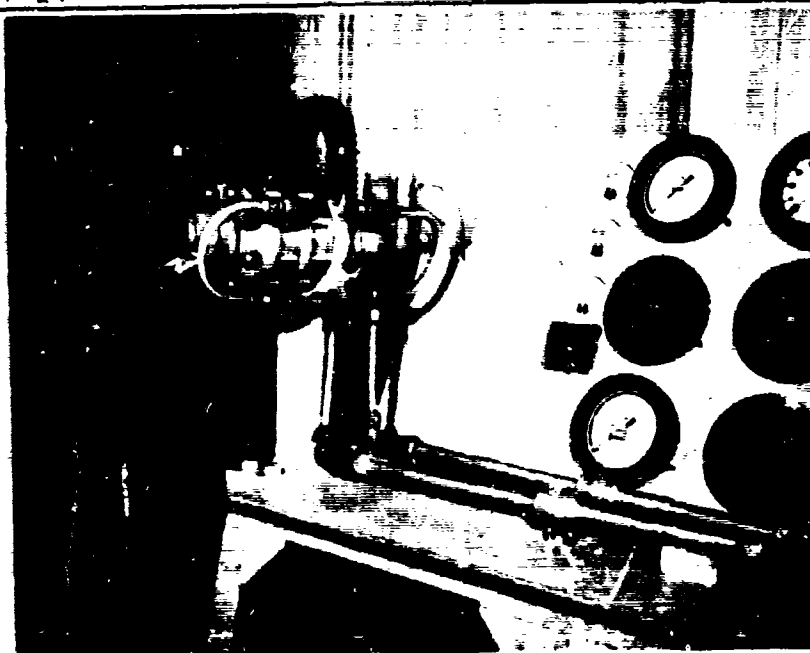


External View



Internal View

Fig. 16 First Generation Chamber With g-Insert

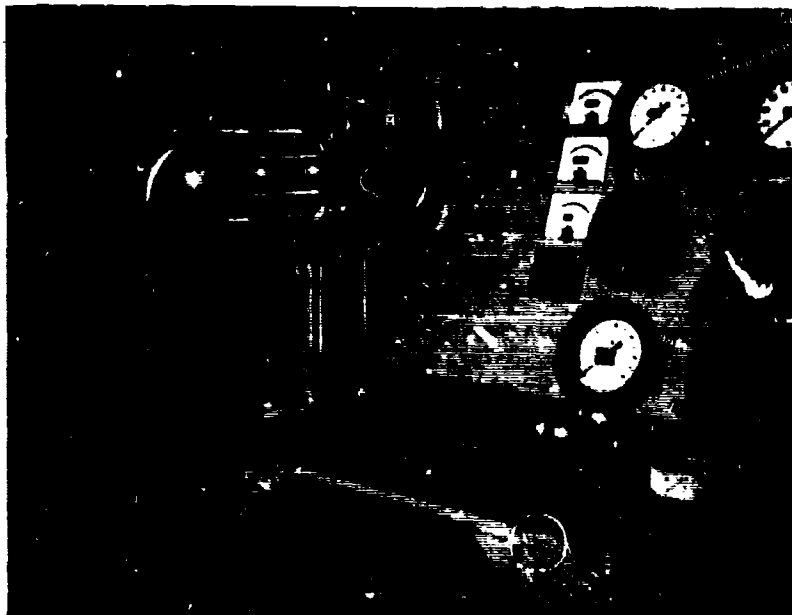


External View

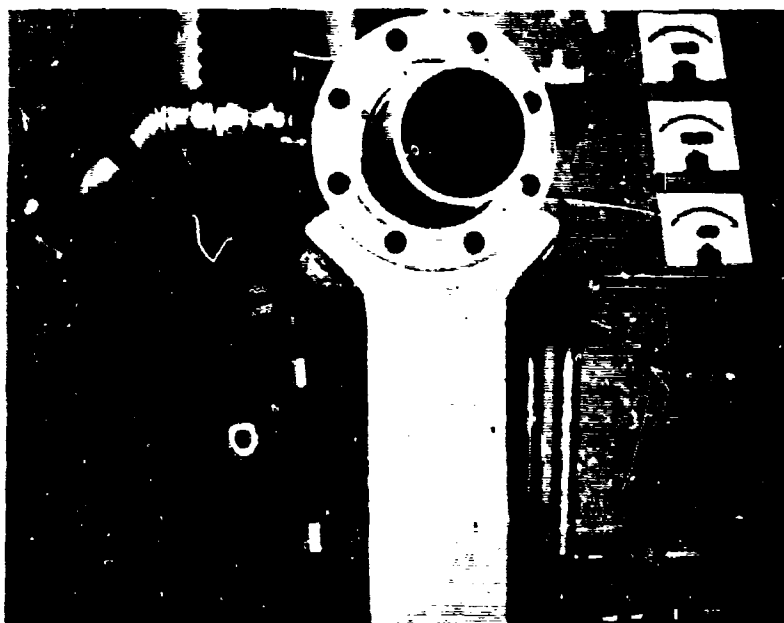


Internal View

Fig. 17 First Generation Chamber With h-Insert



External View



Internal View

Fig.18 First Generation Chamber With 1-Insert

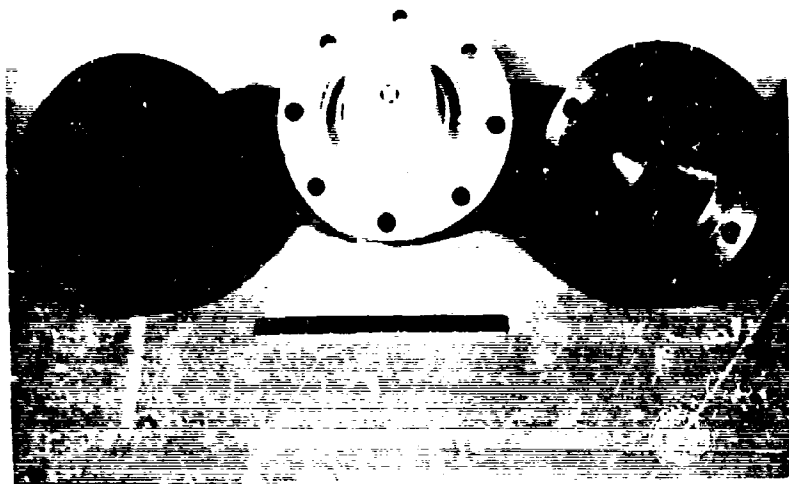


Fig. 19 Radial Exhaust Diffusers

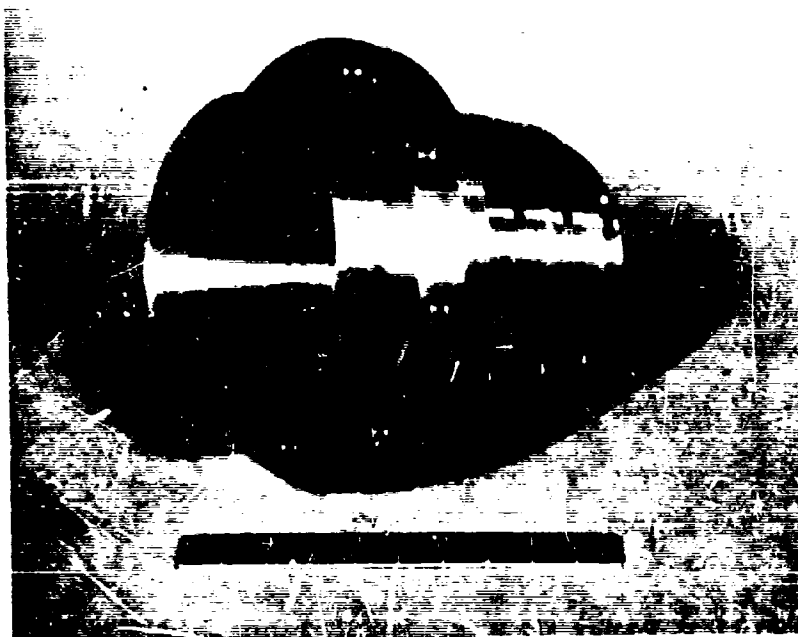
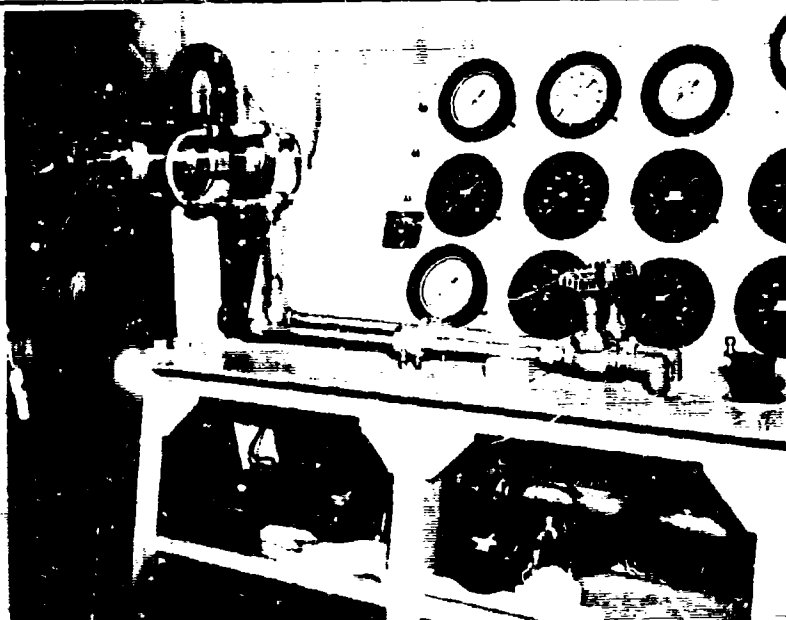


Fig. 20 Injection Housing for Second Generation Chamber

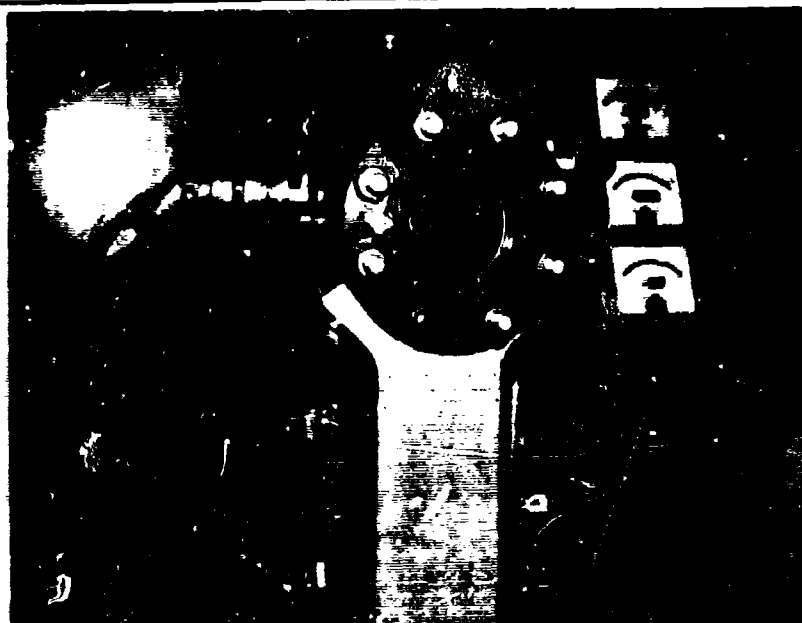


External View

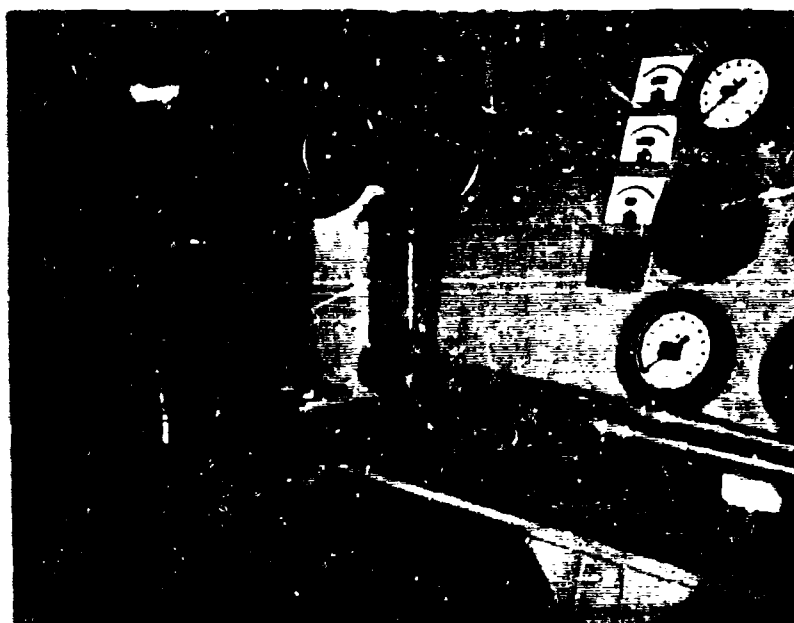


Internal View

Fig.21 Second Generation Chamber



Front View



Side View

Fig. 22 First Generation Visual Chamber

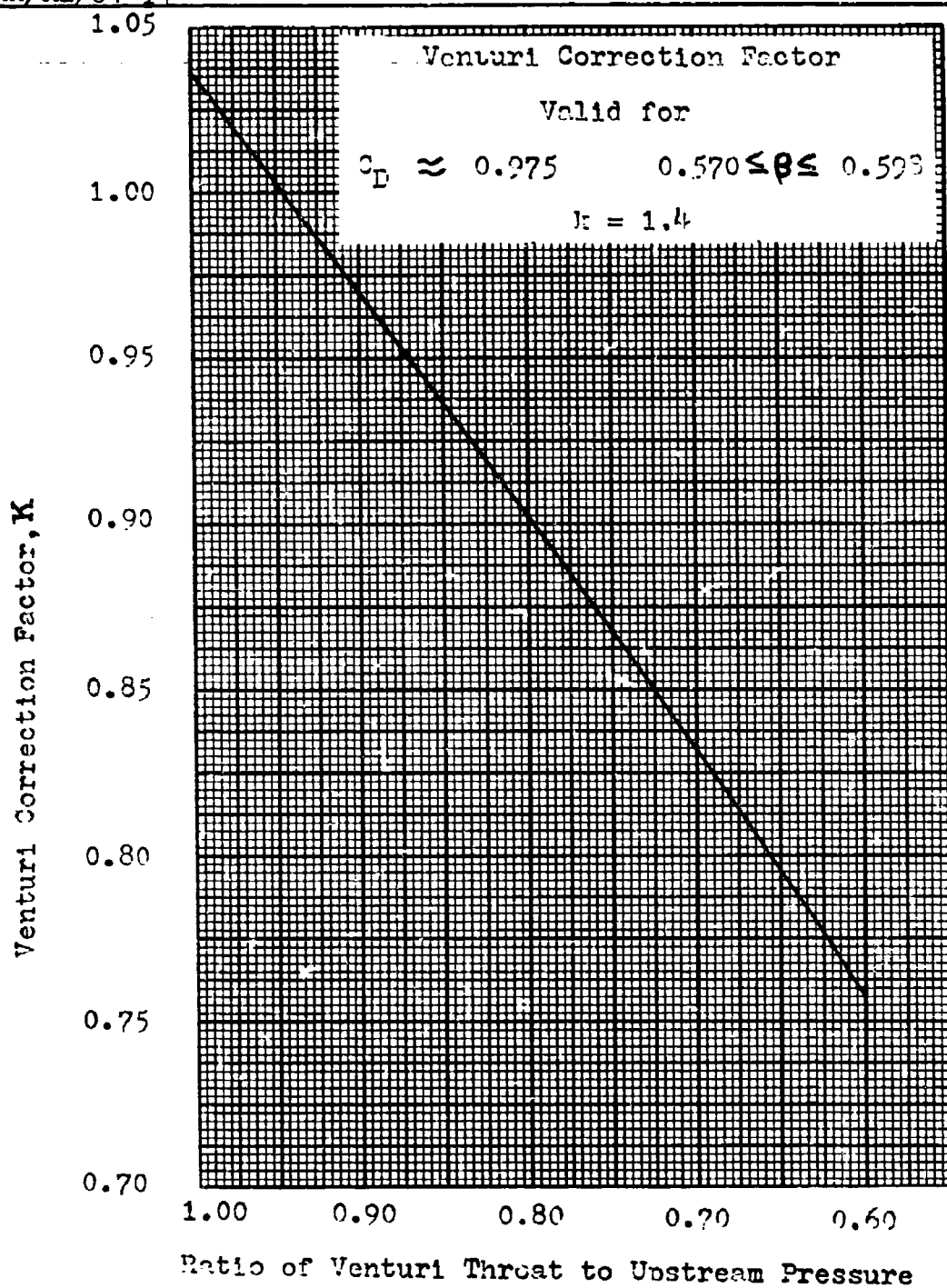


Fig. 23 Correction Factor vs Venturi Pressure Ratio

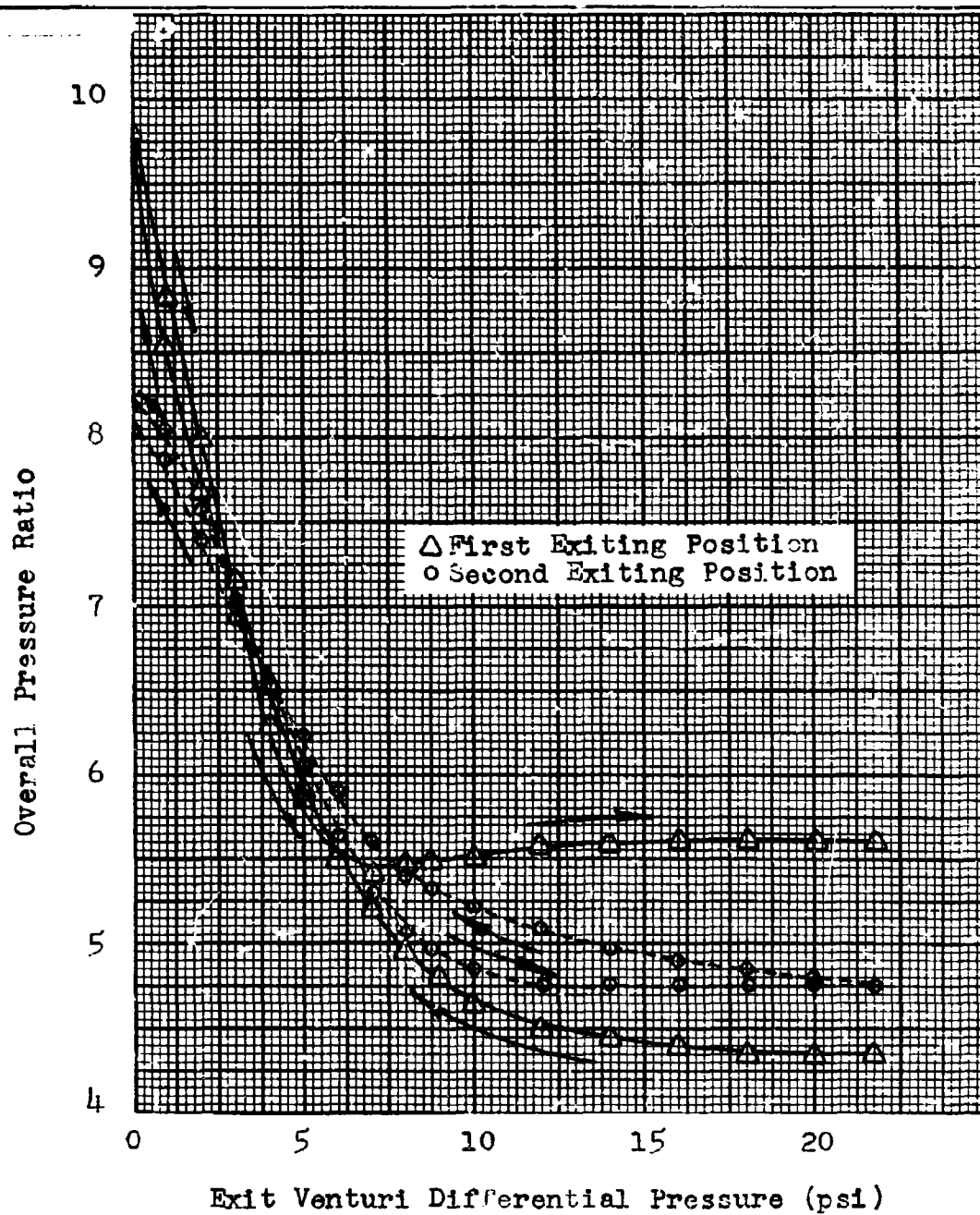


Fig. 24 Effect of Fluid Exiting Position on the Overall Pressure Ratio

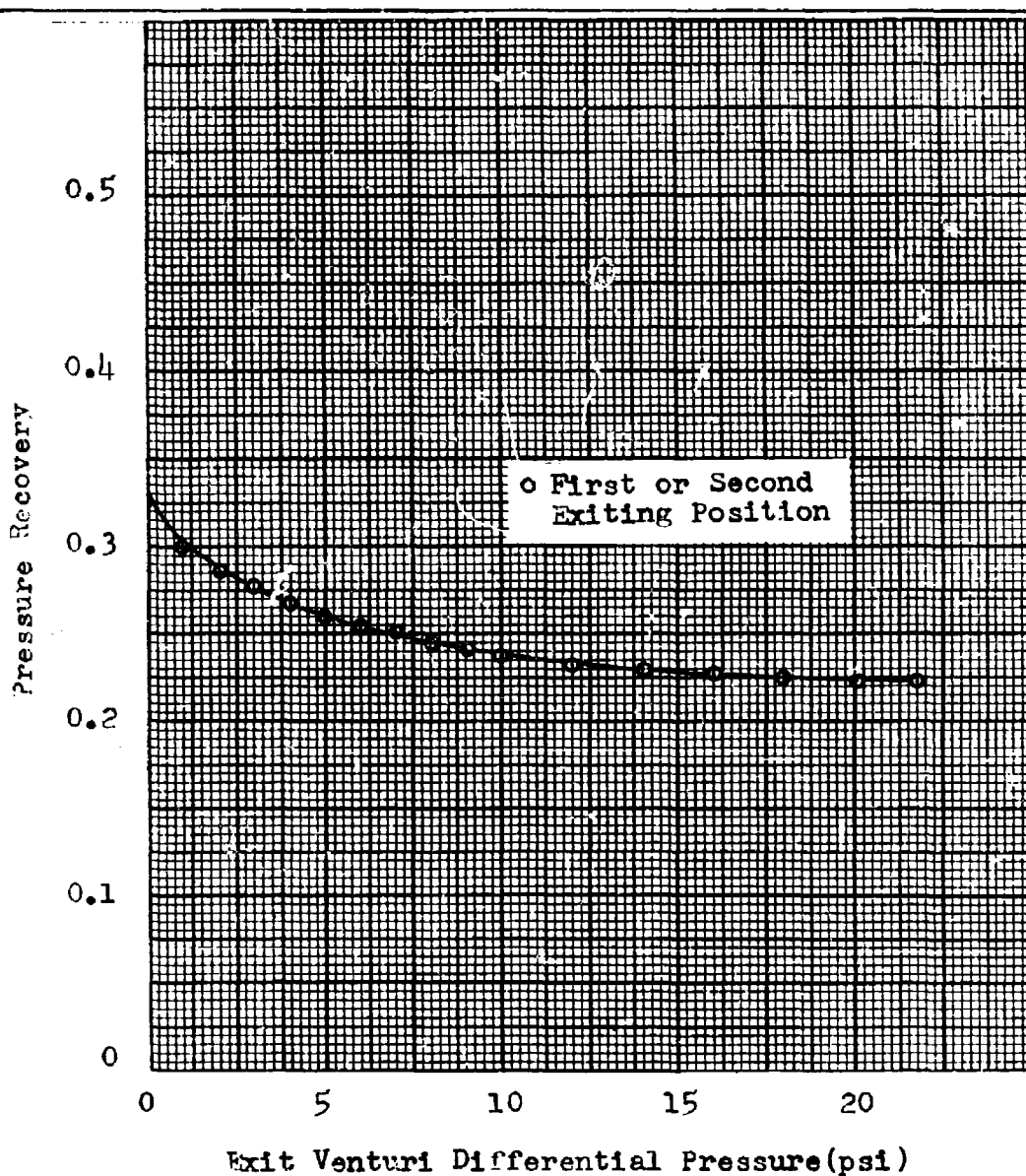


Fig. 25 Effect of Fluid Exiting Position on the Pressure Recovery

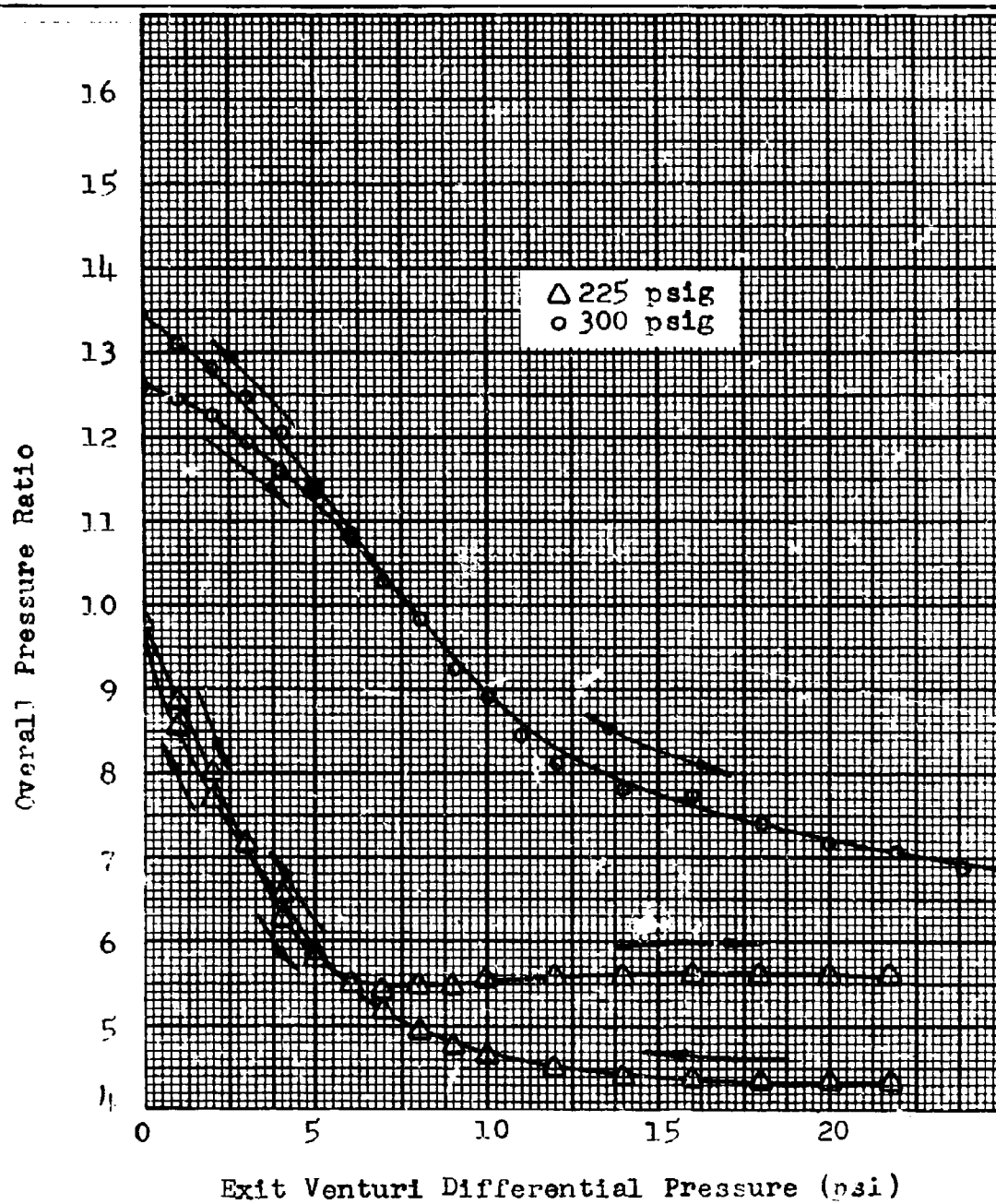


Fig. 26 Effect of Inlet Pressure on the Overall Pressure Ratio for the First Fluid Exiting Position

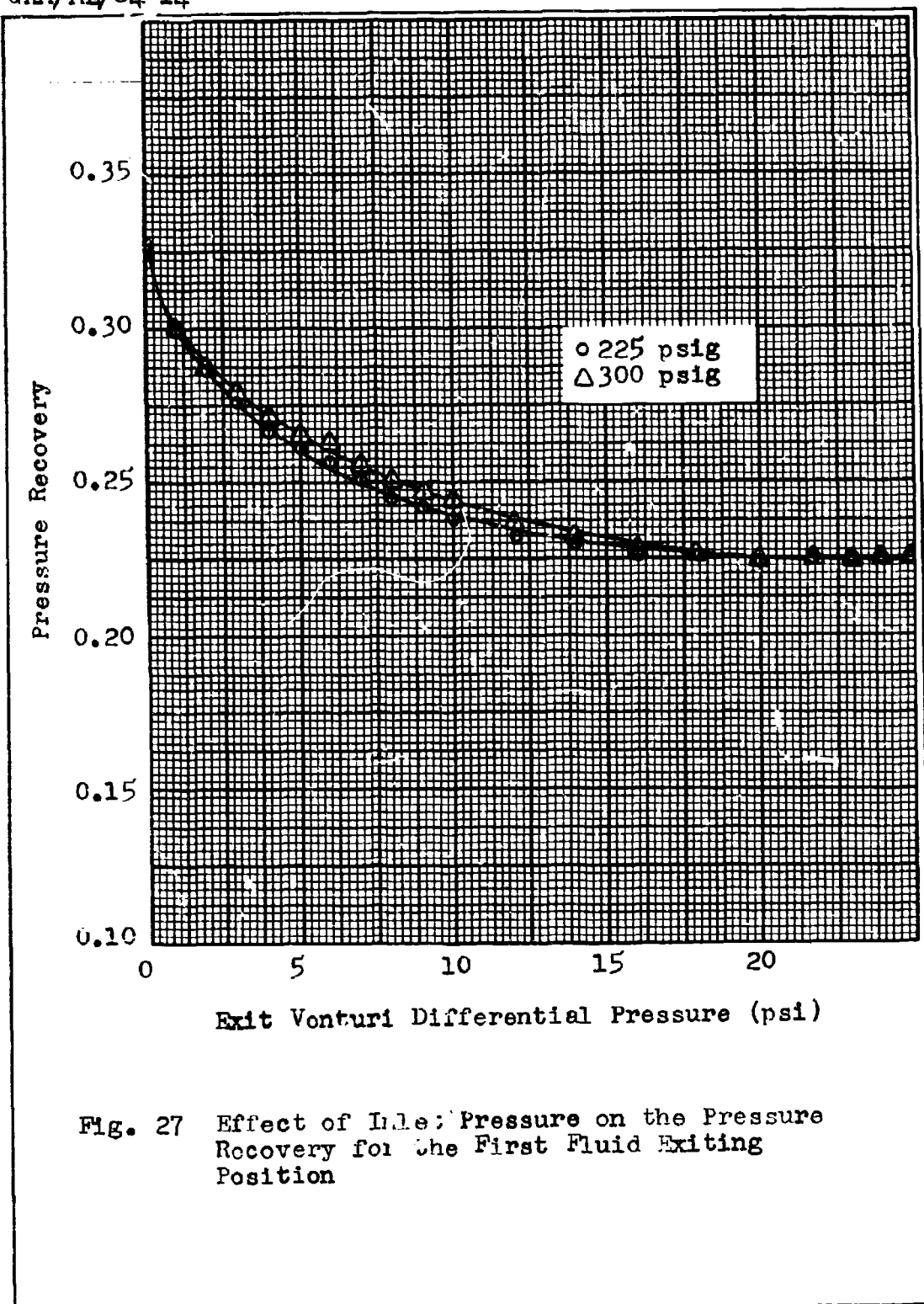


Fig. 27 Effect of Inlet Pressure on the Pressure Recovery for the First Fluid Exiting Position

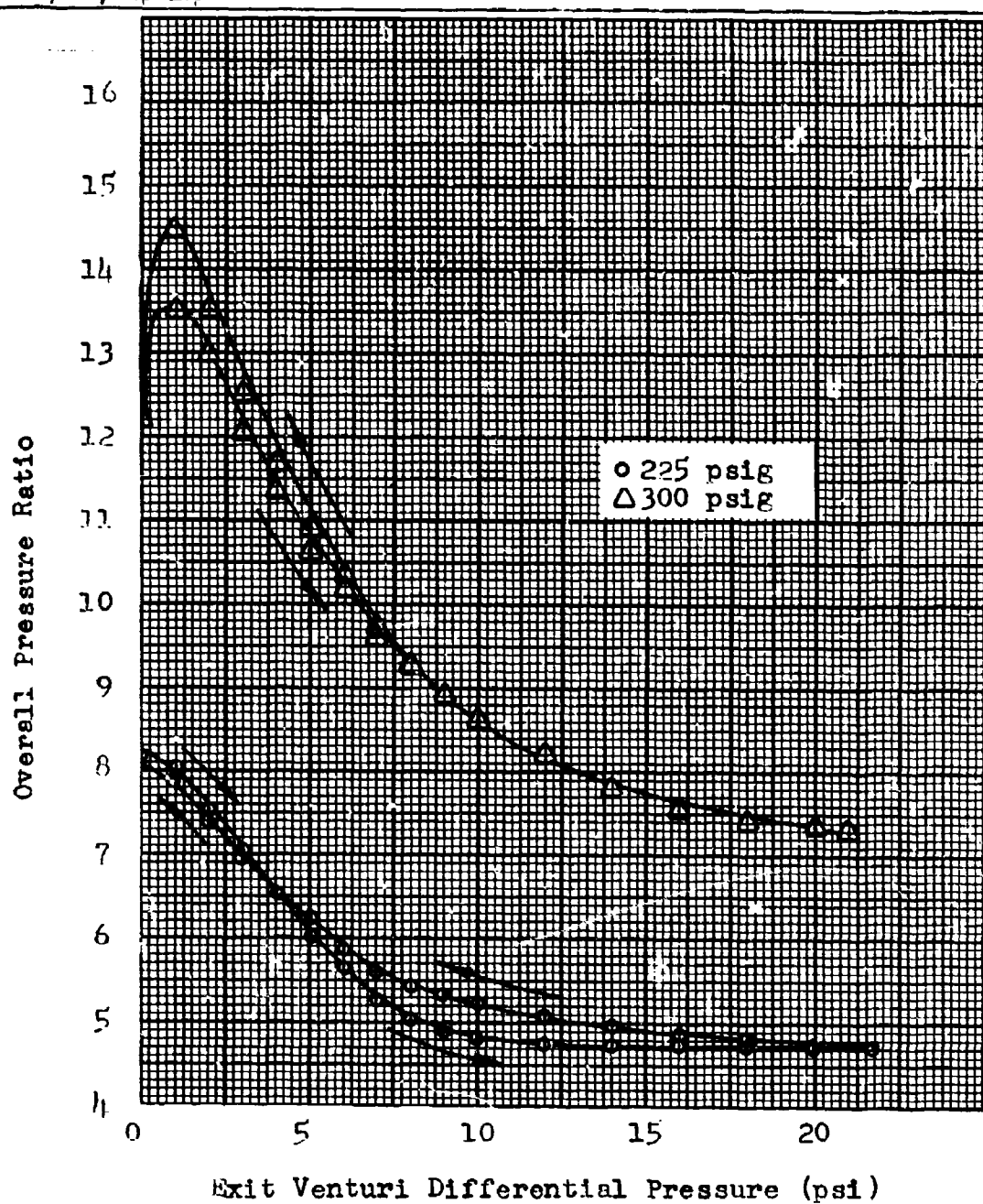


Fig. 28 Effect of Inlet Pressure on the Overall Pressure Ratio for the Second Fluid Exiting Position

GAM/ME/64-11

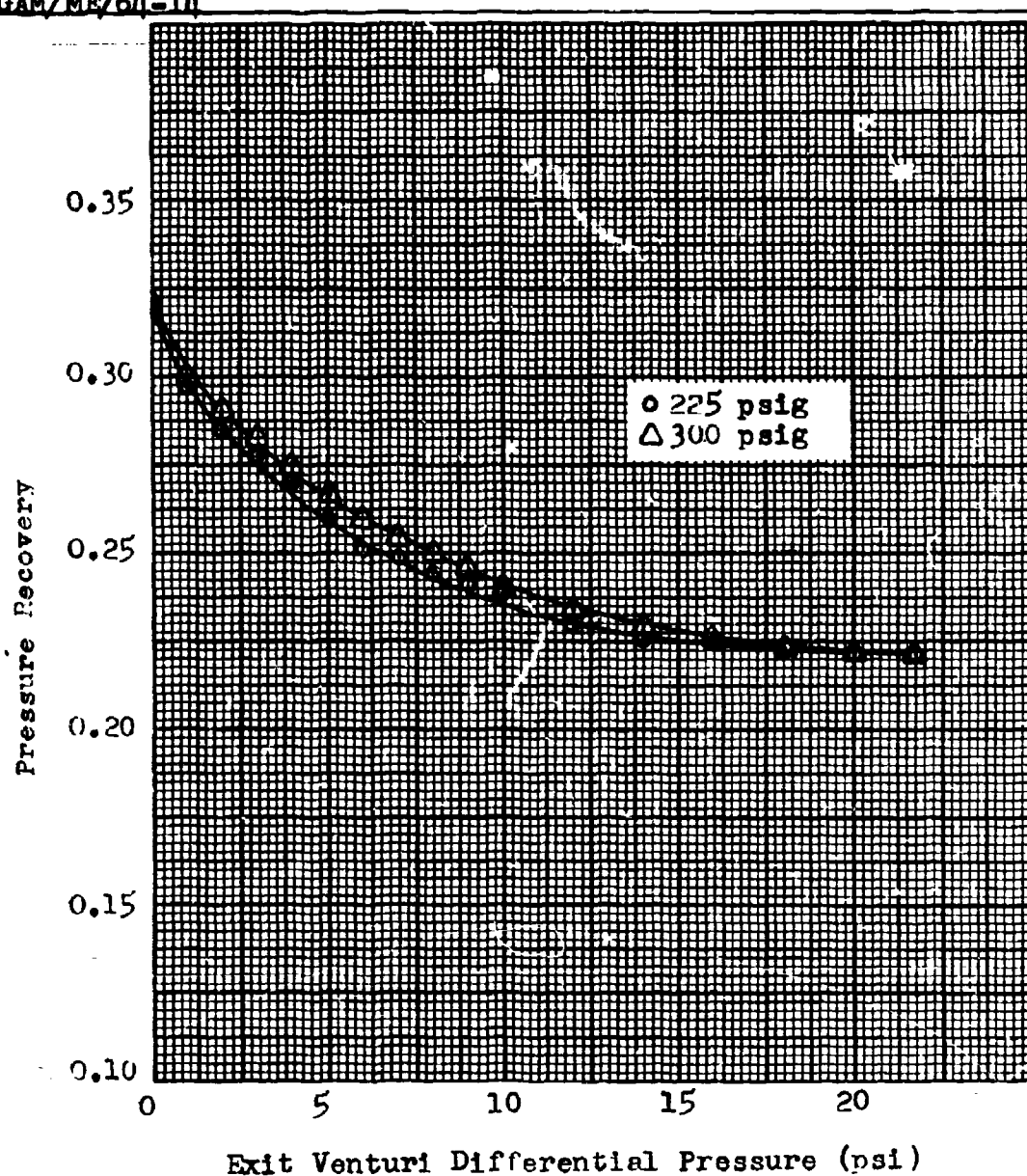


Fig. 29 Effect of Inlet Pressure on the Pressure Recovery for the Second Fluid Exiting Position

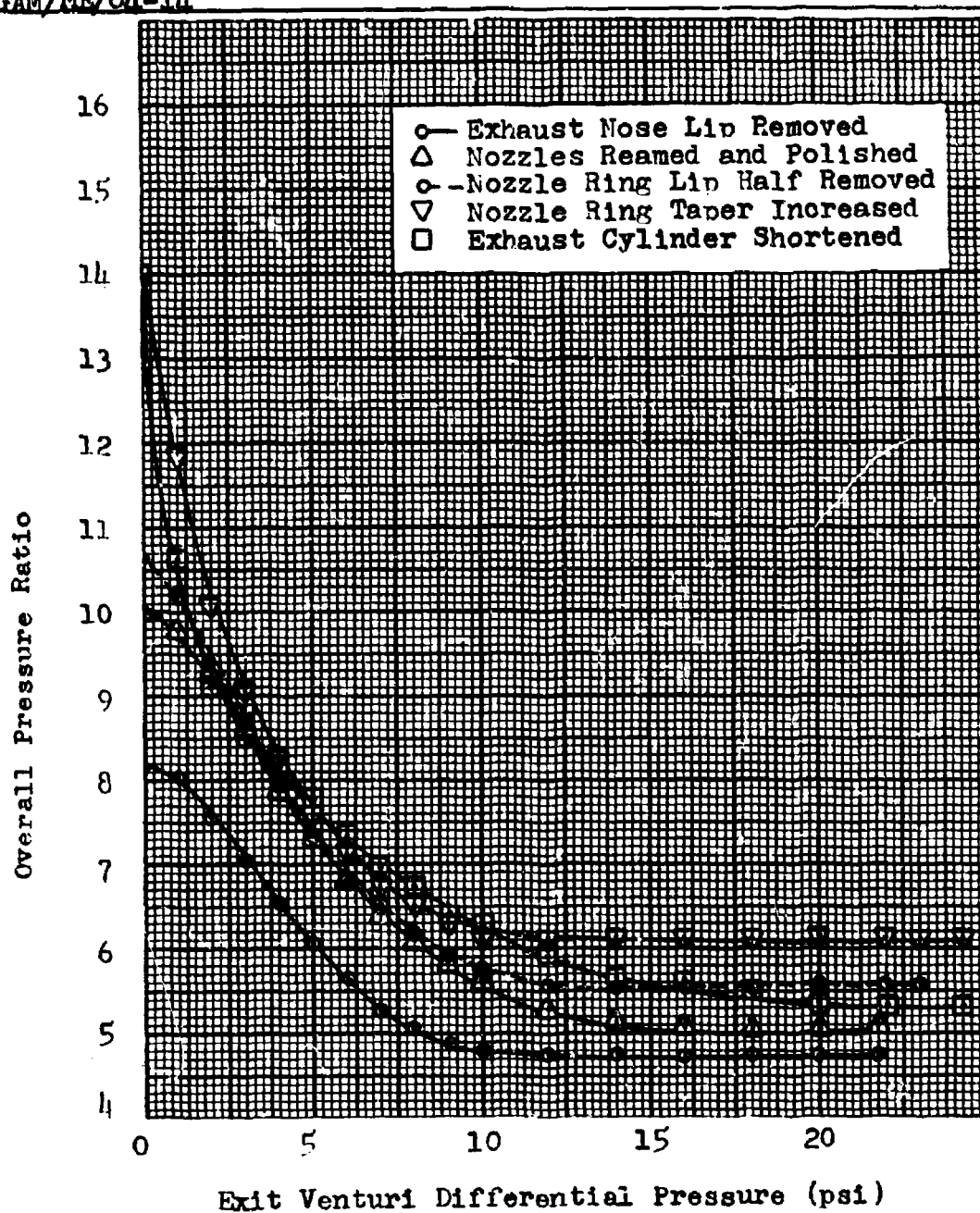


Fig. 30 Effect of Inlet Geometry on the Overall Pressure Ratio

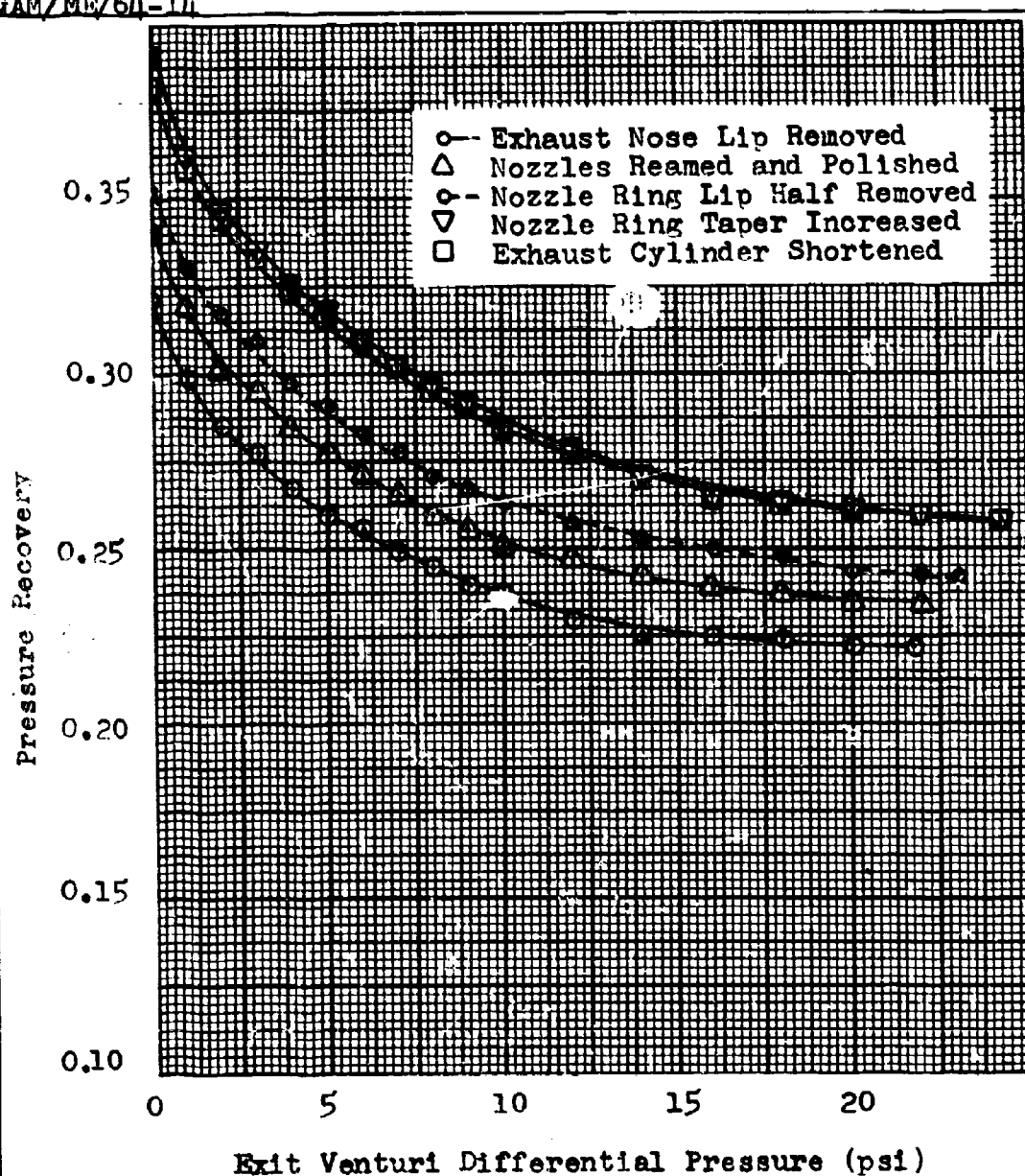


Fig. 31 Effect of Inlet Geometry on the Pressure Recovery

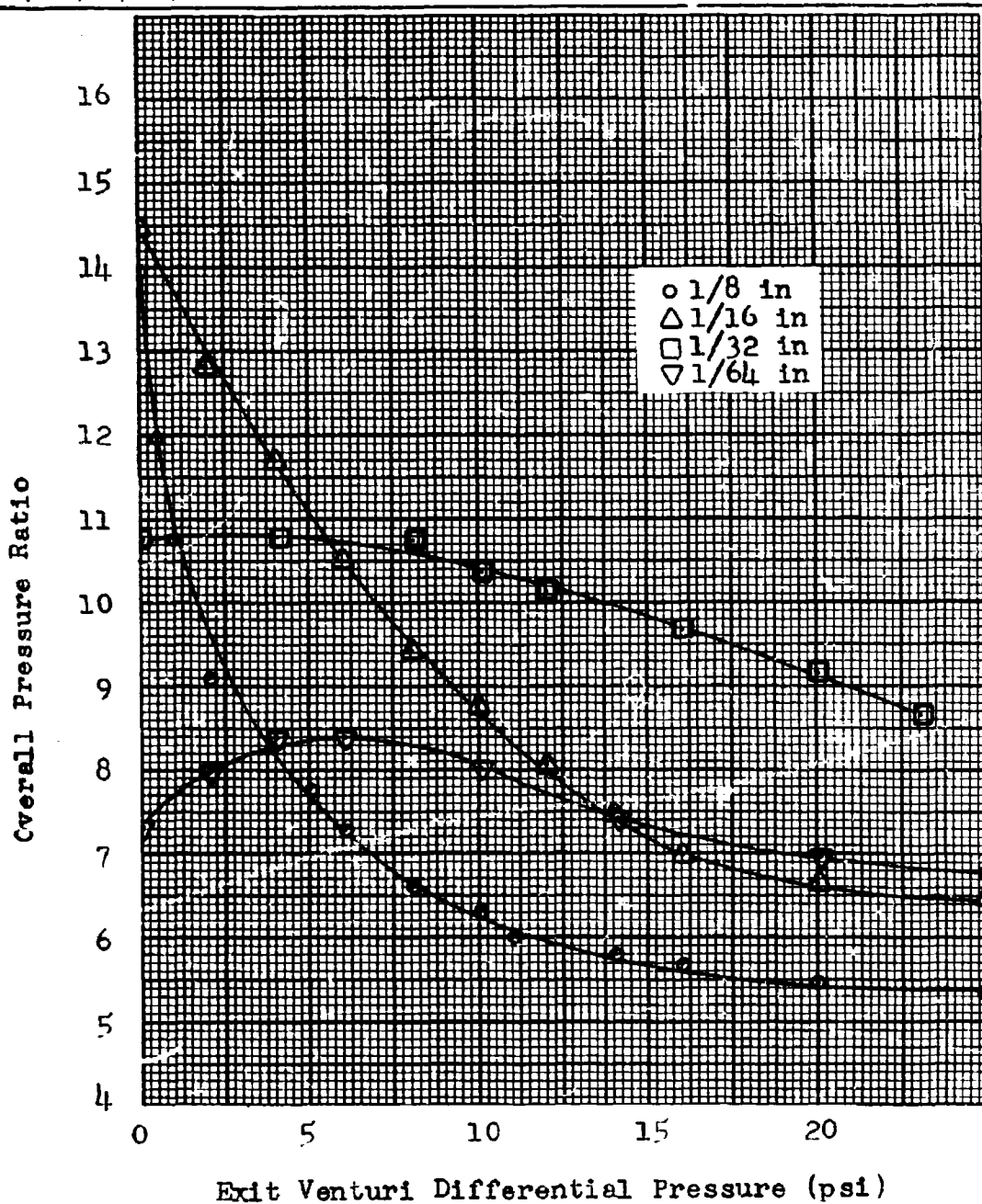


Fig. 32 Effect of Diffuser Gap Spacing on the Overall Pressure Ratio

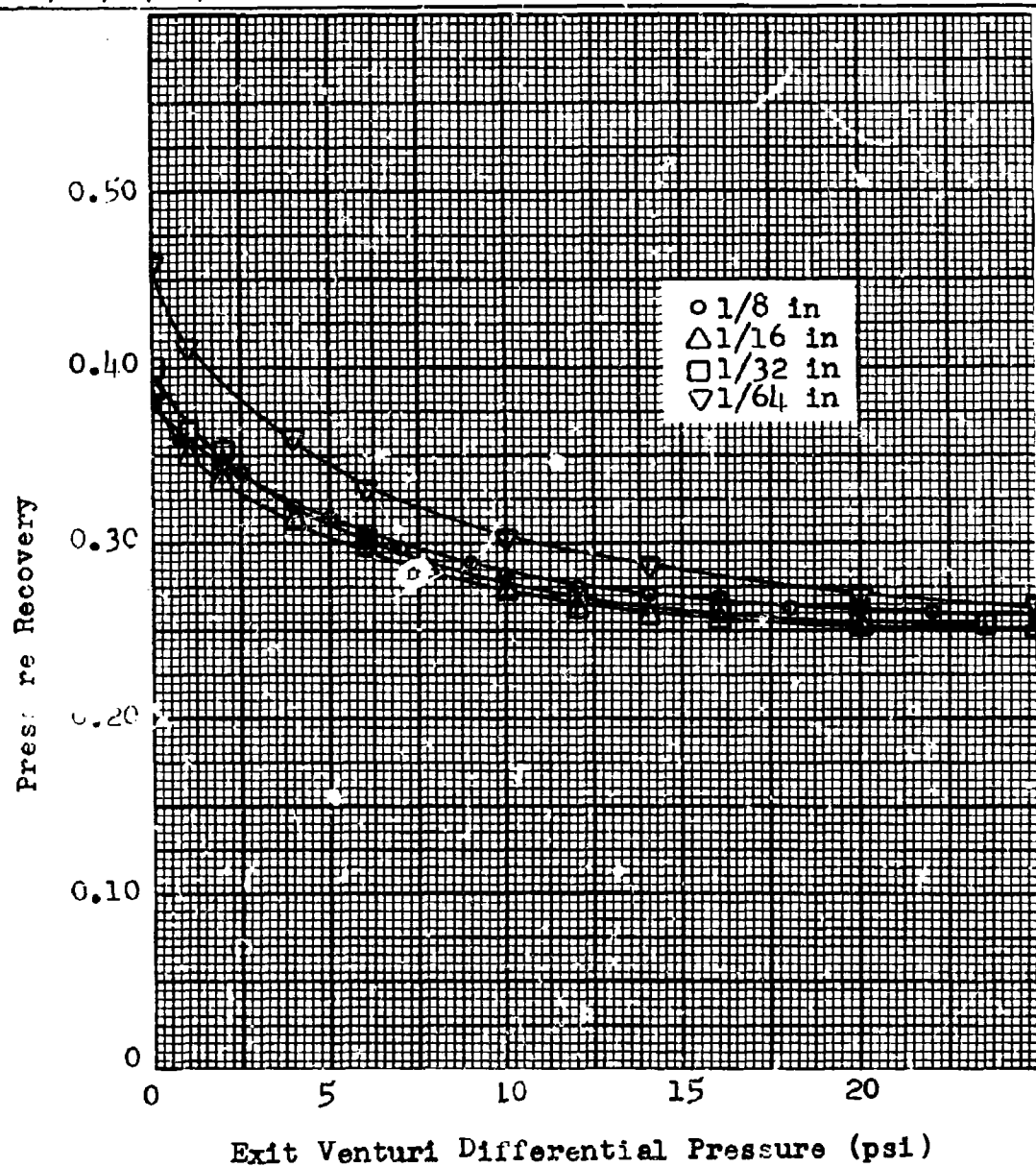


Fig. 35 Effect of Diffuser Gap Spacing on the Pressure Recovery

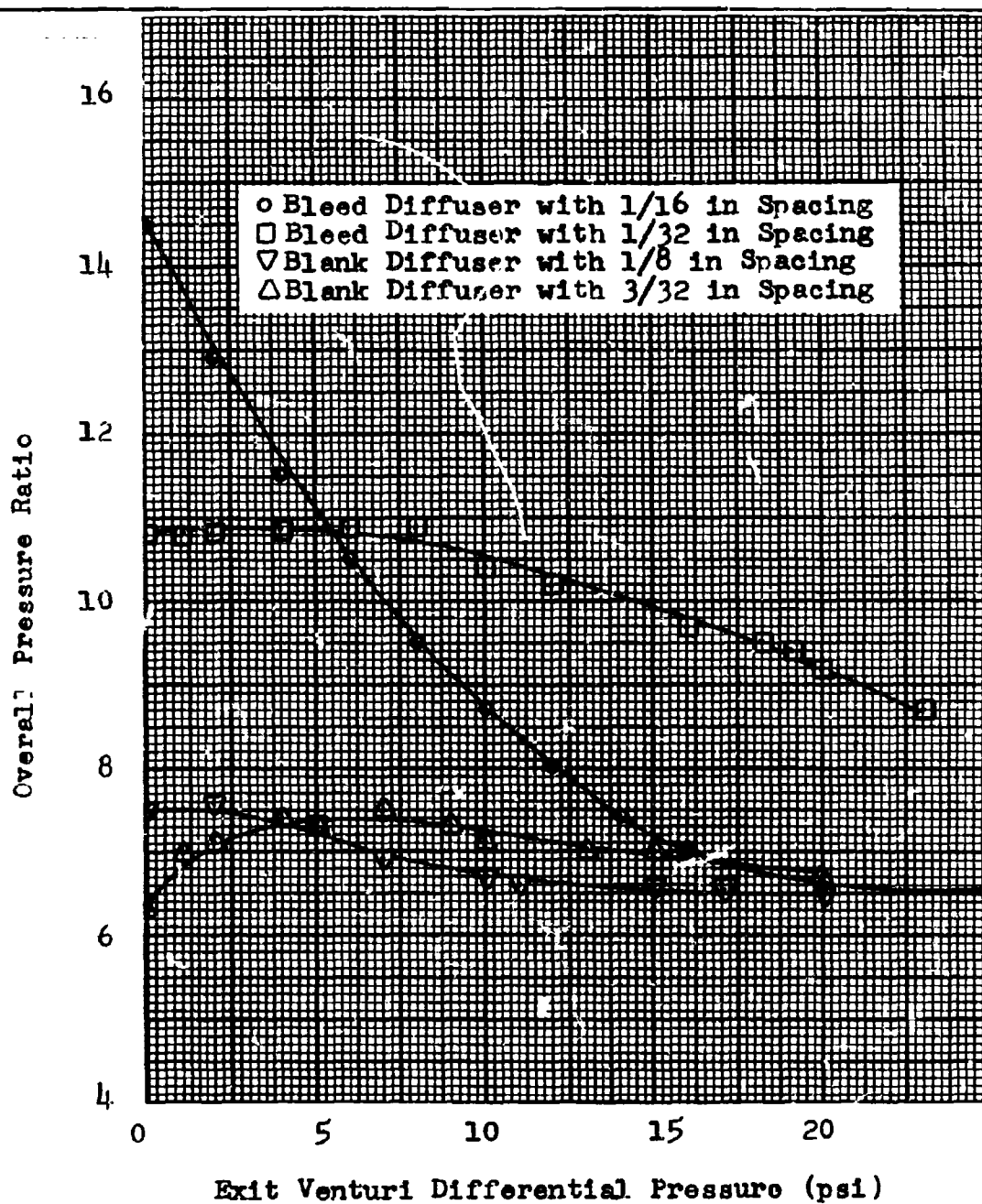


Fig. 34 Overall Pressure Ratio for Blank and Bleed Diffusers

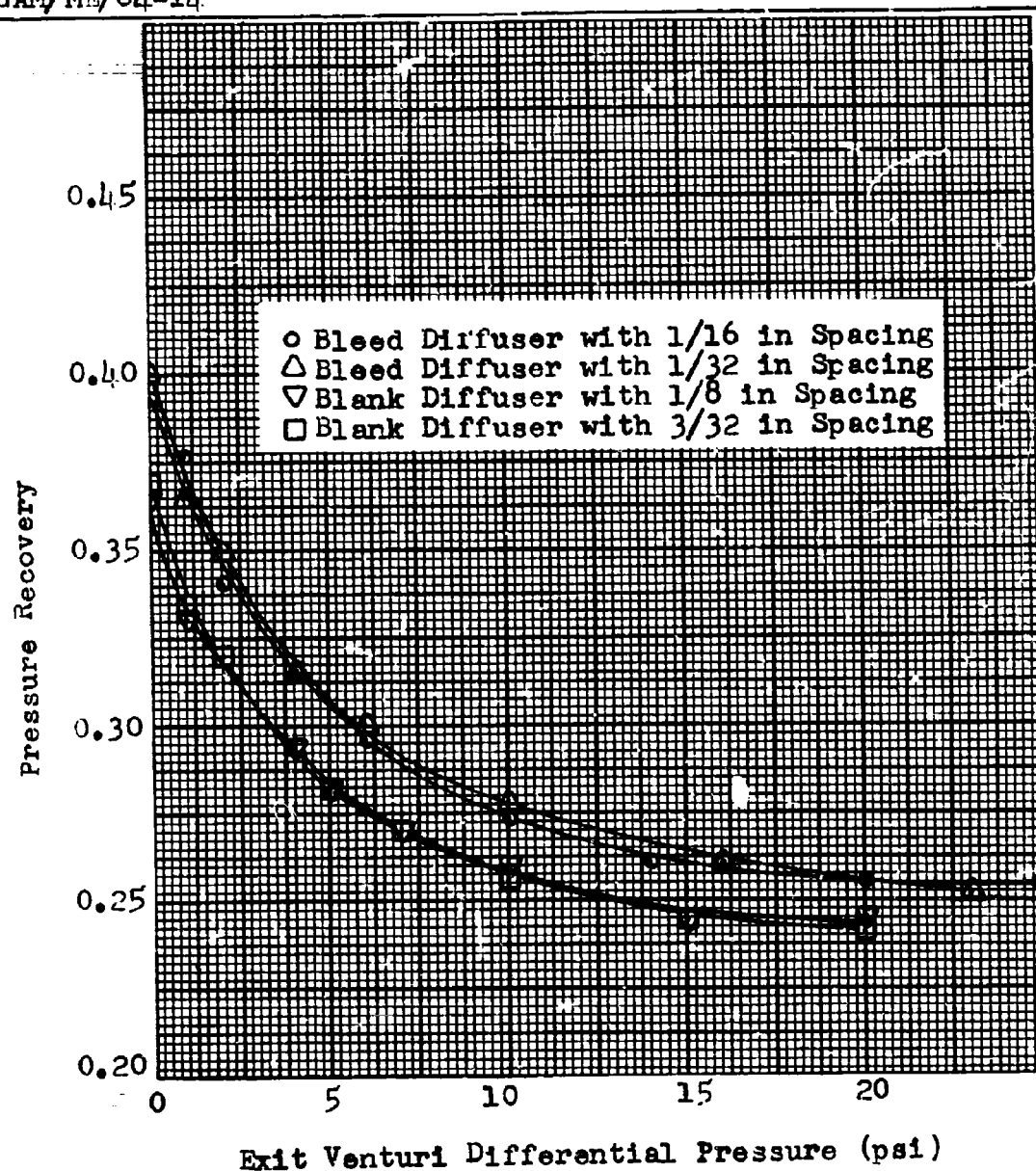


Fig. 35 Pressure Recovery for Blank and Bleed Diffusers

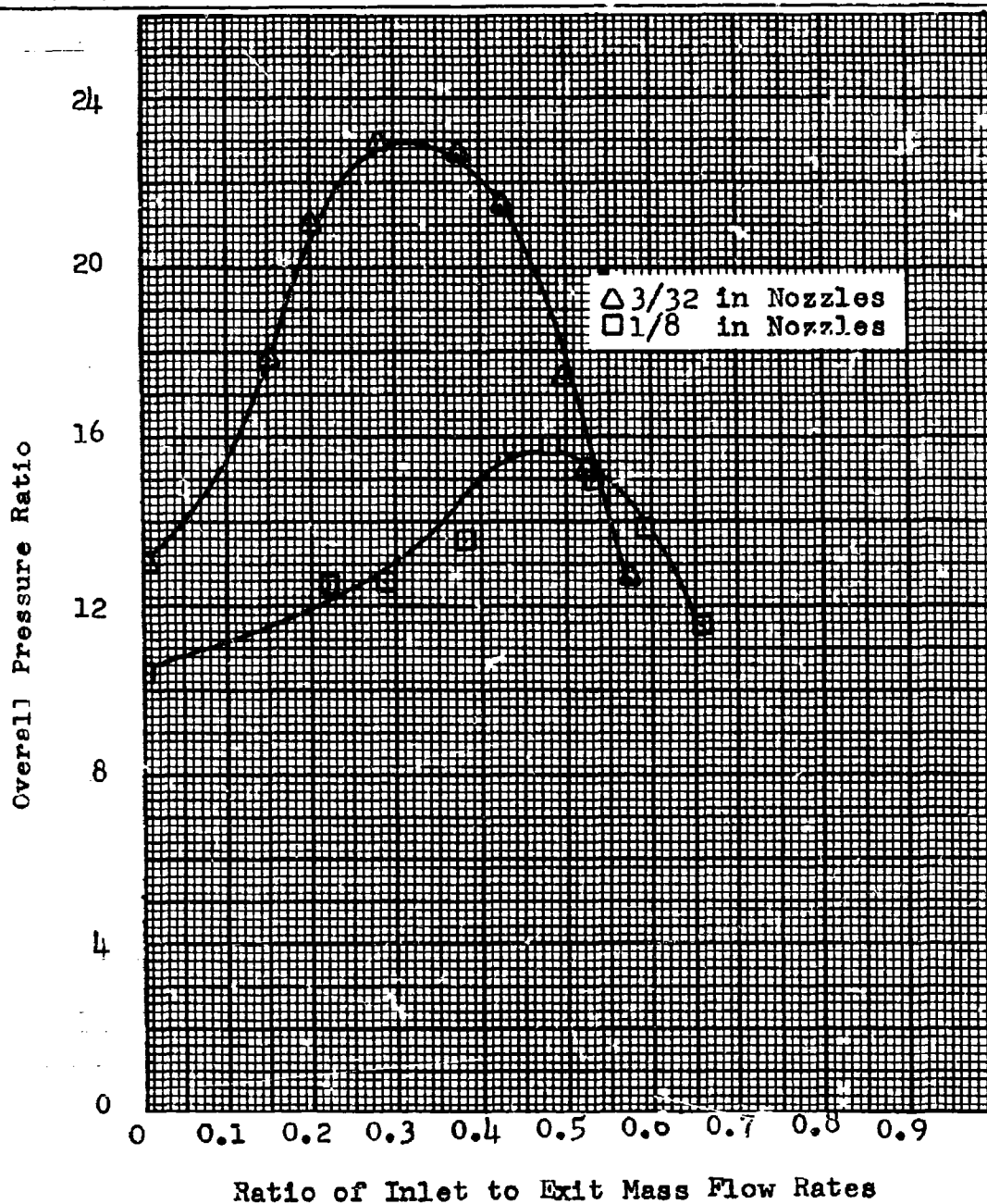


Fig. 36 Overall Pressure Ratio for 3/32 in and 1/8 in Nozzle Rings

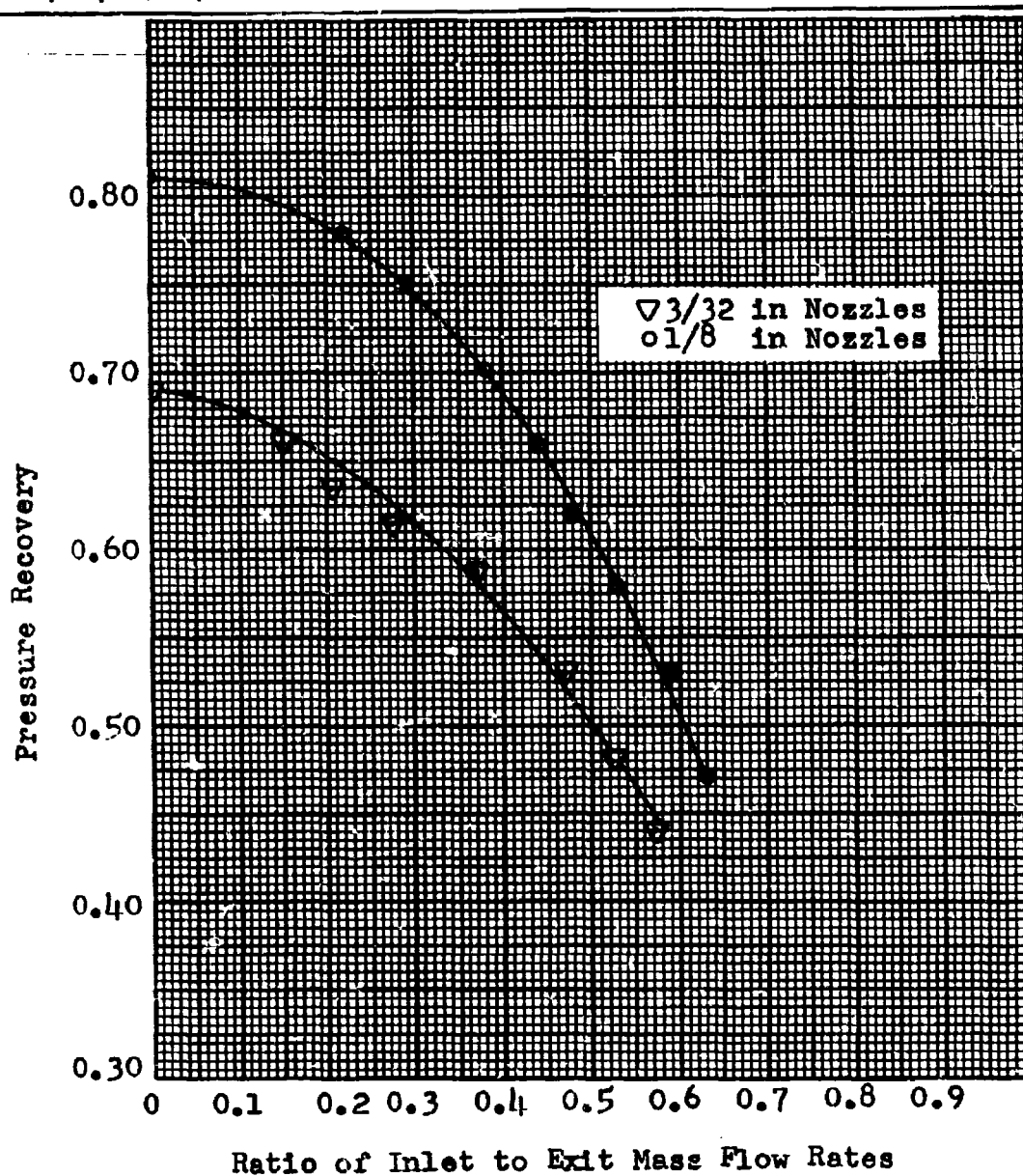


Fig. 37 Pressure Recovery for 3/32 in and 1/8 in Nozzle Rings

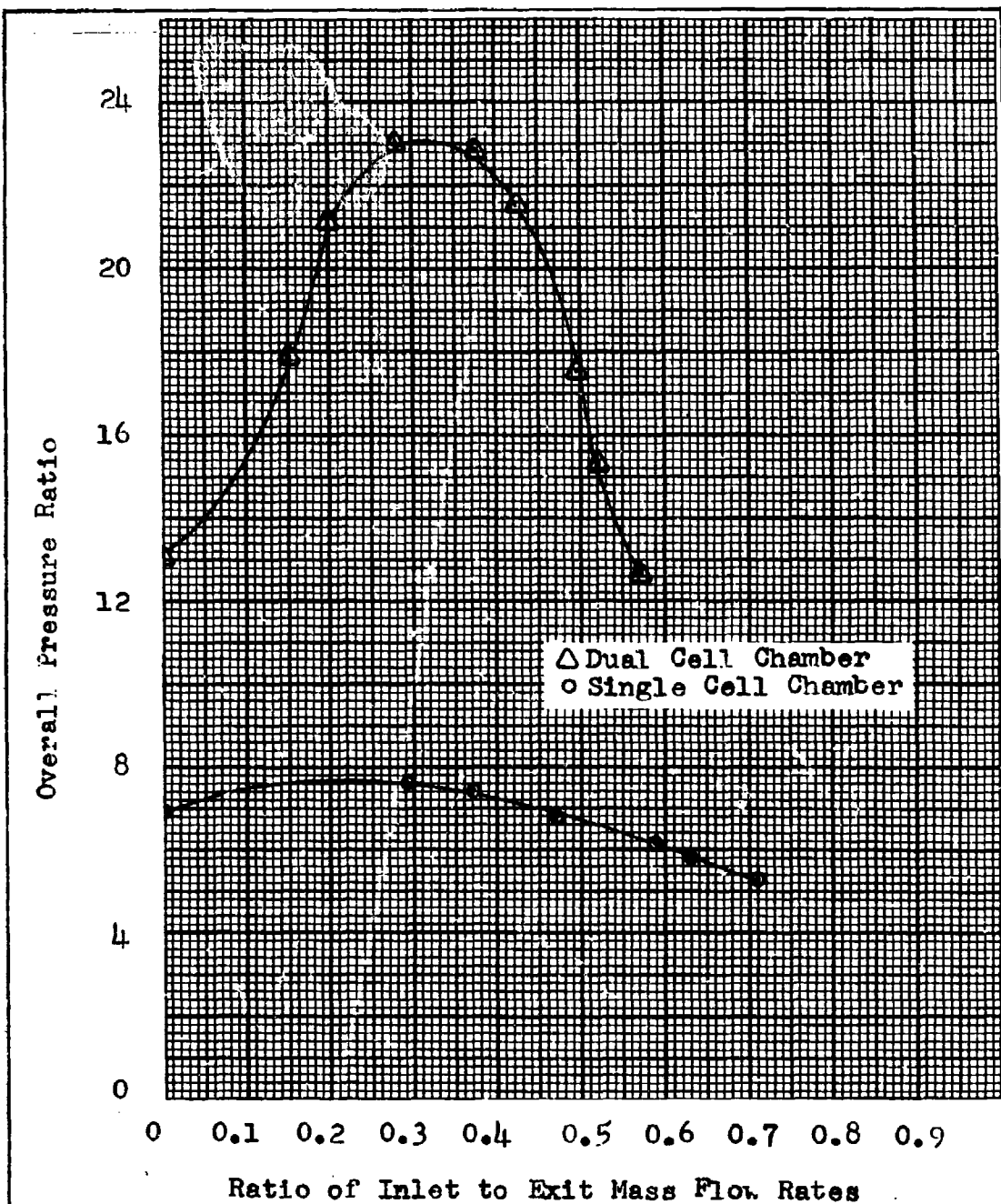


Fig. 38 Overall Pressure Ratio for Single and Dual Cell Chambers

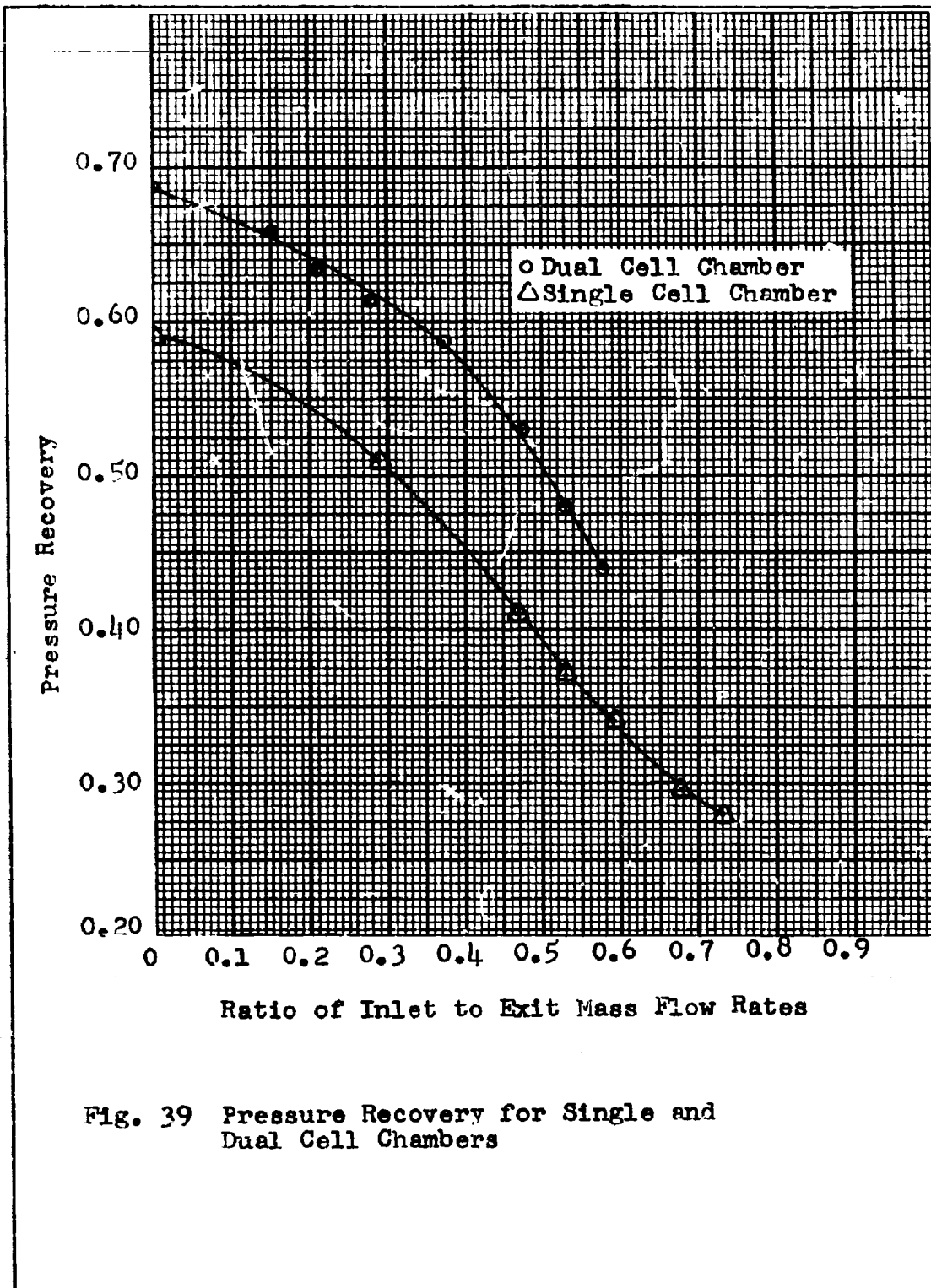


Fig. 39 Pressure Recovery for Single and Dual Cell Chambers

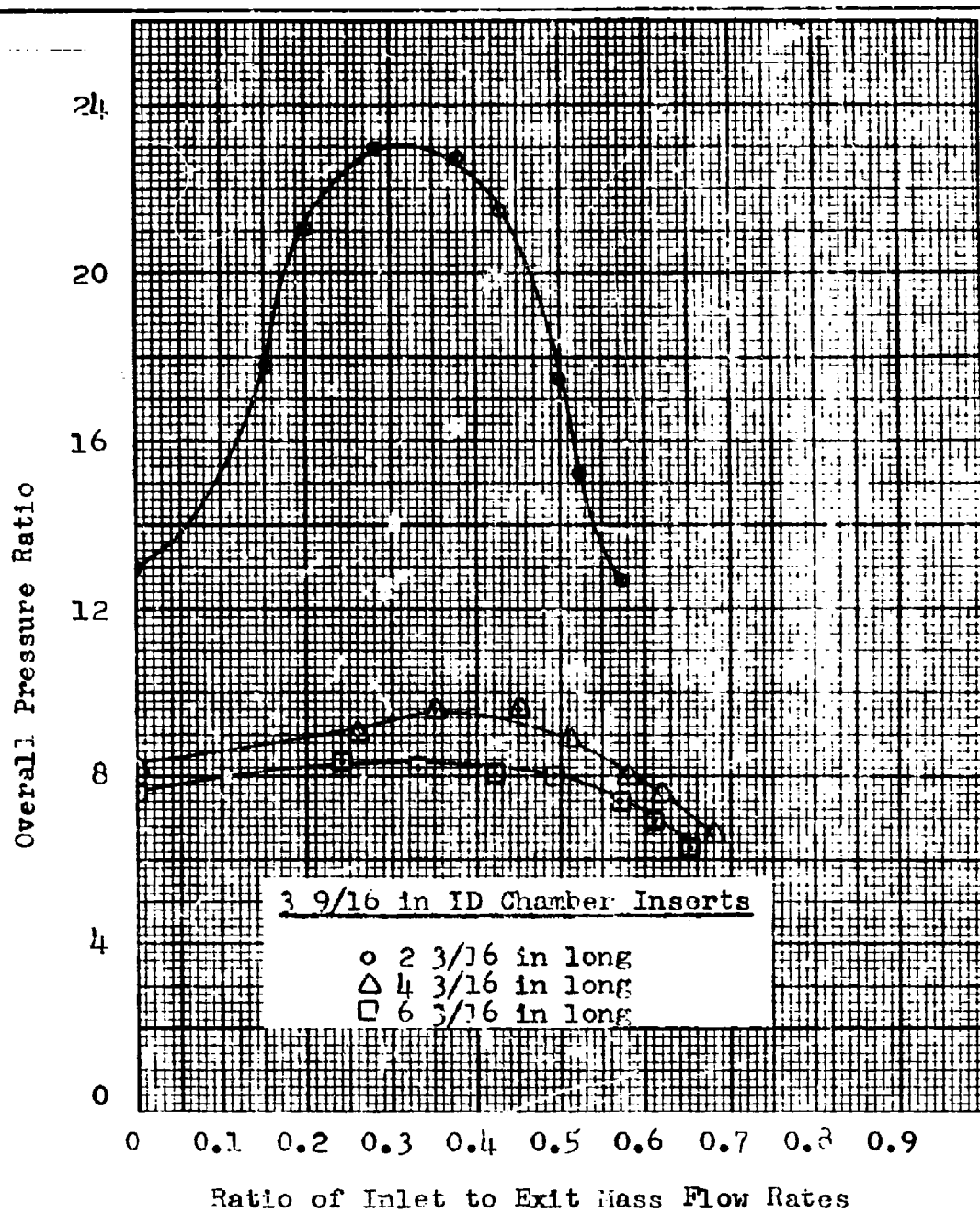


Fig. 40 Overall Pressure Ratio for Three Chamber Inserts

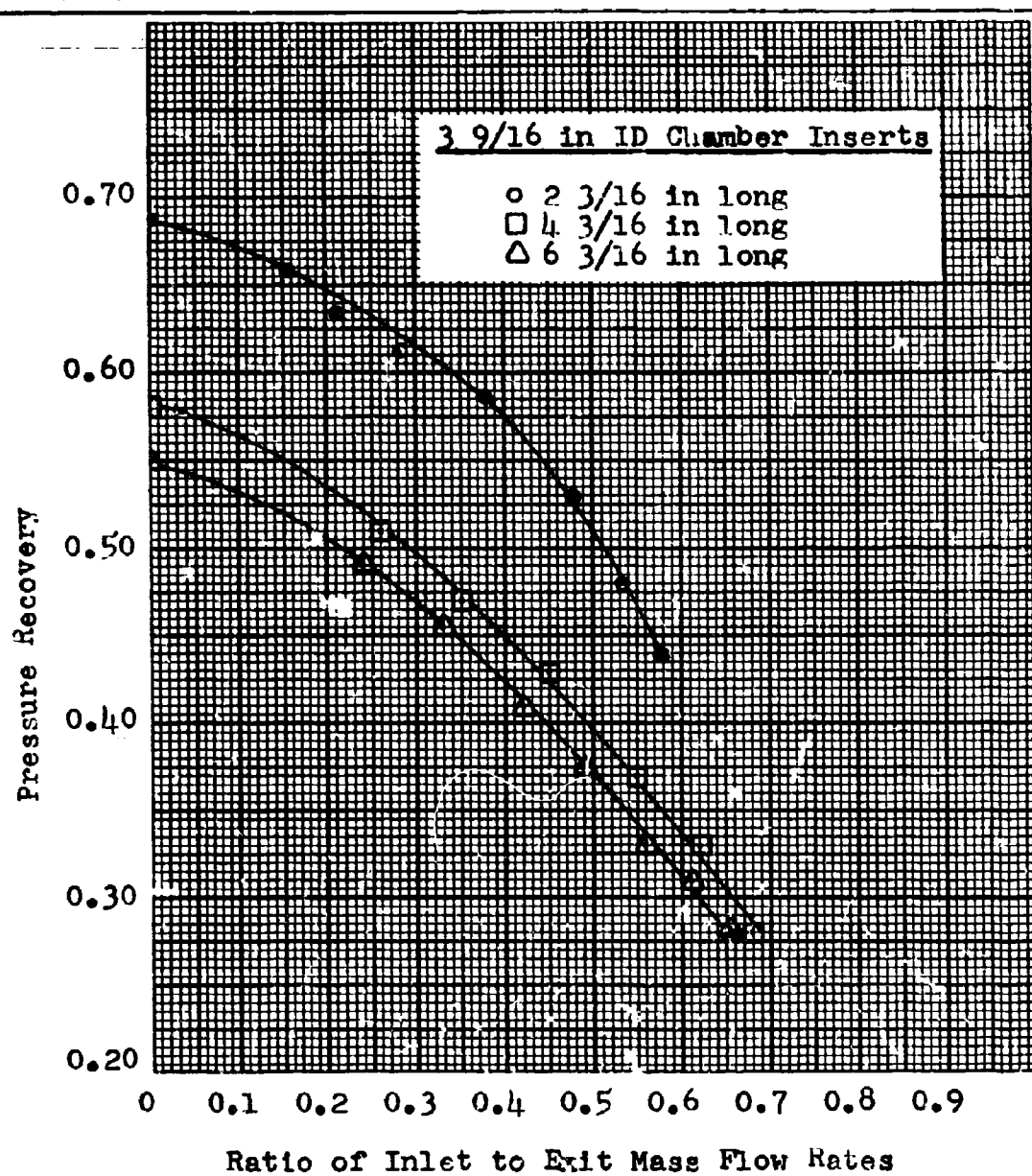


Fig. 41 Pressure Recovery for Three Chamber Inserts

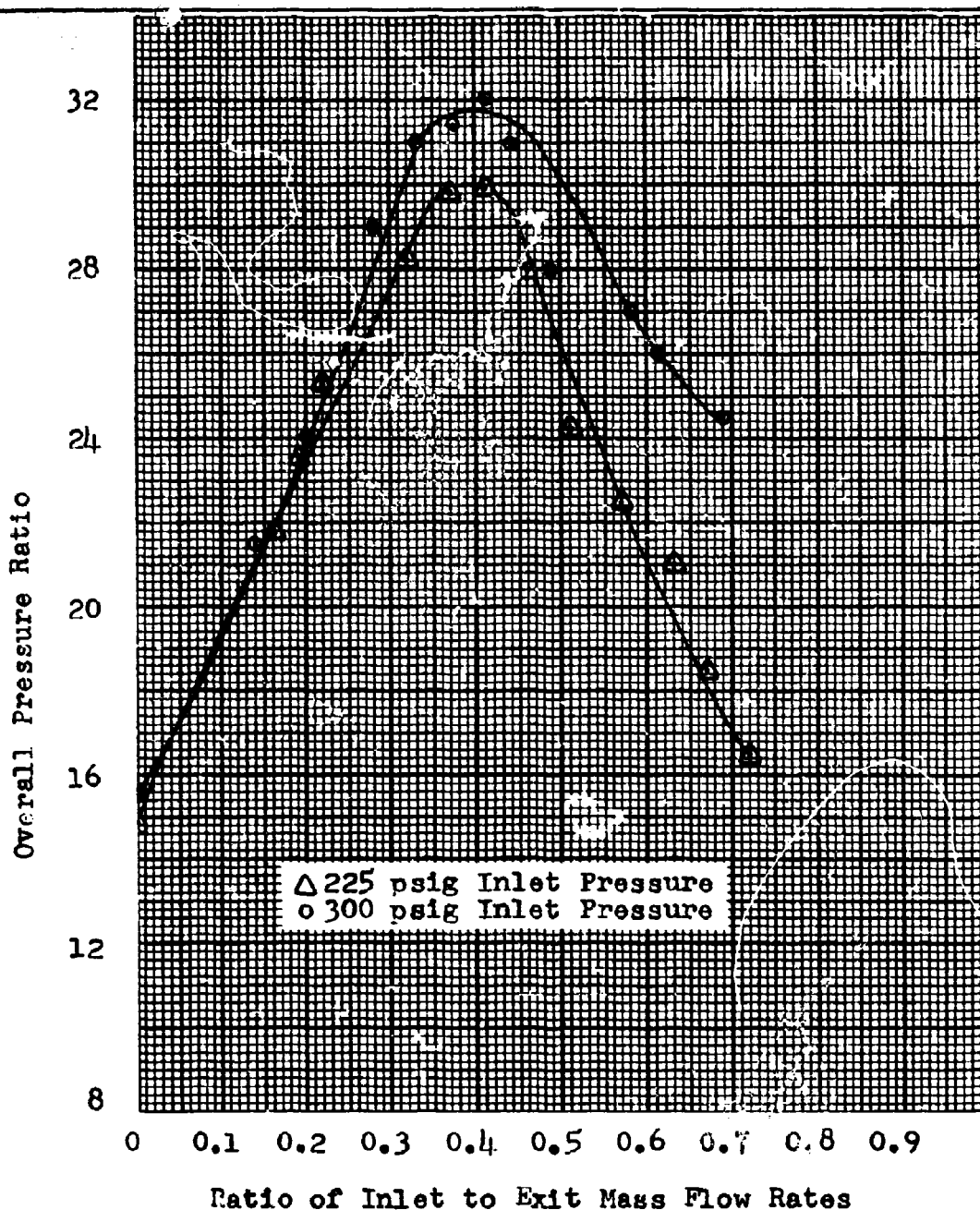


Fig. 42 Second Generation Chamber Overall Pressure Ratio for Two Inlet Pressures

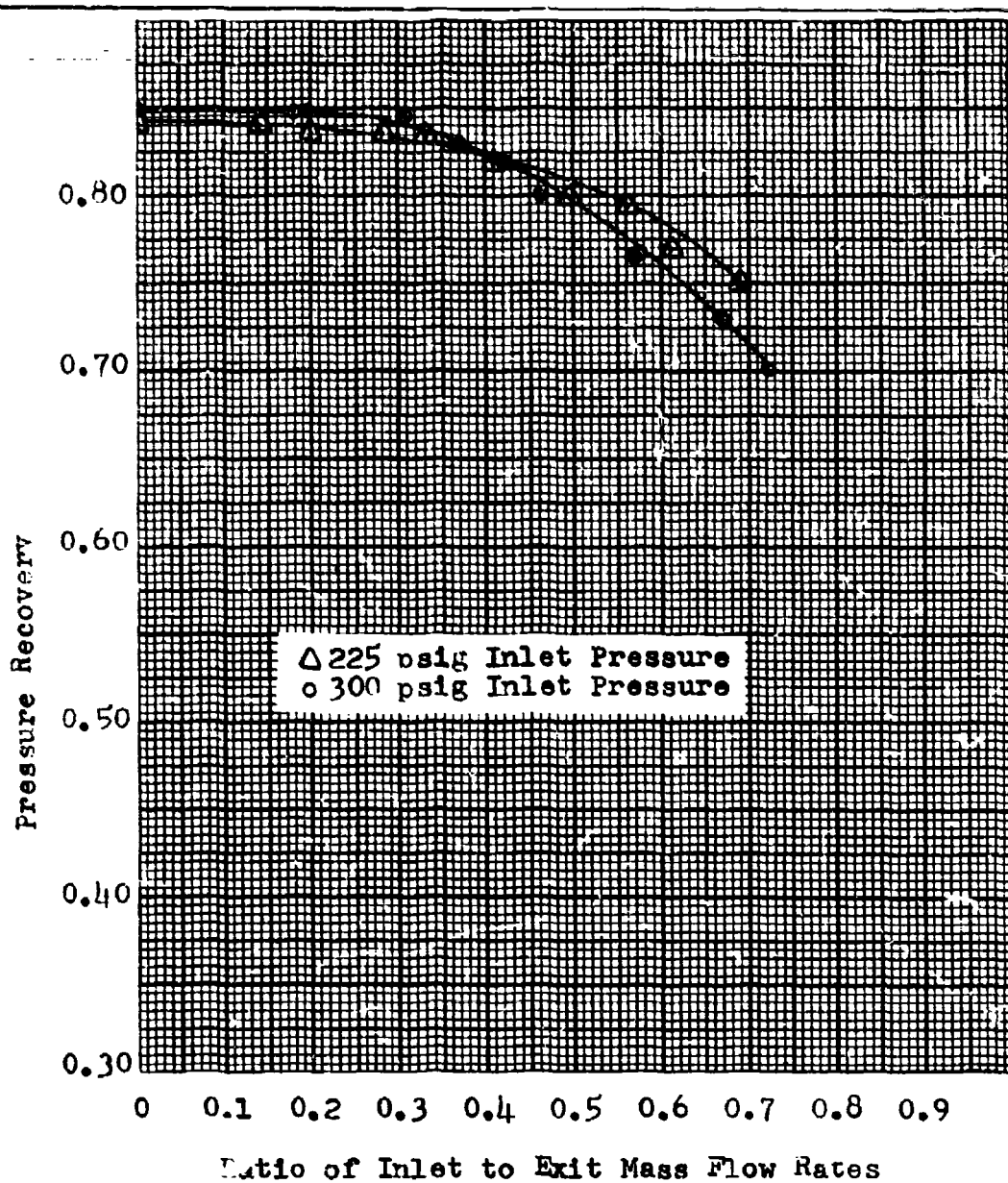


Fig. 43 Second Generation Chamber Pressure Recovery for Two Inlet Pressures

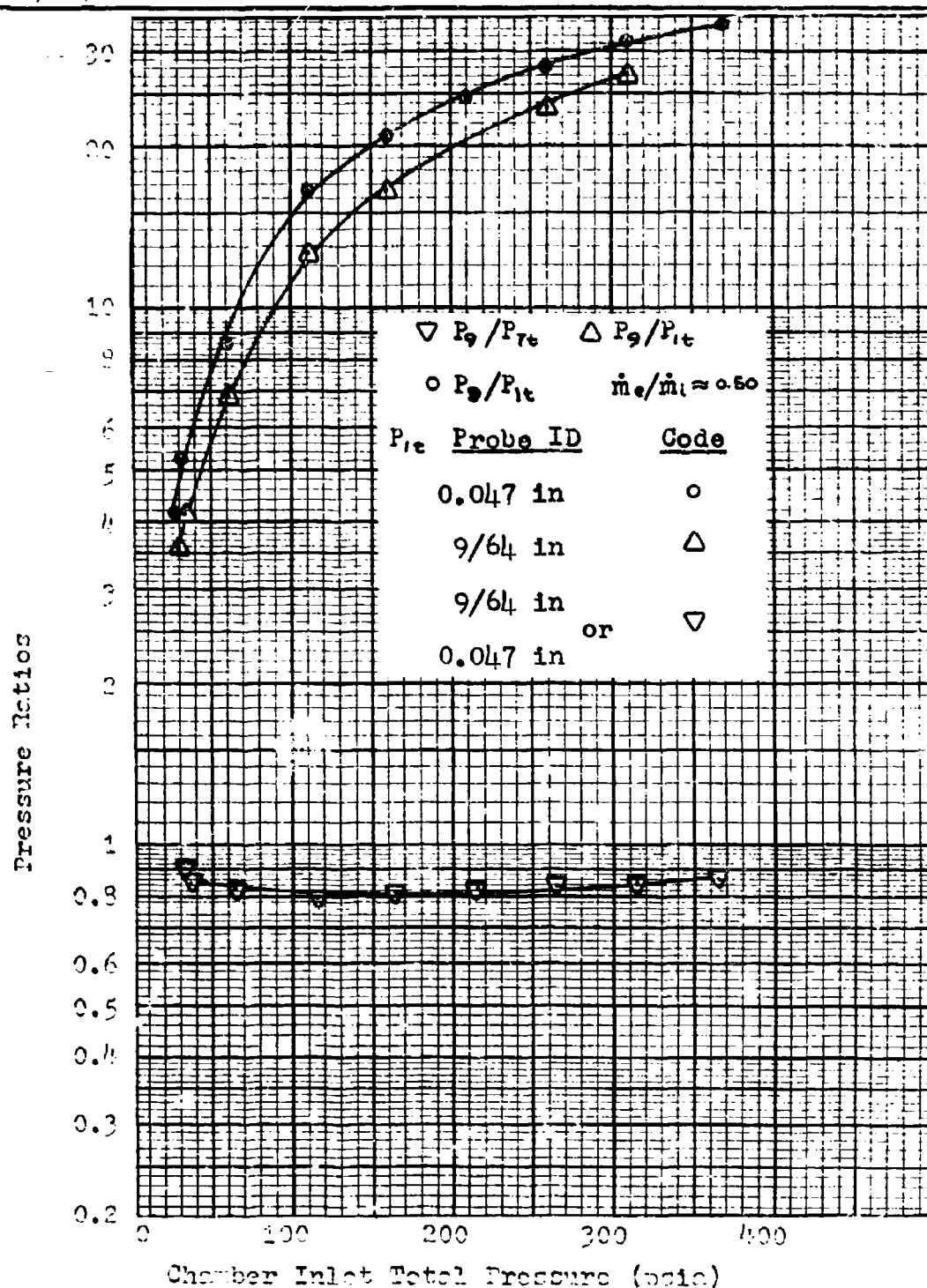


Fig. 44 Second Generation Chamber Pressure Ratios



Fig.45 Flow Pattern for 100 psig Inlet Pressure



Fig.46 Flow Pattern for 200 psig Inlet Pressure

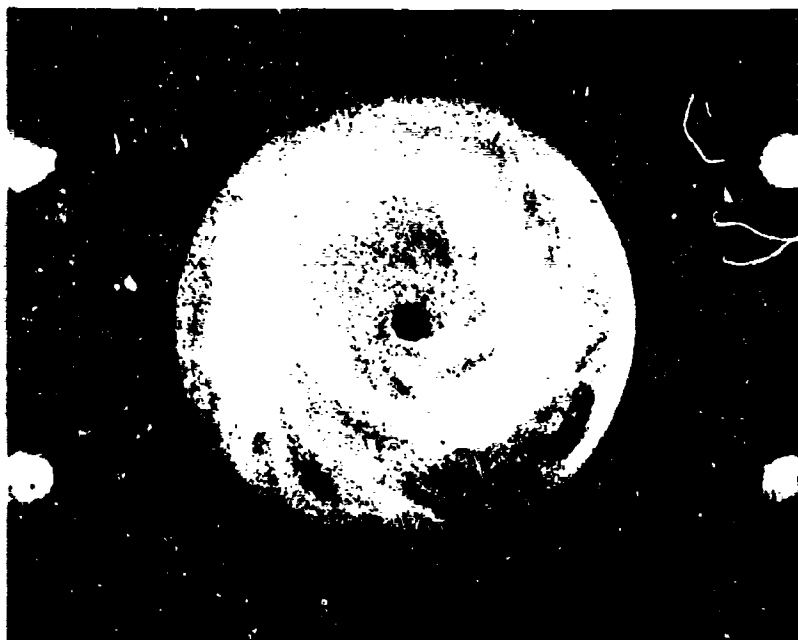


Fig. 47 Flow Pattern for 300 psig Inlet Pressure

GAM/HE/64-14

List of Tables

<u>Table</u>	<u>Page</u>
I Components of First Generation Swirl Chamber . . .	99
II Components of Second Generation Swirl Chamber . .	100

Table I
Components of First Generation Swirl Chamber

Component	Figure Number	Part Number
Blank Diffuser	48 and 53	B-1220I and II
Bleed Diffuser	48 and 54	B-1302
Exhaust Chamber	48	B-1219
Admission Chamber	48	C-1214I and II
Nozzle Ring (Typical)	48 and 51	B-1217I and II
Exit Chamber	48	C-1215I and II
Chamber Insert (Typical)	48	B-1218
Center Disk Flange	48	C-1216

Table II
Components of Second Generation Swirl Chamber

Components	Figure Number	Part Number
Crank Bleed Diffuser	55	C-1522
Exhaust Chamber	49	B-1219
Inlet-Exit Chamber	49	C-1479
Multiple Nozzle Housing	49 and 52	C-1483
Center Disk Flange	49	C-1484

GAM/HE/64-14

Appendix A

Engineering Drawings

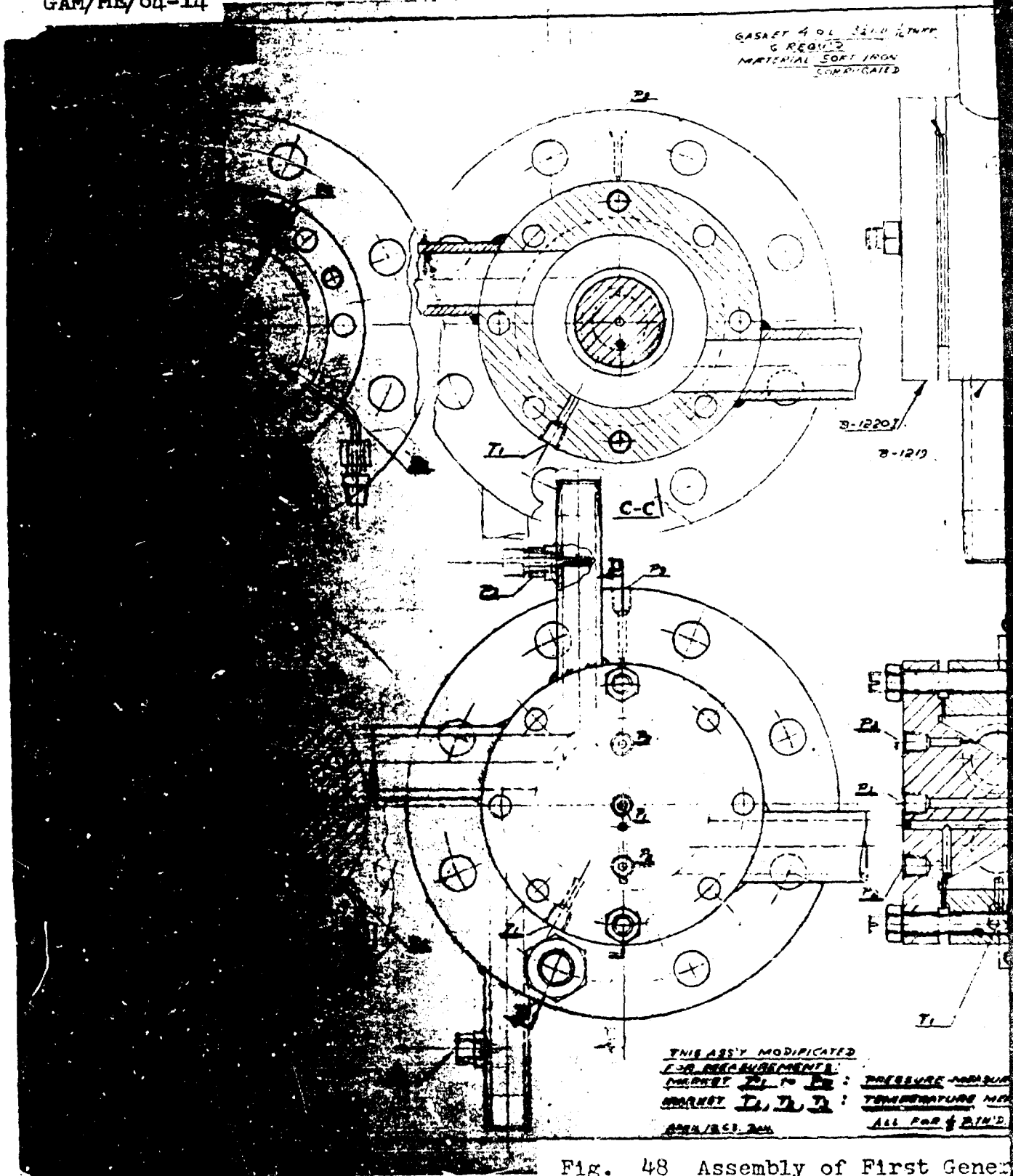
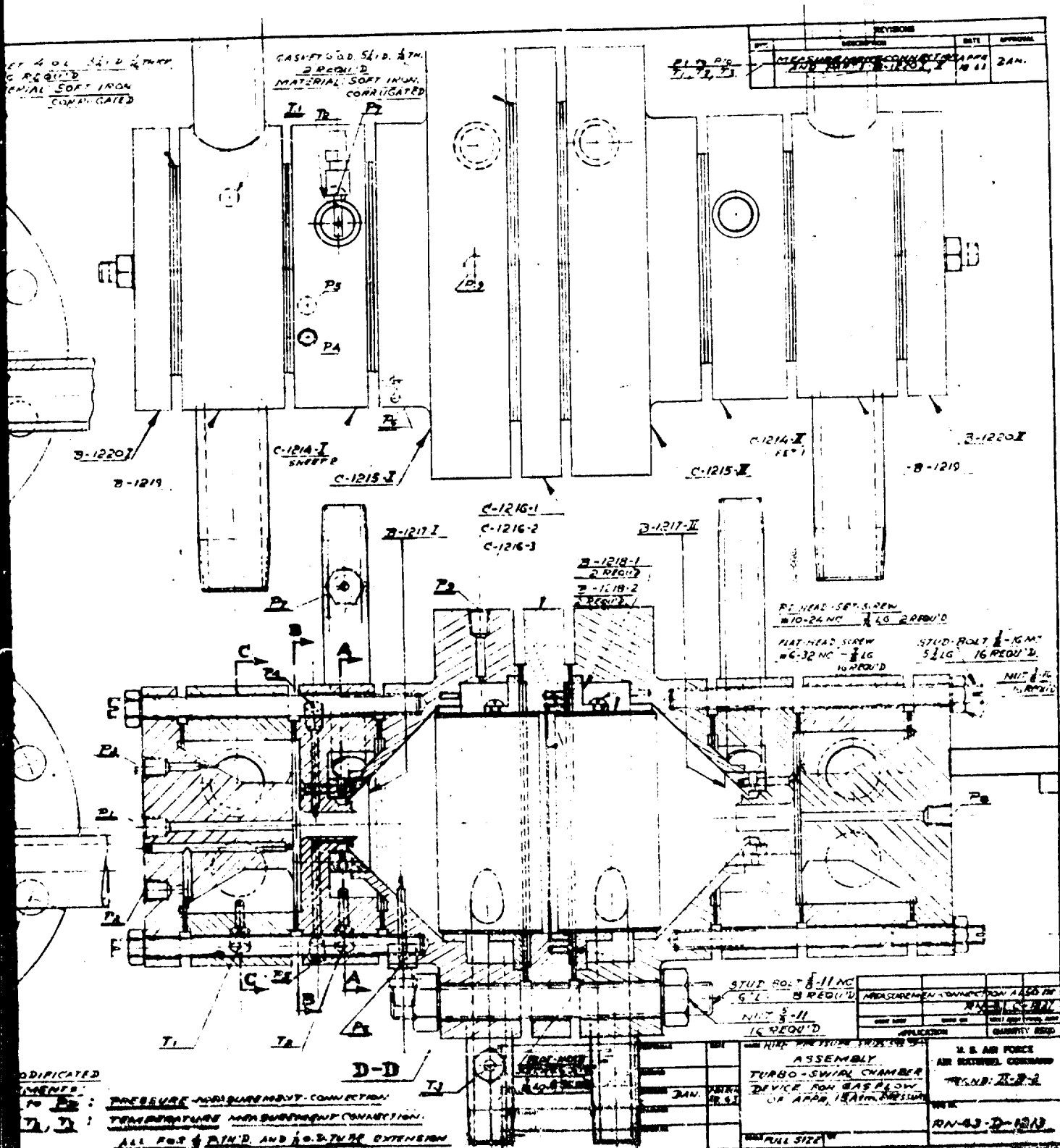


Fig. 48 Assembly of First Generator



Copy of First Generation Dual Cell Swirl Chamber

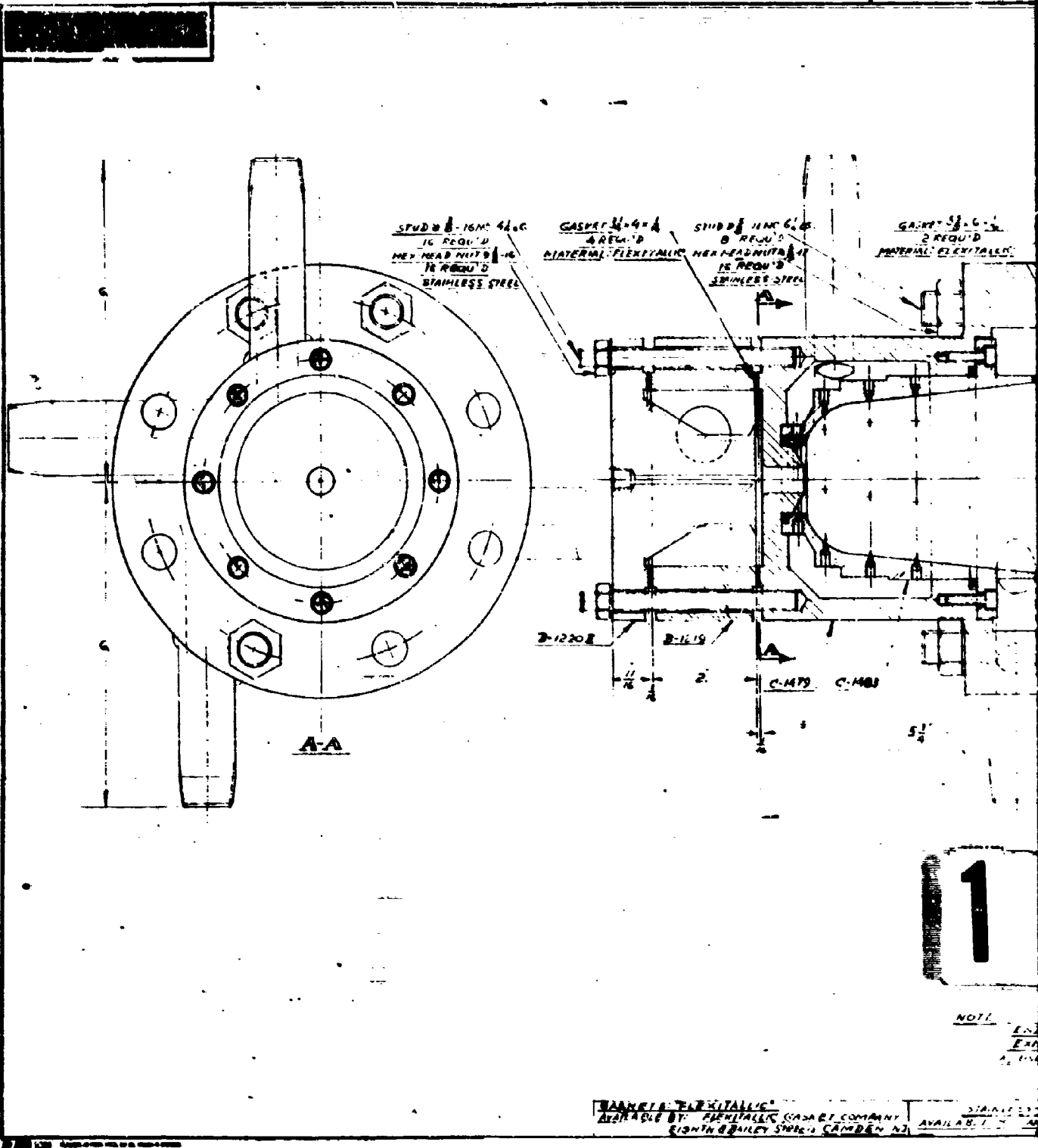
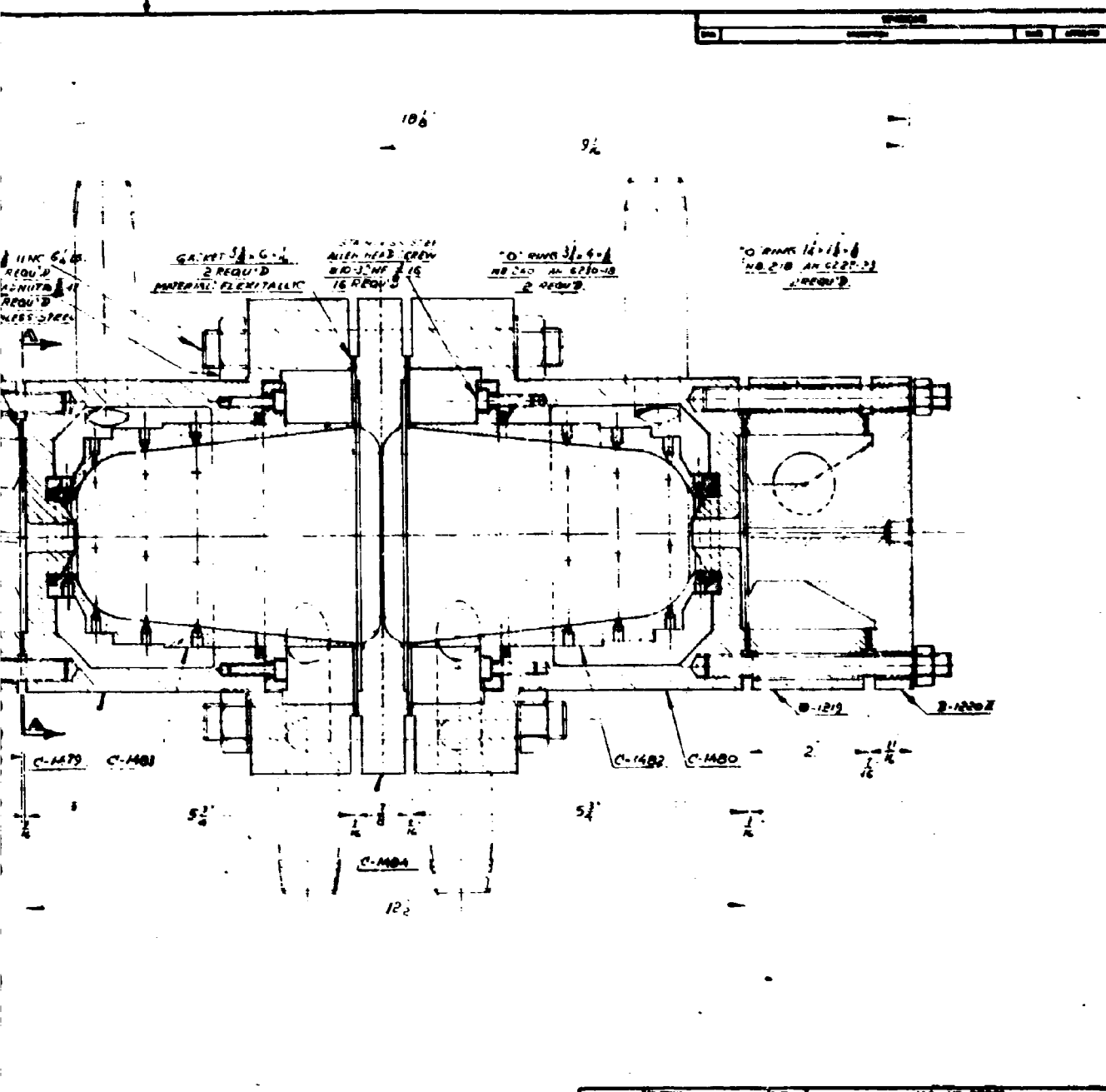


Fig. 49 Assembly of Second Generation



NOTE
 END PLATE: 63-D-1220 (AN)
 EXHAUST CHAMBER: 63-D-1221
 "USE IN SINGLE INJECTION"
 TURBO SWIRL CHAMBER
 ASSY 63-D-1477

STAINLESS STEEL BOLT'S, NUT'S, SCREWS ETC.
 AVAILABLE IN ANTI-CORROSIVE METAL AND DUCT COMPATIBLE
 FOR USE IN HIGH PRESSURE SYSTEMS

U.S. AIR FORCE	
REG. NO. 1-B2	
ASSEMBLY	
TURBO SWIRL CHAMBER FOR	
MULTIPLE INJECTION	
FOR HIGH PRESSURE SYSTEM	
D 63-D-1477	

of Second Generation Dual Cell Swirl Chamber

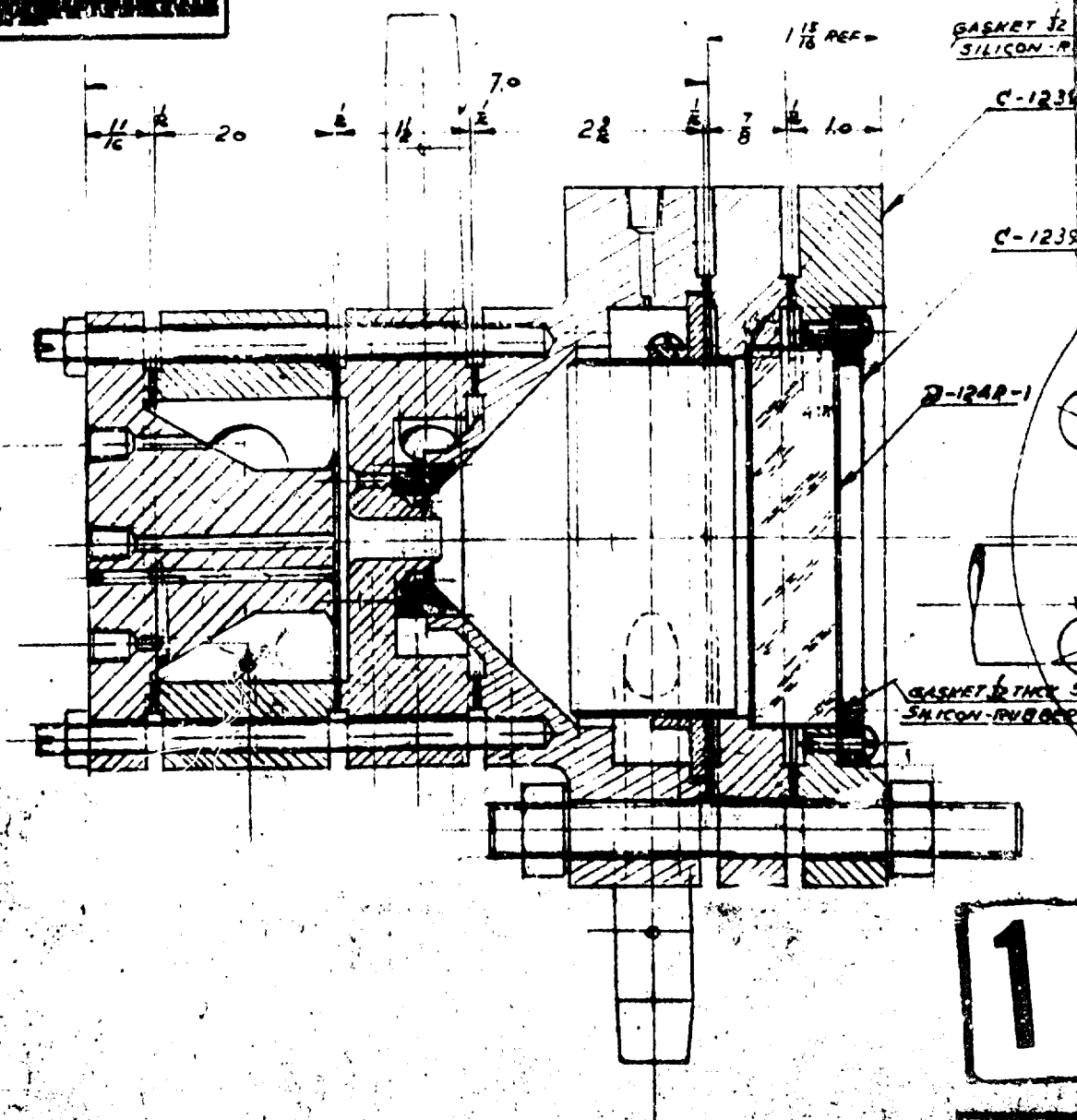
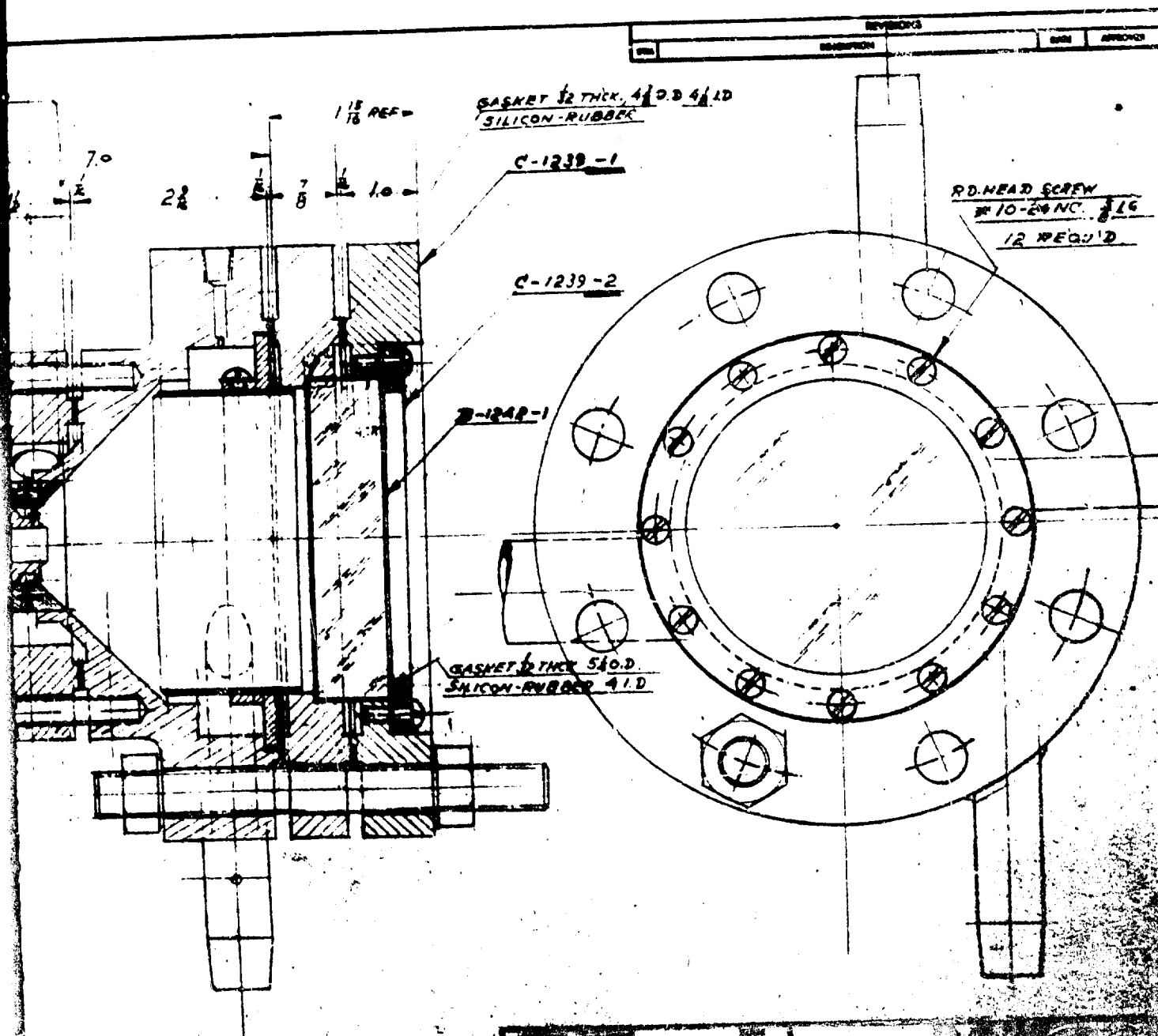


Fig. 50 Assembly of Visual Single Cell Swirl

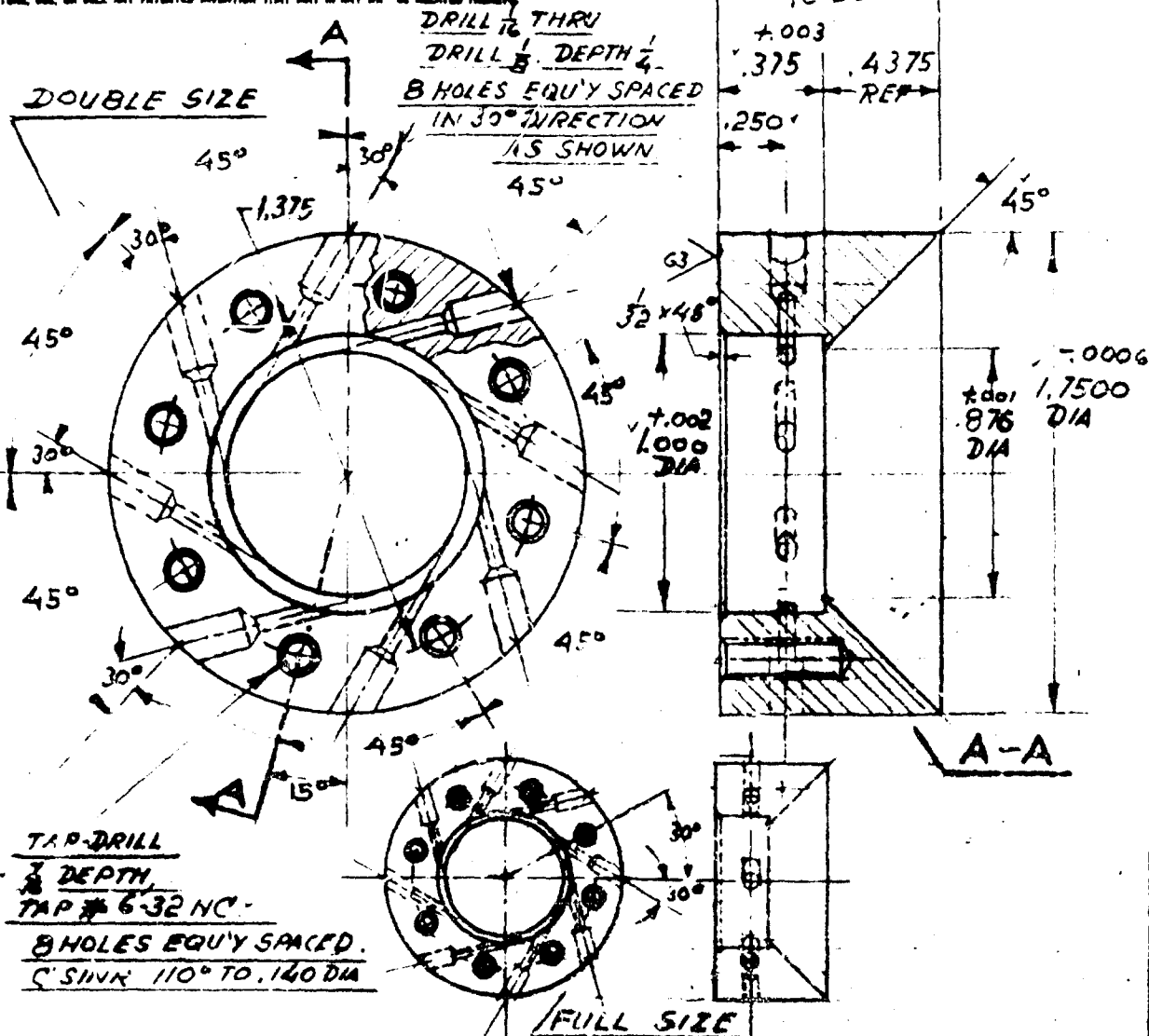


REV	DESCRIPTION	DATE	APPROVED
1	3/16	7/6	
2	7		

60 Assembly of Visual Single Cell Swirl Chamber

GAM/ME/64-14

NOTES: WHEN GOVERNMENT DRAWINGS, SPECIFICATIONS, OR OTHER DATA ARE USED FOR ANY PURPOSE OTHER THAN IN CONNECTION WITH A SPECIFICALLY RELATED GOVERNMENT PROCUREMENT OPERATION, THE UNITED STATES GOVERNMENT THEREBY INCURS NO RESPONSIBILITY, NOR ANY OBLIGATION WHATSOEVER, AND THE FACT THAT THE GOVERNMENT MAY HAVE PROVIDED OR FURNISHED, OR IN ANY WAY SUPPLIED THE SAME DRAWINGS, SPECIFICATIONS, OR OTHER DATA, IS NOT TO BE REGARDED BY REPLICATION OR OTHERWISE AS IN ANY MANNER LICENSES THE REPRODUCER OR ANY OTHER PERSON OR CORPORATION, OR CONVEYING ANY RIGHTS OR PERMISSIONS TO REPRODUCE, USE, OR SELL ANY PATENTED INVENTION THAT MAY IN ANY WAY BE RELATED THERETO.



B-1217-I: LEFT HAND NOZZLE RING

**REMOVE BURRS
FINISH AS NOTED**

UNLESS OTHERWISE SPECIFIED DIMENSIONS ARE IN INCHES TOLERANCES ON			DRAFTSMAN
FRACTIONS	DECIMALS	ANGLES	CHECKER
±	±.003	±	CONSULT ENGINEER
MATERIAL STEEL			DW
TREATMENT			CHAMBER
FINISH			AUTHENTICATION

AF Form 100-2 Rev 18 Previous editions of this form may be used.

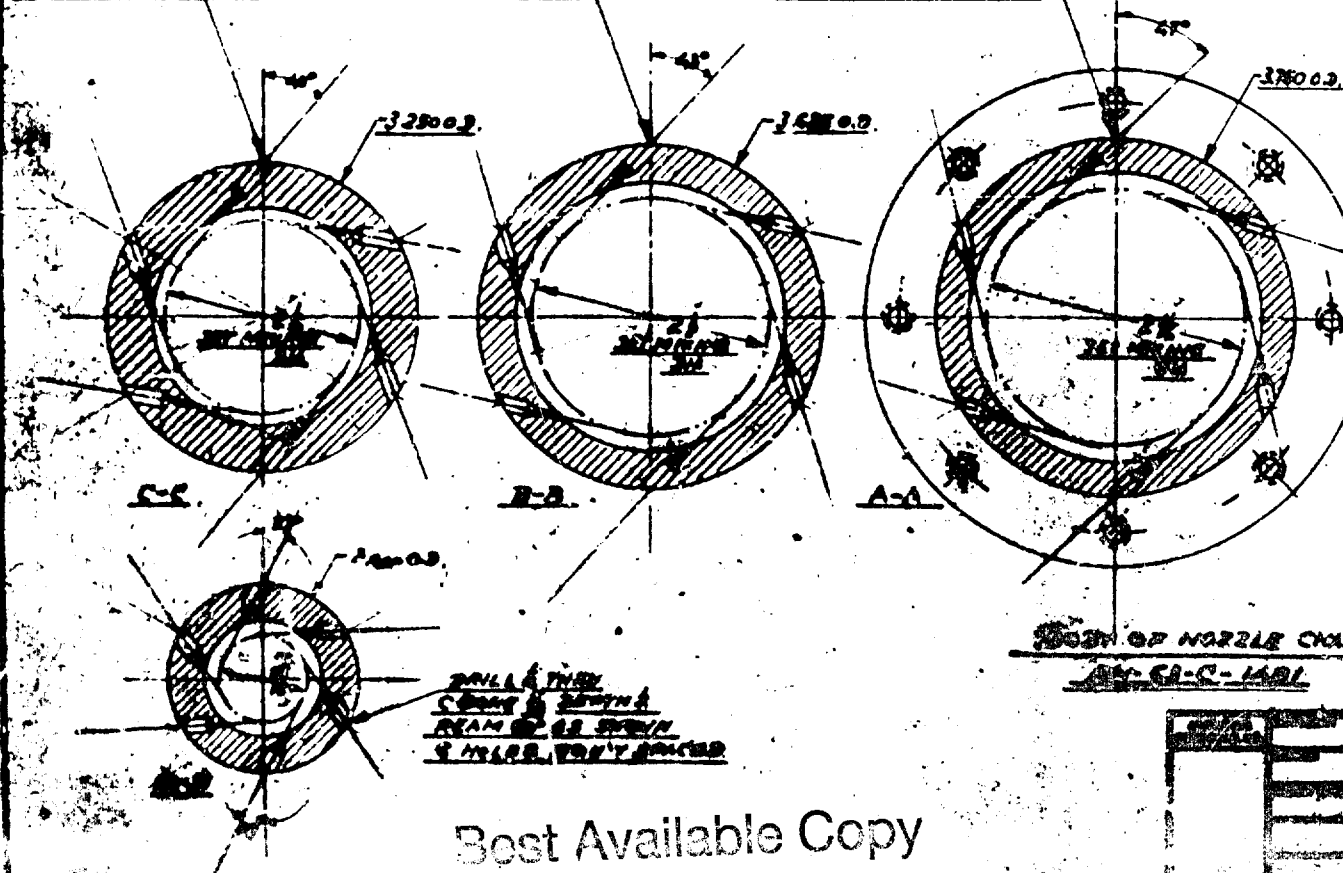
Fig. 51 Nozzle Ring for First Compressor

1

DRILL & TAP
C BORE & DEPTH
REAM 60° AS SHOWN
6 HOLES EQU'Y SPACED

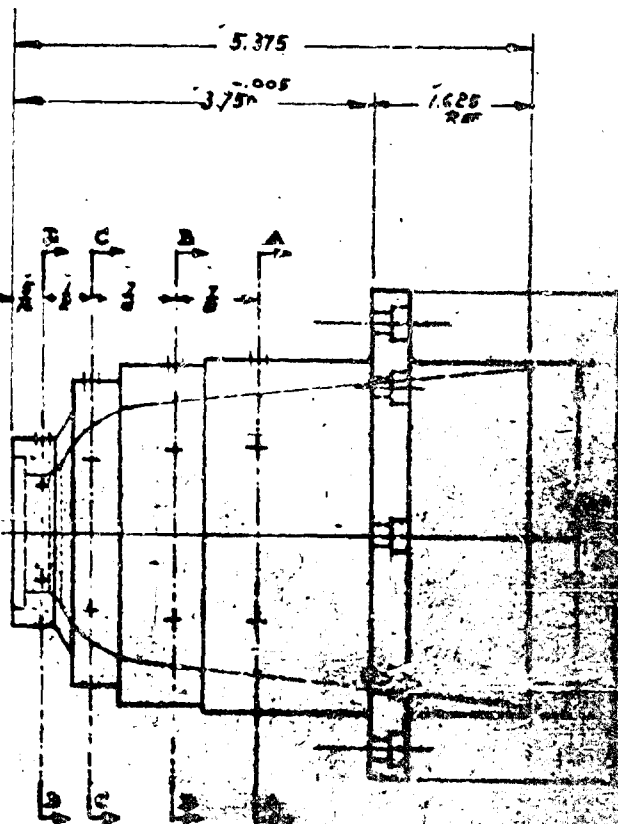
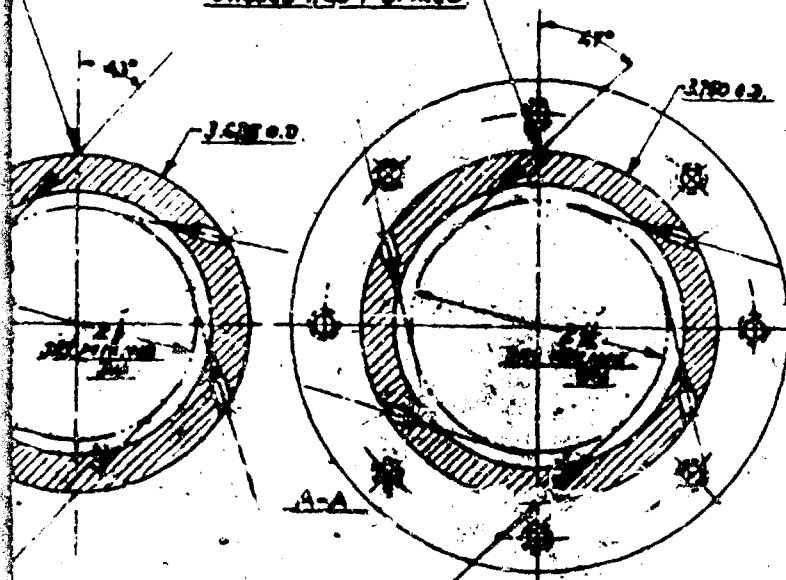
DRILL & TAP
C BORE & DEPTH
REAM 60° AS SHOWN
6 HOLES EQU'Y SPACED

DRILL & TAP
C BORE & DEPTH
REAM 60° AS SHOWN
6 HOLES EQU'Y SPACED



REVISED		DATE	APPROVED
NO.	DESCRIPTION	DATE	APPROVED

2001 1/2 TWIN
 CHARGE 1/2 BIRTH 1/2
 FROM 50 1/2 1/2 1/2
 SAMPLE 1/2 1/2 1/2



BODY OF NOZZLE CHANGED
 NO. 51-C-1601

2001 1/2
 2001 1/2
 1/2 1/2 1/2



Multiple Chamber Housing for Second Generation Chamber

Best Available Copy

2

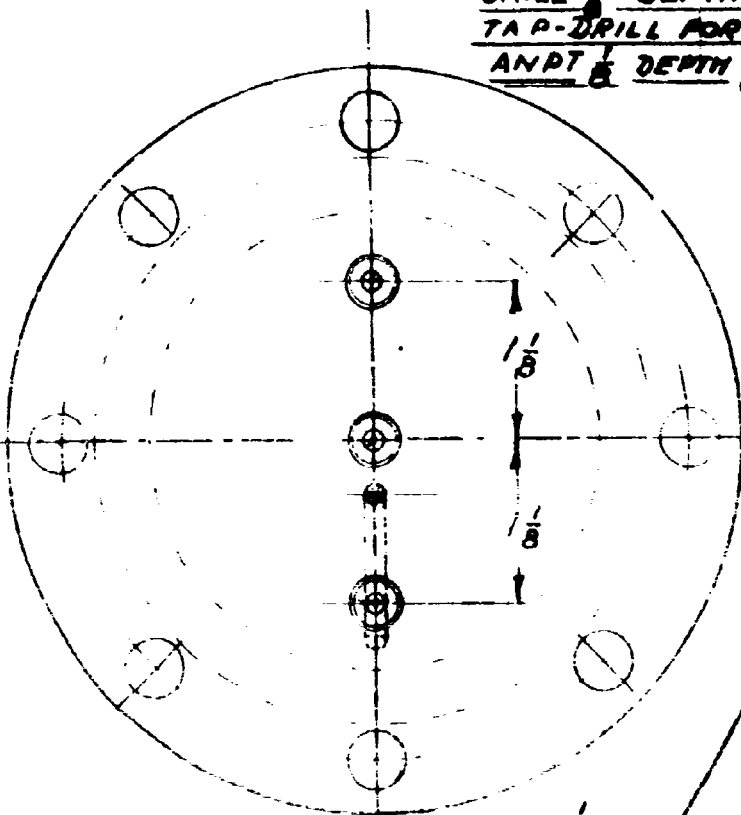
1

DRILL 16 THRU
DRILL DEPTH
TAP-DRILL FOR
ANPT DEPTH

DRILL 7
8 HOLES EQ

-B-1220-J

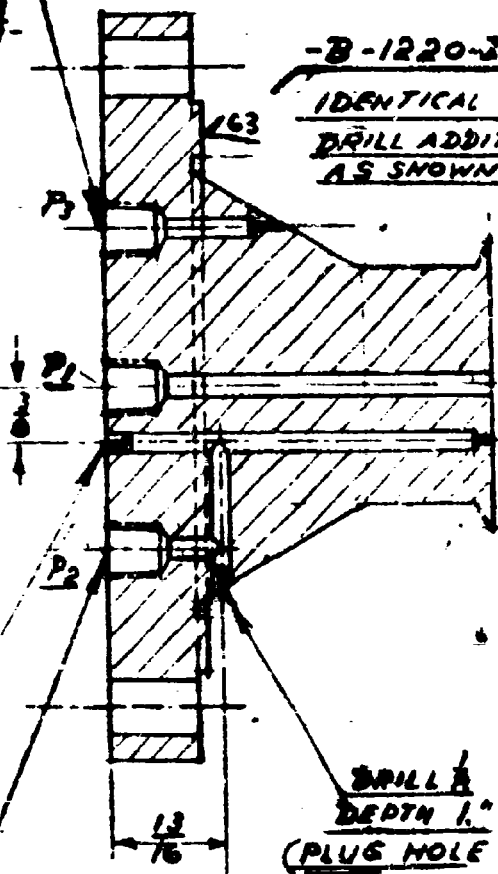
IDENTICAL WITH
DRILL ADDITION
AS SHOWN.



DRILL $\frac{1}{16}$ THRU
DRILL $\frac{1}{8}$ DEPTH $2\frac{5}{8}$
(PLUG HOLE AS SHOWN)

DRILL DEPTH
TAP-DRILL FOR
ANPT, DEPTH

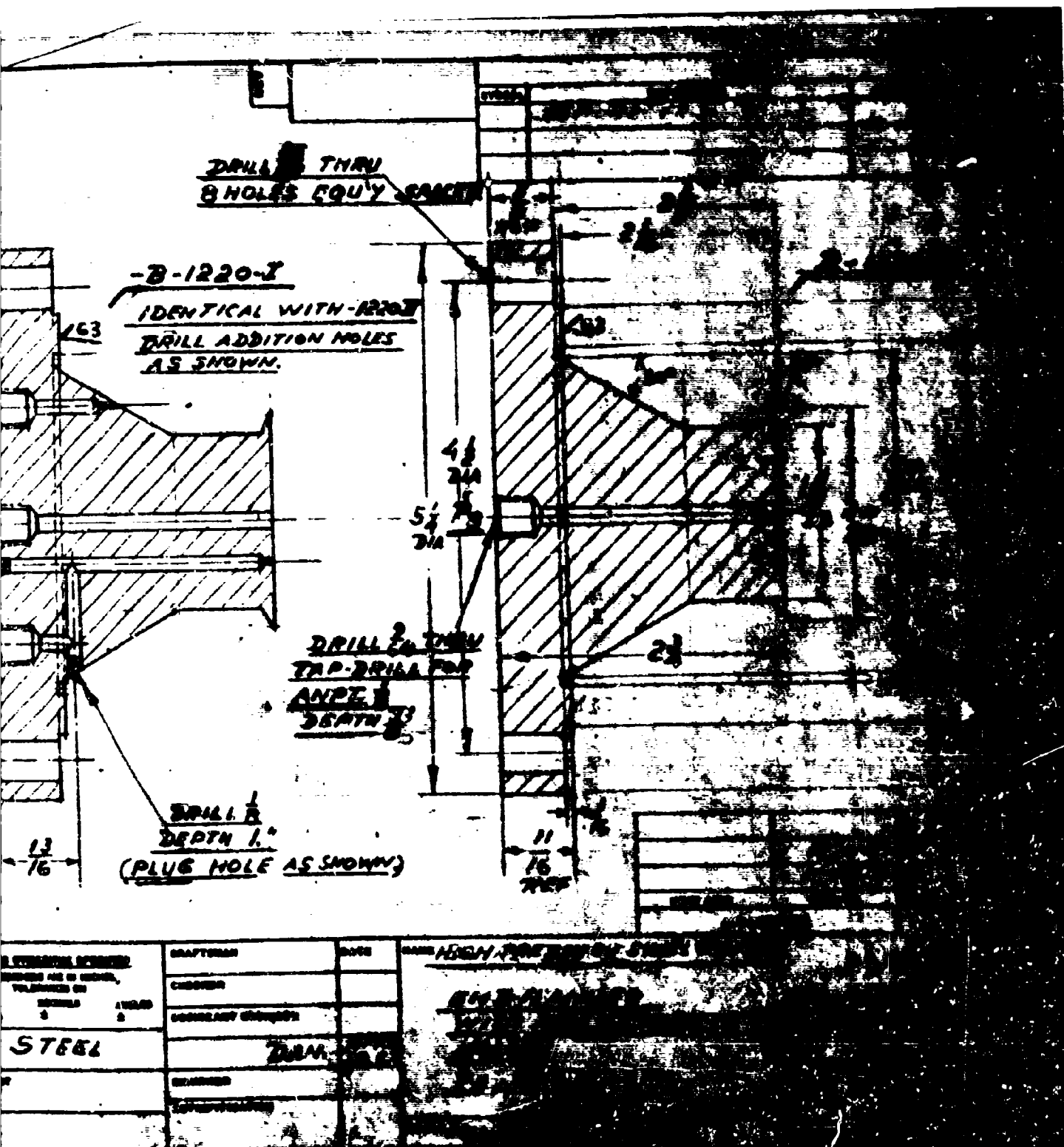
REMOVE BURRS & SHARP EDGES
FINISH AS NOTED



DA
TAP
ANY
DEA

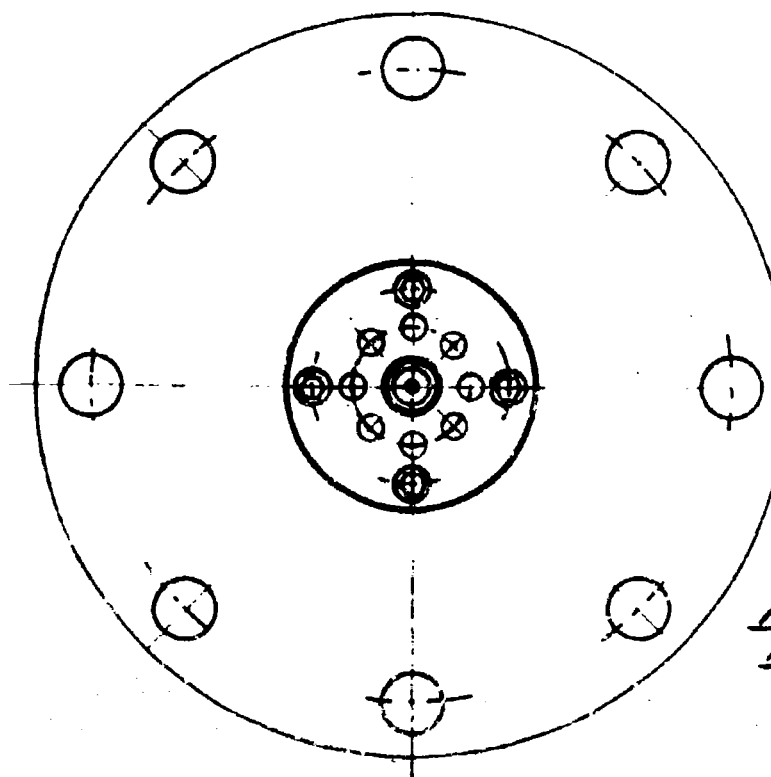
DRILL
DEPTH 1."
(PLUG HOLE AS SH)

WALL STREET JOURNAL COPIES ARE IN ROOM TELETYPE ON			CRAFTMAN
PENDING 2	SPECIALS 2	ANALYST 2	CHECKER
MATERIAL STEEL			COORDINATOR
VERIFICATION			DAN.
PENDING			EXAMINER
PENDING			APPROVED



GAM/ME/64-14

NOTICE: WHEN GOVERNMENT DRAWINGS, SPECIFICATIONS, OR OTHER DATA ARE USED FOR ANY PURPOSE OTHER THAN IN CONNECTION WITH A SPECIFICALLY RELATED GOVERNMENT PROCUREMENT OPERATION, THE UNITED STATES GOVERNMENT THEREBY INCURS NO RESPONSIBILITY, AND ANY RELATIONS WHATSOEVER, AND THE FACT THAT THE GOVERNMENT MAY HAVE FORMULATED, FURNISHED, OR IN ANY WAY SUPPLIED THE SAID DRAWINGS, SPECIFICATIONS, OR OTHER DATA IS NOT TO BE REGARDED BY IMPLICATION OR OTHERWISE AS IN ANY MANNER LICENSES THE HOLDER OR ANY OTHER PERSON OR CORPORATION, OR CONVEYS ANY RIGHTS OR PERMISSION TO REPRODUCE, USE, OR SELL ANY PATENTED INVENTION THAT MAY IN ANY WAY BE RELATED THEREIN.



RN-63-B-1303

RN-63-A-1304

ALLEN HEAD SCREW
1/2 G-32 NC. 1/8 16
6 REQUIRED.

2 REQ

UNION STEEL & CO.			DRAFTSMAN
REINFORCED AND IN VARIOUS			CHECKER
SIZES AND			CONSULT ENGINEER
FOR COLUMNS			DAN
INTERNAL STEEL			LEARNER
TREATMENT			AUTHENTICATOR
FINISH			

AP Form 1000 Sup 60 Replaces Form 1000 of 10-1-54

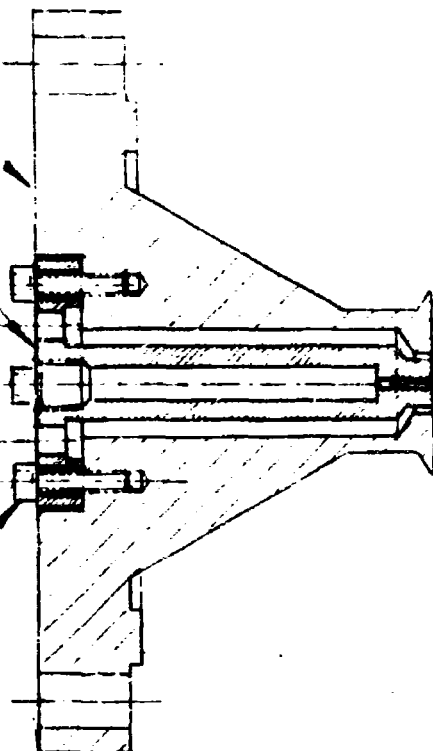
Fig. 54 Cross Section

REV	REVISIONS			
	SYMBOL	DESCRIPTION	DATE	APPROVAL

V-63-B-1303

V-63-A-1304

HEAD SCREW
#32 NC. $\frac{5}{16}$ IN
REQU'D.



2 REQU'D.

NEXT ASSY	USED G3	TEST ASSY	FINAL ASSY
APPLICATION		QUANTITY REQD.	

DESIGNED BY CHECKED APPROVED DATE	DRAFTSMAN	DATE	NAME <u>SWIRL CHAMBER</u> <u>ASSEMBLY</u> <u>REWORK FLANGE-CONE</u> <u>WITH NOZZLE</u>	U. S. AIR FORCE <u>REG. NO. I-B2</u> FIG. NO. <u>RN-63-B-1302</u>
	ENGINEER			
	CONSTRUCTION ENGINEER			
	DAN	JUNE 1952		
	CRAMER		SCALE <u>PIN SIZE</u>	
	AUTHORIZATION			

2

54 Cross Section of Bleed Diffusers

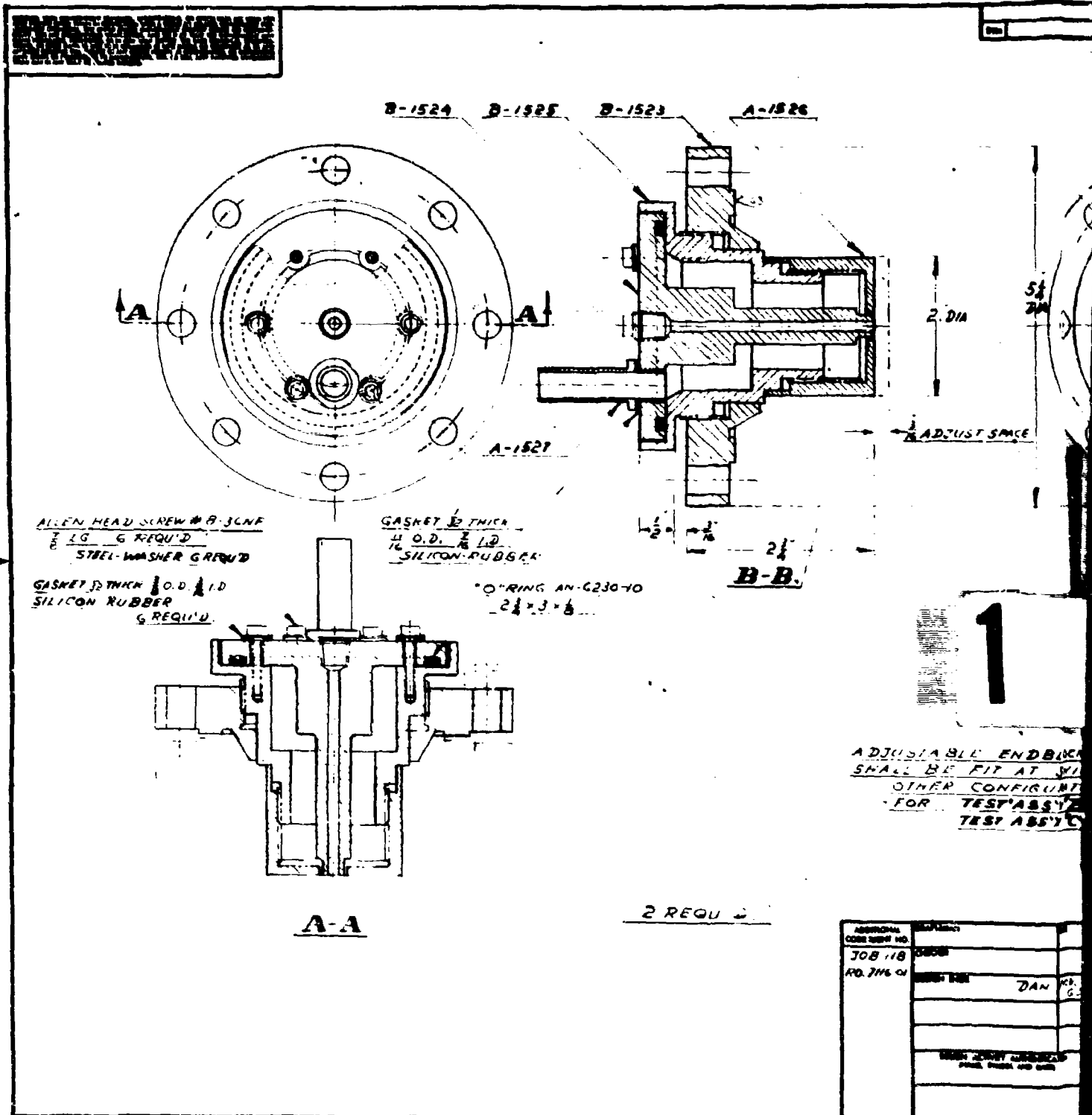
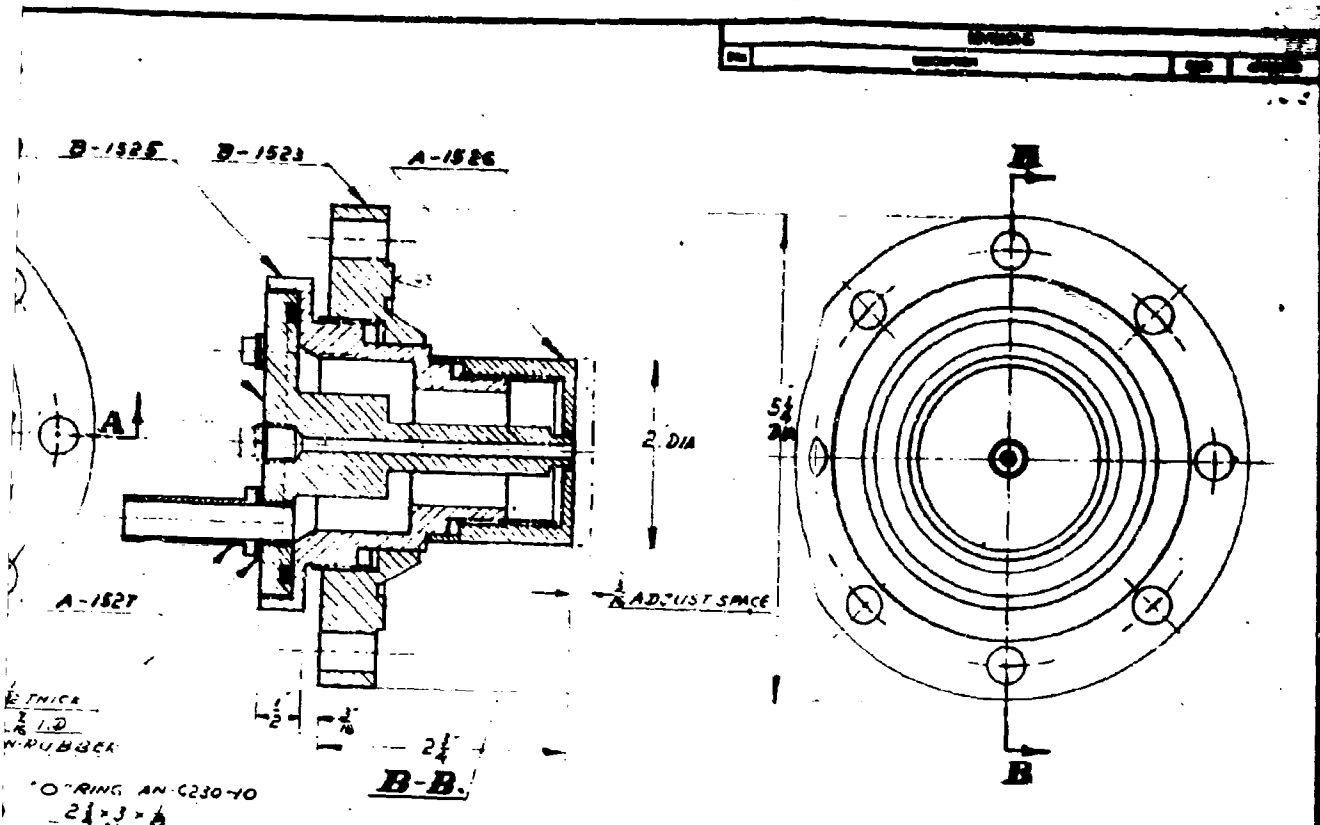


Fig. 55 Crank Diffuser for Second Generation Saturn Car



ADJUSTABLE ENDBLOCK FOR TESTING
 SHALL BE FIT AT SWIRL-CHAMBERS FOR HIGH PRESSURE
 OTHER CONFIGURATION SHOWN
 FOR TEST ASSY "B" RN-63-B-1530 - OAKAL WIND TUNN.
 TEST ASSY "C" RN-63-B-1535 - ELECTRIC WIND TUNN.

2 REQUIRED

ADDITIONAL CODE NO. 708.9 RD 716.01		U.S. AIR FORCE REG. NO. II-B-2 TO SWIRL-CHAMBER HIGH PRESSURE ADJUSTABLE ENDBLOCK WITH RING-SLOT DEVICE TEST-ASSEMBLY "A"	
DATE: JAN 61 BY: DAN		ONE TEST NO. C RN-63-C-1522	

2

Frank Diffuser for Second Generation Swirl Chamber

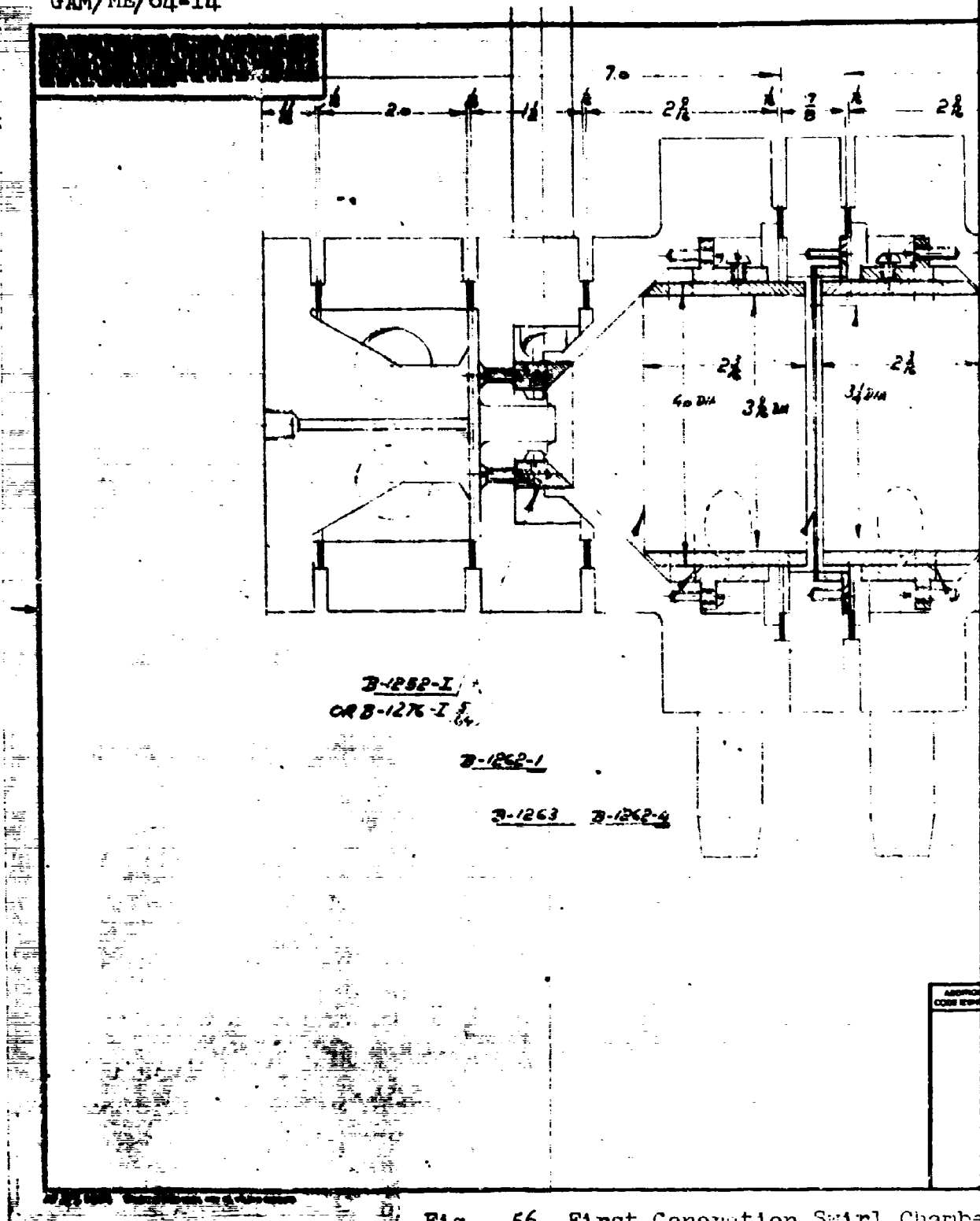
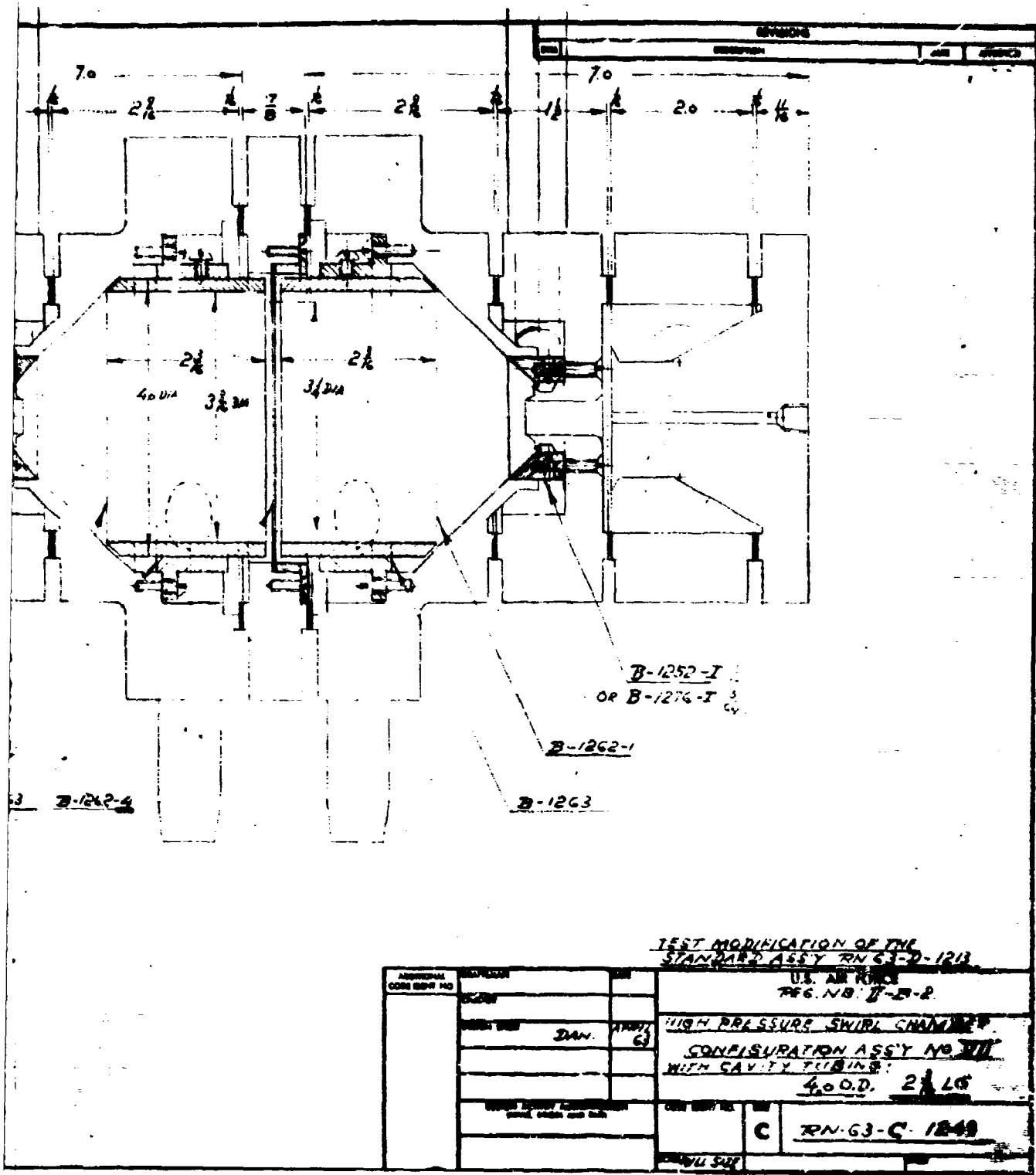
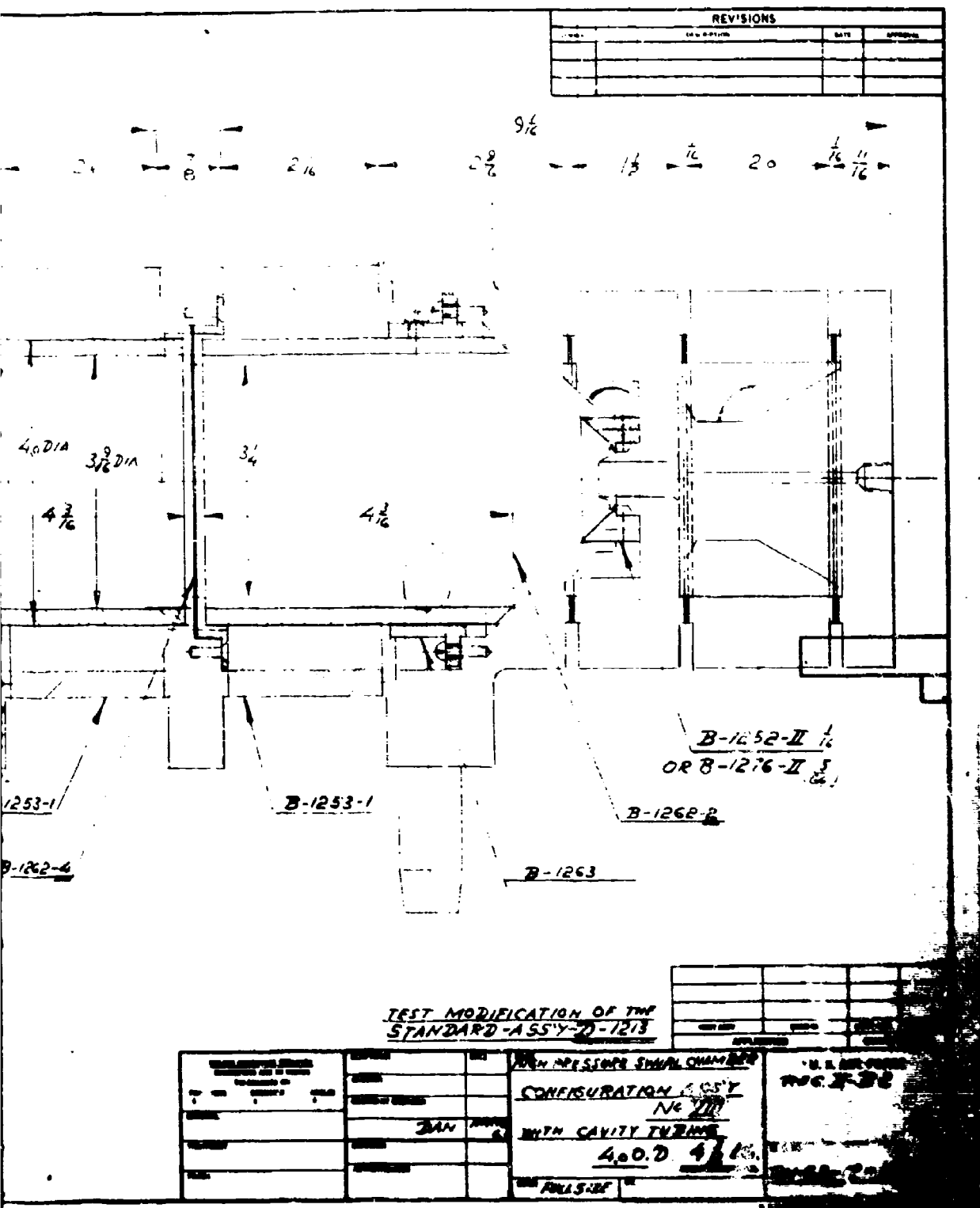


Fig. 56 First Generation Swirl Chamber



First Generation Swirl Chamber with g - Insert



Generation Swirl Chamber with h - Insert

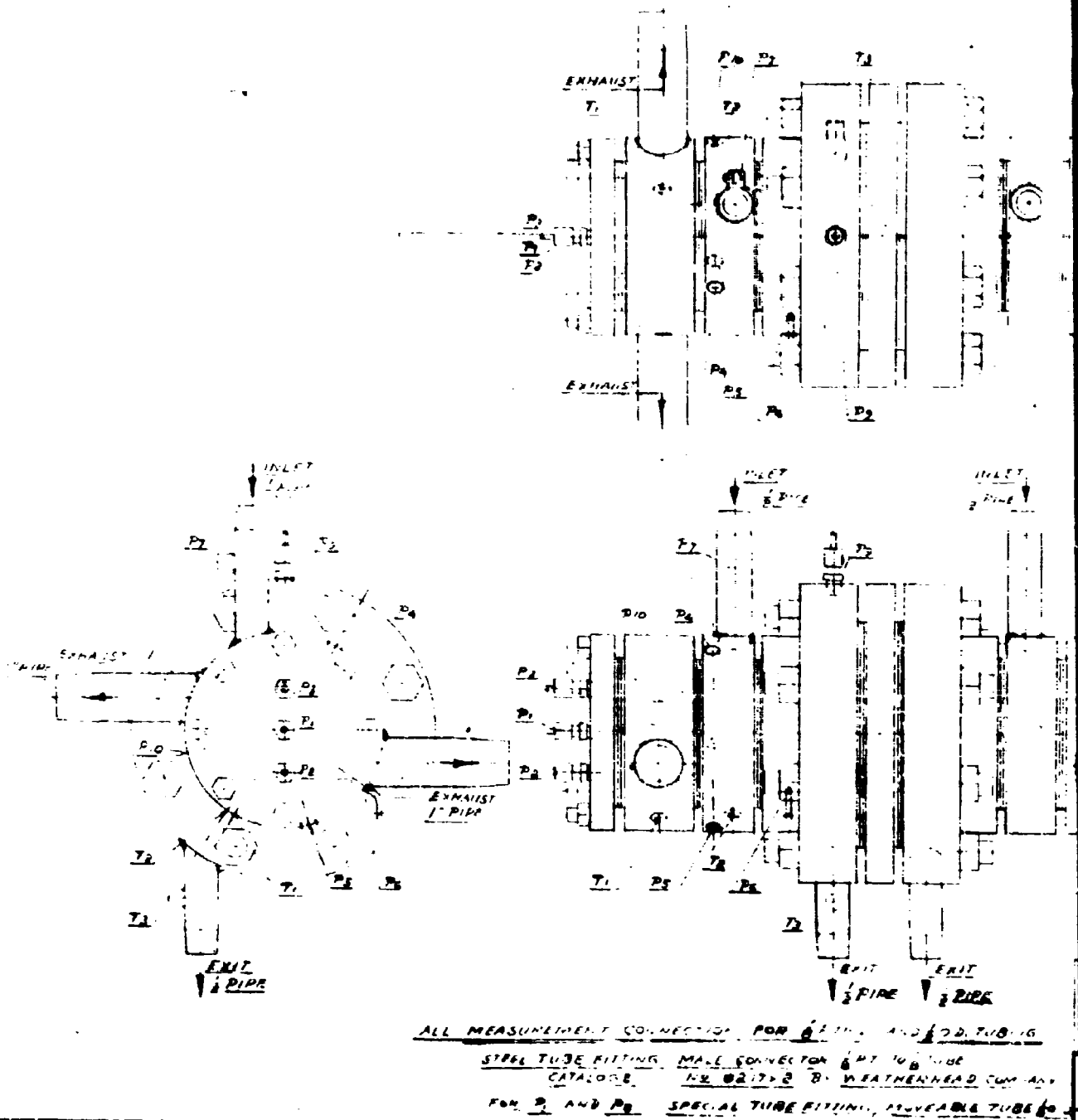
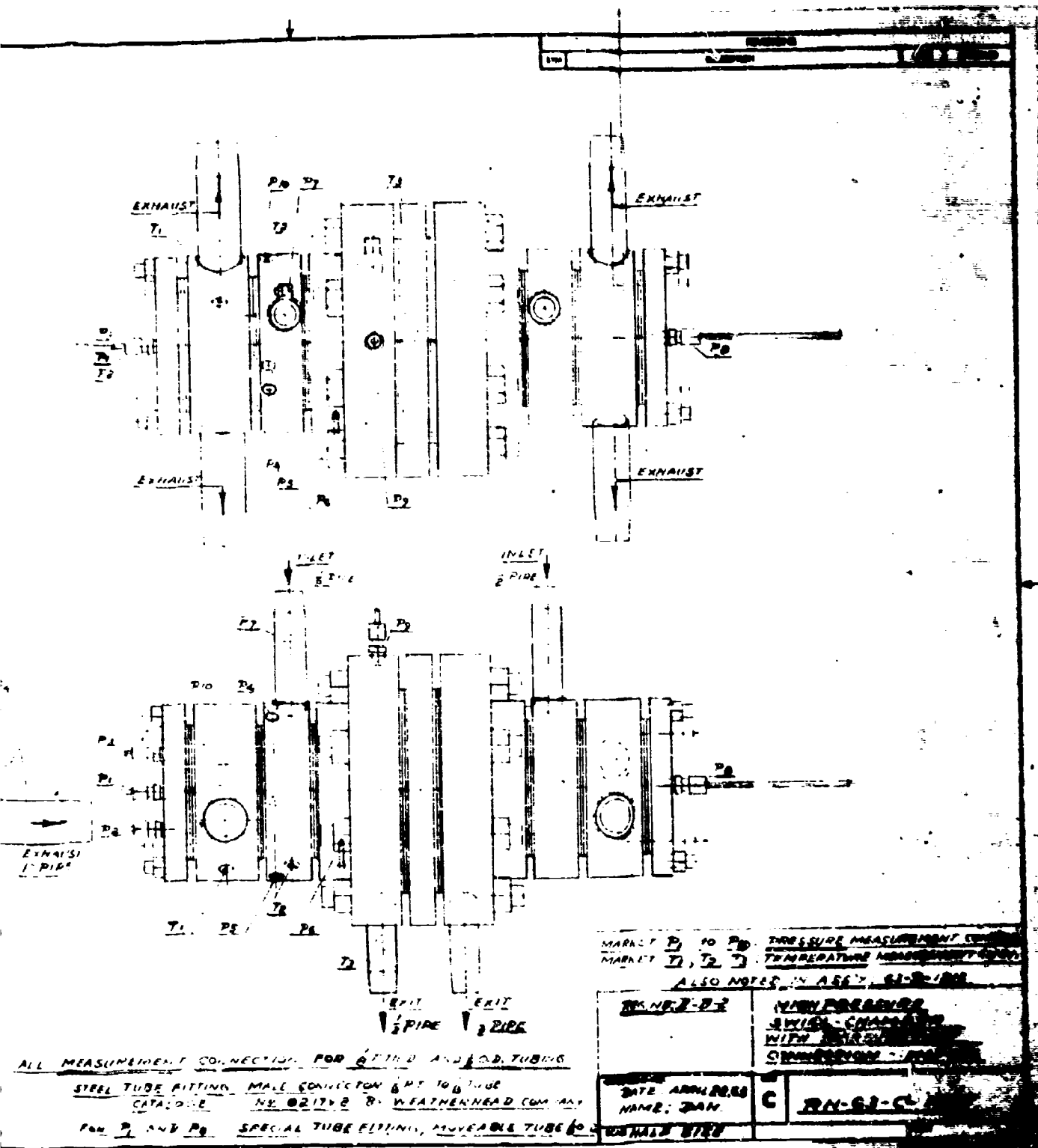


Fig. 59 Pressure and Temperature Connections for First Gear



Pressure and Temperature Connections for First Separation Chamber

GAN/HE/64-14

Appendix B

Swirl Chamber Identification Code
and
Graphical Data

Swirl Chamber Identification Code

Due to the extensive amount of modification and testing on the first generation swirl chamber, a code was developed to facilitate identification of the various tests. The code for the first generation swirl chamber has eight groupings. A typical code is

D-1/16-a-I-3-1/16-239.3-1

The groupings are respectively:

1. Chamber type

D-dual cell swirl chamber

S-single cell swirl chamber

V-single cell visual swirl chamber

2. Nozzle ring type

1/16-one-sixteenth inch nozzle throat diameter; eight nozzles per ring.

3/32-three-thirty second inch nozzle throat diameter; eight nozzles per ring.

1/3-one-eighth inch nozzle throat diameter; eight nozzles per ring.

3. Chamber insert size

a-1 13/16 "ID x 3 1/8" Long

b-1 13/16 "ID x 5 1/8" Long

c-1 13/16 "ID x 7 1/8" Long

- d-2 13/16 "ID x 2 9/16" Long
- e-2 13/16 "ID x 4 9/16" Long
- f-2 13/16 "ID x 6 9/16" Long
- g-3 9/16 "ID x 2 3/16" Long
- h-3 9/16 "ID x 4 3/16" Long
- i-3 9/16 "ID x 6 3/16" Long

- 4. Internal method of exiting fluid (See Figs. 2 and 3).

I-first exiting position

II-second exiting position

- 5. Type of radial exhaust diffuser

B-bleed diffuser

K-blank diffuser

- 6. Diffuser wall spacing--the distance, in inches, between the admission chamber and the radial exhaust diffuser (See Fig. 11).

- 7. Total inlet pressure to the swirl chamber in psia.

- 8. Inlet geometry modifications--each higher number includes the preceeding modifications (See Fig. 11).

0-exhaust nose lip shaved off.

1-nozzle holes reamed and polished.

2-lips on nozzle ring half shaved off.

3-lips on nozzle ring completely removed.

GM/ME/94-14

4-nozzle ring taper increased.

5-exhaust cylinder shortened.

For the second generation chamber the first five groupings and the last group are fixed; therefore, only the sixth and seventh groupings are used to identify tests on the second generation chamber.

List of Graphical Data

Figure		Page
	Qualitative Graphical Data--Performance	
	Parameters as a Function of the Exit	
	Venturi Differential Pressure	
60	D-1/16-g-I-B-1/8-239.2-0	121
61	D-1/16-g-I-B-1/8-314.2-0	122
62	D-1/16-g-II-B-1/8-239.3-0	123
63	D-1/16-g-II-B-1/8-314.3-0	124
64	D-1/16-g-II-B-1/8-239.3-1	125
65	D-1/16-g-II-B-1/8-314.3-1	126
66	D-1/16-g-II-B-1/8-239.2-2	127
67	D-1/16-g-II-B-1/8-314.2-2	128
68	D-1/16-g-II-B-1/8-239.3-3	129
69	D-1/16-g-II-B-1/8-314.3-3	130
70	D-1/16-g-II-B-1/8-239.3-4	131
71	D-1/16-g-II-B-1/8-314.3-4	132
72	D-1/16-g-II-B-1/8-239.4-5	133
73	D-1/16-g-II-B-1/8-314.4-5	134
74	D-1/16-g-II-B-1/16-239.4-5	135
75	D-1/16-g-II-B-1/16-314.4-5	136
76	D-1/16-g-II-B-1/32-239.3-5	137
77	D-1/16-g-II-B-1/32-314.3-5	138

Figure		Page
78	D-1/16-g-II-B-1/64-239.3-5	140
79	D-1/16-g-II-B-1/64-314.3-5	141
80	D-1/16-g-II-N-1/32-239.1-5	142
81	D-1/16-g-II-N-1/16-239.1-5	143
82	D-1/16-g-II-N-3/32-239.1-5	144
83	D-1/16-g-II-N-4/32-239.1-5	145
84	D-1/16-g-II-N-5/32-239.1-5	146

Quantitative Graphical Data--Performance

Parameters and Inlet Mass Flow Rate as
a Function of the Mass Flow Ratio.

85	D-3/32-g-II-B-1/16-239.4-5	147
86	D-3/32-g-II-B-1/16-314.4-5	148
87	D-3/32-g-II-B-1/8-239.4-5	149
88	D-3/32-g-II-B-1/8-314.4-5	150
89	D-3/32-g-II-B-1/4-239.4-5	151
90	D-3/32-g-II-B-1/4-314.4-5	152
91	D-1/8-g-II-B-1/16-239.2-5	153
92	D-1/8-g-II-B-1/8-239.2-5	154
93	D-1/8-g-II-B-3/16-239.2-5	155
94	D-1/8-g-II-B-1/4-239.3-5	156
95	S-3/32-g-II-B-1/8-239.2-5	157
96	S-3/32-g-II-B-1/8-314.2-5	158
97	D-3/32-h-II-B-1/8-239.2-5	159
98	D-3/32-h-II-B-1/8-314.2-5	160

GAM/ME/64-14

Figure		Page
99	D-3/32-1-II-B-1/8-239.2-5	161
100	3/32-239.3	162
101	3/29-314.3	163

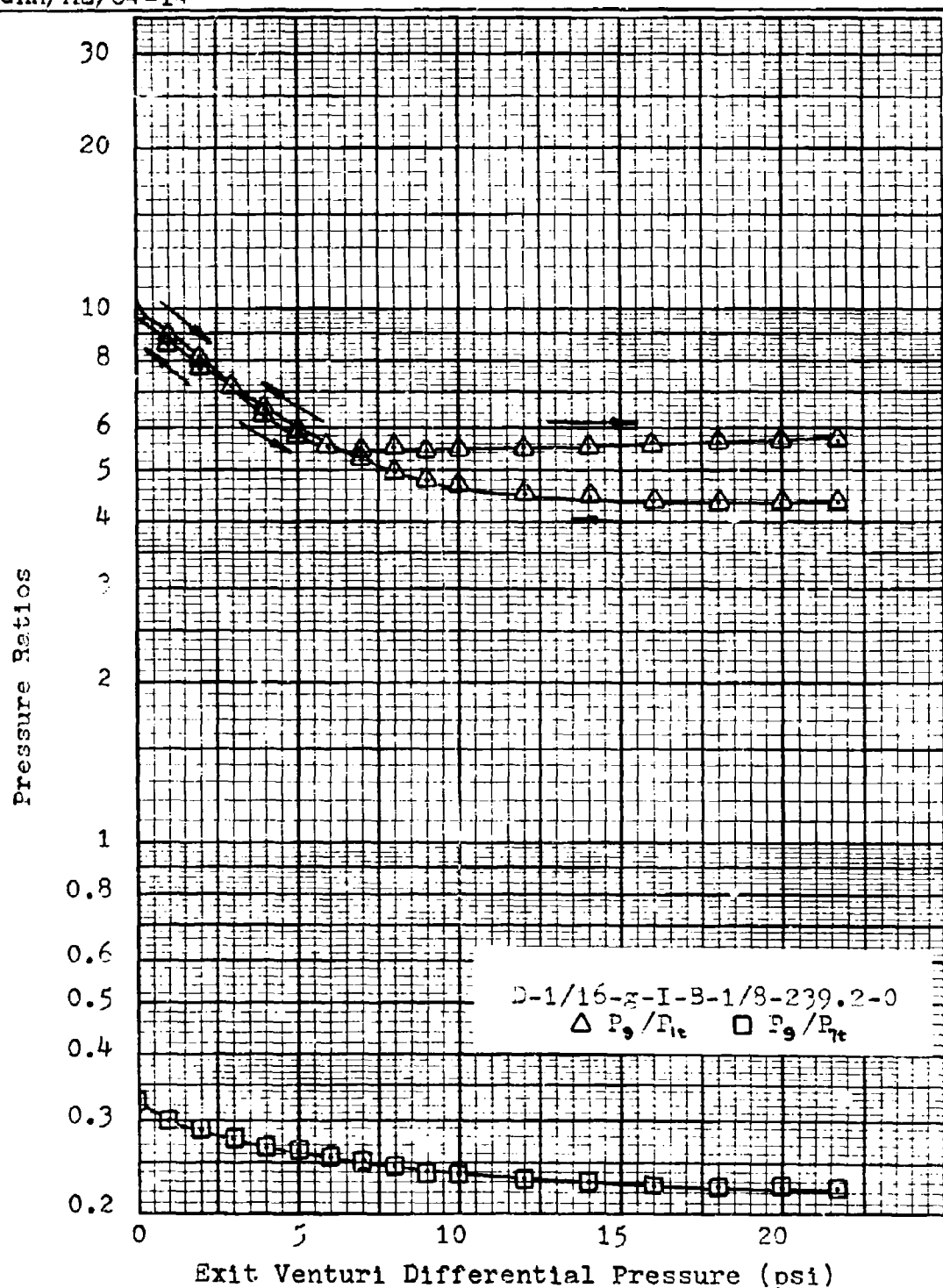
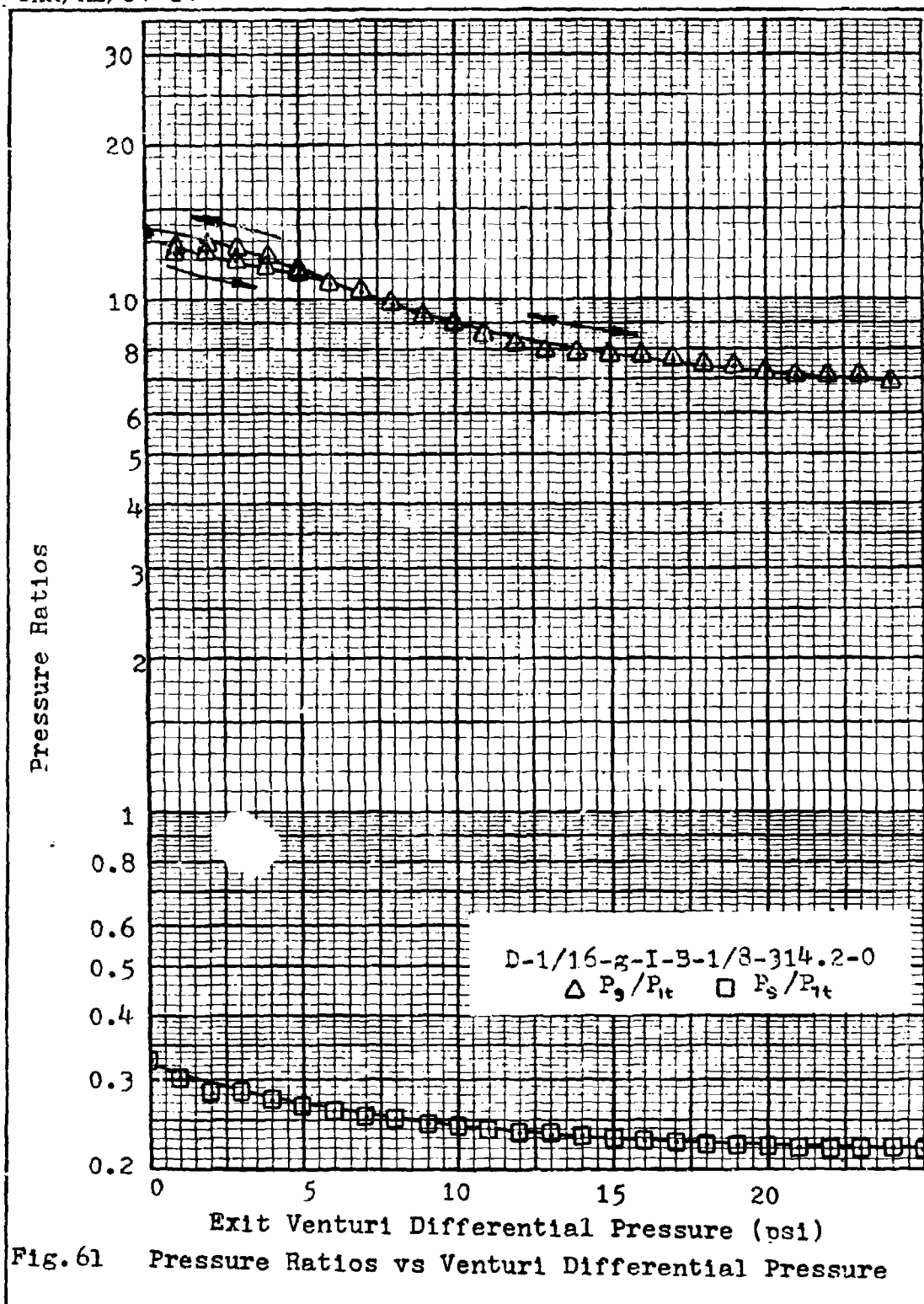
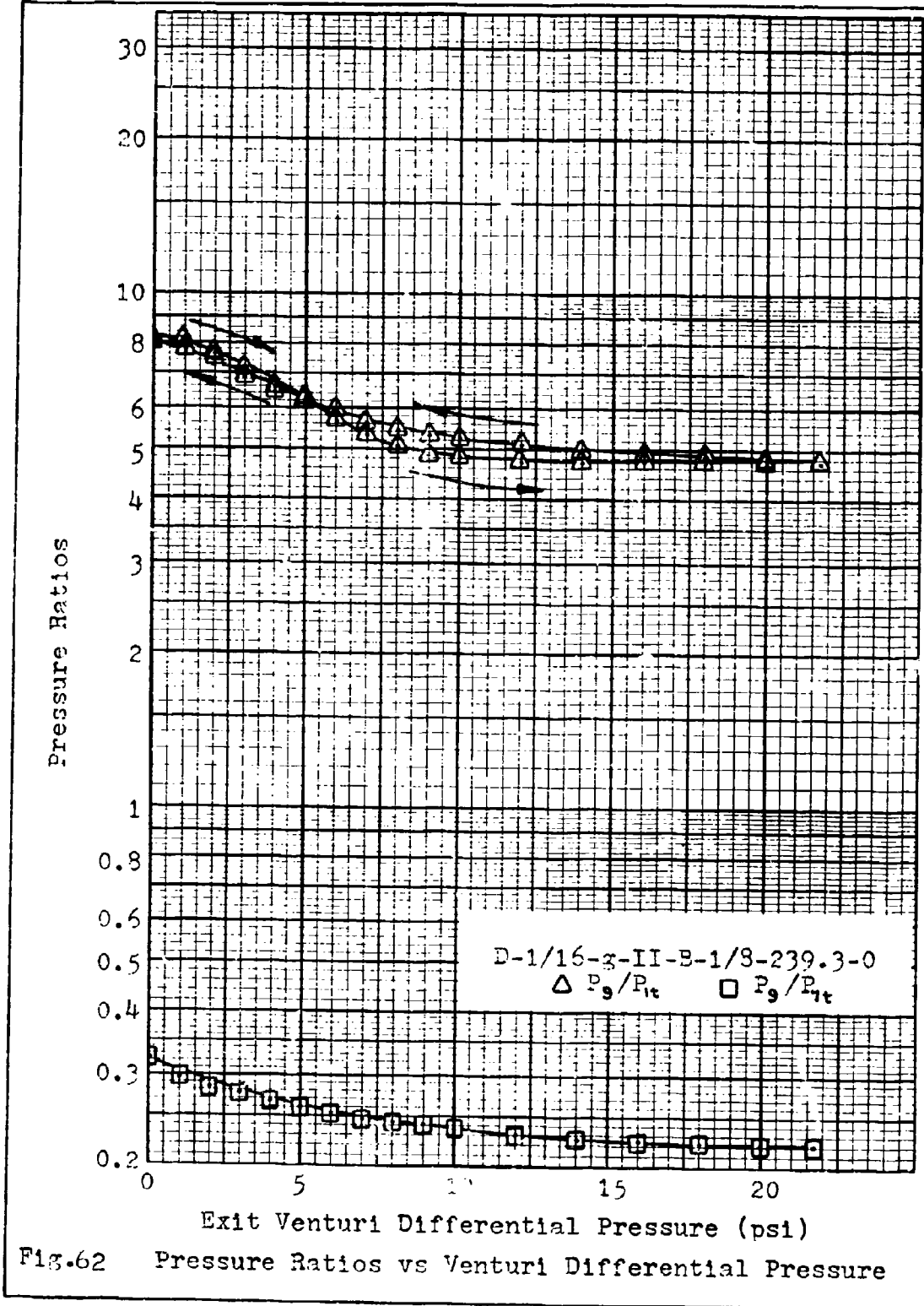
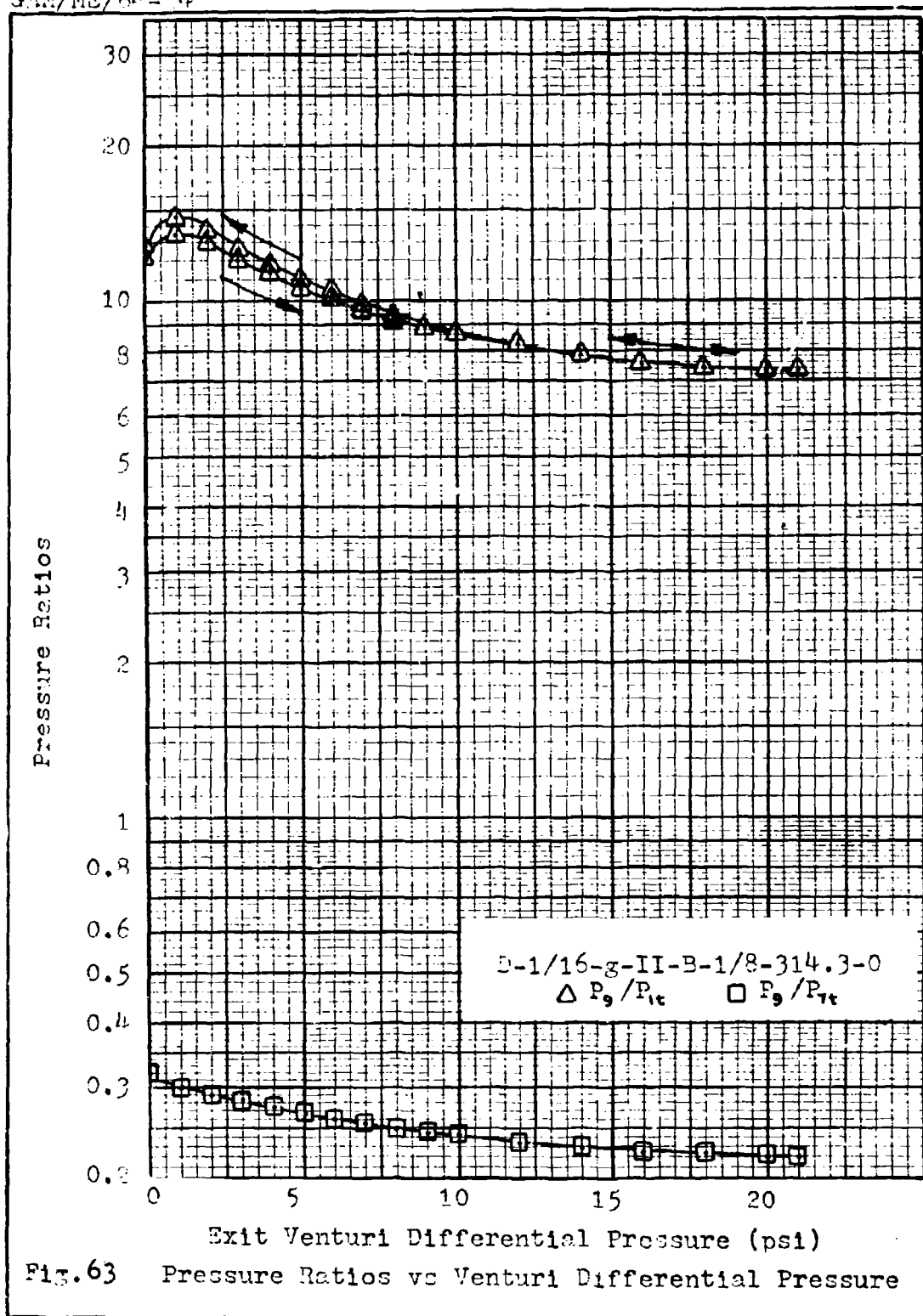
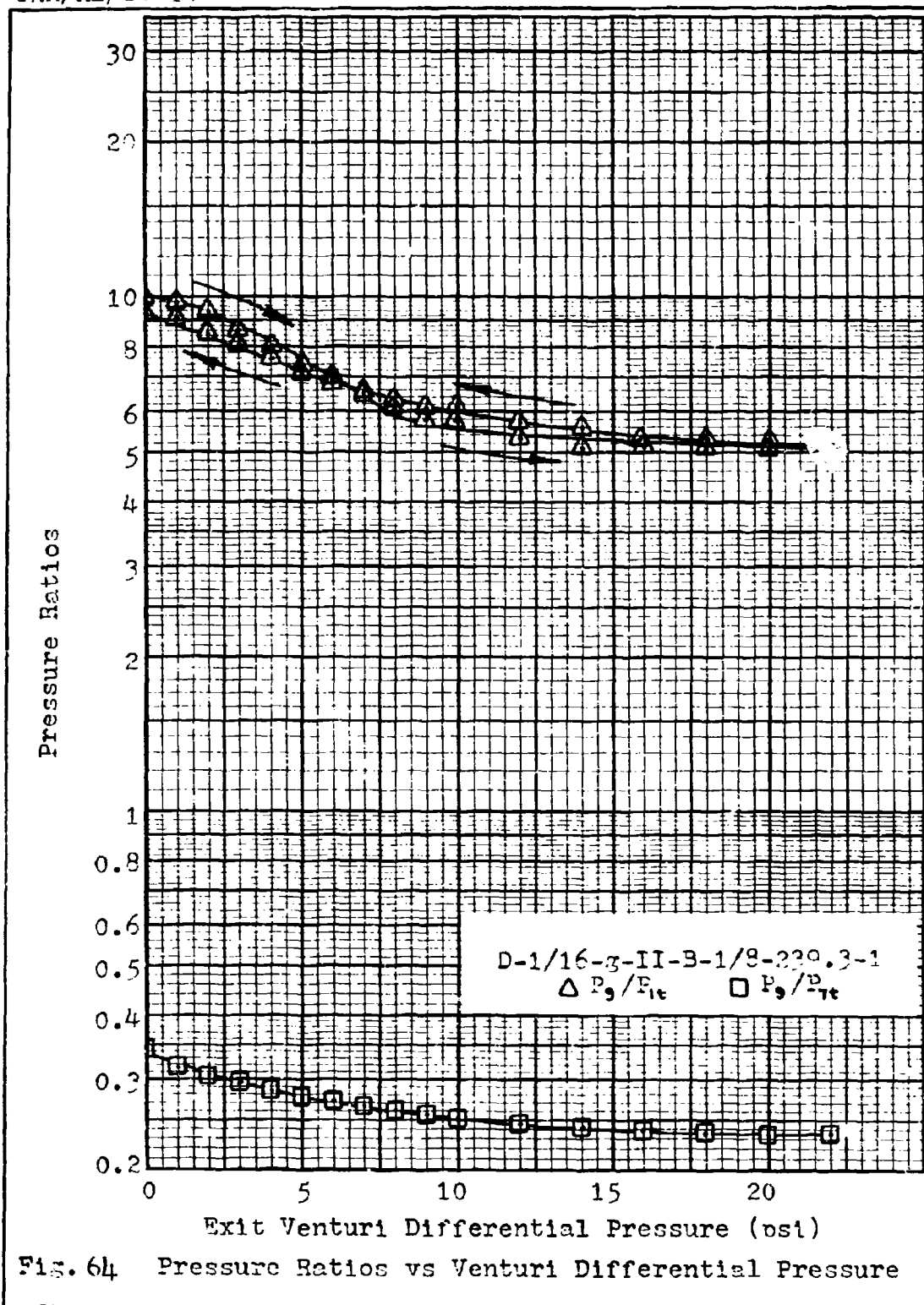


Fig. 60 Pressure Ratios vs Venturi Differential Pressure









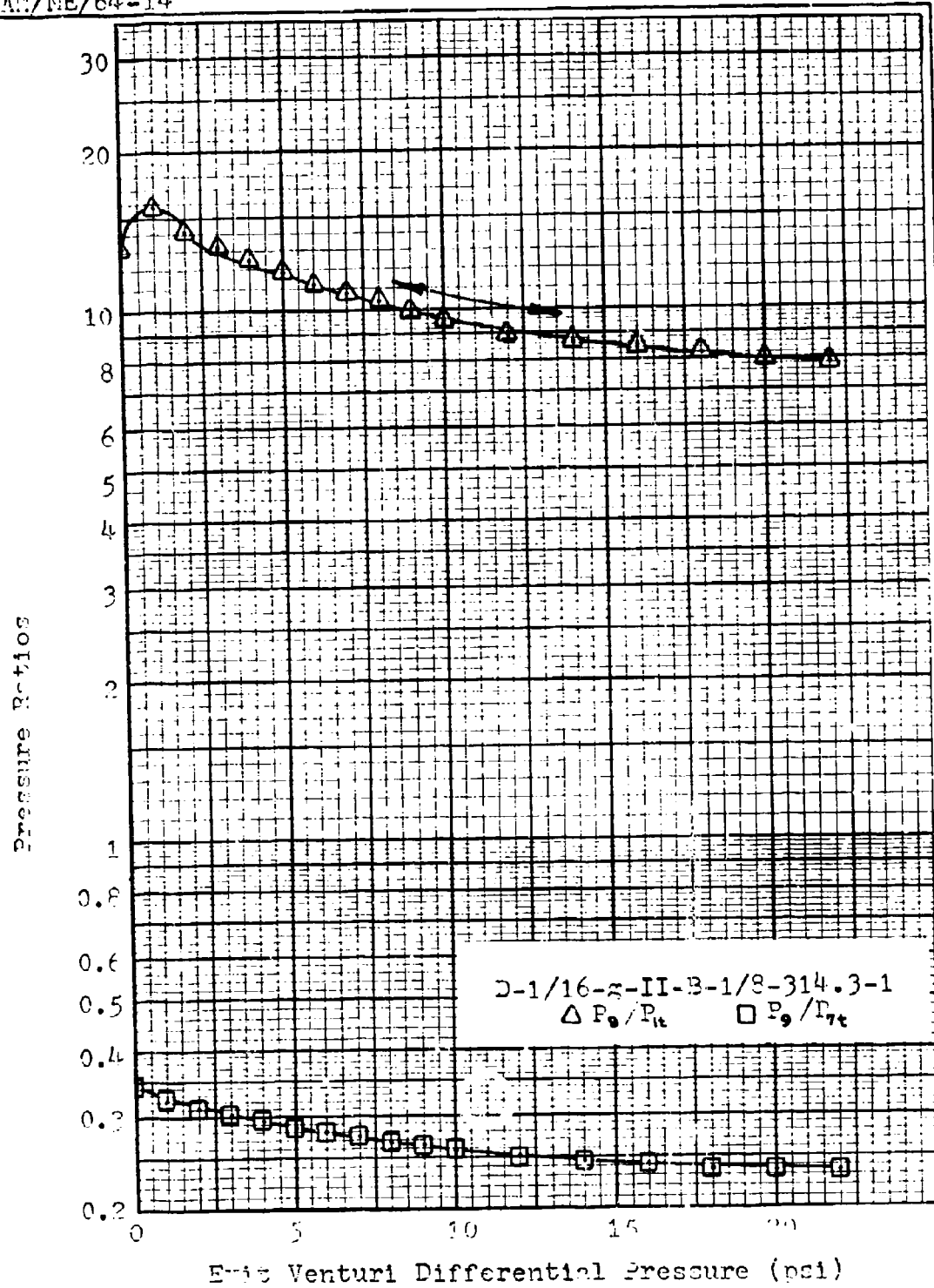
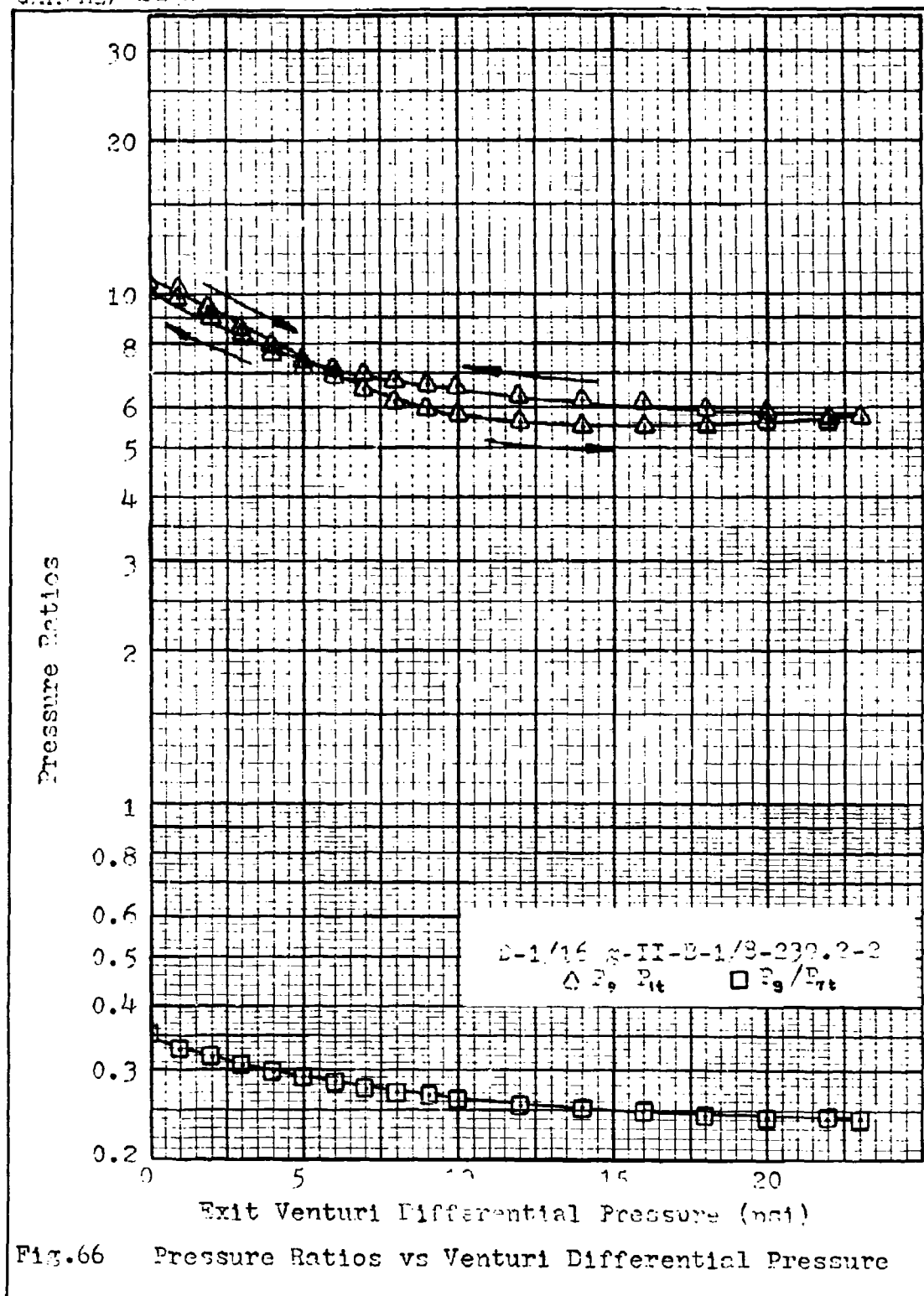


Fig. 65 Pressure Ratios vs Venturi Differential Pressure



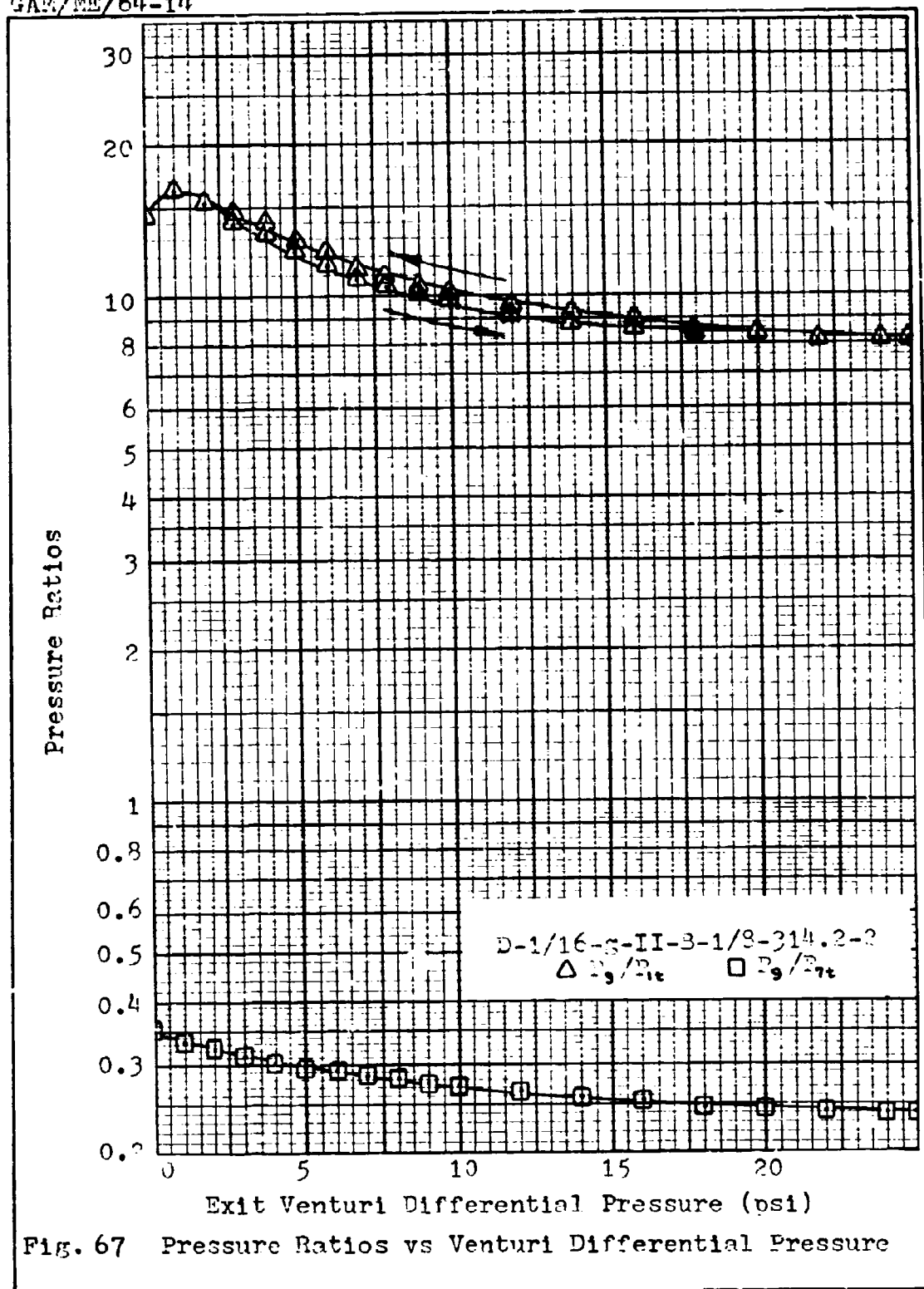


Fig. 67 Pressure Ratios vs Venturi Differential Pressure

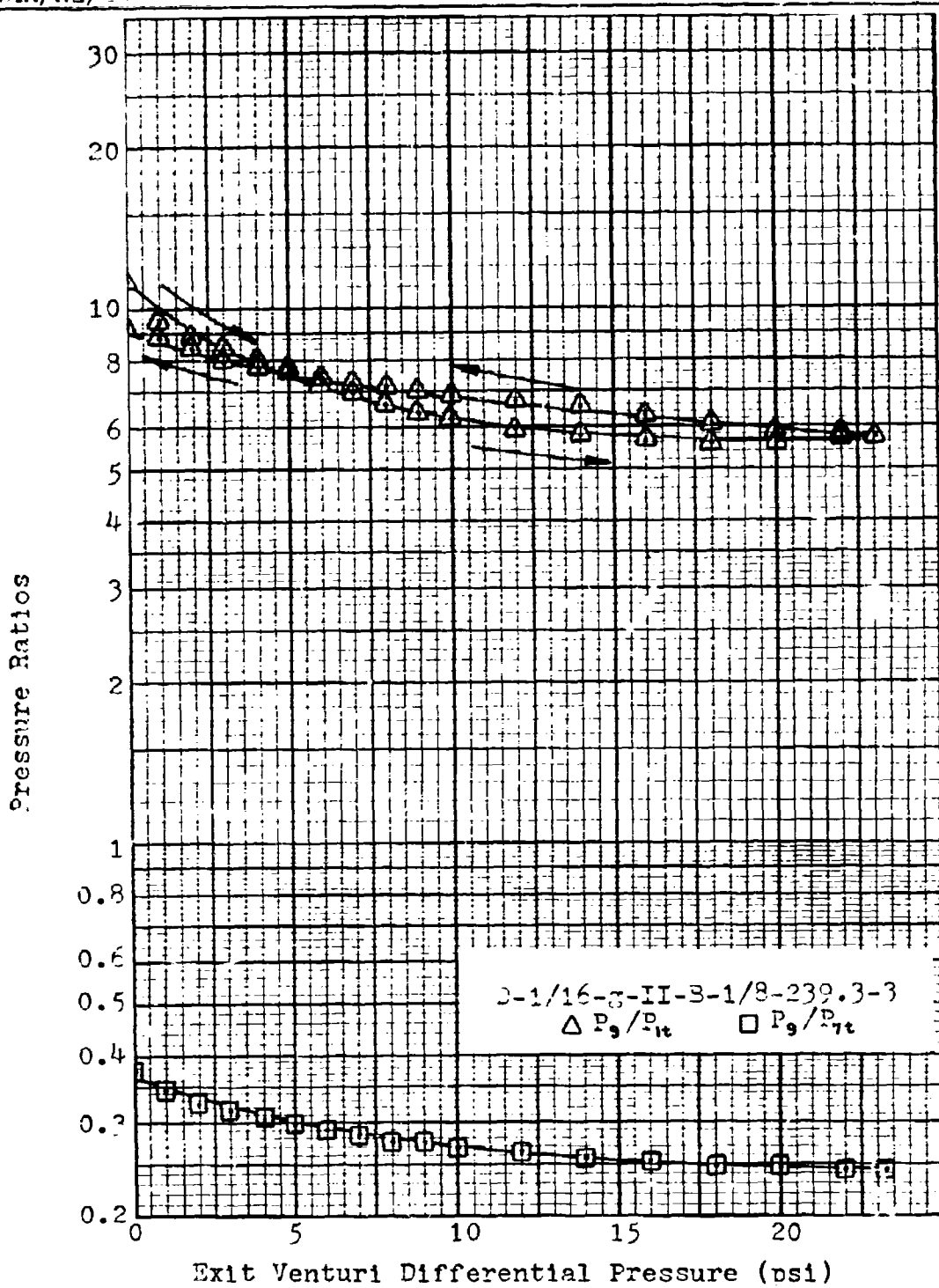


Fig. 68 Pressure Ratios vs Venturi Differential Pressure

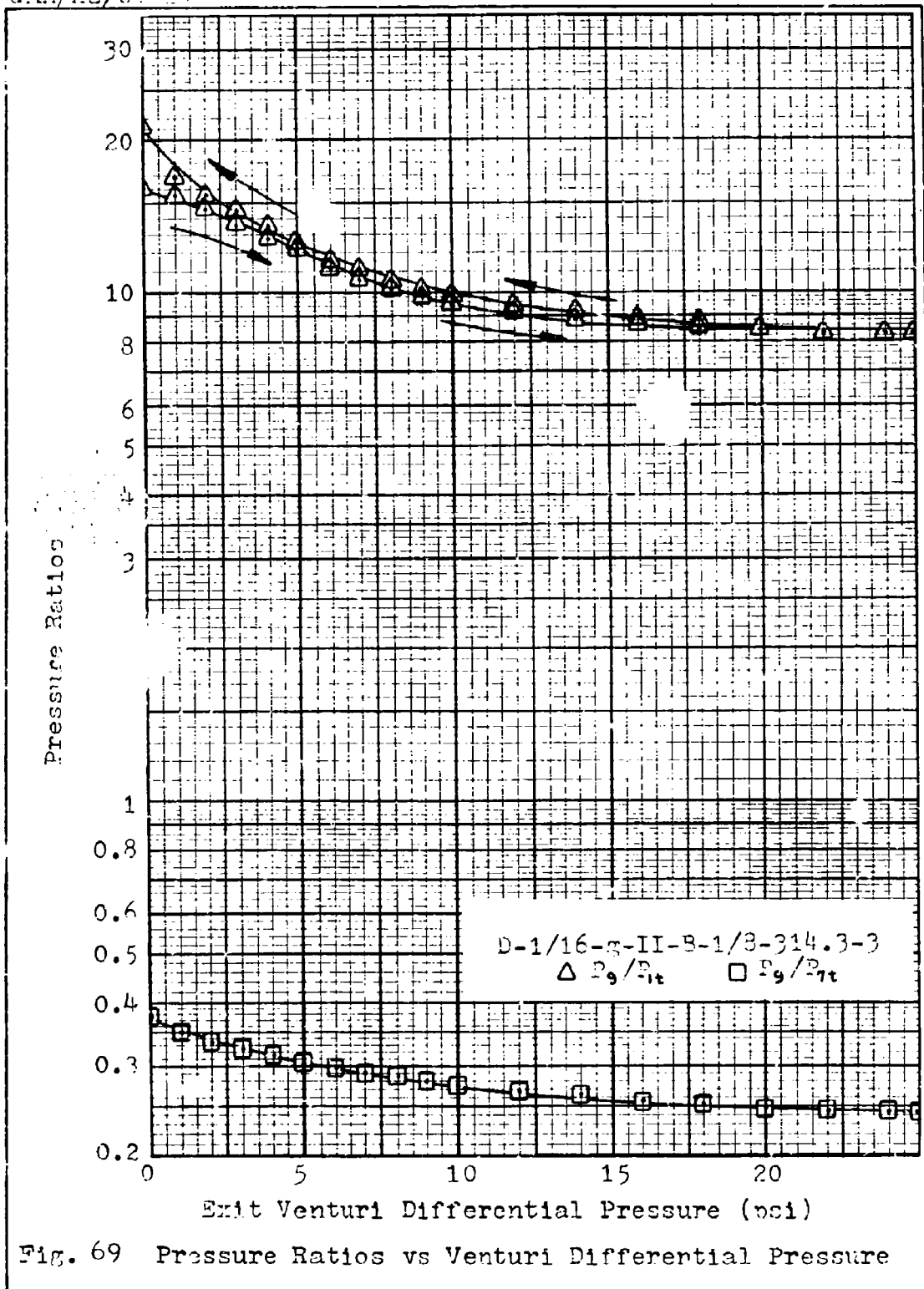
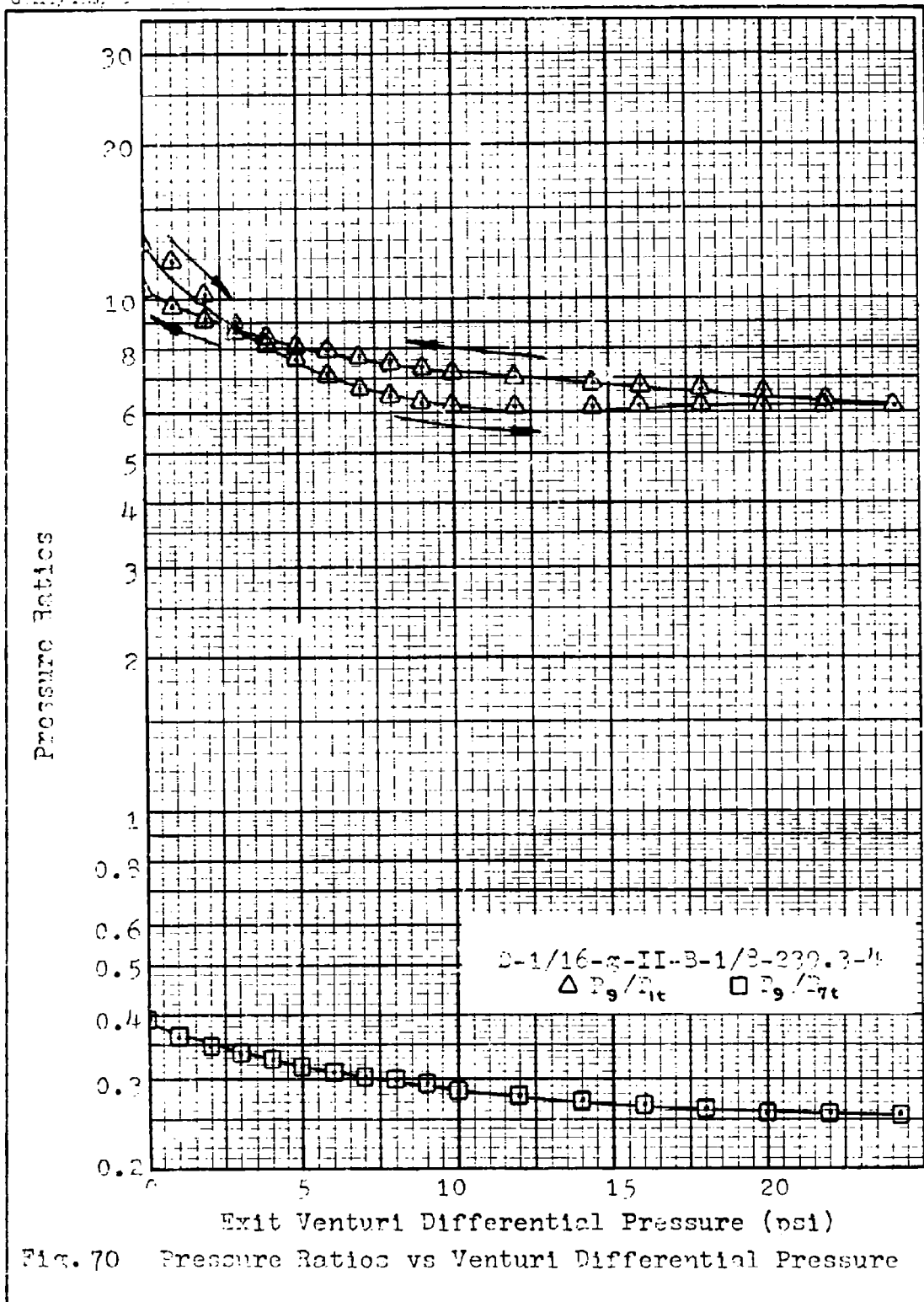


Fig. 69 Pressure Ratios vs Venturi Differential Pressure



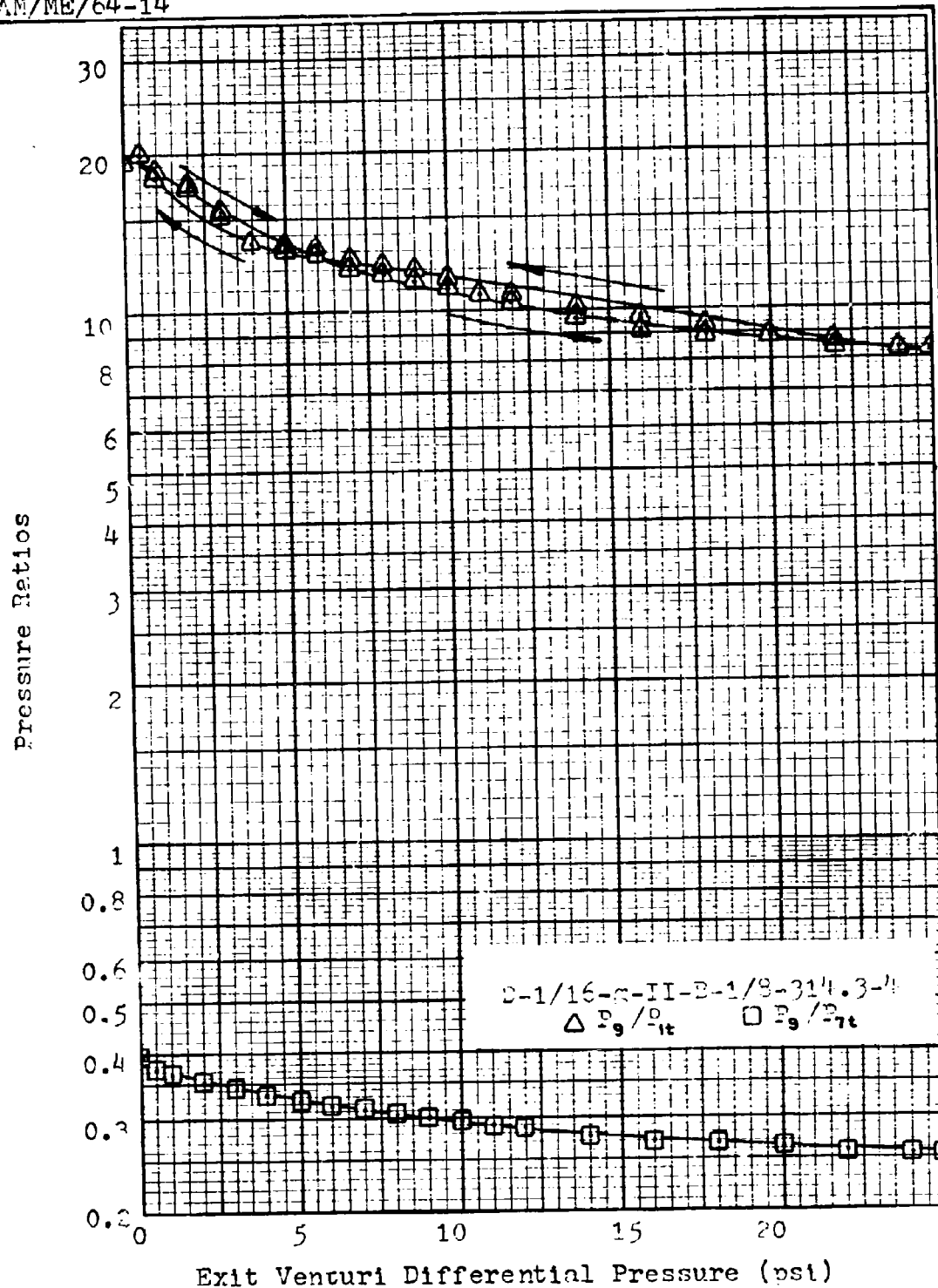
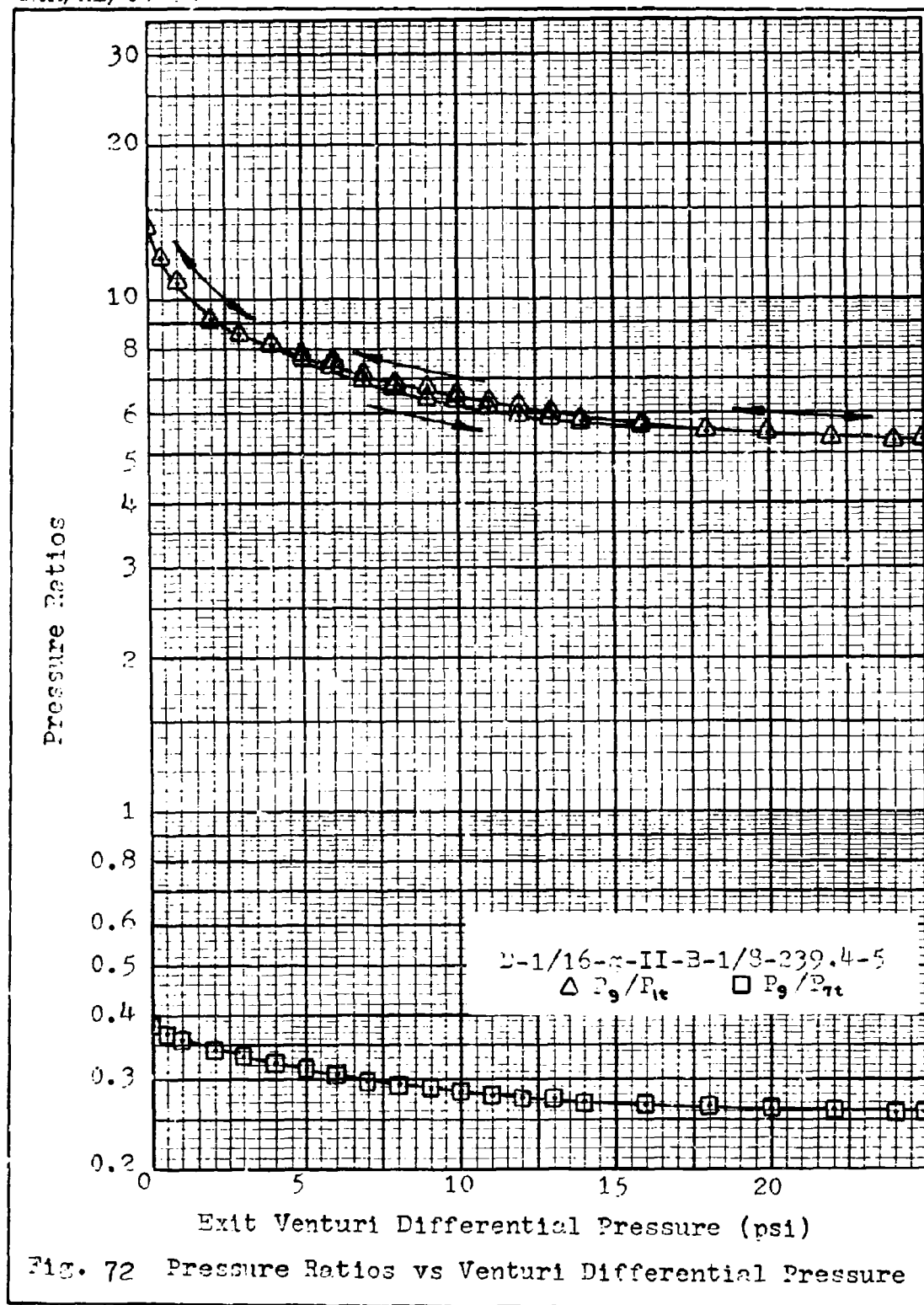


Fig. 71 Pressure Ratios vs Venturi Differential Pressure



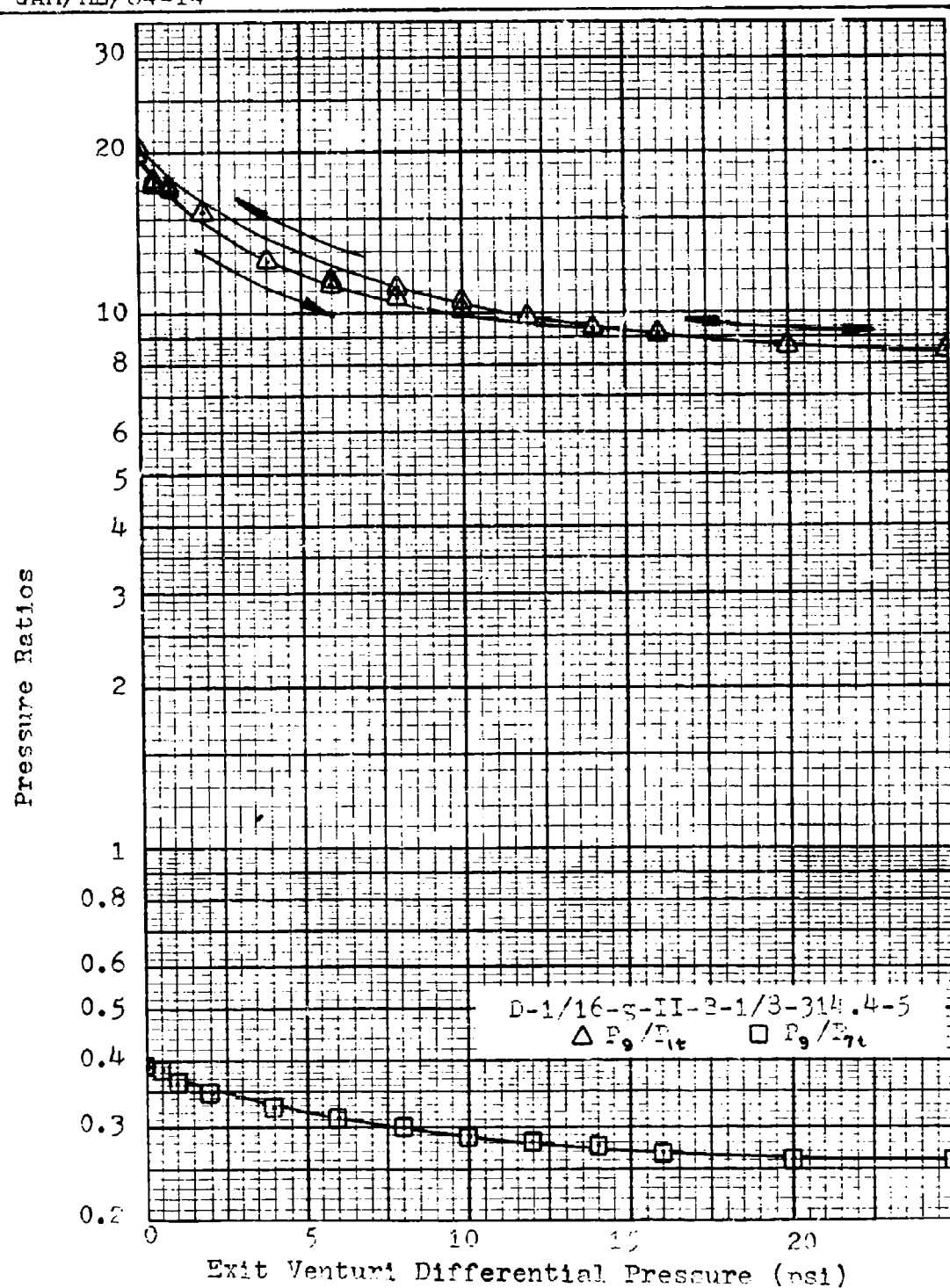
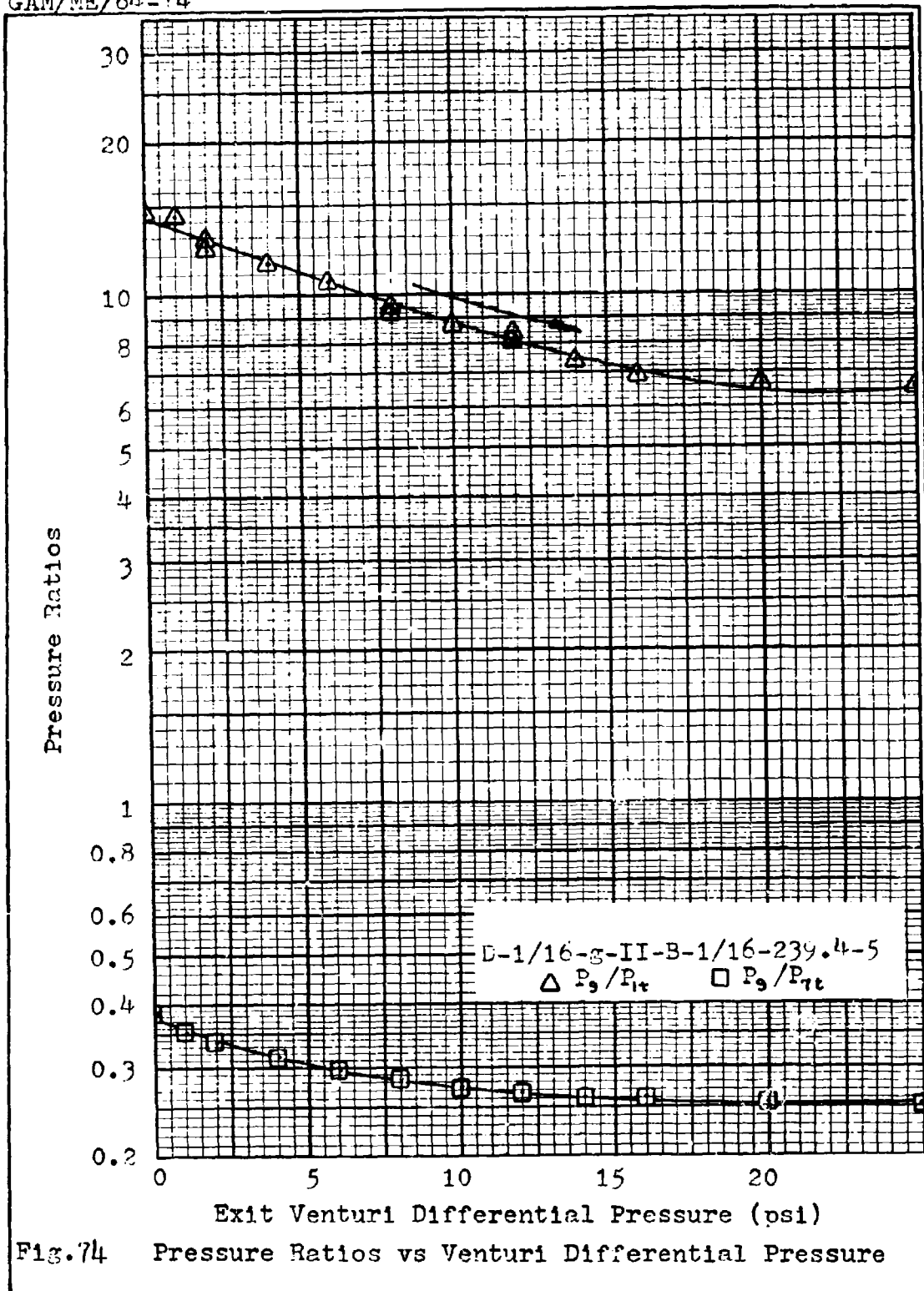
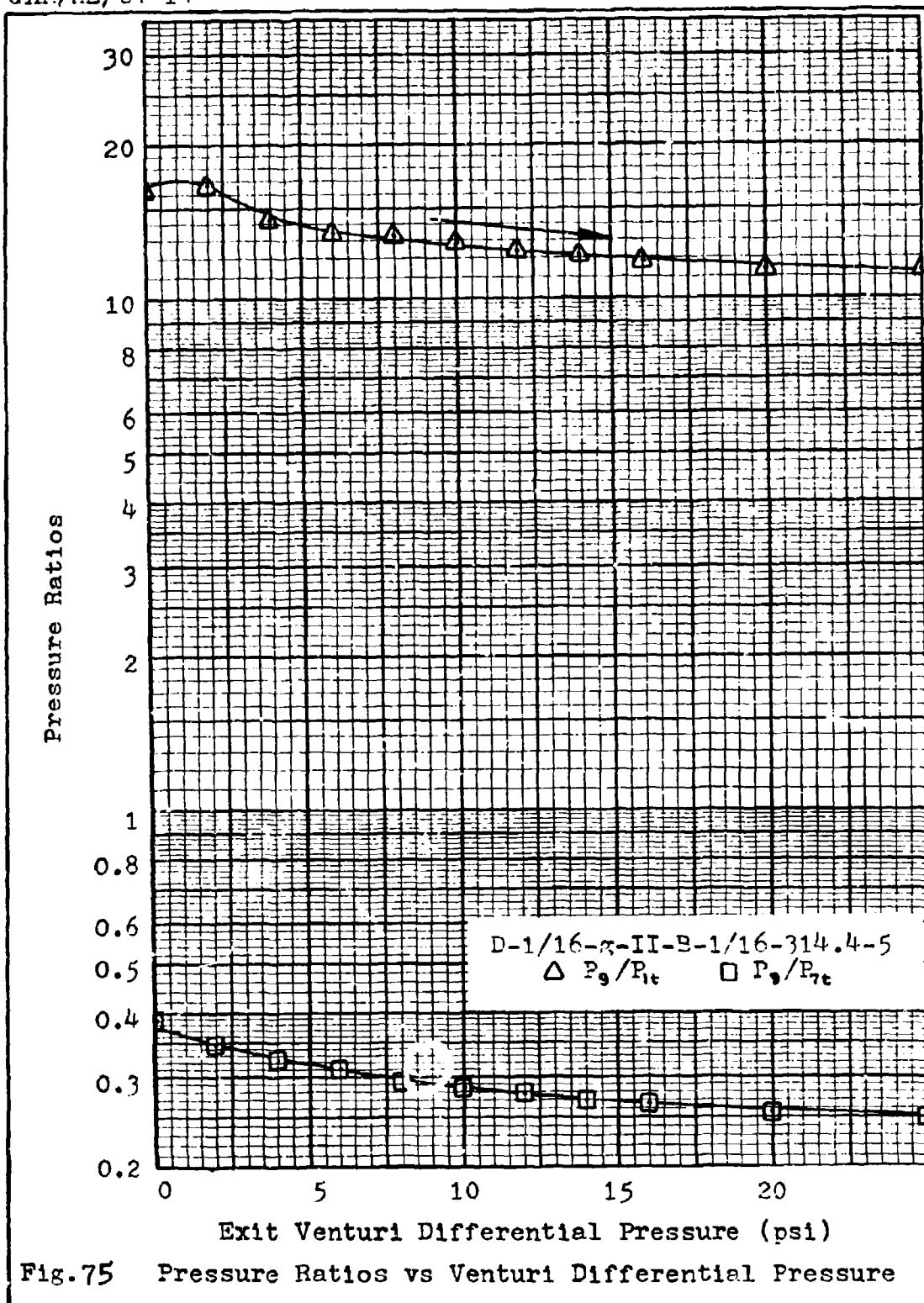
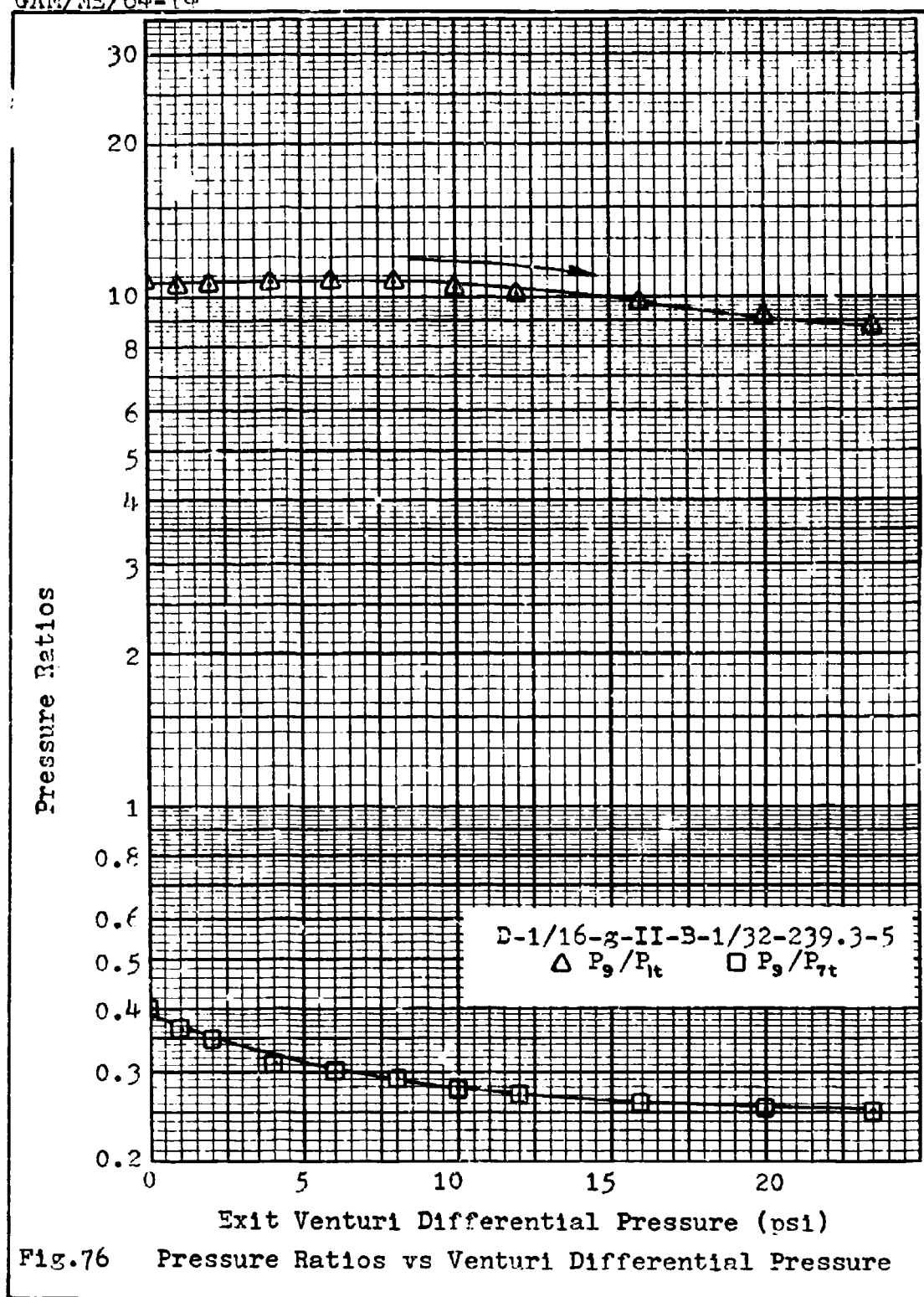
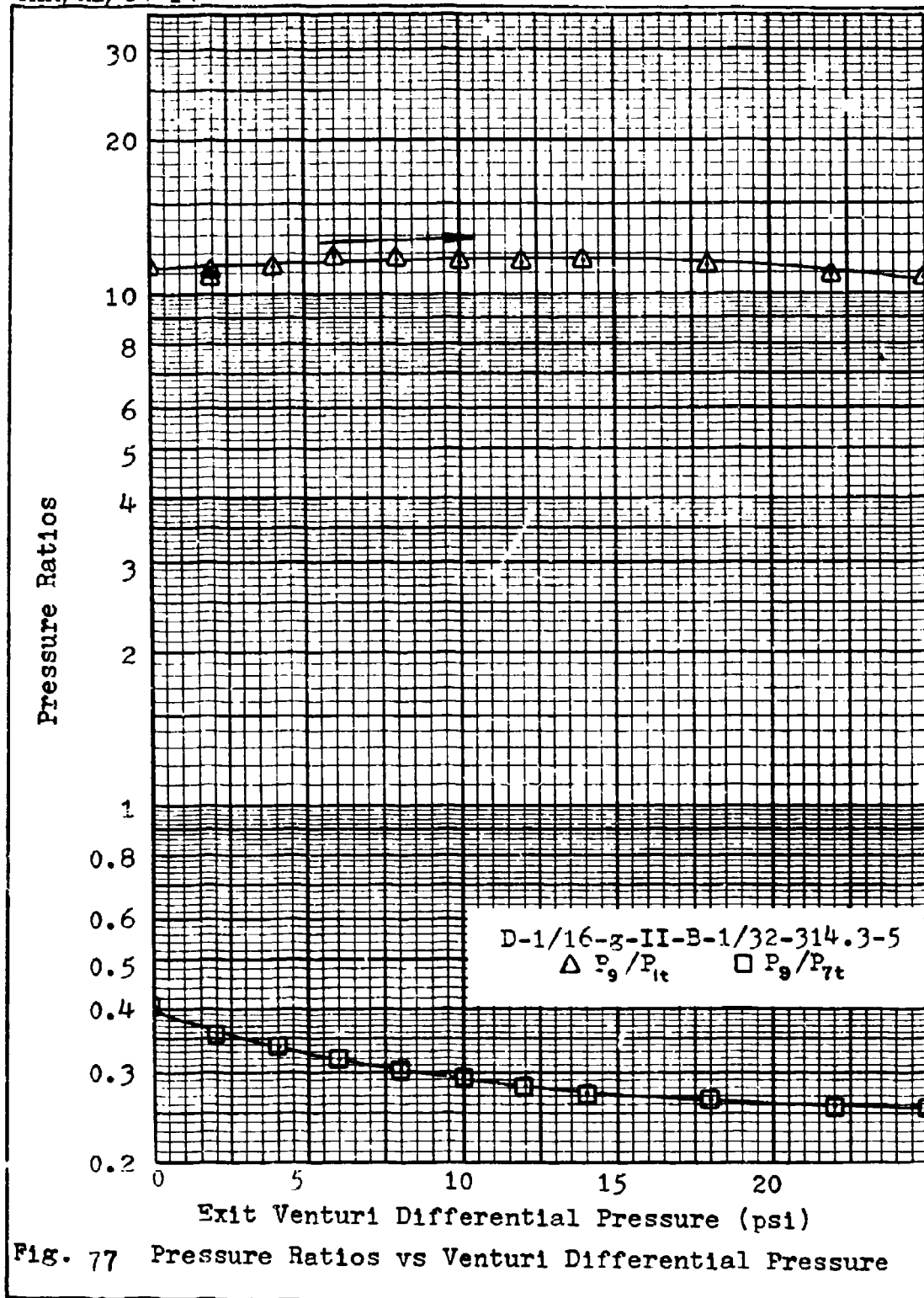


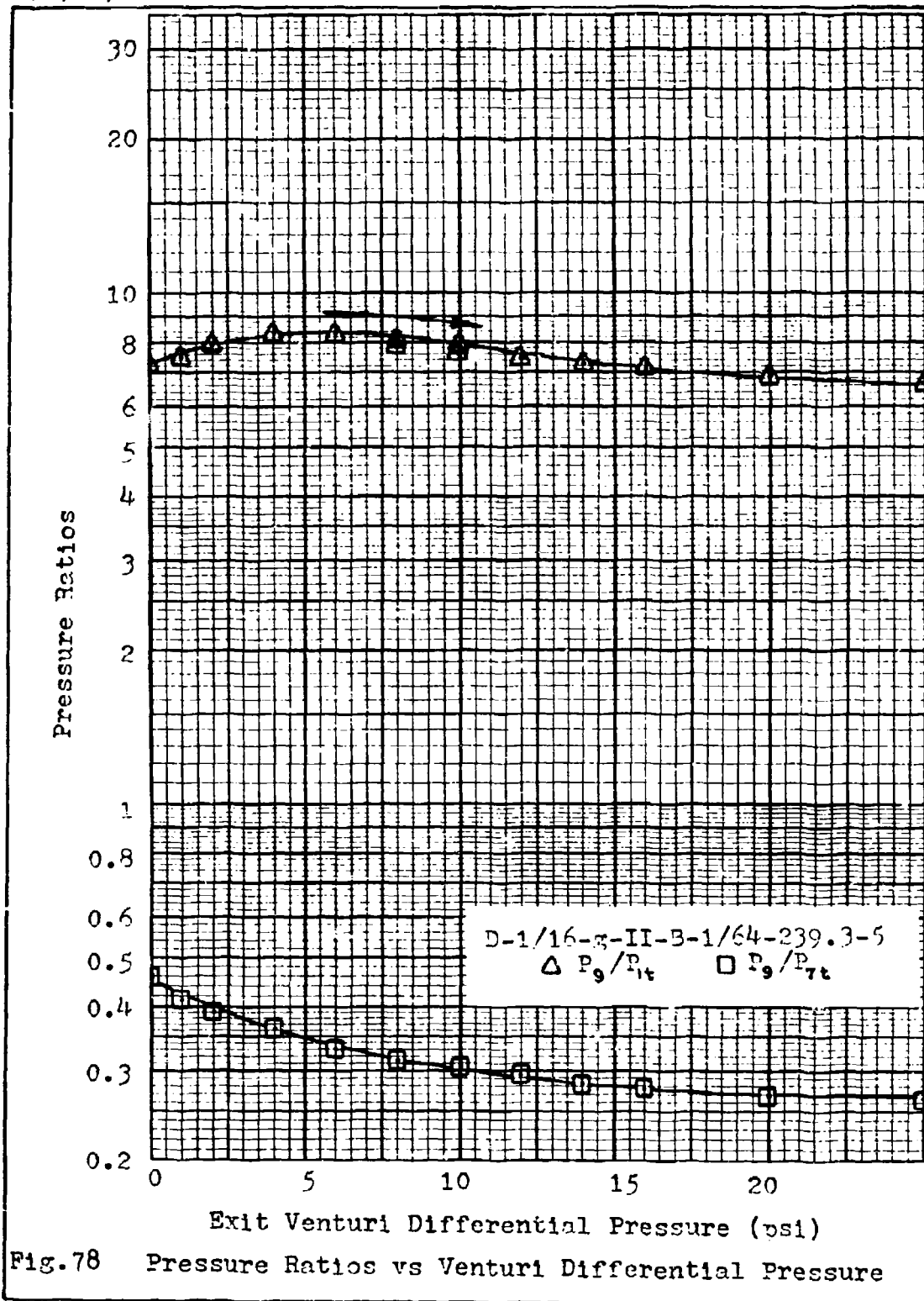
Fig. 73 Pressure Ratios vs Venturi Differential Pressure











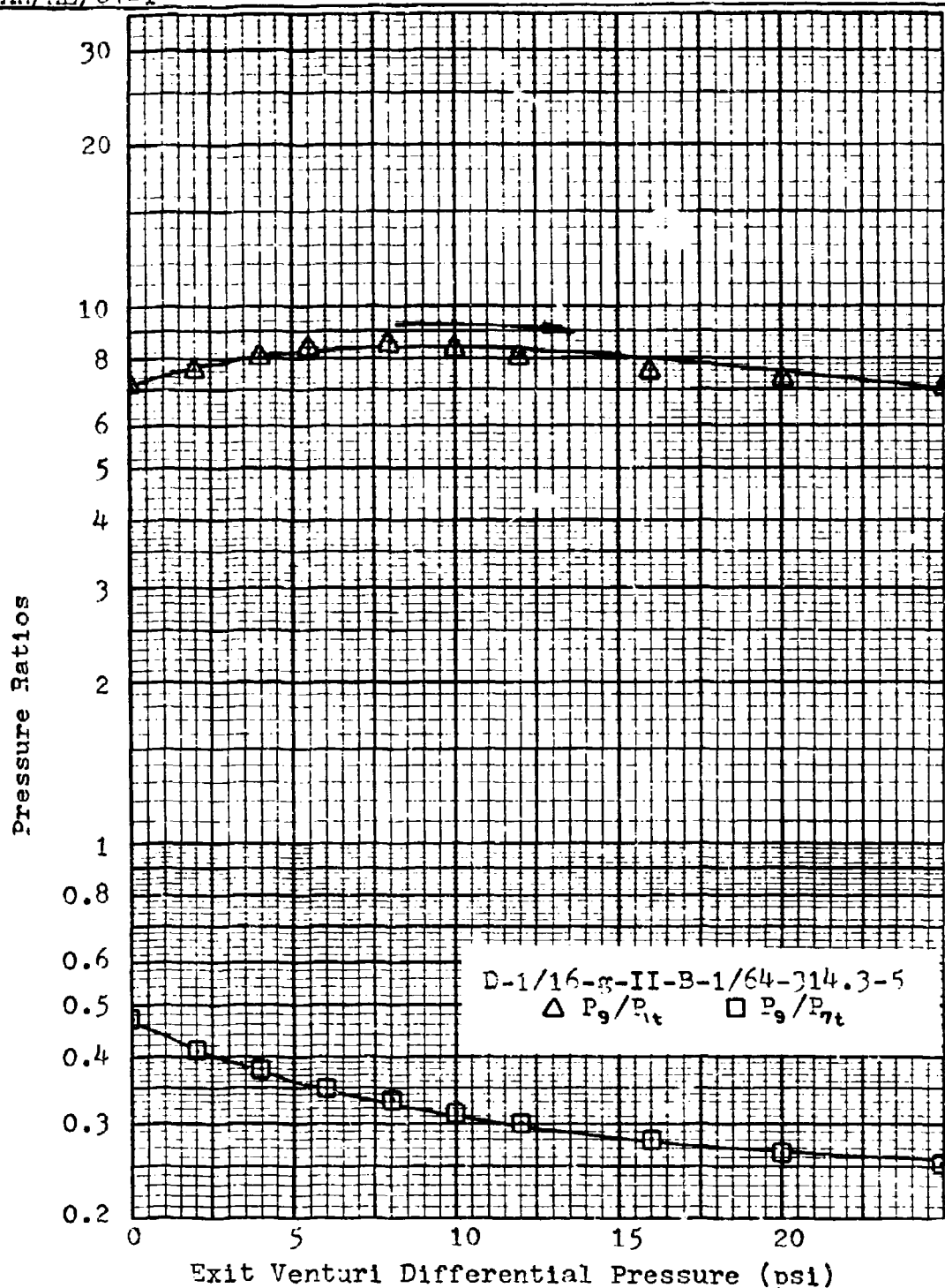
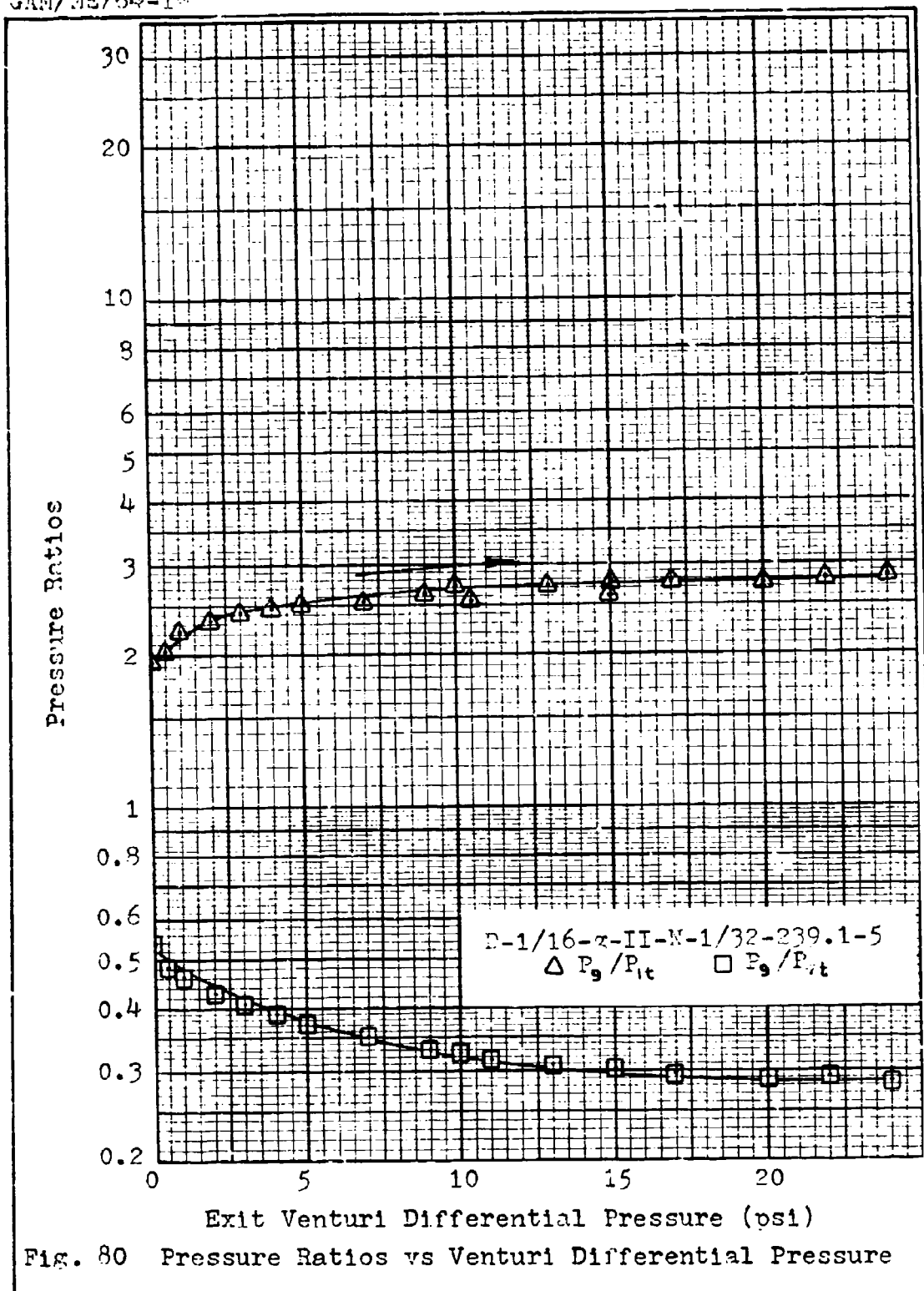
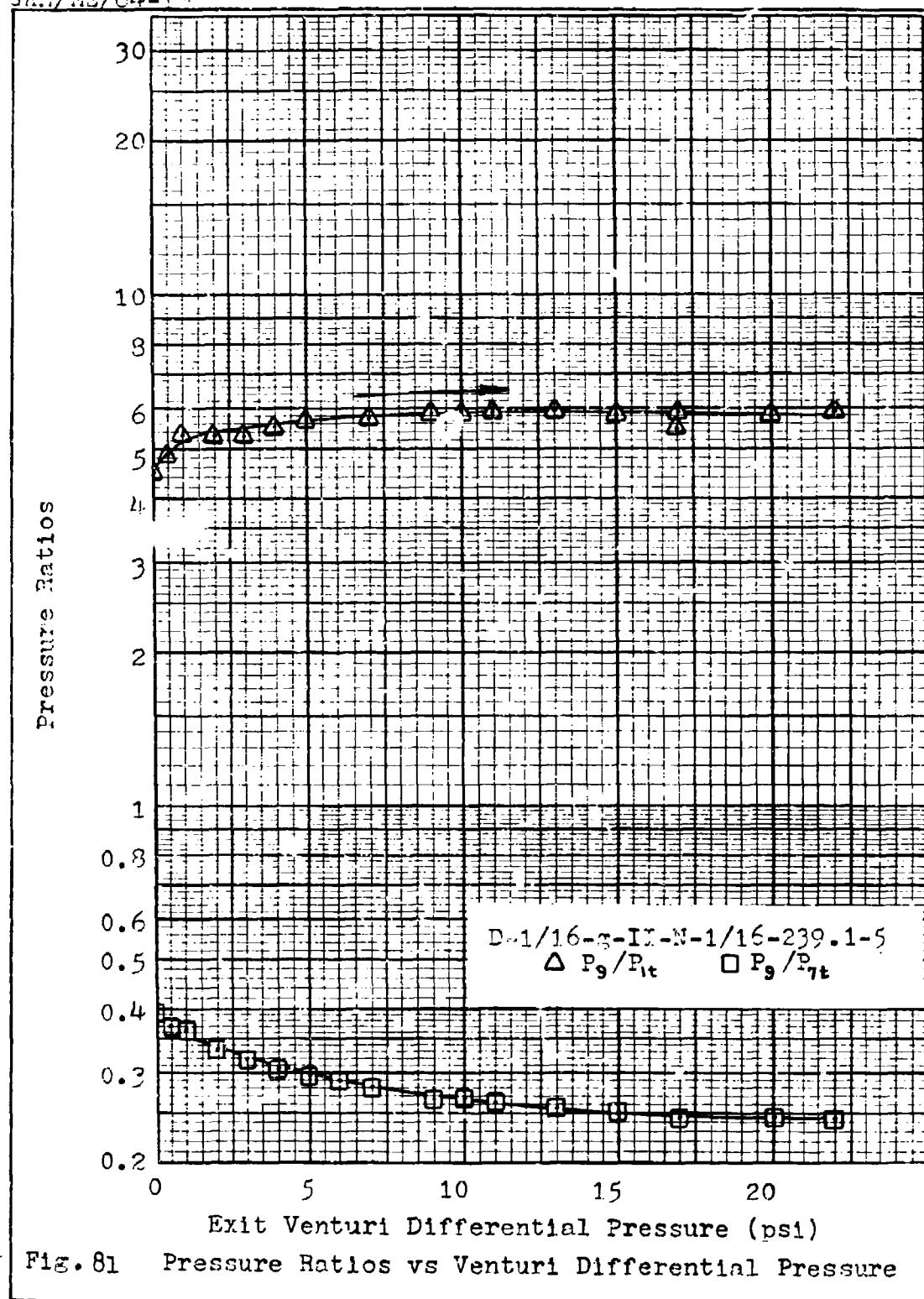
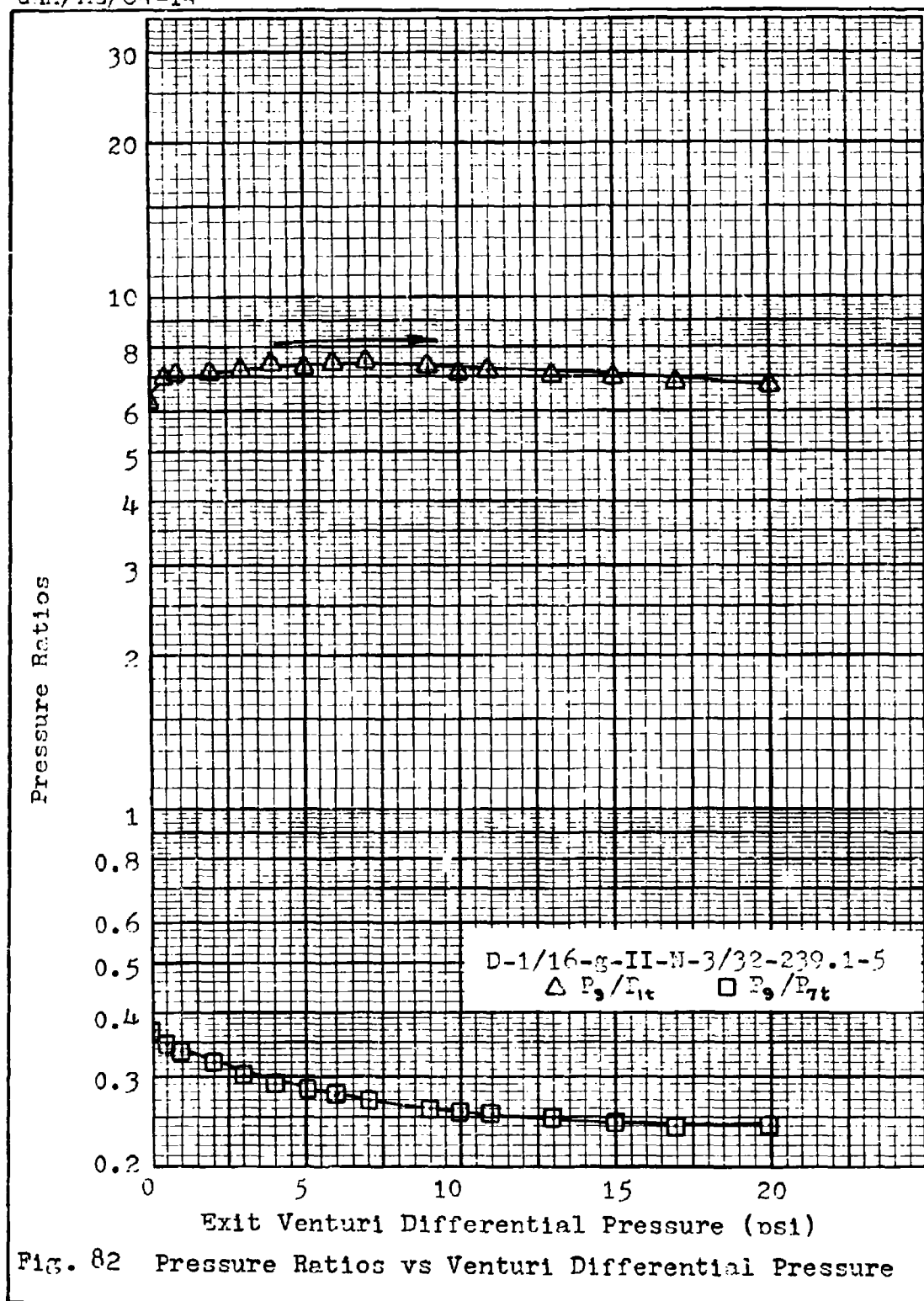
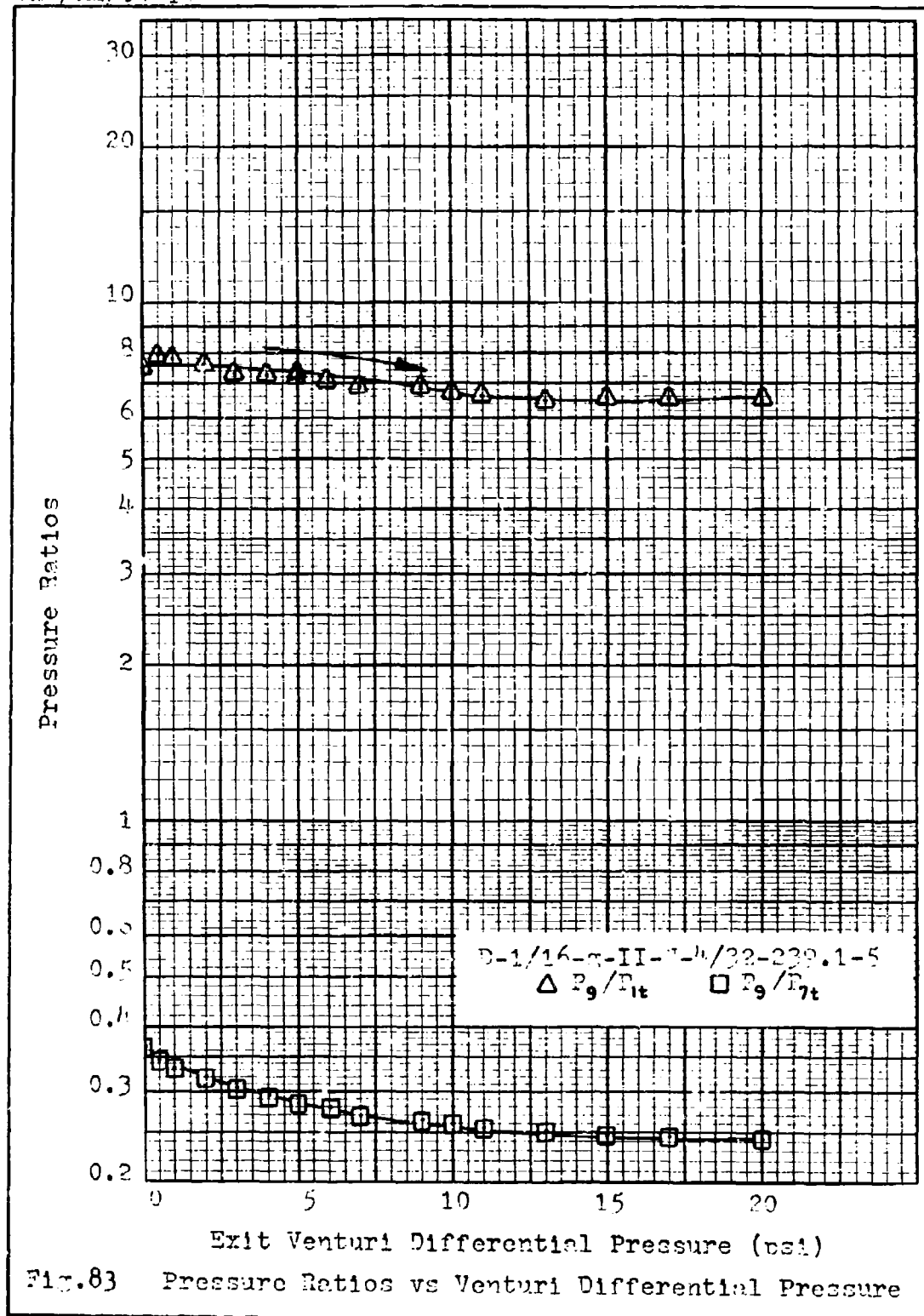


Fig. 79 Pressure Ratios vs Venturi Differential Pressure









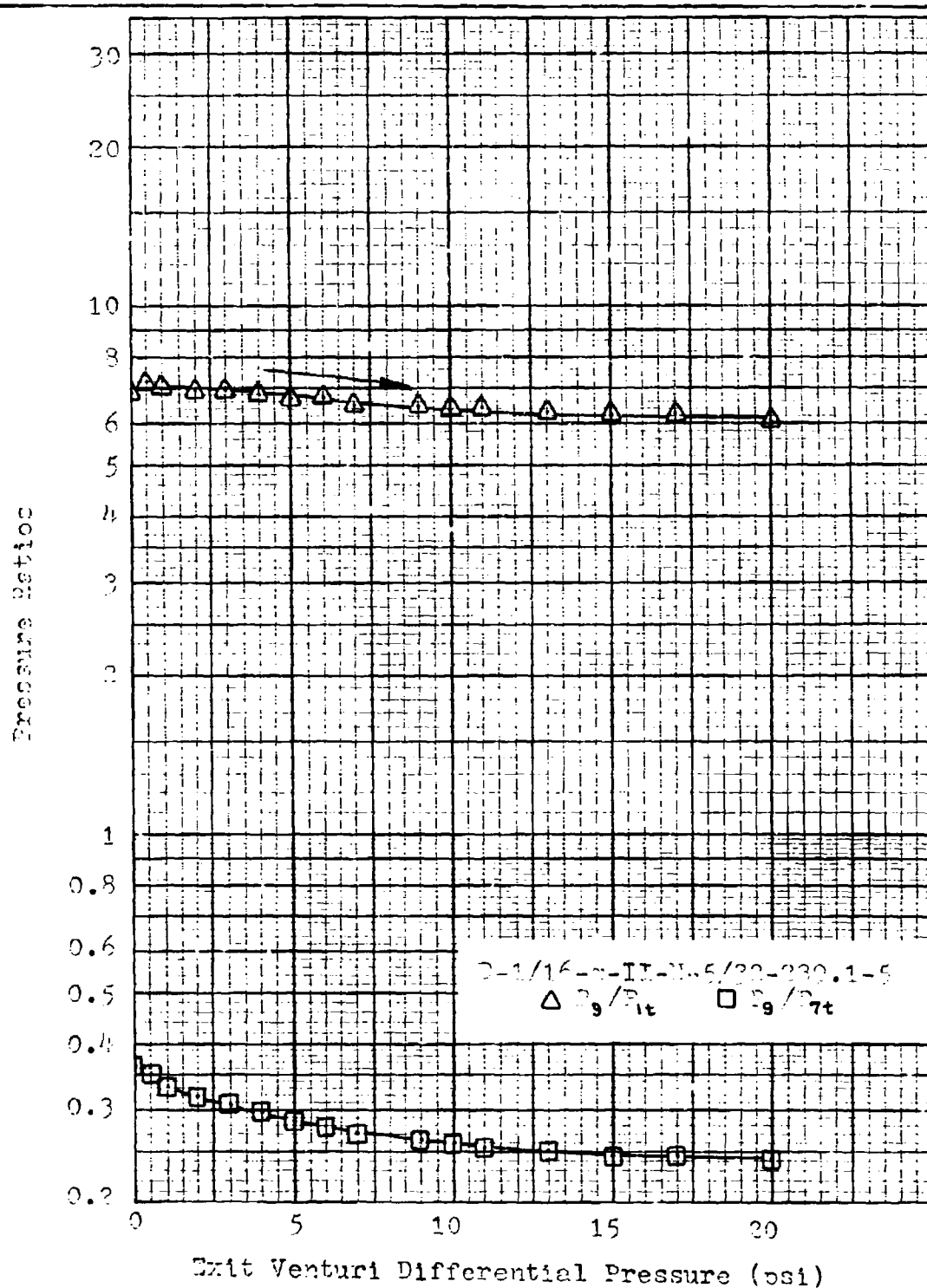
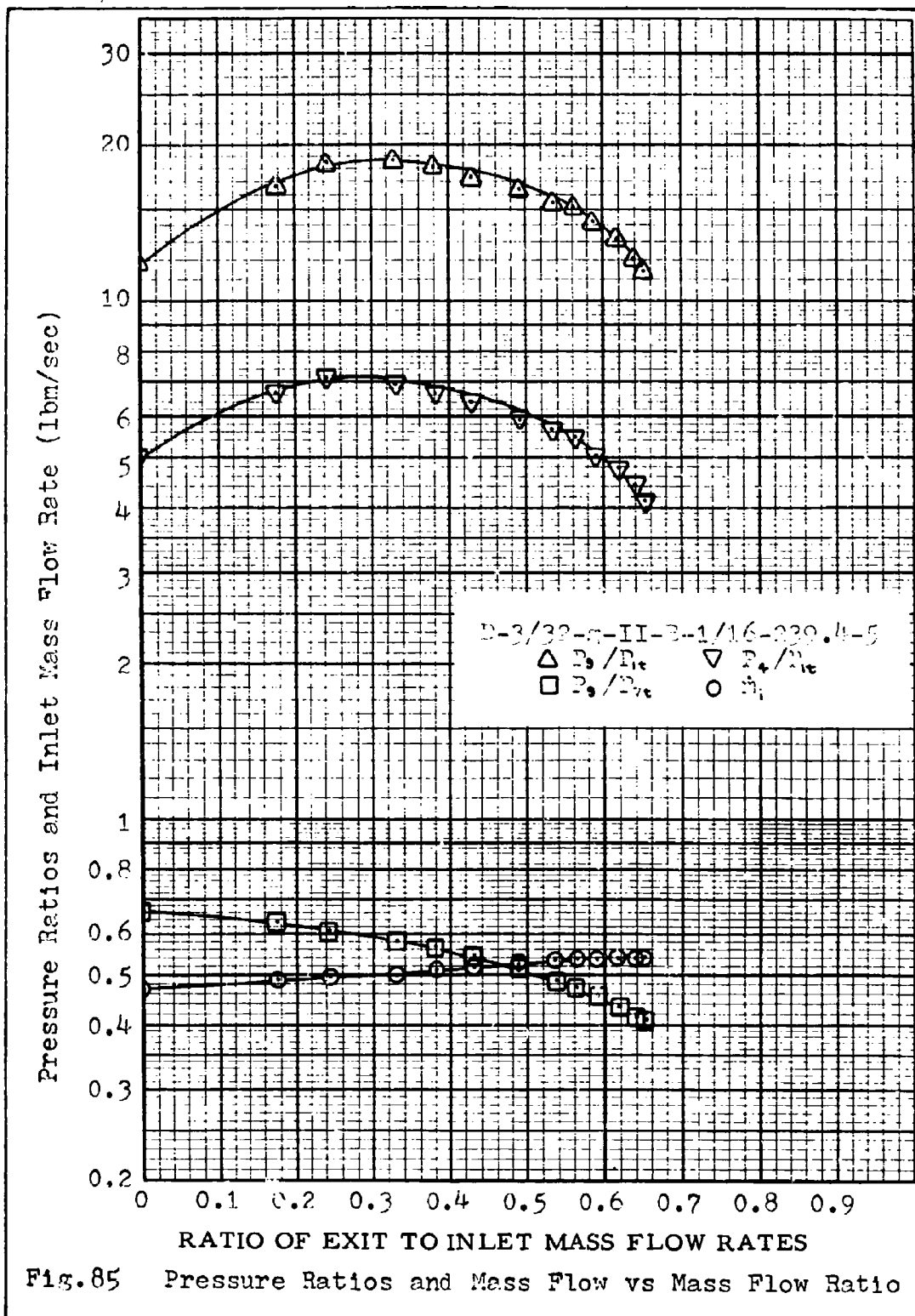
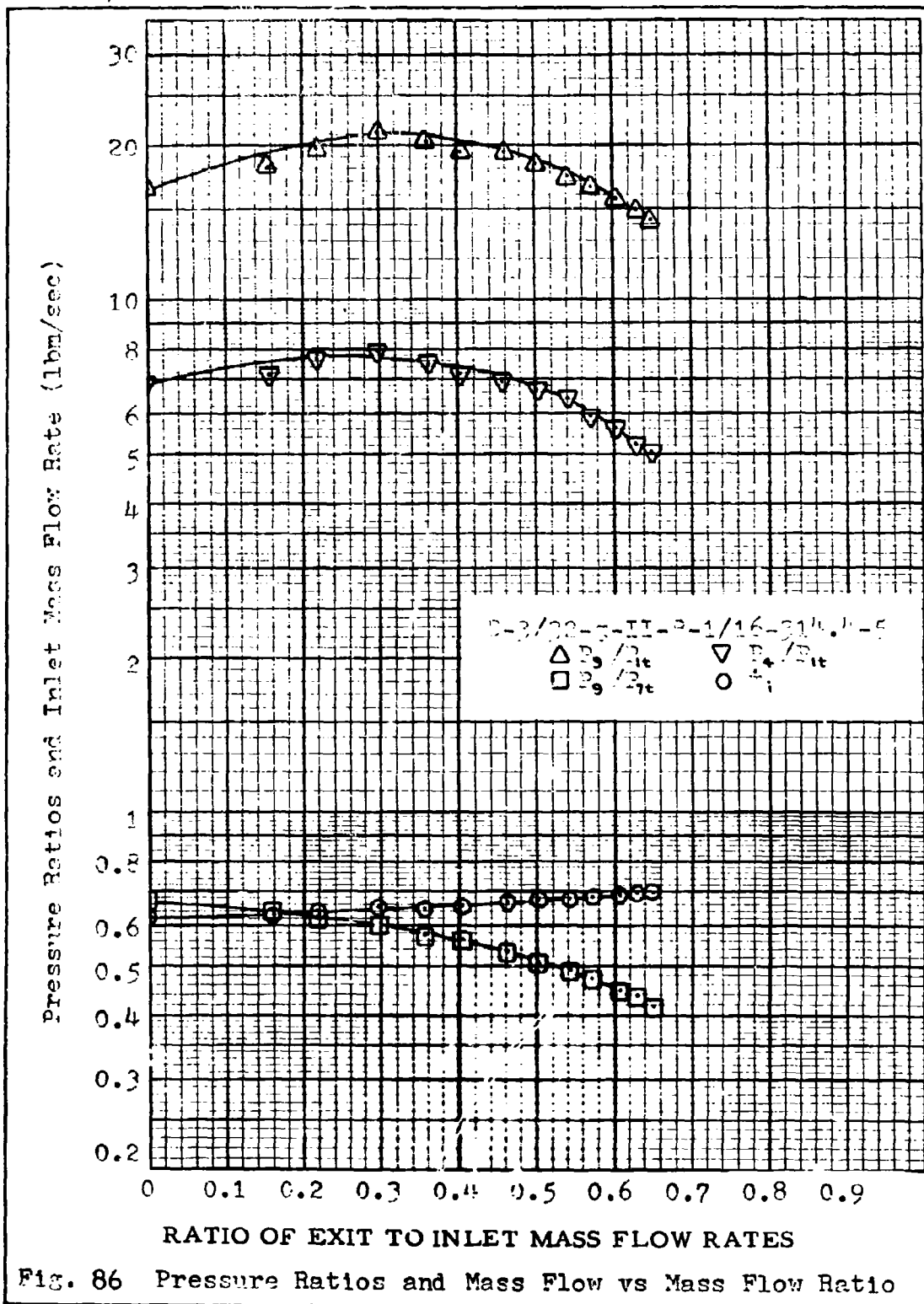


Fig. 8h Pressure Ratios vs Venturi Differential Pressure





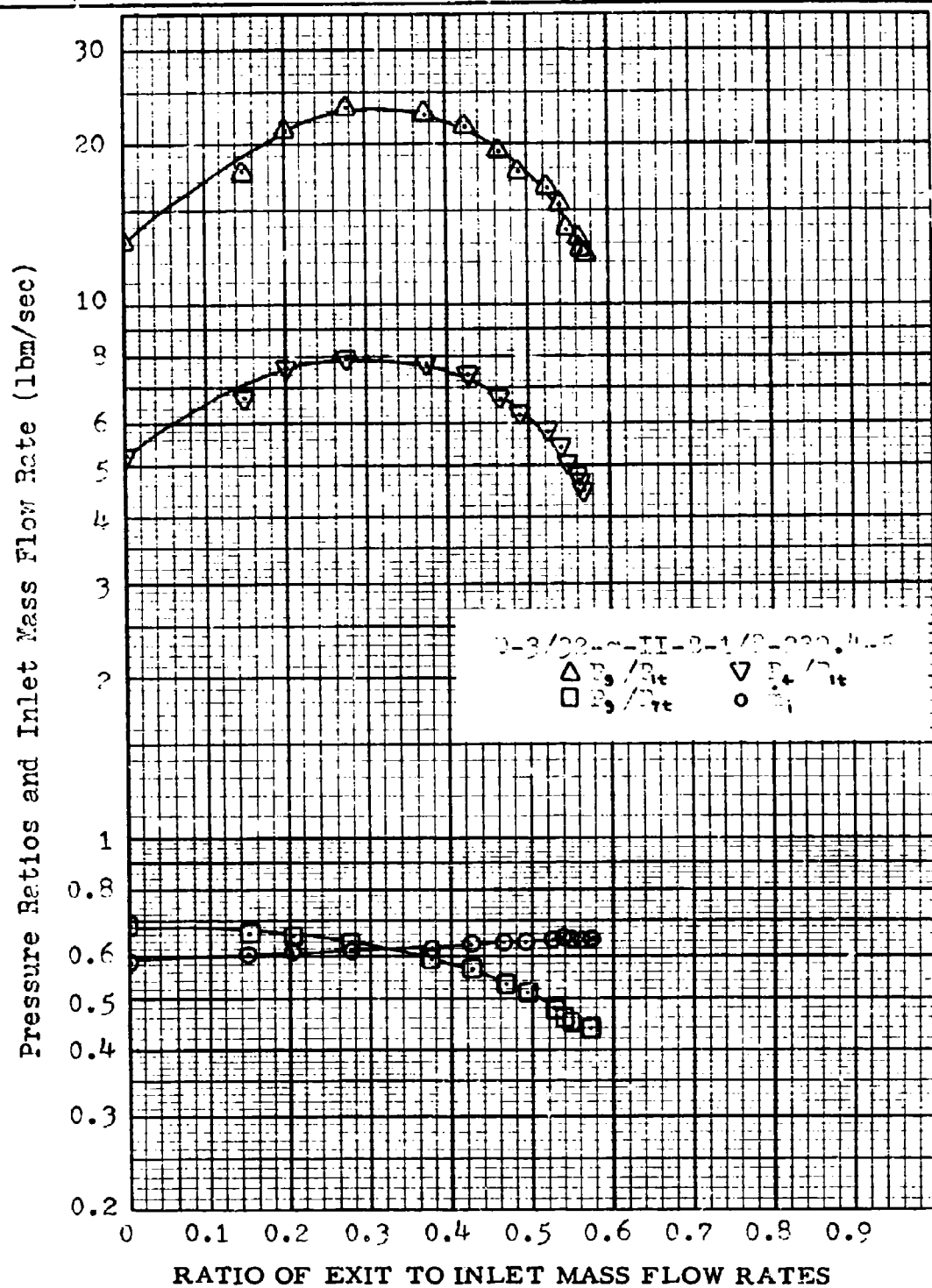
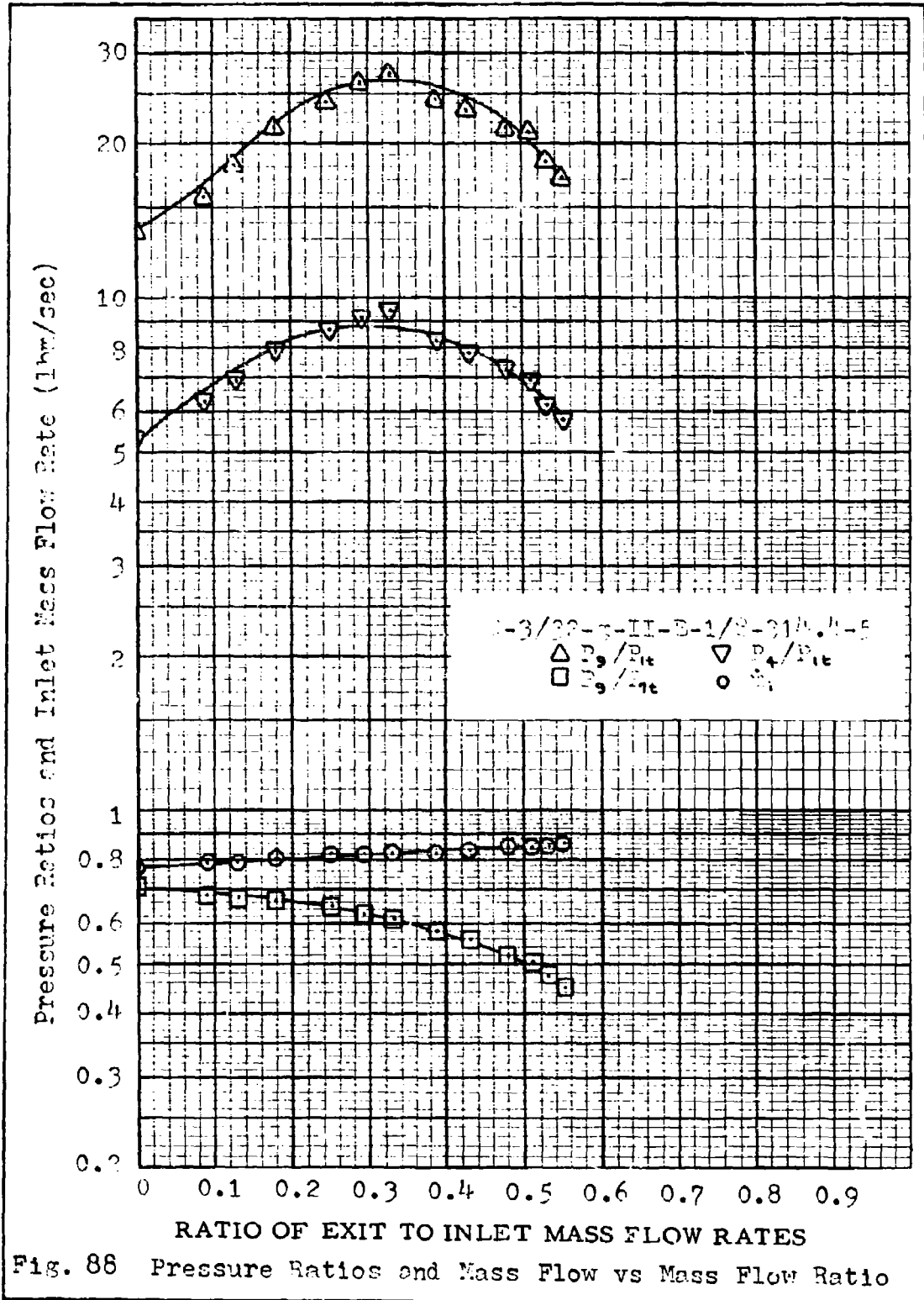
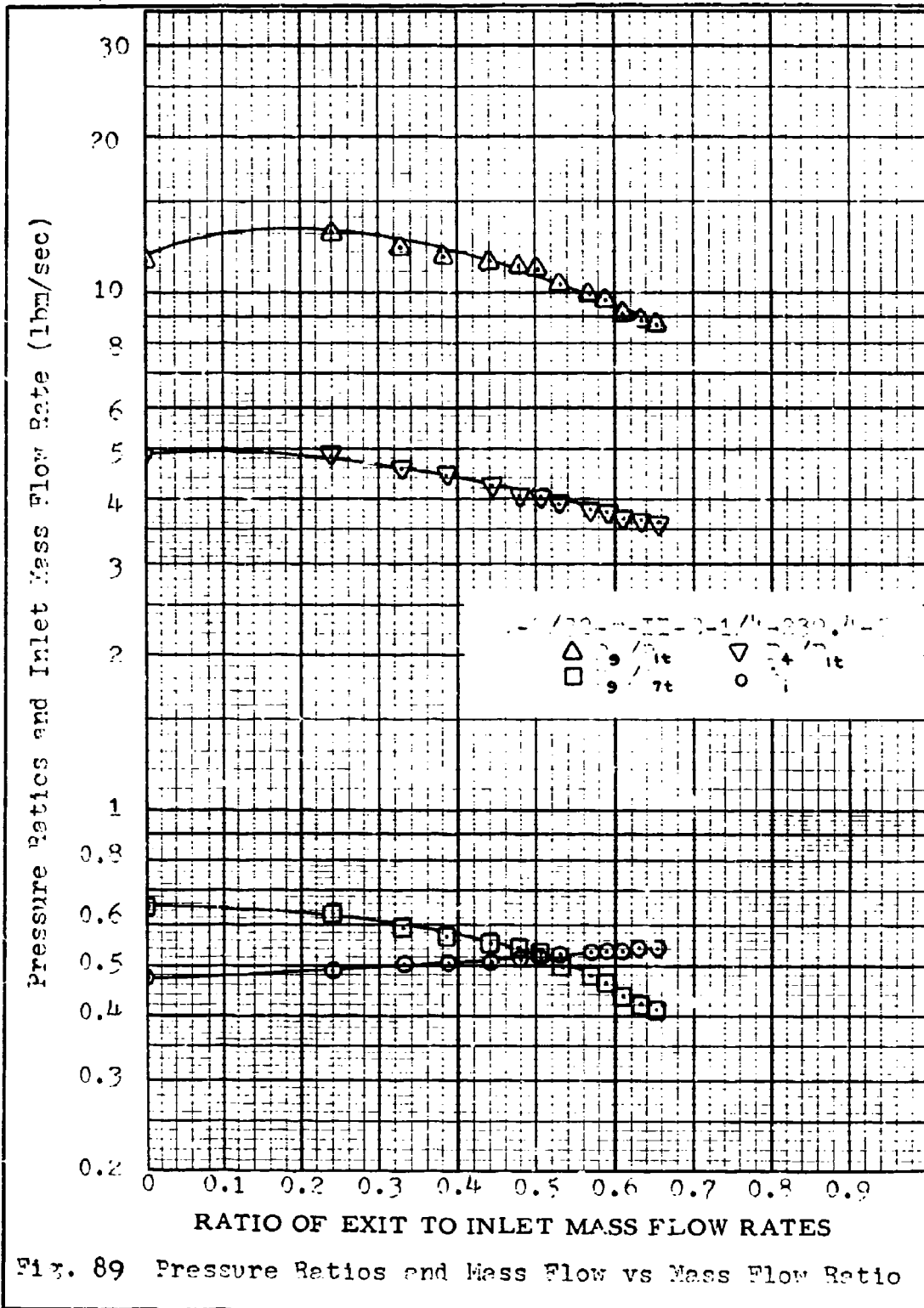
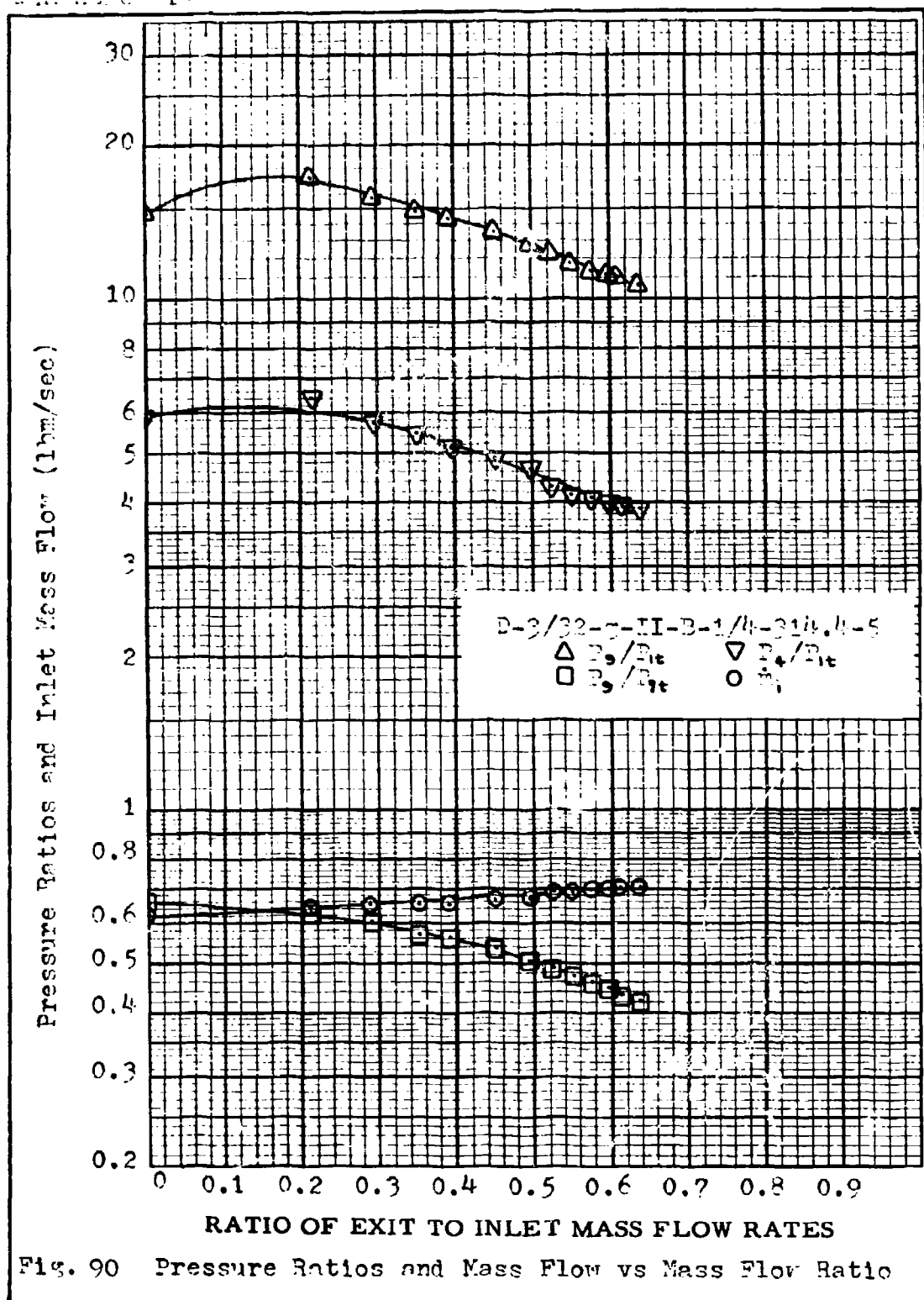


Fig. 87 Pressure Ratios and Mass Flow vs Mass Flow Ratio







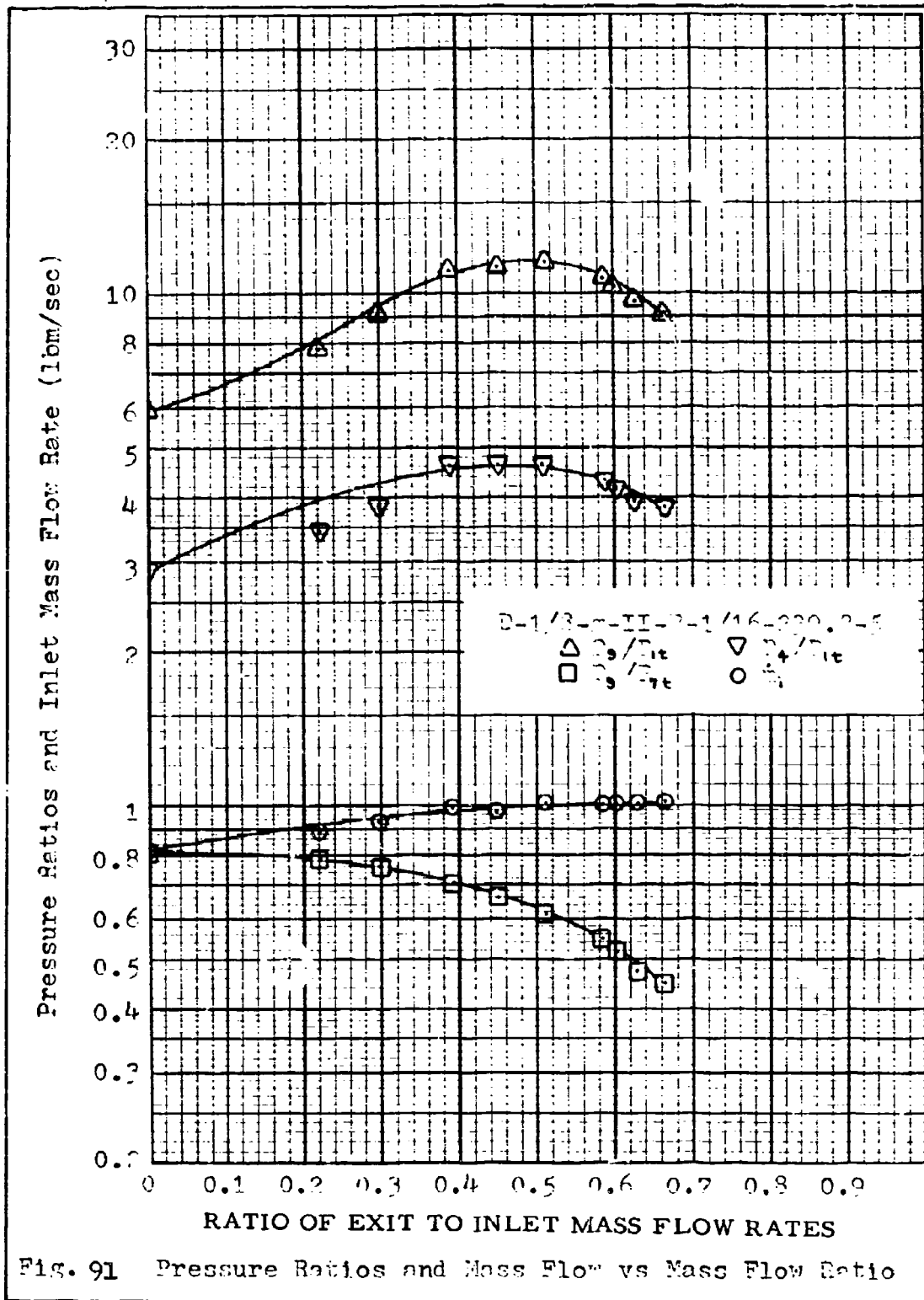


Fig. 91 Pressure Ratios and Mass Flow vs Mass Flow Ratio

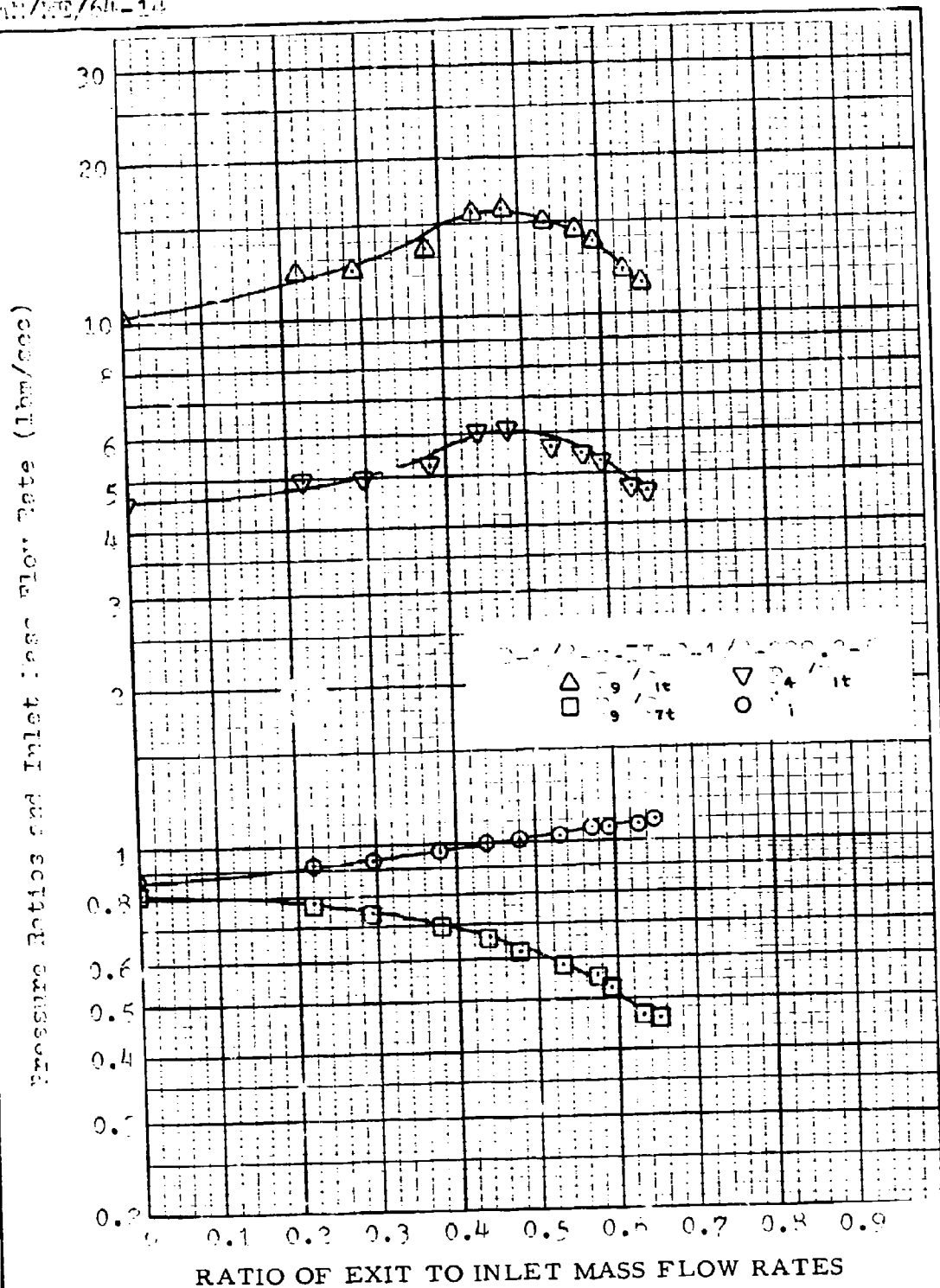
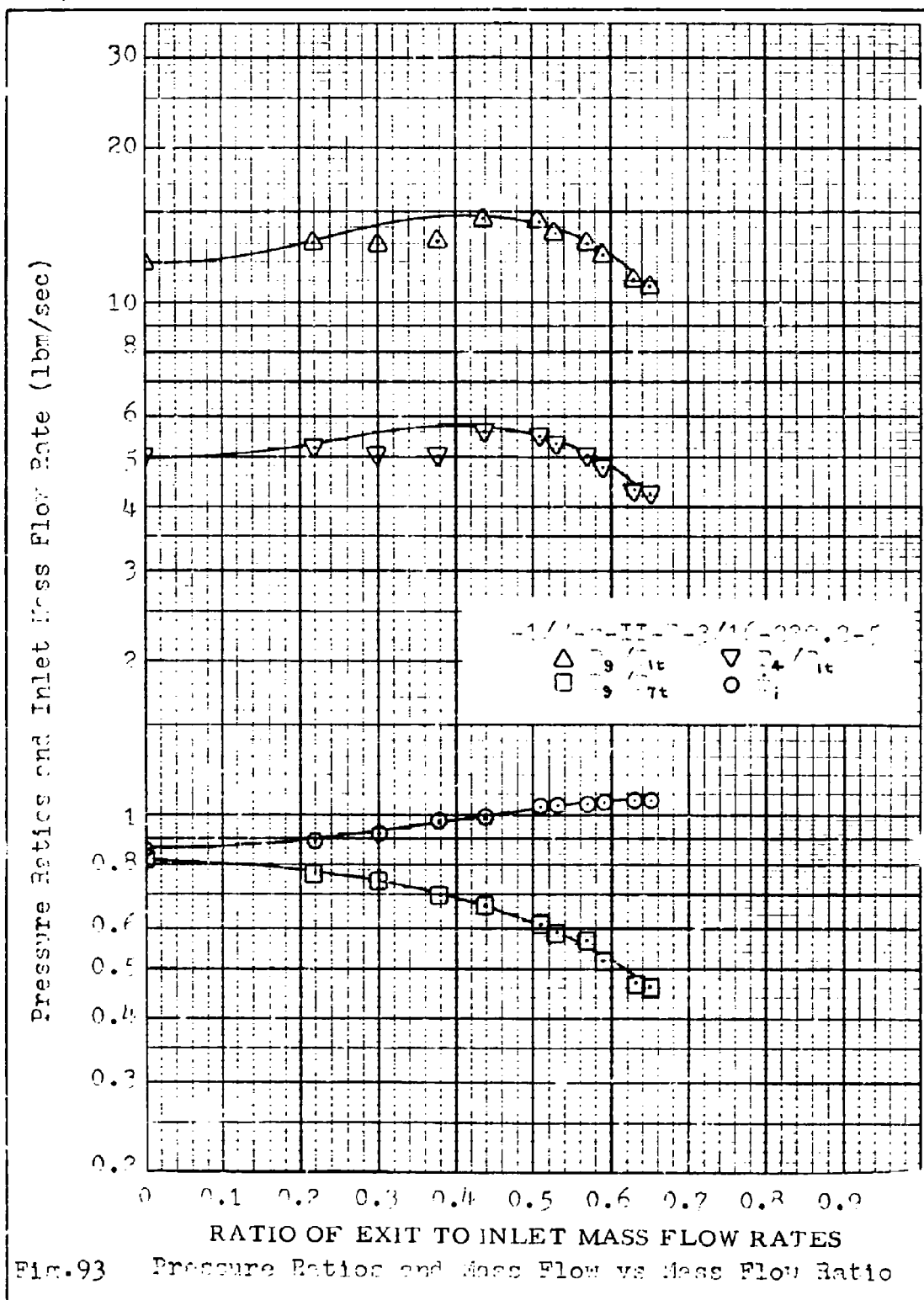
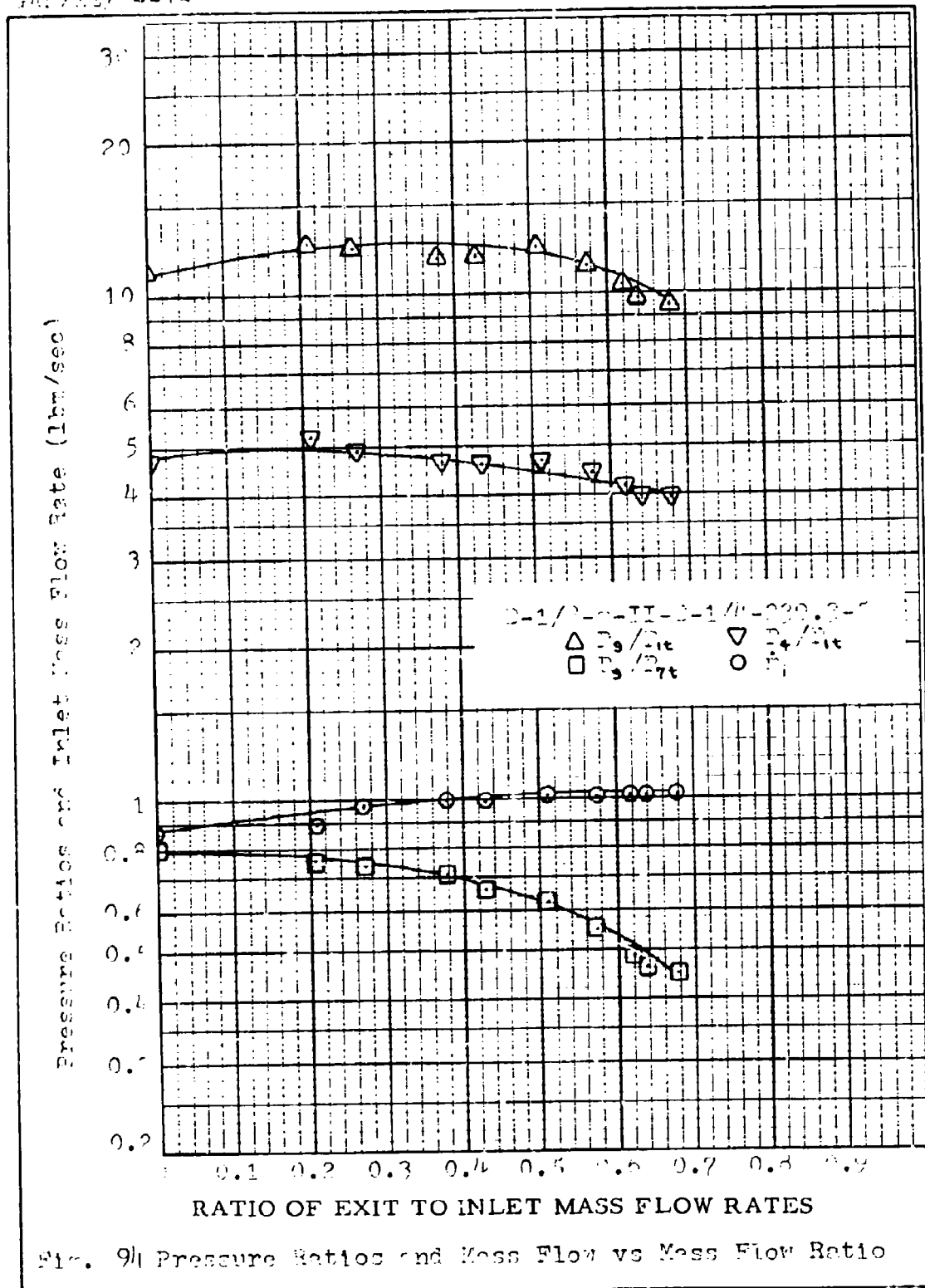
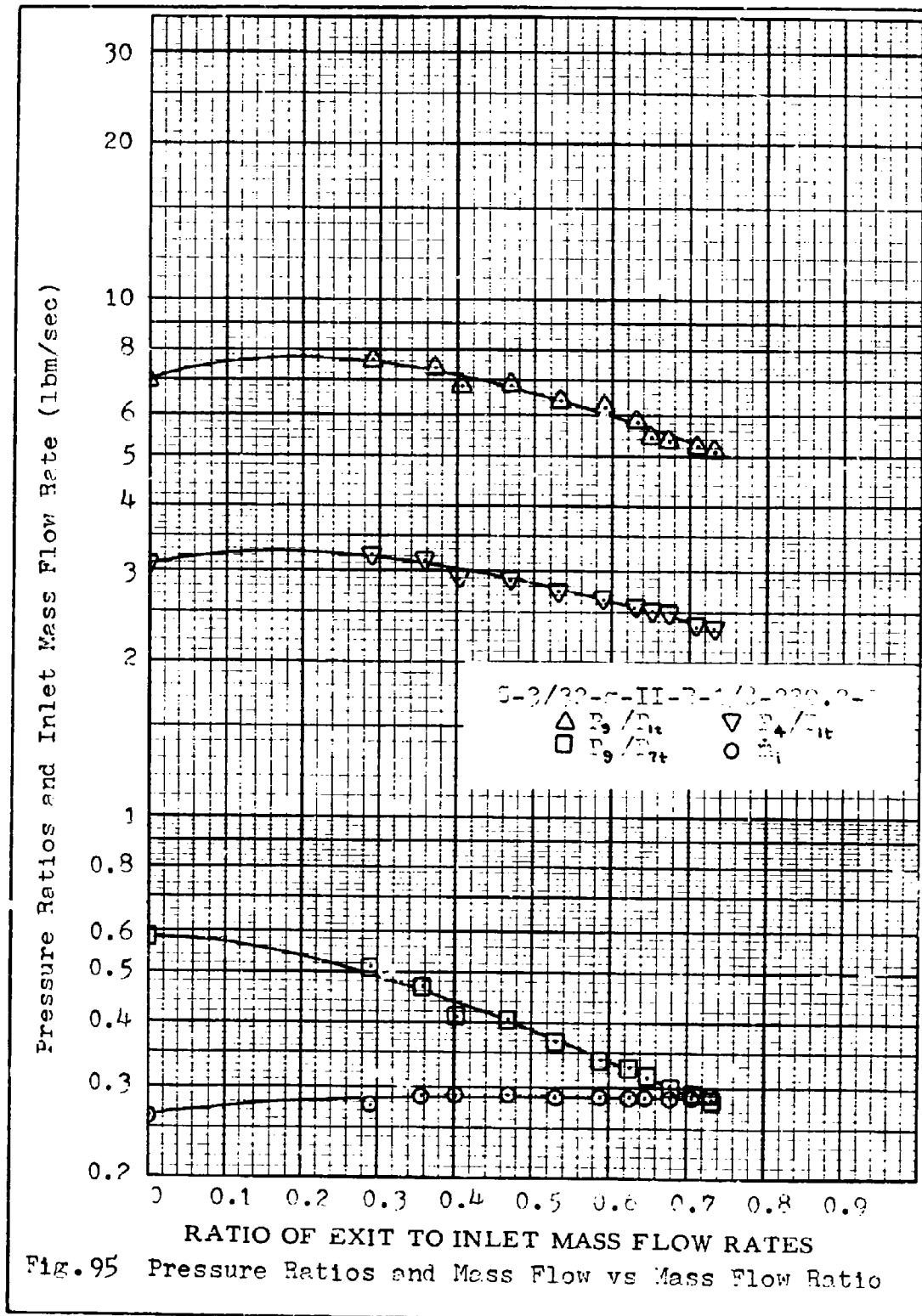


Fig. 92 Pressure Ratios and Mass Flow vs. Mass Flow Ratio







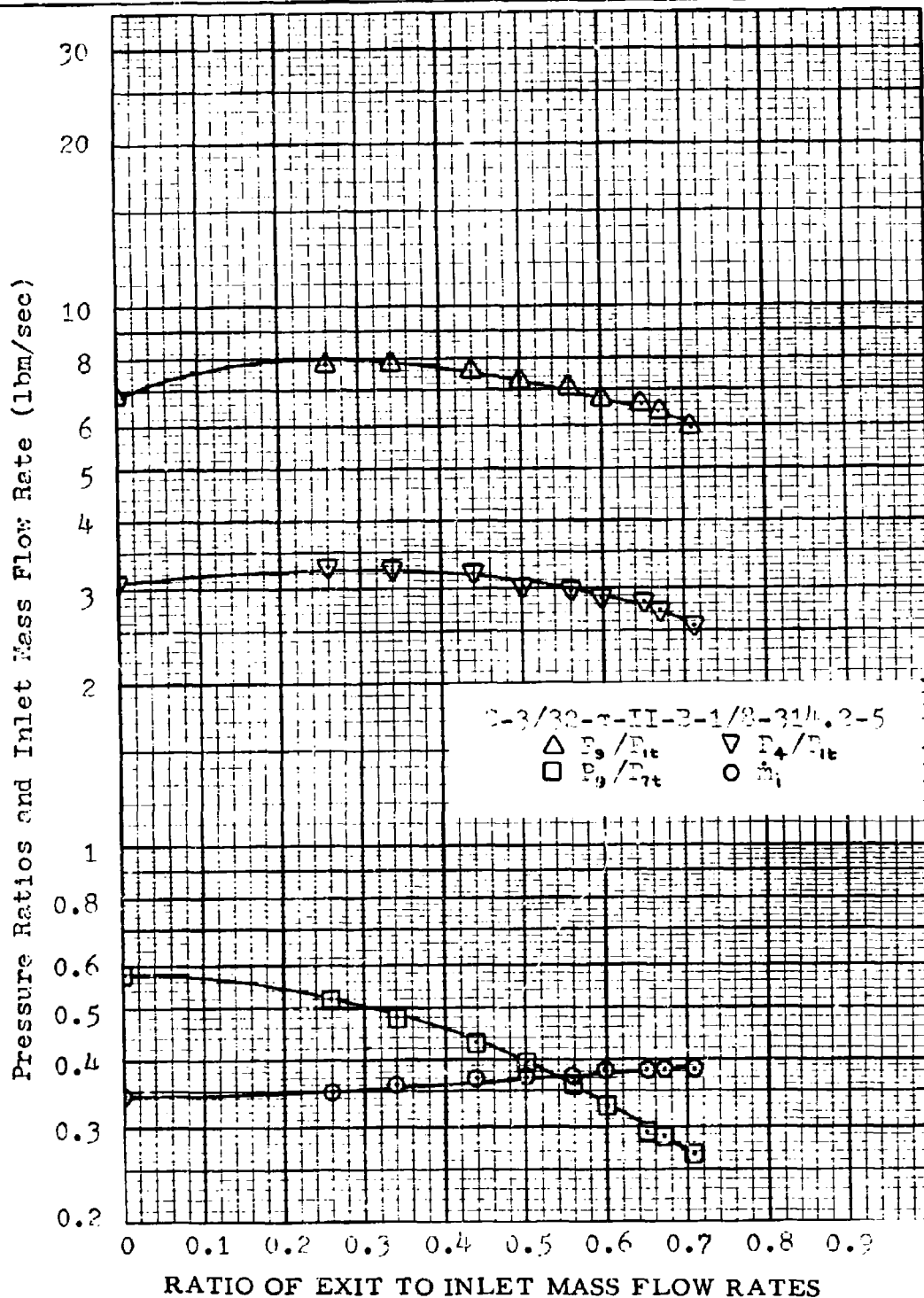


Fig. 96 Pressure Ratios and Mass Flow vs Mass Flow Ratio

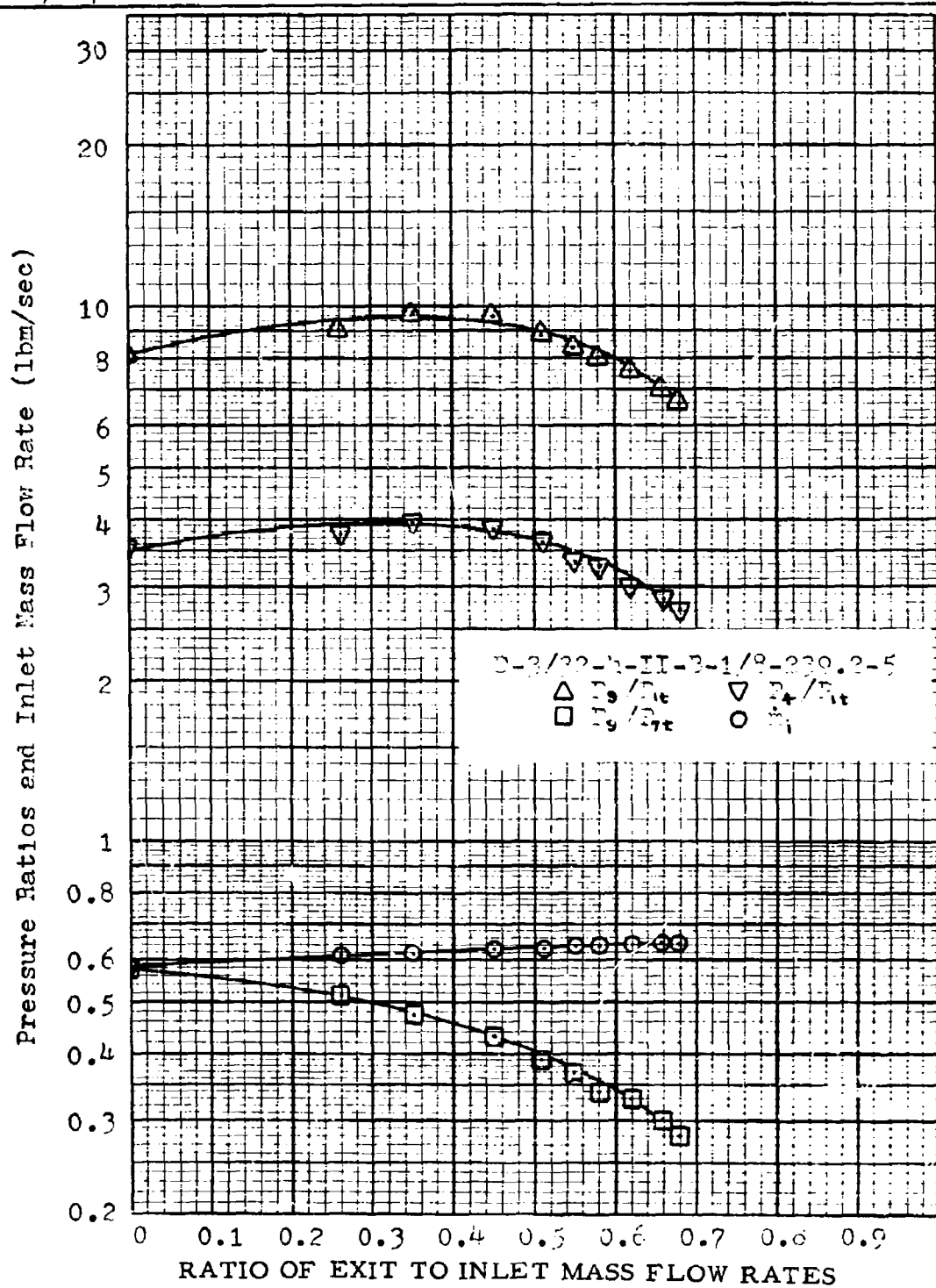


Fig. 97 Pressure Ratios and Mass Flow vs Mass Flow Ratio

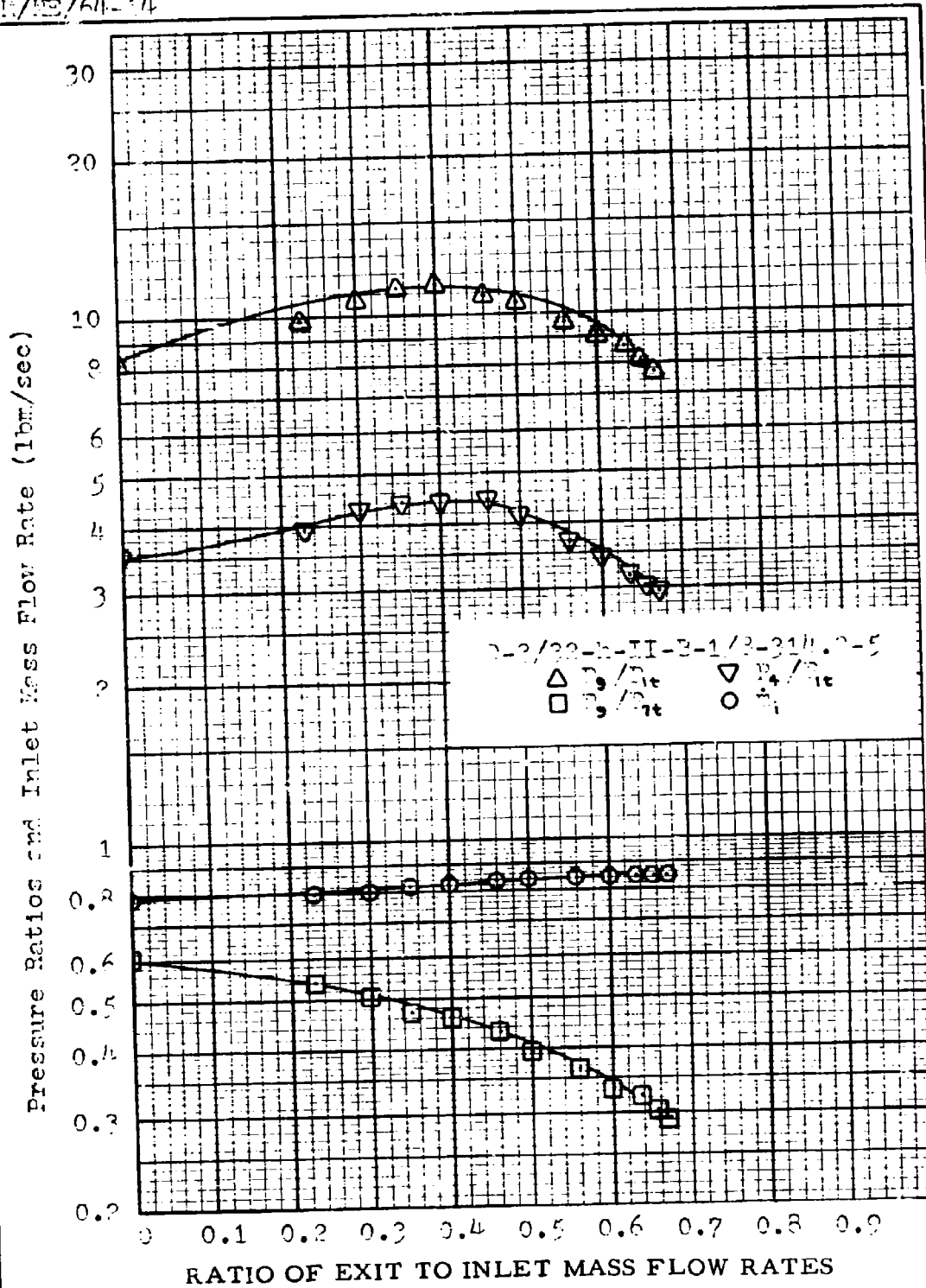


Fig. 98 Pressure Ratios and Mass Flow vs Mass Flow Ratio

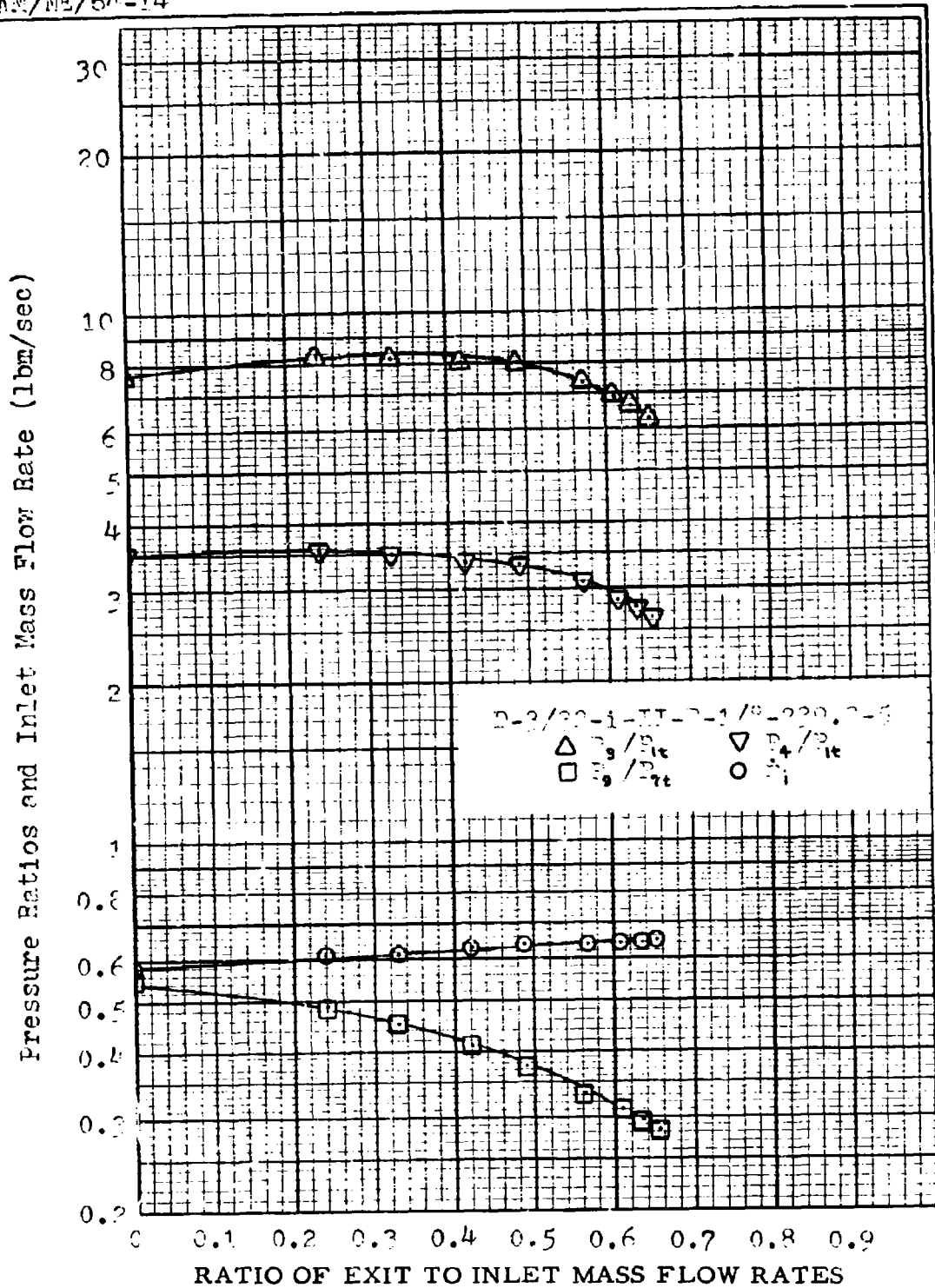
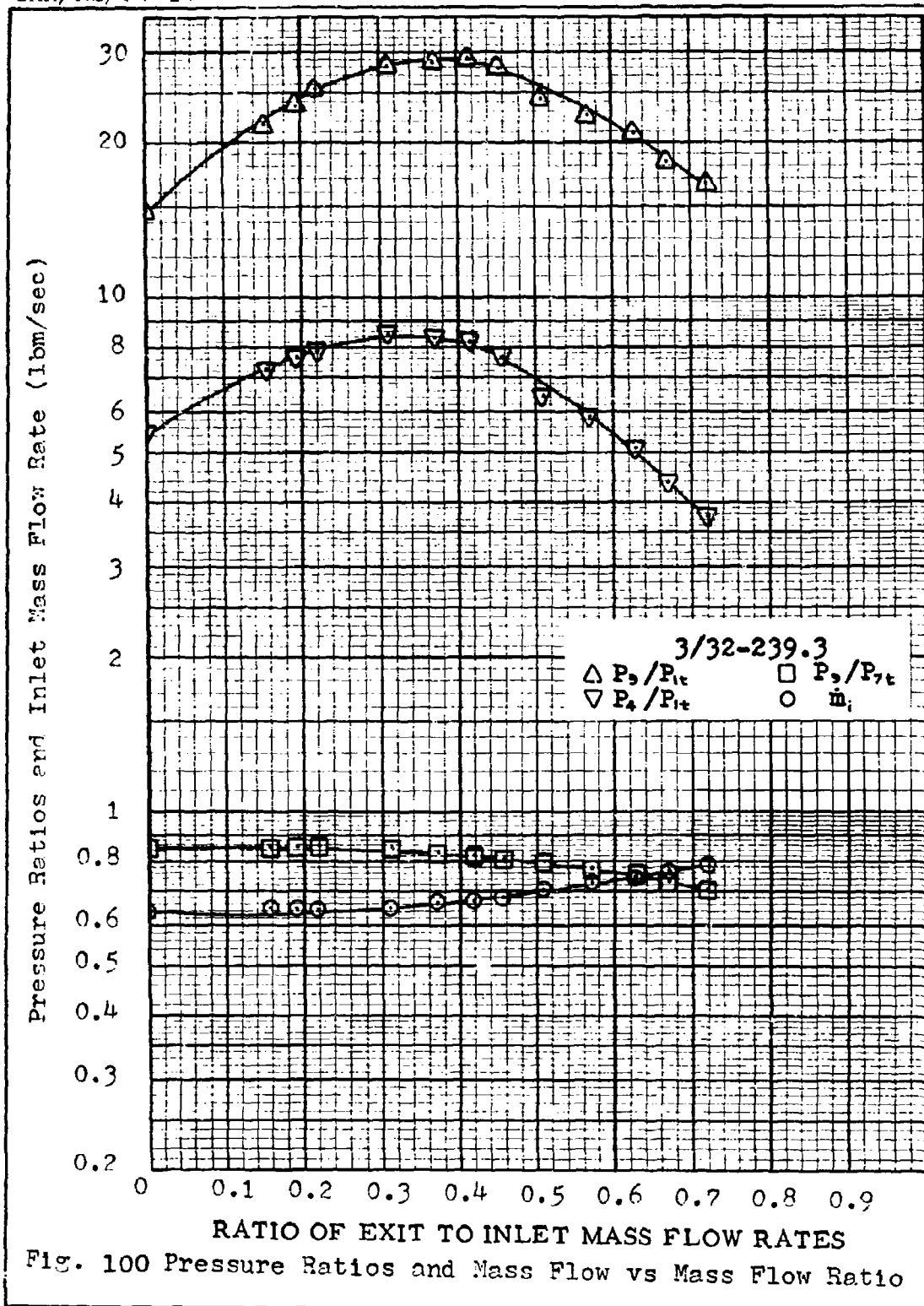
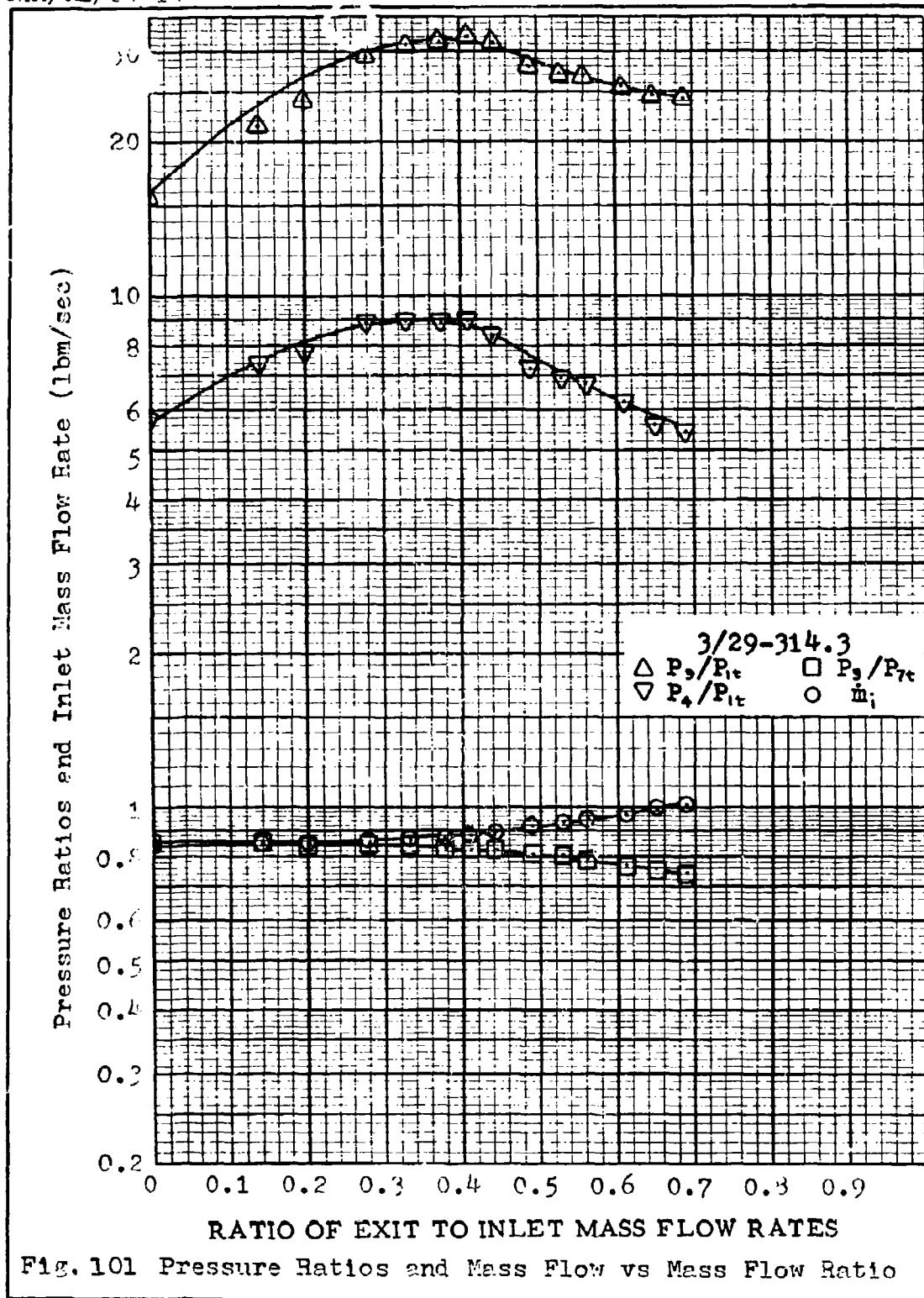


Fig. 99 Pressure Ratios and Mass Flow vs Mass Flow Ratio





Vita

Thomas Daniel Florino, Jr. was born on 18 August 1941 in Dover, New Jersey, the son of Thomas Daniel Florino, Sr. and Angela Florino. After completing his work in 1959 at Bayley Ellard High School, Madison, New Jersey, he enrolled at Parks College of St. Louis University, St. Louis, and in August 1962 he was graduated with the degree of Bachelor of Science in Aeronautical Engineering. After receiving his commission as Lieutenant in the USAF Reserve, he entered active duty in September 1962 to attend the Air Force Institute of Technology.

Permanent address: 27 William St.
Dover, New Jersey 07801

This thesis was typed by Joyce H. Ward.

Vita

Robert Poplawski was born on 20 September 1938 in Amherst, Massachusetts, the son of Bronie Anthony Poplawski, Sr. and Helen Poplawski. After completing his work in 1957 at Saint Michael High School, Northampton, Massachusetts, he enrolled at the University of Massachusetts, Amherst, and in June 1962 he was graduated with the degree of Bachelor of Science in Mechanical Engineering. After receiving his commission as Lieutenant in the USAF Reserve, he entered active duty in September 1962 to attend the Air Force Institute of Technology.

Permanent address: 472 North King Street
Northampton, Massachusetts

This thesis was typed by Joyce H. Ward.

Unclassified

Security Classification

DOCUMENT CONTROL DATA - R&D		
(Security classification of title, body of abstract and indexing annotation must be entered when the overall report is classified)		
1. ORIGINATING ACTIVITY (Corporate author) Air Force Institute of Technology Wright-Patterson Air Force Base, Ohio		2a. REPORT SECURITY CLASSIFICATION Unclassified
		2b. GROUP
3. REPORT TITLE EXPERIMENTAL OPTIMIZATION OF THE REVERSE-FLOW SWIRL CHAMBER		
4. DESCRIPTIVE NOTES (Type of report and inclusive dates) Thesis in partial fulfillment of the requirements for the degree of Master of Science		
5. AUTHOR(S) (Last name, first name, initial) 1/Lt Thomas D. Florino, Jr., and 1/Lt Robert Poplawski		
6. REPORT DATE April 1965	7a. TOTAL NO. OF PAGES 165	7b. NO. OF REFS 4
8a. CONTRACT OR GRANT NO.	8a. ORIGINATOR'S REPORT NUMBER(S) GAM/ME/64-14	
b. PROJECT NO. 7116		
c. Task 711602	8b. OTHER REPORT NO(S) (Air / other numbers that may be assigned this report) ARL 65-66	
d.		
10. AVAILABILITY/LIMITATION NOTICES Qualified requestors may obtain copies of this report from DDC. Report is not releasable to GTS.		
11. SUPPLEMENTARY NOTES	12. SPONSORING MILITARY ACTIVITY Aerospace Research Laboratories, OAR, Thermo-Mechanics Research Laboratory Wright-Patterson Air Force Base, Ohio	
13. ABSTRACT A high pressure-reverse flow vortex chamber is a device designed for the purpose of separating sub-micron particles out of a gas flow. The requirements for separation of sub-micron particles from a curved flow are given, and an equation determining the minimum angular velocity necessary for separation in a vortex flow is presented. Three swirl (vortex) chambers were tested and modified to determine their optimum performance. Results show that inlet geometry, method of injection, injection nozzle size, exhaust diffuser spacing, and internal chamber dimensions are important factors when optimizing chamber performance. The testing and modification has led to the evolution of a swirl chamber that can develop an overall pressure ratio of thirty and a pressure recovery of eighty-five per cent for a chamber inlet total pressure of 300 psig. The internal flow pattern of the swirl chamber was studied using talcum powder for particles and high speed motion picture photography (7,000 frames per second) as an aid in observing gross particle movements. This study has verified the fact that the swirl chambers are basically capable of separating sub-micron particles out of a gas flow.		

DD FORM 1 JAN 64 1473

Unclassified

Security Classification

Security Classification

14	KEY WORDS	LINK A		LINK B		LINK C	
		ROLE	WT	ROLE	WT	ROLE	WT
		<p>Vortex Flow Swirl Chamber Particle Separator Internal Flow</p>					

INSTRUCTIONS

1. **ORIGINATING ACTIVITY:** Enter the name and address of the contractor, subcontractor, grantee, Department of Defense activity or other organization (*corporate author*) issuing the report.

2a. **REPORT SECURITY CLASSIFICATION:** Enter the overall security classification of the report. Indicate whether "Restricted Data" is included. Marking is to be in accordance with appropriate security regulations.

2b. **GROUP:** Automatic downgrading is specified in DoD Directive 5200.10 and Armed Forces Industrial Manual. Enter the group number. Also, when applicable, show that optional markings have been used for Group 3 and Group 4 as authorized.

3. **REPORT TITLE:** Enter the complete report title in all capital letters. Titles in all cases should be unclassified. If a meaningful title cannot be selected without classification, show title classification in all capitals in parentheses immediately following the title.

4. **DESCRIPTIVE NOTES:** If appropriate, enter the type of report, e.g., interim, progress, summary, annual, or final. Give the inclusive dates when a specific reporting period is covered.

5. **AUTHOR(S):** Enter the name(s) of author(s) as shown on or in the report. Enter last name, first name, middle initial. If military, show rank and branch of service. The name of the principal author is an absolute minimum requirement.

6. **REPORT DATE:** Enter the date of the report as day, month, year, or month, year. If more than one date appears on the report, use date of publication.

7a. **TOTAL NUMBER OF PAGES:** The total page count should follow normal pagination procedures, i.e., enter the number of pages containing information.

7b. **NUMBER OF REFERENCES:** Enter the total number of references cited in the report.

8a. **CONTRACT OR GRANT NUMBER:** If appropriate, enter the applicable number of the contract or grant under which the report was written.

8b, 8c, & 8d. **PROJECT NUMBER:** Enter the appropriate military department identification, such as project number, subproject number, system numbers, task number, etc.

9a. **ORIGINATOR'S REPORT NUMBER(S):** Enter the official report number by which the document will be identified and controlled by the originating activity. This number must be unique to this report.

9b. **OTHER REPORT NUMBER(S):** If the report has been assigned any other report numbers (*either by the originator or by the sponsor*), also enter this number(s).

10. **AVAILABILITY/LIMITATION NOTICES:** Enter any limitations on further dissemination of the report, other than those

imposed by security classification, using standard statements such as:

- (1) "Qualified requesters may obtain copies of this report from DDC."
- (2) "Foreign announcement and dissemination of this report by DDC is not authorized."
- (3) "U. S. Government agencies may obtain copies of this report directly from DDC. Other qualified DDC users shall request through _____."
- (4) "U. S. military agencies may obtain copies of this report directly from DDC. Other qualified users shall request through _____."
- (5) "All distribution of this report is controlled. Qualified DDC users shall request through _____."

If the report has been furnished to the Office of Technical Services, Department of Commerce, for sale to the public, indicate this fact and enter the price, if known.

11. **SUPPLEMENTARY NOTES:** Use for additional explanatory notes.

12. **SPONSORING MILITARY ACTIVITY:** Enter the name of the departmental project office or laboratory sponsoring (*paying for*) the research and development. Include address.

13. **ABSTRACT:** Enter an abstract giving a brief and factual summary of the document indicative of the report, even though it may also appear elsewhere in the body of the technical report. If additional space is required, a continuation sheet shall be attached.

It is highly desirable that the abstract of classified reports be unclassified. Each paragraph of the abstract shall end with an indication of the military security classification of the information in the paragraph, represented as (TS), (S), (C), or (U).

There is no limitation on the length of the abstract. However, the suggested length is from 150 to 225 words.

14. **KEY WORDS:** Key words are technically meaningful terms or short phrases that characterize a report and may be used as index entries for cataloging the report. Key words must be selected so that no security classification is required. Identifiers, such as equipment model designation, trade name, military project code name, geographic location, may be used as key words but will be followed by an indication of technical content. The assignment of links, rules, and weights is optional.

465075-
AD
ARL 65-66

APRIL 1965

NOTICE

Following Information was Omitted from ARL Technical Report
No. ARL 65-56, dated April 1965:

THESIS WAS COMPLETED IN APRIL 1964 AND WAS JOINTLY
SPONSORED BY ARL SCIENTISTS AND MEMBERS OF THE
AIR FORCE INSTITUTE OF TECHNOLOGY FACULTY".



DEPARTMENT OF THE AIR FORCE
AIR UNIVERSITY (AETC)

Date: October 29, 2004

Re: Air Force Institute of Technology Thesis (AD0465075)

Please be advised that the distribution statement for "Experimental Optimization of the Reverse-Flow Swirl Chamber", a Master's thesis prepared by 1st Lt. Thomas D. Fiorino, Jr. and 1st Lt. Robert Poplawski, dated April 1965, has been changed from limited to category A – approved for public release.

Signed:

A handwritten signature in cursive script, reading "Bradley S. Liebst".

Bradley S. Liebst, PhD.
Department Head, AFIT/ENY
Air Force Institute of Technology
Wright Patterson Air Force Base
Dayton, OH 45433